Design of a TIMP-3 mutant with an increased half-life for improved protection against cartilage breakdown



Christine Doherty
St Cross College

Supervisors
Dr Linda Troeberg
Prof. Hideaki Nagase

Matrix Biology Group
Kennedy Institute of Rheumatology
Nuffield Department of Orthopaedics, Rheumatology and Musculoskeletal Sciences
University of Oxford

Thesis submitted for the degree of Doctor of Philosophy (D. Phil.) to
University of Oxford
Trinity 2015

Acknowledgements

Four years in the making, 2 different cities, with one steadfast and dedicated supervisor and I have finally submited my thesis. I have had the great luck to have the perfect supervisor and friend in Dr Troeberg. Aside from her astounding scientific knowledge, she is a uniquely gifted teacher. She operates an open-door policy, never once in 4 years have I darkened her door to be asked to come back another time, never once have I asked a question that was not answered and never once have I felt that I was in this entirely alone. She infects her students with her love of science and her sense of humour. It is a great privilege to have spent the last four years as part of her group and to call her a friend.

Prof. Hideaki Nagase has been a fountain for knowledge and frequently stunned even me to silence with his deceptively simple insightful questions. My thesis and knowledge are richer for having known him.

Dr Robert Visse has been an unofficial supervisor from the start, rescuing me from many a mishap, generally before I even knew I needed rescuing. His gentle patience and encouragement have saved many a “bad-lab day”. His generosity of time and spirit has contributed profoundly to my completing this thesis.

The Matrix Biology group has changed so much over the course of my time here, but members past and present will never be forgotten for their friendship, sense of humour and kindness.

My family has been a constant source of encouragement to me throughout this experience and without Andy and Alice this thesis would simply not exist.

I thank you all

Abstract

Thesis title: The design of a TIMP-3 mutant with an increased half-life for improved protection against cartilage breakdown.

Candidate: Christine Doherty, St Cross College

Degree: Doctor of Philosophy (D.Phil.) Trinity 2015

Osteoarthritis (OA) is a degenerative joint disease for which there are currently no disease-modifying drugs. OA is characterised by degradation of cartilage extracellular matrix (ECM) components by catabolic metalloproteinases. Tissue inhibitor of metalloproteinase 3 (TIMP-3) is the endogenous inhibitor of these enzymes, and thus a target for the development of novel OA therapies. Extracellular levels of TIMP-3 are regulated by endocytosis via the scavenger receptor LDL receptor-related protein-1 (LRP-1), reducing its in vivo half-life and chondroprotective activity. The aim of this study was to generate a TIMP-3 mutant resistant to LRP-1 binding but with unaltered affinity for target metalloproteinases and ECM glycosaminoglycans, since we hypothesised such a mutant would have increased chondroprotective activity. LRP-1 ligand-binding motifs have been proposed to consist of a pair of surface lysine residues separated by 21Å. Using in silico molecular modeling of a proposed TIMP-3 structure, we identified 10 pairs of lysine residues potentially satisfying this motif. Site-directed mutagenesis of all of these lysine pairs to alanine generated TIMP-3 mutants with resistance to LRP-1-mediated endocytosis, localising the LRP-1-binding residues to an extended basic patch on the TIMP-3 surface.

TIMP-3 K26A/K45A and TIMP-3 K42A/K110A were further analysed. TIMP-3 K42A/K110A had unaltered affinity for target metalloproteinases, but markedly reduced affinity for ECM glycosaminoglycans. It displayed improved chondroprotection over 24 hours, but was no more effective than Wild-type TIMP-3 over longer time periods, possibly due to its inability to be retained on the ECM. TIMP-3 K26A/K45A, on the other hand, retained high affinity for both target metalloproteinases and ECM glycosaminoglycans, and was found to have a longer half-life in cartilage and improved chondroprotective activity relative to Wild-type TIMP-3. This study thus identified an LRP-1-resistant mutant of TIMP-3 with an increased half-life and protective activity in cartilage, and showed that such behaviour was dependent on maintenance of interaction with the ECM. A similar paradigm may apply to other ECM-associated LRP-1 ligands.

List of Figures **13**

List of Tables **17**

List of abbreviations **18**

Chapter 1: Introduction **22**

1.1 Osteoarthritis (OA) **23**

1.1.1 Incidence of osteoarthritis 23

1.1.2 Treatment 24

1.1.3 Cost of OA 25

1.1.4 Factors contributing to OA 27

1.1.5 Pathology of OA 28

1.2 Cartilage **29**

1.2.1 What is cartilage? 29

1.2.2 Cartilage structure 30

1.2.3 Degradation of cartilage in OA 33

1.2.4 Type II collagen and its degradation in OA 35

1.2.5 Aggrecan and its degradation in OA 36

1.3 Role of proteolytic enzymes in cartilage degradation **39**

1.3.1 Historical background 39

1.3.2 Matrix metalloproteinases (MMPs) 41

1.3.2.1 Collagenases 42

1.3.2.2 Gelatinases 43

1.3.2.3 Stromelysins 44

1.3.2.4 MMPs in OA 44

1.3.3 ADAMTSs 45

1.3.3.1 ADAMTSs in OA 45

1.3.3.2 MMP and ADAMTS cleavage of aggrecan 48

1.4 TIMPs 49
1.4.1 Background 49
1.4.2 TIMP-1 53
1.4.3 TIMP-2 54
1.4.4 TIMP-4 55
1.4.5 TIMP-3 56
1.4.5.1 TIMP-3 inhibitory profile 58
1.4.5.2 Extracellular matrix binding of TIMP-3 60
1.4.5.3 Apoptotic activity of TIMP-3 61
1.4.6 TIMP-3 in disease 62
1.4.6.1. Sorsby's fundus dystrophy 62
1.4.6.2 Role of TIMP-3 in OA 63
1.4.7 Regulation of TIMP-3 64
1.5 Low-density lipoprotein receptor-related protein (LRP-1) 68
1.5.1 History of LRP-1 69
1.5.2 LRP-1 structure 70
1.5.3 LRP-1 ligands and biological function 72
1.5.4 Receptor associated protein (RAP) 74
1.5.5 LRP-1 expression 75
1.5.6 LRP-1 ligand-binding interface 76
1.5.7 LRP-1-mediated signaling 78
1.5.8 LRP-5 and -6 79
1.6 Hypothesis and aims of study 80

Chapter 2: Material and Methods 82

2.1 Reagents 83
2.1.1. Cultured cells 83
2.1.2. Cell culture reagents 83

2.1.3. Protein biochemistry reagents 83
2.1.4. SDS-PAGE and immunoblotting reagents 83
2.1.5. Antibodies 85
2.1.6. Molecular biology reagents 86
2.2. Methods 87
2.2.1. Cell culture 87
2.2.1.1. Bacterial cell culture 87
2.2.1.2. Mammalian cell line culture 88
2.2.1.3. Primary chondrocyte isolation and culture 88
2.2.2. TCA precipitation 89
2.2.3. SDS-PAGE and immunobloting 89
2.2.3.1. Ammediol SDS-PAGE 90
2.2.3.2. Tris-glycine SDS-PAGE 91
2.2.3.3. Immunoblotting 93
2.2.3.4. Coomassie staining 94
2.2.3.5. Densitometry 95
2.2.4. Generation of stable cell lines 95
2.2.4.1. Liposome transfection 95
2.2.4.2. Hygromyin B selection 95
2.2.4.3. Freezing down cell lines 96
2.2.5. Protein purification 97
2.2.5.1. Purification of TIMP-3 for in vitro analysis 97
2.2.5.2. Purification of TIMP-3 and mutants for cell culture analysis 97
2.2.5.3. Purification of RAP 98
2.2.6. Calculation of apparent equilibrium constant, $K_{i(app)}$ 99
2.2.6.1. Calculation of TIMP-3 affinity for MMP-1 99
2.2.6.2. Calculation of TIMP-3 affinity for MMP-2 100
2.2.6.3. Calculation of TIMP-3 affinity for MMP-3 100

2.2.6.4. Calculation of TIMP-3 affinity for ADAMTS-4 101
2.2.6.5. Calculation of TIMP-3 affinity for ADAMTS-5 101
2.2.6.6. Calculation of TIMP-3 affinity for ADAM-17 102
2.2.7. Endocytosis assays 102
2.2.7.1. Immunoblot analysis of TIMP-3 endocytosis from culture medium 102
2.2.8. LRP-1 binding ELISA 103
2.2.9. Heparin binding ELISA 103
2.3. Measuring GAG release from cartilage 104
2.3.1. Cartilage explant dissection 104
2.3.1.1. Generation of DMMB assay standard curve 104
2.3.1.2. Analysis of GAG release by DMMB assay 105
2.3.2. Analysis of GAG release by immunoblotting 106

Chapter 3: Design of an endocytosis-resistant TIMP-3 107

3.1 Introduction 108
3.2 Results 111
3.2.1 Identification of potential LRP-1 binding motif in TIMP-3 111
3.2.1.1 Model of Wild-type TIMP-3 three-dimensional structure 111
3.2.1.2 Potential lysine pairs satisfying the LRP-1 binding motif 113
3.2.2. Generation of TIMP-3 mutants 115
3.2.2.1. TIMP-3 mutant primer design 116
3.2.2.2. Polymerase chain reaction reagent protocol 119
3.2.2.3. Isolation of TIMP-3 mutant DNA 120
3.2.3. Generation of recombinant RAP 125
3.2.3.1. Introduction 125
3.2.3.2. RAP expression and purification 126
3.2.3.3. Discussion 129

Chapter 4: Screening for endocytosis-resistant mutants of TIMP-3 by immunoblotting 131

4.1 Introduction 132

4.2 Results 133

4.2.1 Transient expression of Wild-type and mutant TIMP-3 in HEK-293-EBNA cell line 133

4.2.1.1 Optimising DNA concentration for transient expression of TIMP-3 in HEK-293-EBNA cells 133

4.2.1.2 Optimising expression time for transient expression of TIMP-3 in HEK-293-EBNA cells 135

4.2.2 Optimising medium volume for screening endocytosis-resistance of Wild-type and mutant TIMP-3 in HTB94 cells 137

4.2.2.1 Detection of Wild-type TIMP-3 in HEK-293-EBNA conditioned medium 137

4.2.2.2 Detection of TIMP-3 mutant expression in HEK-293-EBNA conditioned medium 138

4.2.3 Quantification of the rate of TIMP-3 endocytosis by HTB94 chondrosarcoma cells 142

4.2.3.2 Optimisation of HTB94 cell seeding density for endocytosis assay 142

4.2.3.3 Evaluating efficiency of dialysis to remove sodium chlorate from HEK-293-EBNA conditioned media 145

4.2.3.4 Endocytosis of TIMP-3 single mutants by HTB94 cells 148

4.2.3.5 Endocytosis of TIMP-3 double mutants from the medium of HTB94 cells 155

4.2.4. Evaluation of the effect of Wild-type and mutant TIMP-3 on HTB94 cell viability 162

4.3 Discussion 165

Chapter 5: Bioactivity of TIMP-3 mutants 169

5.1 Introduction 170

5.2 Results 170

5.2.1 Generation of stable cell lines for expression of shortlisted mutants 170

5.2.2 Purification of TIMP-3 mutants 173

5.2.3 Resistance of purified TIMP-3 double mutants to endocytosis by HTB94 cells 179

5.2.4 Evaluation of TIMP-3 mutant binding to LRP-1 181

5.2.5 Metalloproteinase inhibitory activity of TIMP-3 mutants 183

5.2.5.1 Affinity of TIMP-3 mutants K26A/K45A and K42A/K110A for MMP-1ΔC 185

5.2.5.2 Affinity of TIMP-3 mutants K26A/K45A and K42A/K110A for MMP-2ΔC 186

5.2.5.3 Affinity of TIMP-3 mutants K26A/K45A and K42A/K110A for MMP-3ΔC 188

5.2.5.4 Affinity of TIMP-3 mutants K26A/K45A and K42A/K110A for ADAMTS-4 190

5.2.5.5 Affinity of TIMP-3 mutants K26A/K45A and K42A/K110A for ADAMTS-5 192

5.2.5.6 Affinity of TIMP-3 mutants K26A/K45A and K42A/K110A for ADAM-17 194

5.2.6 Binding of TIMP-3 mutants to sulfated glycosaminoglycans 197

5.2.6.1 Binding of Wild-type TIMP-3, TIMP-3 K26A/K45A and TIMP-3 K42A/K110A to heparin and heparan sulfate 198

5.2.6.2 Effect of reduced heparin binding on inhibition of ADAMTS-5 200

5.3 Discussion 202

Chapter 6: Chondroprotective effect of TIMP-3 mutants..... 211

6.1. Introduction 212

6.2. Results 214

6.2.1. Resistance of purified TIMP-3 double mutants to endocytosis by primary porcine chondrocytes..... 214

6.2.2. Optimising quantification of GAG release 216

6.2.2.1. Evaluation of GAG release stimulation method 217

6.2.2.2. Evaluation of duration of stimulation period 222

6.2.2.3. Effect of Wild-type and mutant TIMP-3 on chondrocyte viability in IL-1 stimulated porcine cartilage explants 224

6.2.2.4. Inhibition of porcine articular cartilage explant degradation by N-TIMP-3..... 227

6.2.2.5. Inhibition of porcine articular cartilage explant degradation by full-length Wild-type TIMP-3 228

6.2.2.6. Inhibition of GAG release from cartilage explants by TIMP-3 mutant K26A/K45A..... 231

6.2.2.7. Inhibition of GAG release from cartilage explants by TIMP-3 mutant K42A/K110A..... 233

6.2.2.8. Effect of pre-incubation on chondroprotective activity of TIMP-3 K26A/K45A and TIMP-3 K42A/K110A..... 236

6.2.2.9. Effect of TIMP-3 K26A/K45A on time course of GAG release.... 238

6.3. Discussion 240

Chapter 7: Discussion..... 247

7.1. Evaluation of proposed LRP-1-binding motif..... 248

7.2. LRP-1-binding residues of TIMP-3..... 249

7.3. Biological effectiveness of mutants..... 254

7.4. Conclusions and future directions..... 257

Chapter 8: References..... 262

List of Figures

Figure 1: Management regime for treating patients with OA. 25
Figure 2: Direct cost of OA in the UK in 2010. 26
Figure 3: Diagram showing the features of knee OA. 29
Figure 4: Articular cartilage can be functionally and structurally divided into three zones. 31
Figure 5: Primary components of the cartilage ECM that contribute to cartilage function. 33
Figure 6: Structural degradation of cartilage associated with OA. 34
Figure 7: Increased denaturation of type II collagen fibrils with increasing OA 36
Figure 8: Structure of the aggregating proteoglycan aggrecan. 38
Figure 9: Domain structure of matrix metalloproteinases. 43
Figure 10: Cleavage sites on human aggrecan by aggrecanases and MMPs. 49
Figure 11: TIMP-1 interaction with metalloproteinases. 52
Figure 12: TIMP-3 is a central regulator of cartilage degradation. 64
Figure 13: Extracellular levels of TIMP-3 are regulated by the equilibrium between binding to LRP-1 and the ECM. 68
Figure 14: LDL receptors are structurally homologous and composed of repeating subunits. 71
Figure 15: Classes of identified LRP-1 ligands and their proposed intracellular effects. 72
Figure 16: Structure of cysteine–rich complimentary repeats of LRP-1. 77
Figure 17: DMMB standard curve using chondroitin-4-sulfate. 105
Figure 18: RAP binding to LRP-1 is mediated by a di-lysine pair separated by 21Å. 109
Figure 19: Comparison of N-TIMP-3 crystal structure and proposed model of full-length TIMP-3 structure. 113
Figure 20: Model of full-length TIMP-3 structure, highlighting lysine residues. 114
Figure 21: Agilent QuikChange II XL Site-Directed Mutagenesis Strategy. (adapted from Agilent product literature). 116

Figure 22: Primers all 12 TIMP-3 single mutants. 118
Figure 23: Mammalian expression vector encoding C-terminally FLAG-tagged human TIMP-3 121
Figure 24: Restriction digest screening of candidate TIMP-3 single mutants K110A and K157A. 124
Figure 25: Restriction digest screening of TIMP-3 double mutants K42A/K110A and K42A/K157A. 125
Figure 26: Purification of Wild-type RAP 128
Figure 27: Optimization of DNA concentration for transfection of HEK-293-EBNA cells with TIMP-3 135
Figure 28: Optimising expression time for transient expression of TIMP-3 in HEK-293-EBNA cells. 136
Figure 29: Expression of Wild-type TIMP-3 in HEK-293-EBNA conditioned medium. 138
Figure 30: Detection of TIMP-3 single mutant expression in HEK-293-EBNA conditioned medium. 140
Figure 31: Detection of TIMP-3 double mutant expression in HEK-293-EBNA 141
Figure 32: Optimising seeding density of HTB94 cells for endocytosis time course assays. 144
Figure 33: Purified Wild-type TIMP-3 and dialysed Wild-type TIMP-3 conditioned medium have the same half-life on HTB94 cells. 147
Figure 34: TIMP-3 K22A and TIMP-3 K26A have delayed endocytosis compared to Wild-type TIMP-3. 149
Figure 35: TIMP-3 K27A and TIMP-3 K30A are endocytosed at the same rate as Wild-type TIMP-3. 150
Figure 36: TIMP-3 K42A has delayed endocytosis, but TIMP-3 K45A is endocytosed at the same rate as Wild-type TIMP-3. 151
Figure 37: TIMP-3 K52A is endocytosed at the same rate as Wild-type TIMP-3 but TIMP-3 K71A has delayed endocytosis. 152
Figure 38: TIMP-3 K76A is endocytosed at the same rate as Wild-type TIMP-3, but TIMP-3 K89A has an increased rate of endocytosis. 153
Figure 39: TIMP-3 K110A and TIMP-3 K157A have delayed endocytosis compared to Wild-type TIMP-3. 154

Figure 40: TIMP-3 K22A/K110A and TIMP-3 K22A/K157A are not endocytosed by HTB94 cells within 24 hours. 157
Figure 41: TIMP-3 K26A/K45A and TIMP-3 K27A/K45A are not endocytosed by HTB94 cells within 24 hours. 158
Figure 42: TIMP-3 K30A/K52A and TIMP-3 K30A/K76A are not endocytosed by HTB94 cells within 24 hours. 159
Figure 43: TIMP-3 K42A/K110A and TIMP-3 K42A/K157A are not endocytosed by HTB94 cells within 24 hours. 160
Figure 44: TIMP-3 K45A/K89A and TIMP-3 K71A/K157A are not endocytosed by HTB94 cells within 24 hours. 161
Figure 45: The effect of TIMP-3 and mutants on HTB94 cell viability. 164
Figure 46: Generation of HEK-293-EBNA stable cell lines expressing TIMP-3 K26A/K45A and K27A/K45A..... 172
Figure 47: Purification of TIMP-3 K26A/K45A and TIMP-3 K42A/K110A by anti-FLAG affinity chromatography. 175
Figure 48: Purification of TIMP-3 K27A/K45A and TIMP-3 K42A/K157A were expressed at low levels by anti-FLAG affinity chromatography. 176
Figure 49: Titration of TIMP-3 K26A/K45A and K42A/K110A against MMP-1ΔC 178
Figure 50: TIMP-3 mutants K26A/K45A, K30A/K76A and K42A/K110A retain endocytosis resistance after purification in HTB94. 181
Figure 51: Affinity of TIMP-3 mutants for LRP-1 evaluated by ELISA..... 183
Figure 52: Affinity of Wild-type TIMP-3 and TIMP-3 mutants K26A/K45A and K42A/K110A for MMP-1ΔC..... 186
Figure 53: Affinity of Wild-type TIMP-3 and TIMP-3 mutants K26A/K45A and K42A/K110A for MMP-2ΔC..... 188
Figure 54: Affinity of Wild-type TIMP-3 and TIMP-3 mutants K26A/K45A and K42A/K110A for MMP-3ΔC..... 190
Figure 55: Affinity of Wild-type TIMP-3 and TIMP-3 mutants K26A/K45A and K42A/K110A for ADAMTS-4..... 192
Figure 56: Affinity of Wild-type TIMP-3 and TIMP-3 mutants K26A/K45A and K42A/K110A for ADAMTS-5..... 194
Figure 57: Affinity of Wild-type TIMP-3 and TIMP-3 mutants K26A/K45A and K42A/K110A for ADAM-17. 196

Figure 58: Binding by Wild-type TIMP-3, TIMP-3 K26A/K45A and TIMP-3 K42A/K110A to heparin and heparan sulfate..... 199
Figure 59: Effect of heparin on affinity of Wild-type TIMP-3 and TIMP-3 mutants K26A/K45A and K42A/K110A for ADAMTS-5. 201
Figure 60: TIMP-3 mutants K26A/K45A, K30A/K76A and K42A/K110A are resistant to endocytosis by primary porcine chondrocytes. 216
Figure 61: By DMMB assay, IL-1 stimulates highest GAG release from porcine cartilage explants and articular chondrocytes. 219
Figure 62: IL-1 and retinoic acid stimulation of AGEG neo-epitope release from porcine cartilage explants by immunoblotting. 221
Figure 63: Time course of AGEG neo-epitope release from IL-1-stimulated porcine cartilage explants. 223
Figure 64: MTS assay of porcine cartilage explants treated with Wild-type and mutant TIMP-3. 226
Figure 65: N-TIMP-3 inhibits IL-1-stimulated GAG release from porcine articular cartilage explants. 228
Figure 66: 100 nM Wild-type TIMP-3 inhibits GAG release from cartilage.. 230
Figure 67: Inhibition of GAG release from porcine cartilage explants by TIMP-3 K26A/K45A. 232
Figure 68: Inhibition of GAG release from porcine cartilage explants by TIMP-3 K42A/K110A quantified by DMMB assay..... 235
Figure 69: TIMP-3 K26A/K45A retains chondroprotective effect after pre-incubation on cartilage. 237
Figure 70: TIMP-3 K26A/K45A shows improved inhibition of GAG release over time. 240
Figure 71: Localisation of di-lysine pairs on chondroprotective TIMP-3 mutants. 250
Figure 72: Localisation of lysine residues assessed for endocytosis-resistance on a TIMP-3 model. 252
Figure 73: Proposed TIMP-3-LRP-1 binding..... 253

List of Tables

Table 1: Sources of economic cost of OA. 27
Table 2: Summary of general TIMP characteristics. 56
Table 3: Summary of mouse phenotypes resulting from deletion of TIMP genes. 56
Table 4: Suppliers of cell culture reagents. 84
Table 5: Suppliers of SDS-PAGE and immunoblotting reagents. 85
Table 6: Buffers for ammediol SDS-PAGE. 91
Table 7: Composition of 10 % Ammediol SDS-PAGE gels. 91
Table 8: Buffers for the Tris-glycine SDS-PAGE system. 92
Table 9: Composition of 6% Tris-glycine gels. 93
Table 10: Amino acid sequence of FLAG-tagged human TIMP-3. 112
Table 11: Distance between α-carbons of lysine residues in proposed di-lysine pairs of TIMP-3. 114
Table 12: Agilent QuikChange II XL Site-Directed Mutagenesis kit primer design guidelines. 117
Table 13: Design of primers for generation of TIMP-3 K22A. 117
Table 14: Design of primers for generation of TIMP-3 K42A 117
Table 15: PCR mutagenesis reaction components for generation of TIMP-3 mutants using QuikChange II XL-site directed mutagenesis kit. 119
Table 16: PCR parameters for generation of TIMP-3 mutants using QuikChange II XL-site directed mutagenesis kit. 120
Table 17: Yield of purified Wild-type RAP. 129
Table 18: Half-life of TIMP-3 single mutants in HTB94 cells. 155
Table 19: Resistance of TIMP-3 di-lysine mutants to LRP-1-mediated endocytosis by HTB94 cells. 162
Table 20: Summary of purification of shortlisted TIMP-3 double mutants. .. 179
Table 21: Affinity of Wild-type and mutant TIMP-3 for prototypic TIMP-3 target metalloproteinases. 197
Table 22: Effect of heparin on affinity of TIMP-3, TIMP-3 K26A/K45A and TIMP-3 K42A/K110A for ADAMTS-5. 202

List of abbreviations

Å	Angstrom
α_2M	α_2-macroglobulin
ADAM	A disintegrin and metalloproteinase
ADAMTS	A disintegrin and metalloproteinase with thrombospondin motifs
AP	Alkaline phosphatase
ApoE	Apolipoprotein E
APS	Ammonium persulfate
BACE1	B-secretase beta-site amyloid precursor protein
Brij-35	Polyethylene glycol dodecyl ether
CaPPS	Calcium pentosan polysulfate
CHO	Chinise hamster ovary
COMP	Cartilage oligomeric protein
CR	Complementary repeat
CRP	Complementary regulatory protein
CS	Chondroitin sulfate
CTGF	Connective tissue growth factor
DMEM	Dulbecco's modified Eagle's medium
DMMB	Dimethylmethylene blue
DMOAD	Disease modifying osteoarthritis drug
DMSO	Dimethyl sulfoxide
dUTP	deoxynucleotidyl transferase
ECM	Extracellular matrix
EDTA	Ethylenediaminetetraacetic acid
EGF	Epidermal growth factor
ELISA	Enzyme-linked immunosorbent assay
E_o	Total enzyme concentration
ERK	Extracellular-signal-regulated kinases
FAS	Fas cell surface death receptor
FCS	Fetal calf serum
GAG	Glycosaminoglycans
GPC3	Glypican-3
HA	Hyaluronic acid

HEK-293-EBNA	Human embryonic kidney-293-Epstein-bar virus nuclear antigen
HEPES	4-(2-Hydroxyethyl)piperazine-1-ethanesulfonic acid, N-(2-Hydroxyethyl)piperazine-N′-(2-ethanesulfonic acid)
HRP	Horseradish peroxidase
HSPG	Heparin sulfate proteoglycan
IGD	Interglobular domain
IL-1	Interleukin-1
I_o	Total inhibitor concentration
JNK-2	c-Jun N-terminal kinase-2
kDa	kilo Daltons
$K_{i(app)}$	Apparent inhibition constant
KS	Keratan sulfate
LB	Luria Bertani
LDL	Low-density lipoprotein
LDLR	Low-density lipoprotein receptor
LRP	Low-density lipoprotein receptor-related protein
MAG	Myelin-associated glycoprotein
MAP	Mitogen-activated protein
MEF	Mouse embryonic fibroblast
miRNA	MicroRNA
MKK-4	Mitogen-activated protein kinase kinase 4
MMP	Matrix metalloproteinase
MSI	Microsatellite instability
MT-MMP	Membrane-type matrix metalloproteinase
N-TIMP-3	N-terminal domain of tissue inhibitor of metalloproteinase-3
NaCl	Sodium chloride
$NaClO_3$	Sodium chlorate
NMDA	N-methyl-D-aspartate
NMR	Nuclear magnetic resonance
NSAIDS	Non-steroidal anti-inflammatory drugs
OA	Osteoarthritis
OSM	Oncostatin M
p75NTR	P75 neurotrophin receptor
PAPS	3'-phosphoadenosine-5'-phosphosulfate

PAGE	Polyacrylamide gel electrophoresis
PAI-1	Plasminogen activator inhibitor type-1
PAI1	Plasminogen activator inhibitor-1
PBS	Phosphate buffered saline
PCR	Polymerase chain reaction
PDGF	Platelet derived growth factor
PEA	*Pseudomonas exotoxin* A
PKA	Protein kinase pathway
PVDF	Polyvinylidene fluoride
RAP	Receptor associated protein
Rpm	Revolutions per minute
RT-PCR	Real time Polymerase chain reaction
SDS	Sodium dodecyl sulfate
Shh	Sonic hedgehog
siRNA	Small interfering RNA
SirT1	Sirtuin 1
SNP	Sodium nitroprusside
$t_{1/2}$	Half-life
TACE	Tumor necrosis factor converting enzyme
TAK-1	TGF-β-activated kinase 1
TBS	Tris buffered saline
TCA	Trichloroacetic acid
TEMED	N,N,N',N'-tetramethylethane-1,2-diamine
TGFβ	Transforming growth factor-β
TNC	Tris/sodium/calcium assay buffer
TNF	Tumor necrosis factor
TNF-RI	Tumor necrosis factor receptor-1
TRAF	Tumor necrosis factor receptor-associated factors
TRAIL	Tumor necrosis factor-related apoptosis-inducing ligand
TrK	Tyrosine receptor kinase
TUNEL	terminal deoxynucleotidyl transferase dUTP nick end labeling
uPA	Urokinase-type plasminogen activator
v_o	Equilibrium rate of substrate hydrolysis without inhibitor
v_s	Equilibrium rate of substrate hydrolysis with inhibitor
vWf	Von Willebrand factor

WT TIMP-3	Wild-type TIMP-3
λ_{em}	Emission wavelength
λ_{ex}	Excitation wavelength

Chapter 1: Introduction

1.1 Osteoarthritis (OA)

Osteoarthritis (OA) is a chronic degenerative disease affecting synovial or diarthrosis joints. Degeneration of the joint structure causes pain and impairs movement of affected individuals. In addition to the physical impact on the patient, OA also imposes substantial societal and financial burdens. A key event underlying the pathogenesis of OA is degradation of the articular hyaline cartilage layer of the joint, leading to progressive loss of cartilage and joint space narrowing. Additional features include synovial inflammation, subchondral bone remodeling and development of osteophytes (Goldring and Goldring, 2010). Current treatments for OA include use of non-steroidal anti-inflammatory drugs (NSAIDs) and steroids. These drugs provide pain management, but do not have any protective effect on the cartilage and do not moderate the progression of disease. There are currently no disease-modifying osteoarthritis drugs (DMOADs), and OA progression frequently necessitates joint replacement surgery. There is thus considerable interest in development of alternative approaches to treating OA.

1.1.1 Incidence of osteoarthritis

OA is the most common form of arthritis and affects more adults globally than any other rheumatic disease. In the UK, 8.75 million people have sought treatment for OA, of which 4.71 million have sought treatment for knee OA alone. OA is the single most common cause of disability in older adults, ranking 5th worldwide and 9th in developing countries as a cause of years lost to disability (Murray et al., 2012). It is also considered to be the musculoskeletal disease with the highest burden, out-ranking rheumatoid arthritis and

osteoporosis. Globally, it is estimated that 9.6 % of men and 18.0 % of women over 60 years of age have symptomatic OA (Lozano et al., 2012). The joints in the knees, hands, feet, and spine are the most commonly affected, but OA is also relatively common in other joints such as the shoulder and hip joints (Bitton, 2009). Arthritis research UK estimates that due to increasing levels of obesity and population age, it is expected that the number of people seeking treatment for knee OA within the UK will reach 6.5 million by 2020.

1.1.2 Treatment

There are currently no disease-modifying osteoarthritis drugs (DMOADs). OA is thus incurable and as such, the medical community has limited treatment options, and OA is currently a managed disease rather than a cured one. A stepwise regime for this management plan is shown in Figure 1. Initially, exercise and the maintenance of a healthy weight are advised, followed by joint support with taping and braces, and depending on the joint affected, use of walking aids and appropriate footwear. For the patient, the first indication of OA is joint pain and advised pain management methods include use of paracetamol, followed by anti-inflammatory gels and NSAIDs. At later stages, corticosteroid injections are prescribed, and when the patient experiences increasing pain, opioids can be introduced (Hunter and Felson, 2006). Quality of life becomes increasingly affected and the only disease-modifying treatment currently available is joint replacement surgery. According to National Joint Registry records, 85920 knee and 80194 hip replacement surgeries were carried out in England, Wales and Northern Ireland in 2013. Alternative approaches to OA treatment are thus sought.

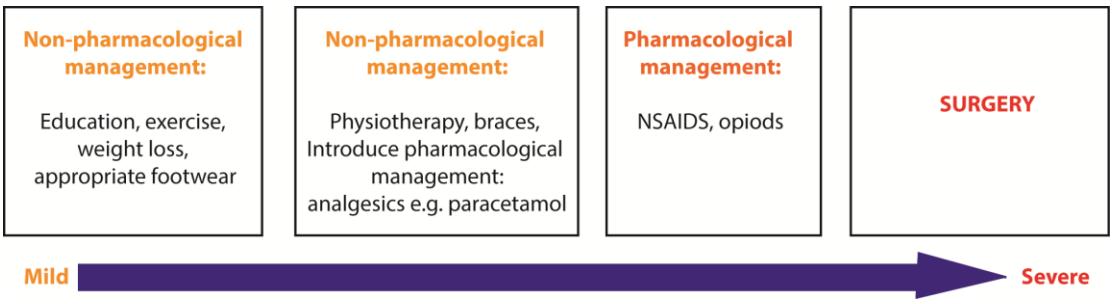


Figure 1: Management regime for treating patients with OA.
OA treatment progresses from initial non-pharmacological intervention to subsequent pharmacological pain management and commonly requires joint replacment surgery in later disease stages. While this treatment regime can be modified according to patient and clinician preference, it highlights the need for the development of disease-modifying OA drugs. Adapted from Hunter and Felson (2006).

1.1.3 Cost of OA

Age is a primary risk factor for OA and almost 25 % of people aged over 75 have sought treatment for knee OA. However, OA also affects younger people, and in the UK, one third of people aged 45 and over have sought treatment for OA. In the UK, an estimated 2.36 million people of working age have sought treatment for knee OA, 840 000 for hip OA, and 620 000 for wrist or hand OA. Figure 2 outlines the direct cost of treating OA in the UK in 2010. First-line management with NSAIDs such as ibubrofen cost £44.8 million and, worryingly, the iatrogenic events associated with NSAID use costs a further £99 million to treat. The co-prescription of proton pump inhibitors with NSAIDs for gastroprotection, and diagnostic arthroscopic surgery, jointly contribute another £12.9 million. The largest direct cost is the joint replacement surgery, at £852 million (Chen et al., 2012).

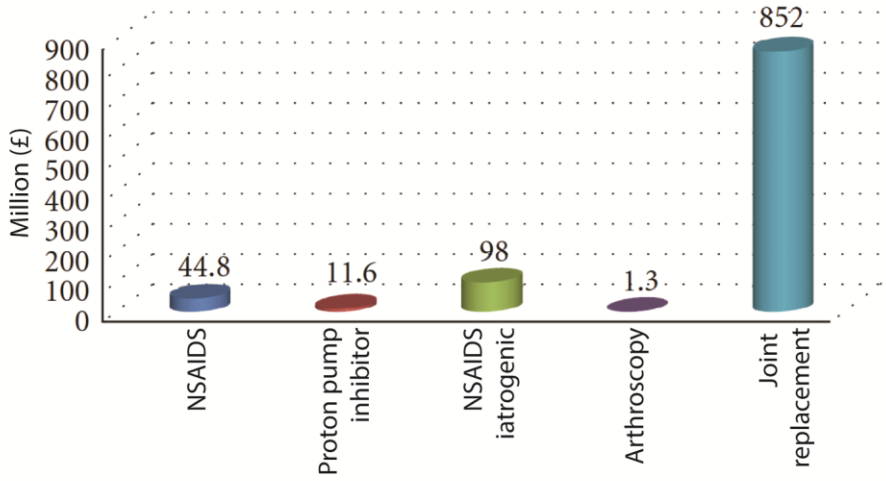


Figure 2: Direct cost of OA in the UK in 2010.

In 2010, diagnostic arthroscopic surgery was the smallest contributing direct cost, followed by the cost of co-prescribing proton pump inhibitors for gastroprotection against the effects of NSAID at 11.6 million. Prescription of NSAIDS for OA management cost £44.8 million and treatment of associated iatrogenic events costs a further £98 million. However, the largest direct cost was the joint replacement surgery, at £852 million. Adapted from Chen et al. (2012).

The costs outlined above refer only to direct medical costs, but the indirect cost of OA is substantial. The Department of Work and Pensions estimates that 36 million workdays were lost to OA in 2002, giving a loss of economic production in excess of £3.2 billion. While this represents a substantial financial burden, it does not give a full picture of the impact of OA in the UK. For example £43 million was spent on community services and £215 million on social services in 2002. Table 1 gives an overview of the economic cost of OA in the UK.

Table 1: Sources of economic cost of OA.

Adapted from Chen et al. (2012).

Direct costs	Indirect costs	Intangible costs
Surgery	Loss of productivity	Pain and suffering
Hospital resources	Absenteeism	Decreased quality of life
Care-giver time	Premature mortality	Potential depression and anxiety
Pharmacological treatment	Disability payments/benefits	
Non-pharmacological treatment		
Costs of treatment side effects		
Research		

1.1.4 Factors contributing to OA

The causes of OA are not fully understood and historically it has been regarded as a disease of old age, and an inevitable consequence of wear and tear of joints. However it is now known to be a multifactorial disease, with a range of risk factors including age, gender, obesity, joint injury or abnormality, occupation, and genetic factors. Women have a higher incidence of OA, with approximately 50 % higher prevalence of hip, hand and wrist OA, 22 % higher prevalence of knee OA and 28 % higher prevalence of foot and ankle OA than men (Jordan et al., 2007). Obesity is a well-validated risk factor for OA due to the increased burden on joints, especially the knee. However, it has been observed that the risk of finger OA is also increased in overweight patients (Verrouil and Mazieres, 1995), indicating a pathological effect beyond increased mechanical burden, potentially of an inflammatory source (Sellam and Berenbaum, 2010).

It has also been hypothesised that abnormal mechanical forces underlie the development of most or all cases of OA and that once OA has set in, abnormal mechanics overwhelm all other factors driving the disease. This hypothesis is supported by research on mouse models of joint injury and the observation that patients experiencing an injury to the joint have a 14-fold increased likelihood of developing OA in that joint (Felson, 2013). However, epidemiological surveys have also confirmed family clustering of hand and knee OA (Felson et al., 1998; Hirsch et al., 1998), indicating an additional genetic component to susceptibility.

1.1.5 Pathology of OA

Historically, OA has been considered to be a disease exclusively of articular cartilage, but now it is generally accepted to be a complex disease involving the entire joint. In addition to progressive failure of articular hyaline cartilage, additional features of OA include subchondral bone remodeling, joint space narrowing, synovial inflammation and changes to bone surrounding the joints leading to osteophyte formation (Goldring and Goldring, 2010) as shown in Figure 3.

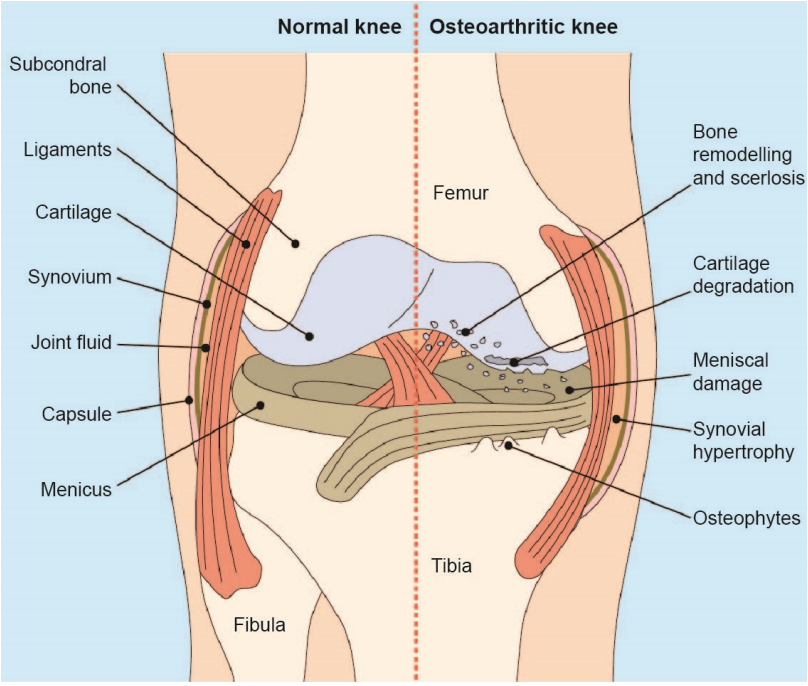


Figure 3: Diagram showing the features of knee OA.
OA is characterised by degradation of articular hyaline cartilage, subchondral bone remodelling, joint space narrowing, synovial inflammation, meniscal damage and osteophyte formation. Adapted from Hunter and Felson (2006).

1.2 Cartilage

1.2.1 What is cartilage?

Articular cartilage is a highly specialized connective tissue and its main function is to provide a smooth, lubricated surface for joint movement and to resist joint compression upon loading. Articular cartilage is devoid of blood vessels and nerve supply and so has limited capacity for healing and repair. Therefore, the preservation of joint homeostasis is fundamental to joint health.

Articular hyaline cartilage is 2-4 mm thick and consists of a single cell type, the chondrocyte. Chondrocytes are sparsely dispersed throughout the cartilage extracellular matrix (ECM) and comprise only 2-3 % of the total cartilage volume (Stockwell, 1967). As chondrocytes are the only cell present

in cartilage, they are responsible for the synthesis, organisation and maintenance of the ECM. They vary in morphology, number and size depending on their location within cartilage.

The cartilage ECM provides structural support for the tissue, functions as a scaffold for tissue organization, and it plays a central role in chondrocyte homeostasis (Aigner et al., 2006; Heinegård and Saxne, 2011). In turn, the chondrocytes regulate the articular cartilage function by synthesizing and secreting both the ECM components and the catabolic enzymes that degrade it.

1.2.2 Cartilage structure

Cartilage can be categorised into 3 zones named according to their distance from the articular surface as the superficial, intermediate and deep zones. The structure and content of each of these zones contributes to the overall function of cartilage. For articular cartilage to resist compressive forces, it must be sufficiently pliable to absorb compressive forces, while maintaining smooth frictionless movement of the joint, without becoming deformed by the compressive forces.

The superficial zone of cartilage is exposed to the joint capsule and makes up 10-20 % of articular cartilage thickness. It consists of collagen type II and IX fibres, aligned parallel to the articular surface (Sophia Fox et al., 2009). The area contains a relatively large number of flattened chondrocytes that secrete lubricin that, together with hyaluronic acid secreted by the synoviocytes, allows smooth gliding motion during joint movement (Gleghorn et al., 2009; Greene et al., 2011). The structural integrity of this zone is fundamental to the protection of the deeper cartilage zones.

Beneath the superficial zone is the intermediate zone, which represents 40-60 % of the total cartilage volume. This zone contains thicker collagen fibrils, with chondrocytes being more spherical but at a lower density that in the superficial zone.

The deep zone lies furthest from the articular surface, and is demarcated from the calcified cartilage at its lower edge by the tidemark. It represents approximately 30 % of the total cartilage volume and provides the greatest resistance to compressive forces due to its high aggrecan content and the arrangement of larger diameter collagen fibrils perpendicular to the articular surface. Chondrocytes localized here are hypertrophic and have a columnar arrangement parallel to the collagen fibers and articular surface (Figure 4).

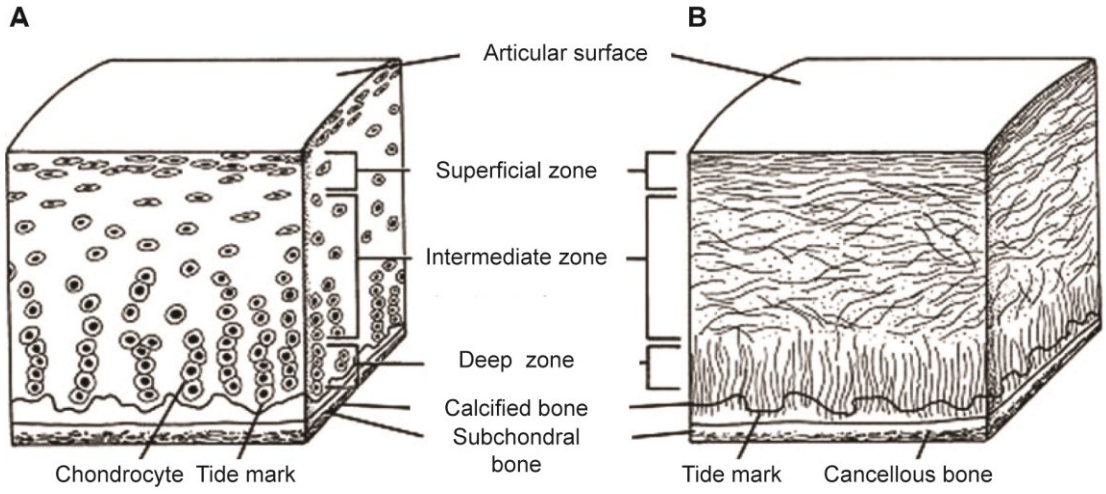


Figure 4: Articular cartilage can be functionally and structurally divided into three zones.

Cartilage can be divided into 3 zones, namely the the superficial, intermediate and deep zones. (**A**) shows the differing chondrocyte morphology in each zone.

Chondrocytes are flattened in the superficial zone, present in reduced density and spherical in the intermediate zone and columnar in the deep zone. (**B**) shows collagen fiber organization in each zone. Collagen fibers are aligned parallel to each other and the articular surface in the the superficial zone. In the intermediate zone, the collagen fibers are thicker and arranged more randomly. In the deep zone, the fibers have an increased diameter and are aligned perpendicular to the articular surface. Adapted from Buckwalter et al (Buckwalter et al., 1994).

The ECM of articular cartilage is composed of a fluid phase of 60-85 % water and a solid organic phase containing ECM proteins (see Figure 5). The ability of articular cartilage to withstand compressive forces is primarily due to the presence of aggrecan, which is contained within the type II collagen framework that gives cartilage its tensile strength. The 2 main structural components of the cartilage ECM, type II collagen and aggrecan, contribute directly to the biomechanical function of healthy cartilage. Cartilage function is therefore dependent on the maintenance of high levels of aggrecan and type II collagen (Figure 5).

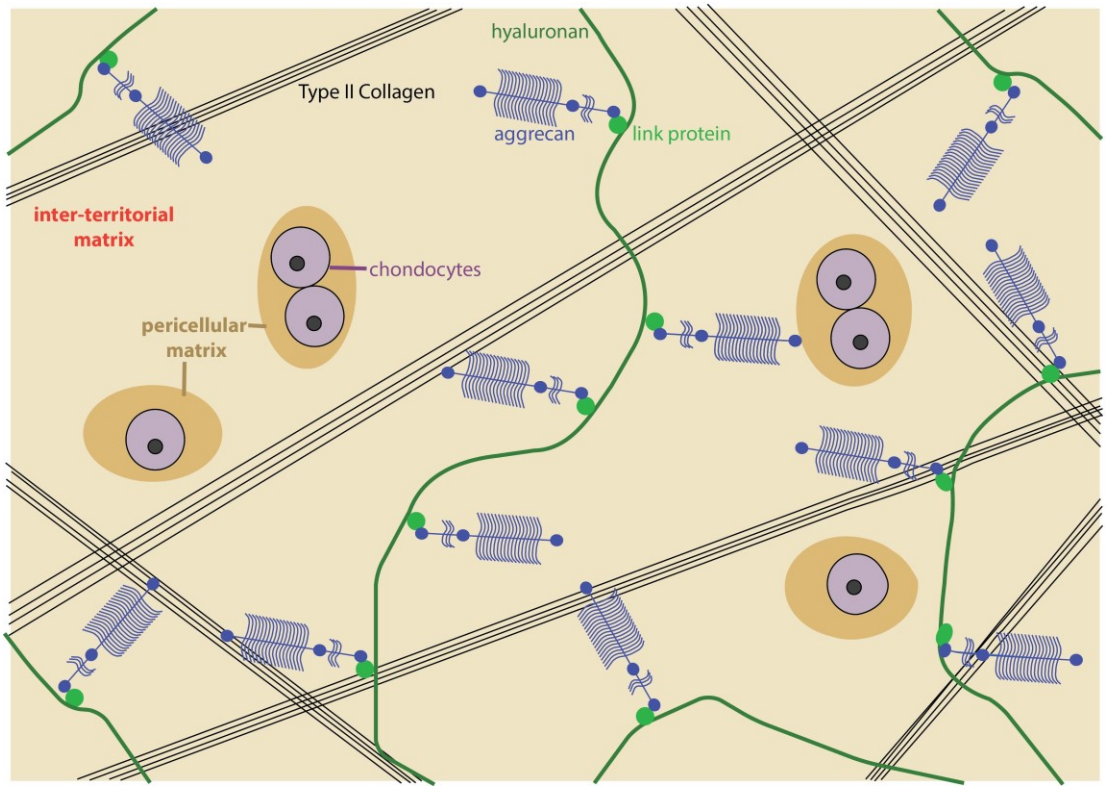


Figure 5: Primary components of the cartilage ECM that contribute to cartilage function.

The interaction between highly negatively charged cartilage proteoglycan aggrecan and type II collagen fibrils is responsible for the compressive and tensile strength of the tissue, which resists load.

The specific location of most MMPs and TIMPs in cartilage has not been identified. Most MMPs and TIMPs (TIMP-1, -2 and -4) are able to move freely in the extracellular environment. Their localisation within cartilage and their diffusion distance from chondrocytes is likely to be affected by the composition of the ECM, the chondrocyte, the density of collagen fibers, the number of actively secreting chondrocytes, the disease state of the cartilage and whether the proteins were present in complex with other components such as endogenous inhibitors or target proteinases.

TIMP-3 and some MMPS (such as MMP-13) are known to bind to the ECM through their interaction with heparan sulfate proteoglycans. They are thus concentrated in the pericellular matrix, where perlecan, the primary heparan sulfate proteoglycan in cartilage is localised. The diffusion distance of TIMP-3 and such MMPs is thus further affected by the degree of ECM sulfation and its degradation (and therefore OA stage). Additionally, binding of TIMP-3 to the ECM has been observed to increase its affinity for its target enzymes e.g. affinity for ADAMTS-5 increased by up to 1000 fold (Troeberg et al., 2014) which would consequently influence the diffusion distances of its target enzymes.

1.2.3 Degradation of cartilage in OA

With progression of OA, the structural organisation of cartilage undergoes fundamental changes, including loss of aggrecan, and consequent loss of its

function of resisting compressibility and facilitating smooth joint movement (Figure 6).

The first sign of collagen degeneration in OA is degradation and loss of the triple helical structure, resulting in fibrillation of the articular cartilage surface and increased friction during joint movement. This collagen damage is due to cleavage of collagen by collagenases (Billinghurst et al., 1997). Figure 7 shows the correlation between degradation of type II collagen and OA progression.

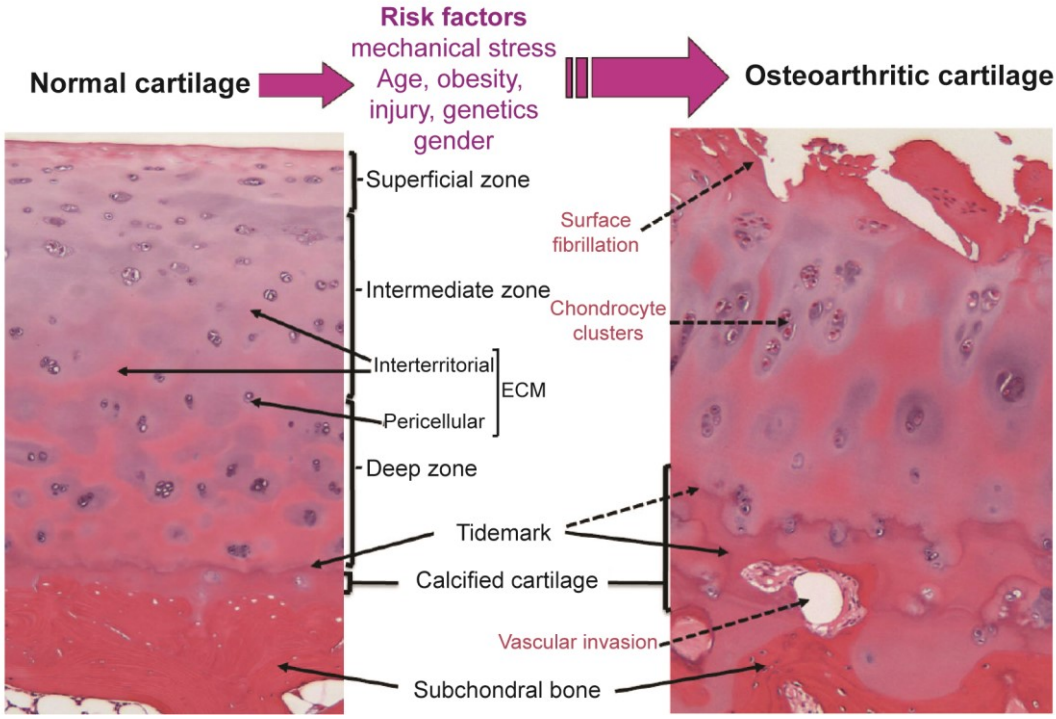


Figure 6: **Structural degradation of cartilage associated with OA.**
As OA progresses, cartilage zones become less defined, and the smooth superficial surface becomes fibrilated. Chondrocytes become hypertrophic and the overall cartilage volume decreases due to aggrecan degradation. Adapted from Goldring et al. (Goldring and Marcu, 2012).

1.2.4 Type II collagen and its degradation in OA

Collagens are the major proteins of the cartilage ECM making up 2/3 of adult articular cartilage dry weight (Eyre et al., 2006). Collagens can be classified according to their function and morphology. Type II collagen is classified as a fibril-forming collagen (Mouw et al., 2014) and is essential in the providing mechanical strength to cartilage.

Compressive forces in the human hip joint are in the region of 1-2 atmospheres for an unloaded joint, rising to 100-200 atmospheres on standing, and 40-50 atmospheres on walking (Afoke et al., 1987). The ability of cartilage to withstand these compressive forces is contingent on the tensile strength of the collagen framework. While these compressive forces are transient, they are high and therefore type II collagen is a key structural and function macromolecule in the functioning of healthy cartilage. Any decrease in collagen-derived tensile strength would result in uncontrolled swelling of the aggrecan component of the ECM, giving softer cartilage and reduced resistance to compression.

The tensile strength that type II collagen confers on cartilage peaks at 30 years of age, and deteriorates thereafter, particularly in the knee and hips joints (Kempson, 1982). It appears that the type II collagen architecture achieved in development cannot be rebuild upon injury of mature cartilage, with newly synthesized fibrils showing reduced tensile strength. It has also been demonstrated that ageing modifies collagen fibrils, leading to accumulation of non-enzymatic glycation products that increase collagen stiffness (Verzijl et al., 2002).

The first sign of collagen degeneration in OA is degradation or loss of the triple helical structure, resulting in fibrillation of the articular cartilage surface and increased friction during joint movement. This collagen damage is due to cleavage of collagen by collagenases (Billinghurst et al., 1997). Figure 7 shows the correlation between degradation of type II collagen and OA progression.

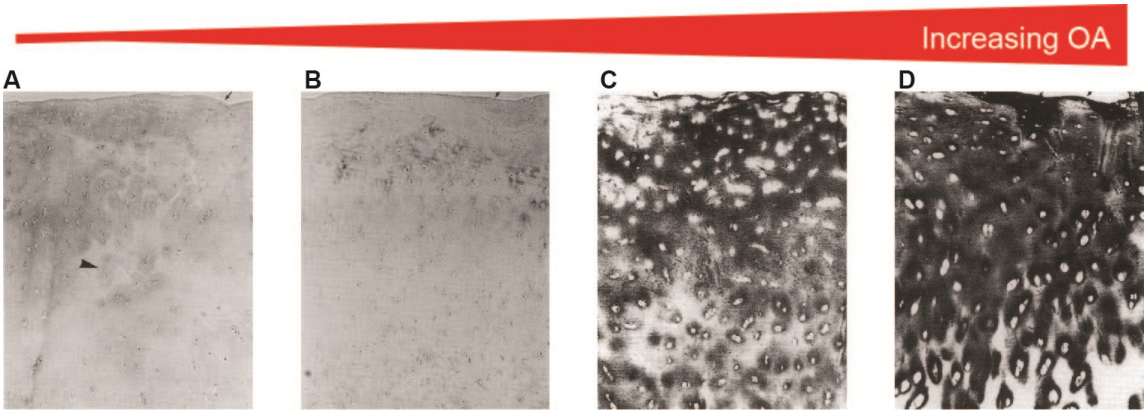


Figure 7: Increased denaturation of type II collagen fibrils with increasing OA
Hollander et al. (Hollander et al., 1995) detected degradation of type II collagen in human articular femoral condylar cartilage using an antibody recognising degraded type II collagen. The increased progression of collagen degradation was correlated with increasing severity of OA using Mankin scores. (**A**) Almost no collagen degradation is visible in early OA cartilage, with (**B**) showing increased staining in superficial zones, indicating increasing degradation with OA progression. (**C**) and (**D**) show increased staining in the intermediate and deep zones respectively, correlated with substantially increased type II collagen degradation as OA progresses.

1.2.5 Aggrecan and its degradation in OA

Aggrecan is fundamental for the maintenance of healthy cartilage, with aggrecan loss being a key early event in the pathology of OA. Aggrecan is a proteoglycan that consists of a core protein with covalently bound glycosaminoglycan (GAG) chondroitin sulfate and keratan sulfate side chains. Aggrecan forms proteoglycan aggregates in the ECM (Watanabe et al., 1998), with each aggregate composed of a central filament of hyaluronic acid (HA), to

which aggrecan molecules are non-covalently attached via interaction of their core protein with link protein (Figure 8A). Aggrecan monomers contain 3 globular domains referred to as G1, G2 and G3 (Figure 8B). The G1 domain is located at the N-terminus of the core protein and interacts with the HA filament. It contains 3 disulfide-bonded domains referred to as A, B and B', with the B domain forming the interaction with HA and the A domain interacting with link protein (Matsumoto et al., 2003; Watanabe et al., 1998). Link protein stabilises the proteoglycan aggregate, helps protect the HA from hyaluronidase or free radical degradation (Rodriguez and Roughley, 2006), and facilitates the binding of newly synthesised G1 to HA (Melching and Roughley, 1990).

The function of the G2 domain is unclear; it does not bind to the HA filament and is separated from the G1 domain by the interglobular domain (IGD), a common site for proteolysis. The G2 and G3 domains are separated by a long region containing numerous GAG attachment sites that can be further divided into 3 differing regions (Doege et al., 1991). The keratan sulfate-rich domain is located close to the G2 region and is followed by the chondroitin-rich domains CS1 and CS2. A typical aggrecan molecule can have up 100 CS side chains and usually a lower number of KS side chains. It is these highly sulfated side chains that give aggrecan its high anionic charge and therefore its ability to attract and hold water in the cartilage.

The G3 domain is located at the C-terminus of the core protein and is composed of 2 epidermal growth factor (EGF)-like repeats, 1 C-type lectin-like domain and 1 complementary regulatory protein (CRP)-like domain. The G3-domain is thought to be required for normal trafficking of aggrecan to the ECM (Zheng et al., 1998). The ability of the lectin-like domain to interact with other

ECM molecules such as tenascins may indicate a role in anchoring aggrecan in the tissue (Aspberg, 2012).

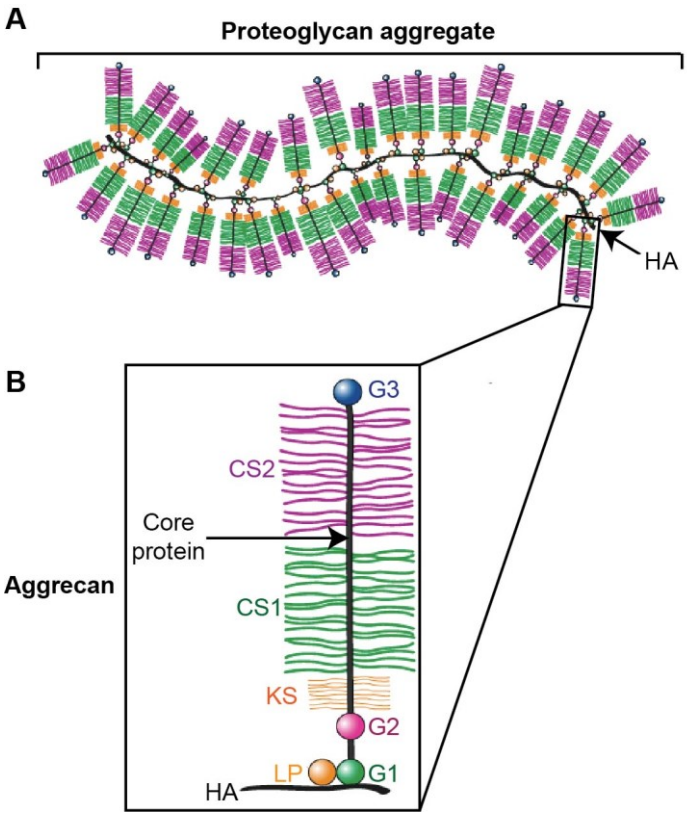


Figure 8: Structure of the aggregating proteoglycan aggrecan.
(**A**) The proteoglycan aggregate is shown, with a central hyaluronan (HA) filament with aggrecan and link protein attached to it. (**B**) The domains of the aggrecan core protein are shown, consistin of the globular regions G1, G2 and G3, separated by the interglobular domains containing keratan sulfate-rich regions (KS) and chondroitin sulfate-rich regions (CS1 and CS2). Adapted from Roughley and Mort (Roughley et al., 2014).

In the presence of water, the highly sulfated GAG side-chains swell and expand within the enclosing type II collagen fibril network. In healthy cartilage, sufficient aggrecan is present such that compression is accommodated by the

displacement of this water and on removal of loading, original swelling is restored.

1.3 Role of proteolytic enzymes in cartilage degradation

1.3.1 Historical background

Aggrecan gives cartilage its resistance to compressibility, and allows for load-bearing of the joint. Osteoarthritic degradation of aggrecan has thus long been the subject of intensive research. In a 1956 study, it was observed that injection of crude papain into rabbit ears caused the ears to lose rigidity and remain completely limp for 18 hours after injection (Thomas, 1956). If left untreated for a further 3-4 days, the ear rigidity returned but was again lost if papain was re-injected. At the time, this observation was assumed to be due to rapid depletion of chondroitin sulfate from the ECM of the ear, but this is now known to be due to aggrecan degradation. Cathepsin D was known to be expressed in ear cartilage, and the observed activity was considered to be “cathepsin D-type”, so cathepsin D was considered responsible for this ECM degradation (Sapolsky et al., 1973). Antisera raised against cathepsin D inhibited up to 90 % of cartilage and proteoglycan degradation at pH 5 (Dingle et al., 1971), supporting the hypothesis that cathepsin D was responsible for the proteoglycan degradation. OA cartilage was however shown to have neutral pH (Sapolsky et al., 1973) and cathepsin D has subsequently been shown to be completely inactive at pH 7.2 (Woessner, 1973). Cathepsin D could therefore not be responsible for cartilage proteoglycan degradation and it was realised that an alternative, unidentified enzyme with proteoglycan-

degrading activity at neutral pH must be responsible for this degradation process.

A neutral “proteoglycanase” was isolated from human OA cartilage and shown to digest proteoglycan at neutral pH. This enzyme was also shown to be metal-dependent and most likely zinc dependent (Sapolsky et al., 1976). In 1977, Ehrlich et al. demonstrated that an enzyme preparation extracted from human OA cartilage degraded proteoglycans at neutral pH and the resulting fragments contained chondroitin sulfate and keratan sulfate (Ehrlich et al., 1977). These so-called proteoglycanases were further found to degrade not only proteoglycans but also type IV collagen, laminin, fibronectin and procollagen (Galloway et al., 1983). Matrix metalloproteinases (MMPs) were considered likely candidates. MMP-3 isolated from human articular cartilage was subsequently found to cleave aggrecan between the GI and G2 N-terminal globular domains at DIPEN^{341} ~ ^{342}FFGVG (Fosang et al., 1991). Cleavage at this site and others was also observed for other MMPs including MMP-1, -2, -7, -8 -9 and -13 (Fosang et al., 1996; Fosang et al., 1993; Fosang et al., 1992), strengthening the hypotheses that MMPs were the main aggrecan-degrading enzymes in OA. MMPs are discussed in more detail in Section 1.3.2.

However, purified synovial fluid taken from OA patients was found to contain 2 major aggrecan core protein populations both with the same N-terminal sequence of ^{374}ARGSV. This differed from the previously observed neo-epitopes of DIPEN^{341}~^{342}FFGVG cleavage, and resulted from cleavage of the aggrecan core protein at the NITEGE^{373}~^{374}ARGSV site located between GI and G2 (Sandy et al., 1992). The ^{374}ARGSV N-terminal sequence had also been observed in interleukin-1 (IL-1) stimulated bovine cartilage cultures

(Sandy et al., 1991). The release of such fragments was not inhibited by the endogenous MMP inhibitors TIMP-1 or TIMP-2 (Hughes et al., 1998), demonstrating that cleavage at this site was independent of MMP activity. The enzymes responsible for this cleavage were termed aggrecanases. These enzymes are discussed in more detail in Section 1.3.3.

1.3.2 Matrix metalloproteinases (MMPs)

The first MMP was discovered in 1962 when skin taken from the resorbing tail of a metamorphosing tadpole was cultured on a collagen gel, and an enzyme able to degrade triple helical collagen at neutral pH was observed (Gross and Lapiere, 1962). This enzyme is now known as MMP-1, subsequent to this discovery, a rapid expansion of the MMP field followed, with 23 vertebrate MMPs identified. The criteria for assignment of proteinases to this family are sequence homology with MMP-1, presence of a cysteine switch motif (PRCGXPD) in the propeptide and a zinc-binding motif (HEXXHXXGXXH) in the catalytic domain (Visse and Nagase, 2003). MMPs are further classified according to their substrate specificity, sequence similarity and domain organisation. These classification groups include collagenases, gelatinases, stromelysins, matrilysins, membrane-type MMPs and other MMPs. The domain structure for MMP-1 is shared with MMP-3 and -13 (Figure 9) (Visse and Nagase, 2003). The domain structure consists of a signal peptide, followed by a propeptide domain containing approximately 80 residues, a catalytic domain of approximately 170 residues, a linker of varying lengths and a hemopexin domain of approximately 200 residues (Nagase et al., 2006).

1.3.2.1 Collagenases

MMP-1 and MMP-13 are termed collagenases as their key functional characteristic is the ability to cleave triple helical collagen type I, II and III at a specific site ¾ from the N-terminus. They however also cleave many other collagenous and non-collagenous molecules such as collagen X and non-collagenous substrates including the ECM molecules fibronectin and aggrecan.

MMP-1 also cleaves substrates not susceptible to MMP-13 including collagen type VII, VIII and XI and ECM molecules vitronectin, tenascin, link protein and versican. MMP-1 also cleaves non-ECM substrates such as ovastatin and proMMP-1, proMMP-2 and proMMP-3 zymogens. (Visse and Nagase, 2003). It has also been demonstrated that MMP-1 degrades IL-1β, but not IL-1α. IL-1β stimulates the expression of MMPs by connective tissue cells, but MMP-1 in turn negatively regulates the activity of IL-1β by mediating its degradation (Ito et al., 1996).

MMP-13 additionally cleaves collagen type VI, IX and X, casein, perlecan and proMMP-9 (Visse and Nagase, 2003). MMP-13 but not MMP-1 cleaves osteonectin thereby increasing its affinity for collagens (Sasaki et al., 1997)

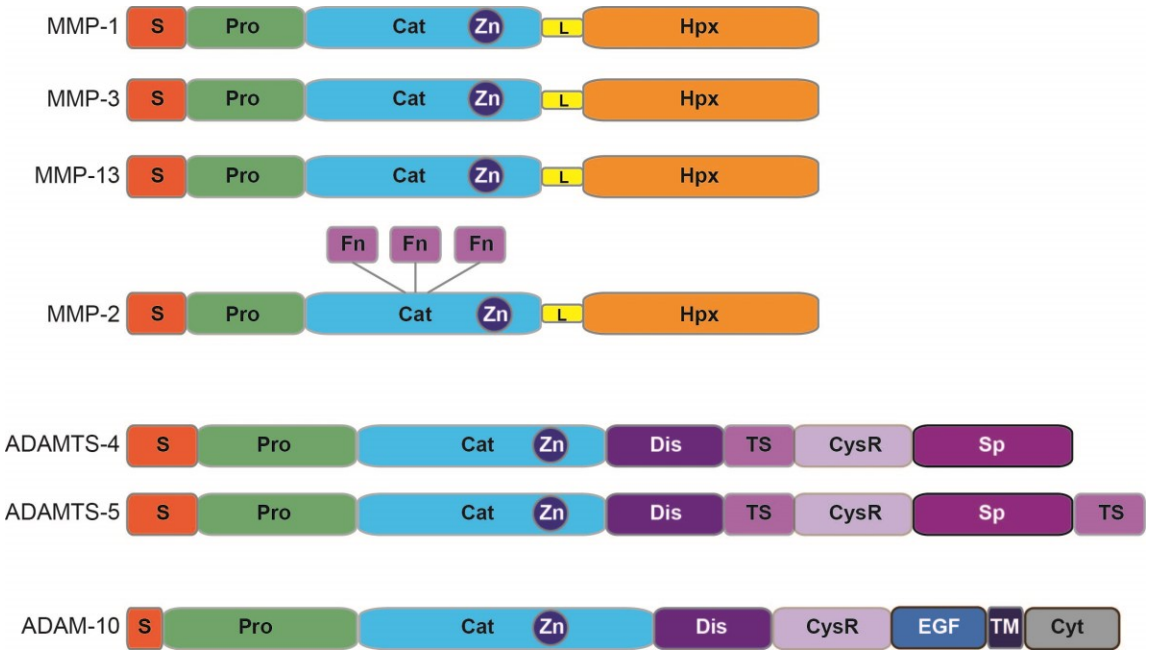


Figure 9: Domain structure of matrix metalloproteinases.
ADAM and ADAMTS domain structure includes an N-terminal signal peptide (S), followed by a propeptide (Pro), catalytic domain (Cat), zinc-containing active site (Zn), disintegrin-like domain (Dis), thrombospondin domain (TS), cysteine-rich domain (CysR), epidermal growth factor-like domain (EGF), with C-terminal transmembrane (TM) and cytoplasmic domains (Cyt). Adapted from Visse and Nagase (2003).

1.3.2.2 Gelatinases

This group consists of MMP-2 and MMP-9, also known as gelatinase A and B respectively. Both enzymes contain 3 repeats of a type 2 fibronectin domain inserted in their catalytic domains (see Figure 9). These type 2 fibronectin domains bind to gelatin, collagens and laminin. Both MMP-2 and MMP-9 cleave the ECM molecules gelatin, vitronectin, aggrecan, link protein, SPARC, myelin basic protein, laminin and versican. Non-ECM substrates include IL1-β and proTNFα.

MMP-2 specifically cleaves latent TGF-β and proMMP-9 and proMMP-13 zymogens, latent tissue growth factor β (TGFβ) (Yu and Stamenkovic, 2000) and fibroblast growth factor receptor 1 (FGFR1). MMP-9-specific substrates

include proTGFβ2 (Yu and Stamenkovic, 2000), IL-2Rα (Sheu et al., 2001), angiotensin I and angiotensin II (Diekmann and Tschesche, 1994).

1.3.2.3 Stromelysins

MMP-3 and MMP-10 are also known as stromelysin 1 and stromelysin 2 respectively. While both MMP-3 and MMP-10 cleave gelatin, elastin, fibronectin, aggrecan, link protein and proMMP-1, proMMP-7, proMMP-8 and proMMP-9 zymogens (Nakamura et al., 1998; Visse and Nagase, 2003), MMP-3 has the higher proteolytic efficiency. Additionally MMP-3 also cleaves proMMP-3, and proMMP-13, E-cadherin (Lochter et al., 1997; Noe et al., 2001), u-PA (Ugwu et al., 1998) and PAI-1 (Lijnen et al., 2000).

1.3.2.4 MMPs in OA

As stated in Section 1.2.4, type II collagen is the main collagen present in cartilage and it provides cartilage with tensile strength. In vitro studies have shown that in bovine and human cartilage explants, collagen degradation occurs only after aggrecan has been degraded (Pratta et al., 2003). Collagen degradation is mainly due to MMPs, in particular MMP-13, which are activated by serine proteinases (Milner et al., 2001). Of the collagenases (MMP-1, -8, -13 and -18), expression of MMP-13 is most increased in OA (Billinghurst et al., 1997) and MMP-13 is considered to be the main collagenase involved in OA. This is supported by the observation that conditional expression of MMP-13 induces OA in mice (Neuhold et al., 2001) while MMP-13 deficient mice are protected in a surgical mouse model (Little et al., 2009). Work in our laboratory has also shown that MMP-1 also cleaves type II collagen (R. Visse, Y.Tominaga, Wang, H.Nagase.). However, due to substantial differences

between murine and human forms of the enzyme, the involvement of MMP-1 in OA cannot be studied in a mouse model (Balbin et al., 2001).

1.3.3 ADAMTSs

The first aggrecanase was purified from IL-1-stimulated bovine nasal cartilage and called aggrecanase 1 or A Disintegrin And a Metalloproteinase with Thrombospondin motifs 4 (ADAMTS-4) due to its sequence homology with ADAMTS-1 (Tortorella et al., 1999). This was quickly followed by the identification of another aggrecanase homologous to ADAMTS-1, which was cloned from bovine cartilage and called aggrecanase-2 or ADAMTS-5. The ADAMTS enzymes are zinc-dependent metalloproteinases of the metzincin family (Fosang et al., 2008) and are related to MMPs and ADAMs (A Disintegrin And Metalloproteinase).

ADAMTS domain structure consists of a signal peptide followed by a propeptide, a catalytic domain with a zinc-binding motif, a disintegrin-like domain, a central thombospondin domain, a cysteine rich region and a spacer domain (Figure 9) (Stanton et al., 2011b). Of the ADAMTS family, ADAMTS-4 is the only family member to contain only one thrombospondin domain (Stanton et al., 2011b) ADAMTS-5 has a similar domain structure to that of ADAMTS-4 but has a second thombospondin motif at its C-terminus (Figure 9). In vitro studies have shown that ADAMTS-5 is the most active aggrecanase (Gendron et al., 2007; Stanton et al., 2011a).

1.3.3.1 ADAMTSs in OA

Studies comparing arthritis in Wild-type and *Adamts5*$^{-/-}$ mice revealed that ADAMTS-5 is the principal aggrecan-degrading enzyme in mice, with *Adamts5*$^{-/-}$ mice developing less severe cartilage damage in both surgical and antigen-

induced models of OA (Glasson et al., 2005; Stanton et al., 2005). Both studies demonstrated that ablation of ADAMTS-5 blocked cleavage of aggrecan in the interglobular domain and substantially reduced aggrecan loss. ADAMTS-5-deficient mouse chondrocytes incubated with oncostatin M (OSM) were shown to have substantially increased expression of ADAMTS-4 mRNA, however no accompanying increase in aggrecanolysis was observed (Rogerson et al., 2010). ADAMTS-1 is expressed in articular and growth plate cartilage and has been shown to cleave aggrecan at physiologically relevant sites. However, *Adamts1*$^{-/-}$ mice were not protected from accelerated aggrecanolysis in an inflammatory model of arthritis (Little et al., 2005). This further supported the hypothesis that ADAMTS-5 is the primary aggrecan-degrading enzyme in murine cartilage.

The identity of the primary aggrecan-degrading enzyme in human cartilage has been controversial (Fosang et al., 2008). By RT-PCR, Naito et al. found that ADAMTS-4 was predominantly expressed in human OA cartilage while ADAMTS-5 was constitutively expressed in both OA and normal cartilage. They immunolocalised ADAMTS-4 to chondrocytes in the aggrecan-depleted areas of the OA cartilage, with this staining strongly correlating with high Mankin scores (Naito et al., 2007), indicating that ADAMTS-4 is the main aggrecanase in human OA.

In 2004, the Nagase group reported that the non-catalytic domains of human ADAMTS-4 influenced both its interaction with the ECM and its proteolytic abilities (Kashiwagi et al., 2004). They then published a study showing that these domains have similar effects on human ADAMTS-5 (Gendron et al., 2007). While the ADAMTS-4 spacer domain was essential for

matrix localisation, the cysteine-rich domain influenced ADAMTS-5 localisation. In keeping with other ADAMTS family members, very little proteolytic activity was detected with the ADAMTS-5 catalytic domain alone. The sequential inclusion of the carboxyl-terminal domains increased ADAMTS-4 and -5 activity against aggrecan. Both enzymes demonstrated optimal activity over a broad range of pHs from 7.0 to 9.5 demonstrating a broad activity at pH 7.0-9.5. Under physiological conditions, human ADAMTS-5 had a reported 1,000-fold higher aggrecanase activity than ADAMTS-4 (Gendron et al., 2007). This suggested that ADAMTS-5 was the major aggrecanase in human cartilage in addition to being the primary aggrecan-degrading enzyme in mice (Glasson et al., 2005; Stanton et al., 2005). In a recent study, Ismail et al. (2015) identified ADAMTS-5 as a major aggrecanase in human chondrocytes in response to IL-1 treatment and showed that the TRAF-6/TAK-1/MKK-4/JNK-2 signaling axis mediated this IL-1-induced aggrecanolysis.

The expression of ADAMTS-4 and -5 in human cartilage has been extensively studied both in normal and OA cartilage, with contradictory findings reported, as reviewed by Fosang (2010). Most studies show that ADAMTS-4 expression can be induced by pro-inflammatory cytokines such as IL-1β or TNFα, while ADAMTS-5 is constitutively expressed (Bau et al., 2002; Naito et al., 2007; Song et al., 2007). Variation in the findings reported is thought to be due to variation in species, age, anatomical location, sample collection and processing, as well as differing definitions of early and late OA.

However, another study suggested that both ADAMTS-4 and ADAMTS-5 are involved in cartilage degradation in human OA (Song et al., 2007). Following siRNA knockdown of ADAMTS-4 and ADAMTS-5, human normal

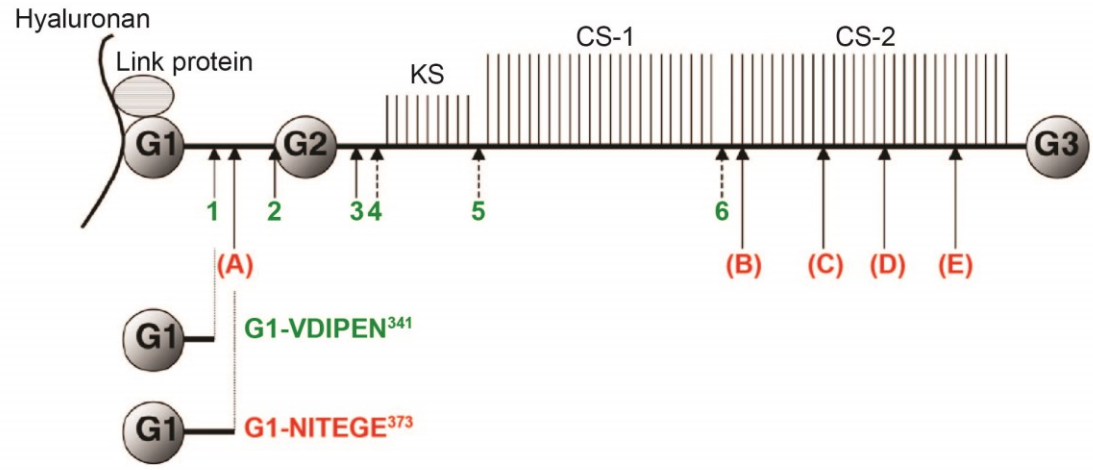
cartilage explants and chondrocytes were treated with or without TNF-α or OSM and GAG release and aggrecanase neo-epitope formation quantified. In this study it was found that both ADAMTS-4 and ADAMTS-5 contribute to cartilage degradation (Song et al., 2007).

1.3.3.2 MMP and ADAMTS cleavage of aggrecan

Subsequent to the identification of the “aggrecanase” cleavage site of NITEGE^{373}~^{374}ARGSV (Sandy et al., 1992) and “MMP” site DIPEN^{341}~^{342}FFGVG, aggrecan cleavage has been well studied. Figure 10 shows additional aggrecanase and MMP cleavage sites found within the IGD and at multiple sites in the chondroitin sulfate-rich region (Nagase and Kashiwagi, 2003). These sites include GELE^{1480}~^{1481}GRGD (Vankemmelbeke et al., 2001), KEEE^{1667}~^{1668}GLGS (Tortorella et al., 2002), TAQE^{1771}~^{1772}AGEG and VSQE^{1871}~^{1872}LGQR (Tortorella et al., 2000). These sites are more readily cleaved than NITEGE^{373}~^{374}ARGSV (Tortorella et al., 2002; Tortorella et al., 2000), for reasons that are not clear, but may include increased accessibility.

While both MMPs and ADAMTSs can cleave aggrecan in vitro, it is now generally believed that ADAMTSs are responsible for the “pathological” cleavage of aggrecan in the IGD in OA, since this “aggrecanase” cleavage results in release of the majority of the aggrecan molecule from the cartilage matrix. MMPs are considered to participate in normal physiological turnover of aggrecan (Sandy, 2006).

A



B

(A)	RNITEGE^{373} ~ ^{374}ARGSVIL	1	FVDIPEN^{341} ~ ^{342}FFGVGGE
(B)	STASELE^{1545} ~ ^{1546}GRGTIGI	2	TAFTSED^{441} ~ ^{442}LVVQVTA
(C)	TTFKEEE^{1714} ~ ^{1715}GLGSVEI	3	HAFCFRG^{666} ~ ^{667}ISAVPSP
(D)	QAPTAQE^{1819} ~ ^{1820}AGEGPSG	4	not determined
(E)	EPTISQE^{1919} ~ ^{1920}LGQRPPV	5	not determined
		6	not determined

Figure 10: Cleavage sites on human aggrecan by aggrecanases and MMPs. (**A**) Aggrecan has 3 globular domains (G1, G2 and G3) and is connected to hyaluronan by link protein. A keratan sulfate-rich region and 2 chondroitin sulfate-rich regions are located in the interglobular domain between G2 and G3. Sites cleaved by aggrecanases are shown in red (A)-(E) and sites cleaved by MMPs are shown in green (1-6). (**B**) Cleavage sites for aggrecanase and MMP cleavage of aggrecan are listed with resulting N-and C-terminal neoepitopes. Adapted from Nagase and Kashiwagi (2003).

1.4 TIMPs

1.4.1 Background

Tissue Inhibitors of Metalloproteinases (TIMPs) are endogenous inhibitors of MMPs, ADAMTSs and ADAMs, with the first TIMP discovered in the 1970s. In 1975, Bauuer et al. (Bauer et al., 1975) determined that an

inhibitor of collagenase was present in the medium of cultured human skin fibroblasts and that this inhibitor appeared to be produced by the cells. It was demonstrated that this inhibitor abolished over 90 % of collagenase activity while displaying no activity against trypsin. A second study published later in the same year found that a single inhibitor isolated from human serum inhibited 4 human collagenases from skin, rheumatoid synovium, gastric mucosa and granulocytes (Woolley et al., 1975). A further study in 1976 demonstrated that a collagenase inhibitor isolated from human cartilage and bovine cartilage and aorta was an effective inhibitor of human skin collagenase (Kuettner et al., 1976). Based on their findings, Kuettner et al. went on to suggest that collagen turnover in cartilage might be under “a strict control via an enzyme-inhibitor-complex” and that a deficiency of inhibitor may be related to cartilage collagen degradation in disease. Collagenase inhibitory activity was detected in skin, bone, and uterine cultures and it was subsequently proposed that all connective tissues synthesize collagenase inhibitors in order to control local enzyme activity (Murphy et al., 1977). A later study showed that the purified inhibitor inhibited collagenase activity with 1:1 stoichiometery (Welgus et al., 1979) and that the inhibitor ranged in size from 25-31kDa (Vater et al., 1979; Welgus et al., 1979). This collagenase inhibitor was later purified from rabbit bone and found to inhibit multiple metalloproteinases, including collagenase, gelatinase, proteoglycanase, human leukocyte collagenase and human leukocyte gelatinase, and was therefore termed Tissue Inhibitor of Metalloproteinase (Cawston et al., 1981).

It is now known that there are 4 human TIMPs, namely TIMP-1, -2, -3 and -4 and all have been extensively characterized and shown to possess common

structural features. Mammalian TIMPs contain an N-terminal domain consisting of approximately 125 residues and a C-terminal domain of approximately 65 residues. Each domain contains 6 conserved cysteine residues, which form 3 disulfide bridges per domain, stabilising the domain structure (Murphy et al., 1991; Williamson et al., 1990). Recombinant forms of TIMP N-terminal domains have stable native structures and are fully active inhibitors of MMPs (Murphy et al., 1991).

Human TIMPs share approximately 40 % sequence identity, with TIMP-2 and TIMP-4 being the most similar with 50 % sequence identity (Brew and Nagase, 2010). TIMP-3 has 38 % sequence identity with TIMP-2 and 30 % identity with TIMP-1 (Pavloff et al., 1992). The first structure reported for a TIMP was a model based on a multidimensional NMR study of the N-terminal domain of TIMP-2 (Williamson et al., 1994). This model proved to be in good agreement with structures later determined by higher resolution X-ray crystallography, including full-length TIMP-1 in complex with MMP-3 (Gomis-Ruth et al., 1997), TIMP-2 in complex with MT1-MMP (Fernandez-Catalan et al., 1998), TIMP-2 (Tuuttila et al., 1998) and N-TIMP-3 in complex with TACE (Wisniewska et al., 2008).

The X-ray structure of the TIMP-1-MMP-3 complex shows TIMP-1 to have a wedge-shaped structure (Gomis-Ruth et al., 1997), with the wedge slotting into the active-site cleft of the MMP-3 catalytic domain such that the conserved N-terminal C^1 residue of the TIMP coordinates the catalytic Zn^{2+} of the MMP. The X-ray crystal structure for MT1-MMP-TIMP-2 complex was also generated, with TIMP-2 described as being “elongated wedge-shaped” with the wedge slotting into the active site of MT1-MMP (Fernandez-Catalan et al., 1998). 60-

75 % of interactions between a TIMP and a metalloproteinase are facilitated by a ridge formed by the 5 N-terminal residues (C^1-T-C-V-P^5 in TIMP-1) and the loop residues (M^{66}-E-S-V-C^{70} in TIMP-1), and stabilized by a disulfide bond between C^1 and C^{70}), as shown in Figure 11.

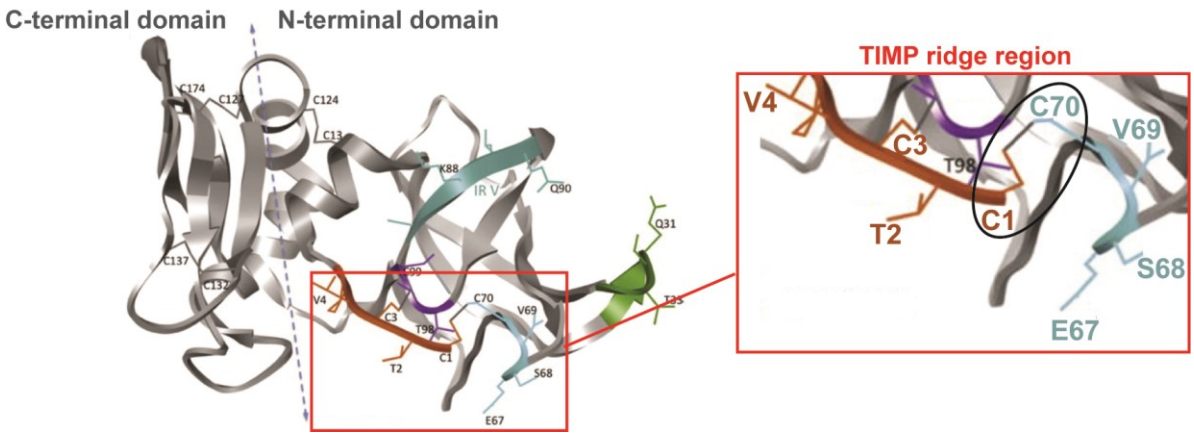


Figure 11: TIMP-1 interaction with metalloproteinases.
Ribbon structure of TIMP-1 showing the ridge region that interacts with MMPs. The ridge is formed by interaction of conserved N-terminal residues C^1-T- C-V-P^5 (shown in brown) with residues of the loop M^{66}-E-S-V-C^{70} (shown in blue), and is stabilised by formation of a disulfide bond between C^1 and C^{70}. Adapted from Brew and Nagase (Brew and Nagase, 2010).

Despite their similarities, differences do exist between the 4 TIMPS in their inhibitory range, tissues in which they are expressed and localization within tissues. TIMP-3 is often quoted as being unique amongst TIMPs in that it binds to the ECM whilst all other TIMPs are soluble, its inhibitory range includes ADAMs and ADAMTSs, and it is the cause of Sorsby's Fundus Dystrophy. Here, each of the TIMPs is discussed individually, starting with an overview of the soluble TIMPs (TIMPs -1, -2 and -4). As TIMP-3 is the subject of this study, it will be discussed in more detail in Section 1.4.5 to Section 1.4.7.

1.4.2 TIMP-1

TIMP-1 has a more restricted inhibitory range than the other TIMPs, as it does not inhibit MT1-MMP and has a relatively low affinity for MT-MMPs in general (Will et al., 1996). However, it does have a higher affinity for MMP-3 and MMP-7 than do TIMP-2 and TIMP-3 (Hamze et al., 2007) and it also inhibits ADAM-10 activity (Amour et al., 2000).

TIMP-1 has been shown to promote cell growth in keratinocytes and fibroblasts (Bertaux et al., 1991; Hayakawa et al., 1992), but it has also been shown to suppress growth in human breast epithelial cells by inducing cell cycle arrest at G_1 (Taube et al., 2006).

TIMP-1 also has anti-apoptotic effects on various cell types, including human breast epithelial cells and activated hepatic stellate cells (Liu et al., 2003; Murphy et al., 2002), which has led to TIMP-1 serum levels and expression in cancerous tissues being associated with poor patient prognosis in many cancer types (Nakopoulou et al., 2002).

TIMP-1 is expressed in the breast and female reproductive system, in particular in the cervix, uterine tissue and endometrium. It is also expressed in the gastro-intestinal tract, including in salivary glands, stomach, duodenum and pancreas.

TIMP-1 null mice exhibit significant learning and memory impairment which was not thought to be related to direct action of TIMP-1 on memory, but linked to the effect of abnormal ECM turnover on neuron development (Chaillan et al., 2006; Jourquin et al., 2005). Other TIMP-1 null mice studies have identified alterations in reproduction and steroidogenesis, implicating a role for TIMP-1 in regulating the murine reproductive cycle (Nothnick, 2001).

TIMP-1 has also been shown to be a regulator of heart tissue remodeling, with TIMP-1 null mice displaying exacerbated left ventricular remodeling following myocardial infarction (Creemers et al., 2003). TIMP-1 general characteristics and the TIMP-1 null mouse phenotypes are summarized in Table 2 and Table 3 respectively.

1.4.3 TIMP-2

It has been reported that TIMP-2 has potent growth-promoting activity in a wide range of cells including mouse embryo fibroblasts, mouse leukemia cells, human erythro-leukemia cells, human gingival fibroblasts, normal human skin fibroblasts and epithelial keratinocytes (Hayakawa et al., 1994; Hayakawa et al., 1992). However a later study reported that while TIMP-2 promoted the growth of lung adenocarcinoma cells, human melanoma cells, and a Burkitt's lymphoma cell line, this response had not been observed for normal human colon and lung fibroblasts (Nemeth et al., 1996). It was then further demonstrated that TIMP-2 promoted cell growth only when cells were treated with insulin in addition to TIMP-2 and in fact, TIMP-2 exhibited an inhibitory effect on cell growth in the absence of insulin (Nemeth et al., 1996).

However, TIMP-2 suppresses growth factor-mediated cell proliferation through interaction with $\alpha_3\beta_1$ integrin (Seo et al., 2008). All TIMPs exhibit anti-angiogenic activity, but only TIMP-2 and TIMP-3 exhibit this activity independent of their MMP inhibitory activity.

TIMP-2 can mediate the activation of pro-MMP-2 by interacting with the hemopexin domain of pro-MMP-2 and facilitating complex formation with cell surface-bound MT1-MMP. This complex homodimerise with a second cell surface MT1-MMP, which cleaves the pro-domain of pro-MMP-2 (Strongin et

al., 1995). TIMP-2-null mice exhibit phenotypes associated with the central nervous system. They display symptoms of altered motor dysfunction due to peripheral and central nerve defects resulting from abnormal ECM turnover (Jaworski et al., 2006) and reduced neuronal differentiation.

TIMP-2 general characteristics and the TIMP-2 null mouse phenotype are summarized in Table 2 and Table 3 respectively.

1.4.4 TIMP-4

TIMP-4 is expressed primarily in the heart, with lower levels of expression in the kidney, placenta, colon and testes. No transcripts have been detected in the liver, brain, lung, thymus and spleen. This expression pattern suggests that TIMP-4 may function in a tissue-specific manner in ECM homeostasis (Greene et al., 1996). N-TIMP-4 but not full length TIMP-4 inhibits ADAM-17 activity (Lee et al., 2005) and it has been reported that TIMP-4 also inhibits ADAM-28 activity (Mochizuki et al., 2004).

Timp4-null mice display various cardiac defects, reflecting the expression profile of this inhibitor (Koskivirta et al., 2010). The general characteristics of TIMP-4 are summarized in Table 2.

Table 2: Summary of general TIMP characteristics.

	TIMP-1	TIMP-2	TIMP-3	TIMP-4
Expression	Most tissues	Most tissues	Most tissues	Heart, kidney, Brain
MMP inhibition	Weak for MMP-14, -16, -19 and -24	All	All	Most
Adamalysin inhibition	ADAM-10	ADAM-12	ADAM-10, -12, -17, -28, -33 ADAMTS-1,-2 (weak), -4, -5	ADAM-17, -28, -33 (weak)
ECM bound	No	No	Yes	No

Table 3: Summary of mouse phenotypes resulting from deletion of TIMP genes.

Mouse phenotype resulting from deletion of TIMP genes	
***Timp1*$^{-/-}$**	• Learning and memory impairment • Exacerbated left ventricular remodeling after myocardial infarction • Increased MMP-9 activity in aveoli giving enhanced acute lung injury after bleomycin exposure • Hyperphagia and obesity in female mice
***Timp2*$^{-/-}$**	• Impaired pro-MMP-2 activation by MMP-14 • Motor dysfunction • Delayed neuronal differentiation
***Timp3*$^{-/-}$**	• Air space enlargement in lungs • Enhanced apoptosis during mammary gland involution • Increased spontaneous OA • Increased inflammation and reduced tissue repair in liver regeneration model • Dilated cardiomyopathy • Tumour invasion • Emphysema
***Timp4*$^{-/-}$**	• Impaired cardiac function with age • Increased susceptibility to myocardial infarction

1.4.5 TIMP-3

TIMP-3 has the broadest inhibition profile of the mammalian TIMPs and *Timp3*$^{-/-}$ knockout has most profound phenotype of the *Timp* knockouts. *Timp3*-null mice develop spontaneous air space enlargement in the lungs, which is observed as early as 2 weeks after birth and increases with age. This space enlargement is due to an increase in MMP activity, leading to ECM degradation

and ultimately cell death (Leco et al., 2001). It has also been shown that *Timp3*-null mice have increased spontaneous cartilage degradation with aging (Sahebjam et al., 2007), due to increased ECM degradation by MMPs and ADAMTSs, in particular ADAMTS-5 and MMP-13. TIMP-3 deficiency also leads to dilated cardiomyopathy due to excessive matrix modeling by MMPs, in particular MMP-9 (Fedak et al., 2004).

TIMP-3 inhibits the activity of ADAM-17, or TNFα converting enzyme (TACE) (Mohammed et al., 2004), and so plays a role in TNFα release (Brennan et al., 1995; Malik and Balkwill, 1988). *Timp3*-null animals exhibit an increase in ADAM17 activity that in turn causes an increase in release of TNF levels and activation of TNF signaling in the liver. This leads to increased inflammation and reduced tissue repair in a liver regeneration model (Mohammed et al., 2004), thus demonstrating that TIMP-3 is a central regulator of inflammation and tissue injury.

An imbalance in TIMP-3 expression has been linked to cardiovascular disease, tumour invasion and metastasis, and emphysema (Brew and Nagase, 2010). Various mutations in TIMP-3 cause Sorsby's fundus dystrophy, as inherited form of macular dystrophy (Langton et al., 2000). Reduced TIMP-3 expression has been linked to colon cancer by epigenetic mechanisms including MicroRNA-191 and higher aberrant methylation of the TIMP-3 promoter (Guan et al., 2013; Qin et al., 2014). Also a frameshift mutation has been linked to colon cancer, this frameshift mutation resulted in gain or loss of a single cytosine residue giving rise either to a premature stop at codon 180 or in the case of deletion the additional of 13 residues before temination (Brueckl et al., 2005).

Less TIMP-3 is present in degraded human OA cartilage compared to normal cartilage (Morris et al., 2010). Addition of the N-terminal inhibitory domain of TIMP-3 (N-TIMP-3) blocks aggrecan degradation in articular cartilage explants stimulated with IL-1α or retinoic acid (Gendron et al., 2003). Similarly, intra-articular injection of N-terminal or full-length TIMP-3 inhibited cartilage degradation in a rat meniscal tear model (Black et al., 2007). These studies indicate that TIMP-3 has the capacity to block cartilage degradation and are the foundation of the present study, which aims to generate a TIMP-3 mutant with improved chondroprotective activity.

In addition to inhibiting MMPs, TIMP-3 also inhibits the activity of ADAMs (Amour et al., 2000; Amour et al., 1998) and ADAMTSs (Hashimoto et al., 2001; Kashiwagi et al., 2001; Wang et al., 2006). As described in Section 1.3, the ADAMs enzyme family of membrane-bound enzymes are often referred to as “sheddases” due to their ability to cleave the extracellular regions of transmembrane proteins, thereby releasing soluble ectodomains. ADAM-17 is such an enzyme and was the first non-MMP metalloproteinase shown to be inhibited by TIMP-3. ADAM-17 catalyses the release of soluble TNF-α from the cell membrane and also the shedding of transforming growth factor α (TGF-α) (Black, 2002). The ability to inhibit ADAM-17 confers on TIMP-3 an important role in regulating the inflammatory process in inflammation-driven diseases, including rheumatoid arthritis and cancer (Murphy and Nagase, 2008; Rocks et al., 2008). Inhibition of ADAM-17 by TIMP-3 differs from TIMP-3 inhibition of MMPs in that it shows cooperative binding (Wei et al., 2005). TIMP-3 is also an effective inhibitor of ADAM-10, 12, 28 and -33.

TIMP-3 is also a potent inhibitor of ADAMTSs, including ADAMTS-4 and -5. It has been observed that TIMP-3 inhibition of ADAMTS-4 is increased 4-fold by aggrecan and sulfated GAGs (Wayne et al., 2007). They found that interaction of chondroitin-6-sulfate with the thrombospondin and spacer domains of ADAMTS-4 mediated this interaction. The resulting chondroitin-6-sulfate-ADAMTS-4 complex had improved TIMP-3 binding affinity relative to ADAMTS-4 alone.

While N-TIMP-3 is a relatively weak inhibitor of ADAMTS-2, its affinity was observed to increase in the presence of heparin (from a K_i of 602 nM to 160 nM) (Wang et al., 2006). However in 2008, calcium pentosan polysulfate (CaPPS), a calcium salt of chemically sulfated beechwood xylosan, was shown to increase TIMP-3 affinity for ADAMTS-4 and ADAMTS-5 more than 100-fold, while having no effect on TIMP-3 affinity for MMP-1, -2 and -3. (Troeberg et al., 2008). This effect was observed only for ADAMTS-4 containing the spacer domain and ADAMTS-5 containing the cysteine-rich domain. Later studies by the same group revealed that the mechanism of this affinity increase was via formation of an electrostatically-driven trimolecular complex (Troeberg et al., 2012). It was also shown that the increase in affinity correlated with the ability of both ADAMTS-5 and TIMP-3 to bind to CaPPS. An ECM-soluble TIMP-3 mutant (TIMP-3 K26/27/30/76E + R163/K165Q), which retained its ADAMTS-5 inhibitory activity, showed greatly reduced CaPPS-binding relative to Wild-type TIMP-3, and as such showed no increase in ADAMTS-5 affinity. This study identified that the inhibitory activity of N-TIMP-3 was increased by the same magnitude as that of full length TIMP-3 by CaPPS, indicating that the minimal complex-forming interface is present on the N-terminal domain of TIMP-3. The

complex was determined to be electrostatic in nature, as NaCl concentrations in excess of 400 mM prevented complex formation. The optimum CaPPS chain length was determined to be 11 saccharide units (Troeberg et al., 2012).

1.4.5.2 Extracellular matrix binding of TIMP-3

It has long been known that TIMP-3 binds to the ECM, with this being one of the fundamental characteristics of the protein upon initial identification (Pavloff et al., 1992). This binding was subsequently shown to be mediated by ECM GAGs (Yu et al., 2000), but the exact molecular basis of the binding remained unknown. In 2007, Lee et al. successfully identified the ECM binding-motif of TIMP-3 (Lee et al., 2007). N-TIMP-3 had been shown not to bind to the ECM, so it appeared that ECM binding motif of TIMP-3 must be confined to the C-terminal domain. However, following mutagenesis and systematic exchange of mutated TIMP domains, the ECM binding motif of TIMP-3 was identified as being comprised of residues from both the N- and C-terminal domains. Mutation of 6 residues, 4 on TIMP-3 N-terminal domain (K26, K27, K30 and K76) and 2 on the C-terminal domain (R163 and K165), ablated ECM binding (Lee et al., 2007). These residues were located on the opposite face of the molecule to the metalloproteinase-binding ridge, in keeping with the ability of ECM-bound TIMP-3 to inhibit metalloproteinase activity. This was further found to agree with subsequent studies in which this TIMP-3 mutant inhibited ADAMTS-5 activity with similar affinity to Wild-type TIMP-3, although no increase in affinity was observed in the presence of CaPPS (Troeberg et al., 2012). This was thought to be due to the inability of this TIMP-3 mutant to form a trimolecular complex with ADAMTS-5 and CaPPS. A recent study has shown that TIMP-3 binding to heparan sulfate or E-type chondroitin sulfate increased

TIMP-3 affinity for ADAMTS-5 by 1000-fold, indicating that these GAGs induced a conformational change in either the enzyme or the inhibitor (Troeberg et al., 2014).

1.4.5.3 Apoptotic activity of TIMP-3

TIMP-3 has been shown to have a pro-apoptotoic effect on normal and malignant human cells in culture and in vivo, with smooth muscle cells, HeLa human epithelial melanoma cell, HT1080 fibrosarcoma cells and MCF-7 breast cancer cells reportedly affected (Ahonen et al., 1998; Baker et al., 1999). It has been proposed that TIMP-3 promotes cell death by stabilising TNF-α receptors on the cell surface, leading to an increased susceptibility to apoptosis (Smith et al., 1997). The pro-apoptotic activity of TIMP-3 has been mapped to the N-terminal domain which also possesses the MMP inhibitory activity (Bond et al., 2000). It has been demonstrated that exposure to recombinant TIMP-3 or N-TIMP-3 and adenoviral expression of TIMP-3 stabilises several death receptors, including tumor necrosis factor receptor I (TNF-RI), Fas cell surface death receptor (FAS) and TNF-related apoptosis-inducing ligand receptor I (TRAIL-RI), thereby sensitizing cells to ligand-induced apoptosis (Ahonen et al., 2003). In this same study, it was also shown that TIMP-3 induced caspase-8-dependent apoptotic signaling of these death receptors. In a recent publication, Qi et al. found that TIMP-3-mediated apoptosis in endothelial cells was independent of MMP inhibitory activity and was mediated by a caspase-independent cell death pathway, involving a focal adhesion kinase (FAK)-dependent survival pathway (Qi and Anand-Apte, 2015).

1.4.6 TIMP-3 in disease

1.4.6.1. Sorsby's fundus dystrophy

TIMP-3 is the only TIMP to have an associated genetically linked disease. Sorsby's fundus dystrophy (SFD) was first identified in 1949, when it was referred to as a "fundus dystrophy with unusual features". It is an autosomal dominant degenerative disease of the macula with onset between the 3rd and 6th decade of life. Progression is rapid and is followed by loss of peripheral vision (Sorsby and Mason, 1949). The disease is characterized by extracellular deposits within the eye and thickening of Bruch's membrane, the basement membrane separating the retinal pigment epithelium from the blood supply (Majid et al., 2007).

Twelve mutations in the human TIMP-3 gene had been identified as causes of SFD (Gliem et al., 2015; Weber et al., 1994). Eight of these mutations are located in exon 5, that encodes for the C-terminal domain of TIMP-3, with 10 leading to the introduction of an additional (namely S156C, G166C, G167C, Y168C, S170C, Y172C, Y174C, Y177C, S181C and Y182C). The E139X mutation introduces a premature stop codon that deletes most of the C-terminal domain. Langton et al. have previously shown that full-length TIMP-3 S156C, G166C and S181C mutants and the truncated E139X mutant share a common phenotype of the gives rise to an MMP-inhibitory ECM localized TIMP-3 dimer when expressed in COS-7 cells, (Langton et al., 1998; Langton et al., 2000).

Immunohistochemical analysis revealed that the Bruch's membrane in the eyes of SFD patients was enriched with TIMP-3 protein compared to non-diseased controls (Fariss et al., 1998). This accumulation was not associated with an increase in mRNA expression, and Langton et al. showed that SFD

mutations induced multimerisation of the mutated TIMP-3, which led to a resistance to degradation and consequent accumulation of the mutant TIMP-3 (Langton et al., 2005).

1.4.6.2 Role of TIMP-3 in OA

Gendron et al. demonstrated that TIMP-3 inhibits ADAMTS-4- and ADAMTS-5-associated GAG release in IL-α-stimulated bovine nasal cartilage explants and in retinoic acid-stimulated porcine cartilage explants (Gendron et al., 2003). TIMP-3 levels are reduced in OA cartilage and *Timp3*$^{-/-}$ mice have increased spontaneous cartilage degradation upon aging (Sahebjam et al., 2007) (Morris et al., 2010). This implies that an imbalance between MMPs/aggrecanases and TIMP-3 enhances ECM degradation in cartilage. Intra-articular injection of N-terminal or full-length TIMP-3 inhibited cartilage degradation in a rat meniscal tear model (Black et al., 2007). Due to its ability to inhibit both aggrecanase and collagenase activity, TIMP-3 is a considered a central regulator of cartilage degradation (Figure 12), with the capacity to block cartilage degradation in OA.

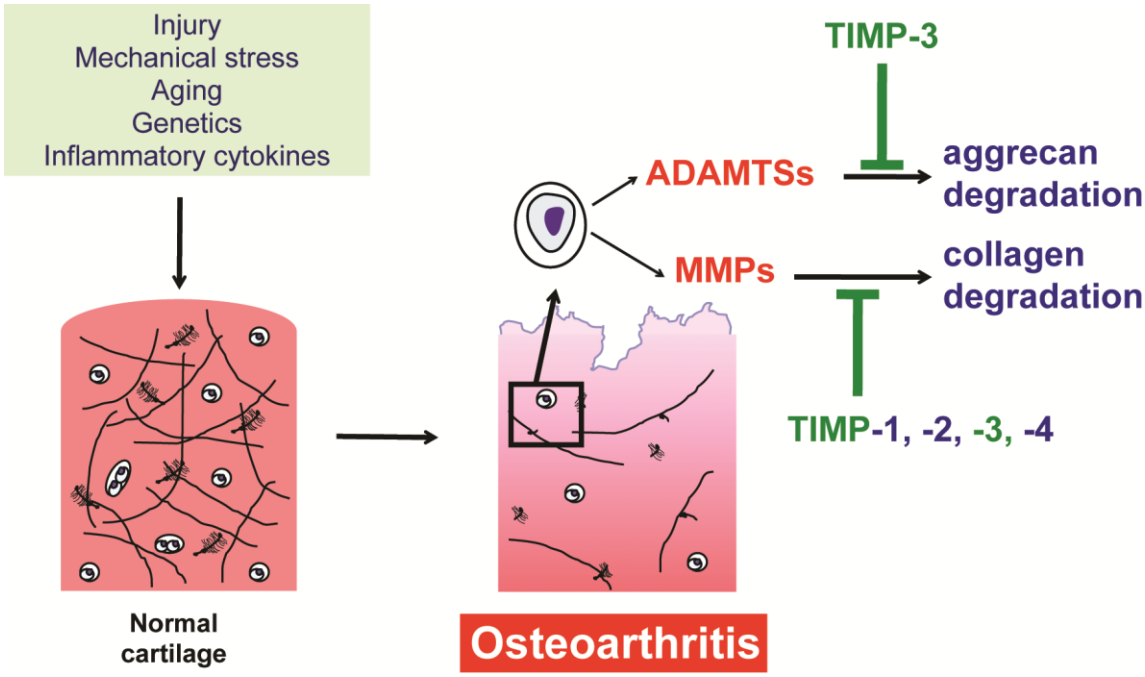


Figure 12: TIMP-3 is a central regulator of cartilage degradation.
Various factors such as injury and mechanical stress have been shown to increase metalloproteinase activity in cartilage, leading to increased degradation of key ECM molecules (aggrecan and type II collagen) and hence to initiation of OA. TIMP-3 is the only member of the TIMP family of metalloproteinase inhibitors to inhibit both the aggrecan-degrading activity of ADAMTS-4 and -5 and the collagenase activity of MMPs in cartilage, indicating that TIMP-3 has a central chondroprotective protective role.

1.4.7 Regulation of TIMP-3

TIMP-3 is regulated at the mRNA level by TGF-β and OSM. In primary normal bovine or human osteoarthritic chondrocytes, TGF-β has been shown to increase TIMP-3 mRNA levels in a dose-dependent fashion (Su et al., 1996). Up-regulation of TIMP-3 gene expression by TGF-β is mediated by serine/threonine and thyrosine kinases (Su et al., 1998). OSM, a cytokine of the IL-6 family, was found to up-regulate TIMP-3 mRNA and protein expression in articular chondrocytes in a dose- and time-dependent manner (Li and Zafarullah, 1998). No synergy between TGF-β and OSM was observed.

Human chorionic gonadotrophin has also been shown to induce a biphasic increase in TIMP-3 mRNA expression in rat periovulatory granulosa cells via the Protein Kinase pathway (Li and Curry, 2009). TIMP-3 expression can also be epigenetically modified. A range of microRNAs have been associated with a decrease in TIMP-3 expression, including miR-21 in glioma cells (Gabriely et al., 2008), miR-206 in HEK-293-EBNA cells (Limana et al., 2011), miR-221 and miR-222 in hepatocarcinoma and non small cell lung cancer cells (Garofalo et al., 2009) and miR-181b in hepatocytes and hepatocellular carcinoma cells (Wang et al., 2010).

Epigenetic regulation of TIMP-3 by the Class III histone deacetylase (HDAC) sirtuin 1 (SirT1) has also been reported. Cardellini et al. found that reduced SirT1 levels are associated with reduced TIMP-3 expression, and that inhibitors of SirT1 activity reduce TIMP-3 expression (Cardellini et al., 2009). Conversely, they found that SirT1 overexpression led to an increase in TIMP-3 expression.

SirT1 has been shown to play a protective role in cartilage, with mice lacking active SirT1 displaying increased cartilage degradation (Gabay et al., 2013). SirT1 expression is reduced in human OA cartilage (Dvir-Ginzberg et al., 2008), with the level of expression inversely correlating with the degree of cartilage damage (Fujita et al., 2011). The mechanism by which SirT1 protects cartilage is unclear. In addition to its ability to increase TIMP-3 expression (Cardellini et al., 2009), SirT1 is thought to inhibit expression of MMP-8, -9 and -13 (Gabay et al., 2013). Studies with broad-range HDAC inhibitors suggest that other HDAC promote cartilage degradation. For example, Young et al. (2005) found that the HDAC inhibitors trichostatin A and sodium butyrate

inhibited IL-1- and oncostatin M-induced expression of MMP-1, MMP-13, ADAMTS-4, ADAMTS-5 and ADAMTS-9 in bovine nasal cartilage explants and primary chondrocyte cultures. The role of specific HDACs in cartilage homeostasis and OA pathogenesis thus requires further study.

Despite the existence of these multiple transcriptional and translational mechanisms for regulating TIMP-3 levels, it has been demonstrated that extracellular levels of TIMP-3 are predominantly regulated post-translationally by endocytosis (Troeberg et al., 2008). This was illustrated by the observation that HTB94 human chondrosarcoma cells transfected with the expression plasmid for TIMP-3 contained high levels of TIMP-3 mRNA, but had non-detectable levels of TIMP-3 protein in the culture medium, unless endocytosis was blocked by addition of cytochalasin D or sulfated GAGs such as heparin or CaPPS. Sulfated GAGs increased TIMP-3 cartilage levels by sequestering the inhibitor extracellularly and preventing its internalization.

Endocytosis could also be inhibited by adding RAP, an antagonist of ligand binding to low-density lipoprotein (LDL) receptors. Accumulation of TIMP-3 upon addition of RAP to human chondrosarcoma cells or porcine articular chondrocytes indicated that TIMP-3 is a ligand for one of the family of LDL receptors (Troeberg et al., 2008), of which there are 13 mammalian members. Using radiolabeled TIMP-3, Scilabra et al. found that TIMP-3 endocytosis was substantially reduced in LRP-1-deficient PEA-13 mouse embryonic fibroblasts, and that addition of RAP had no effect on TIMP-3 endocytosis in PEA-13 cells, indicating that TIMP-3 endocytosis was mediated by LRP-1 (Scilabra et al., 2013). TIMP-3 endocytosis was to show similar kinetics in HTB94 chondrosarcoma cells, uterine fibroblasts and monocyte-like

THP-1 cells. The initial rate of endocytosis was observed to be rapid, but slowed down after 10 hours to only minimal levels. Scilabra et al. determined that this was related to shedding of the LRP-1 receptor from the cell surface.

In a manner similar to that shown for RAP (Laatsch et al., 2012), it has been proposed that on being endocytosed, the TIMP-3-LRP-1 complex is targeted to the early endosome. Upon maturation of early endosomes to late endosomes, pH reduces, causing dissociation of LRP-1 from TIMP-3. LRP-1 is then recycled back to the plasma membrane, while TIMP-3 is targeted to the lysosome for degradation. This model is supported by Scilabra et al., who detected TIMP-3 degradation products in the culture medium of HTB94 human chondrosarcoma cells following endocytosis (Scilabra et al., 2013).

This same group further observed LRP-1-independent endocytosis of TIMP-3 in PEA-13 cells, RAP-treated HTB94, mouse embryonic fibroblasts cells and Chinese hamster ovary (CHO) cells, albeit at a slower rate. The mechanism of this LRP-1-independent endocytic process remains unknown.

Heparin blocks TIMP-3 endocytosis by inhibiting its binding to LRP. This suggests there is an overlap between the LRP-1 binding site and the ECM binding site. Recently, it has been shown that heparan sulfate and E-type chondroitin sulfate also block TIMP-3 binding to LRP-1 (Troeberg et al., 2014). This suggests that control of TIMP-3 trafficking involves dynamic regulation between ECM binding and LRP-1-mediated endocytosis (Figure 13) (Troeberg et al., 2014).

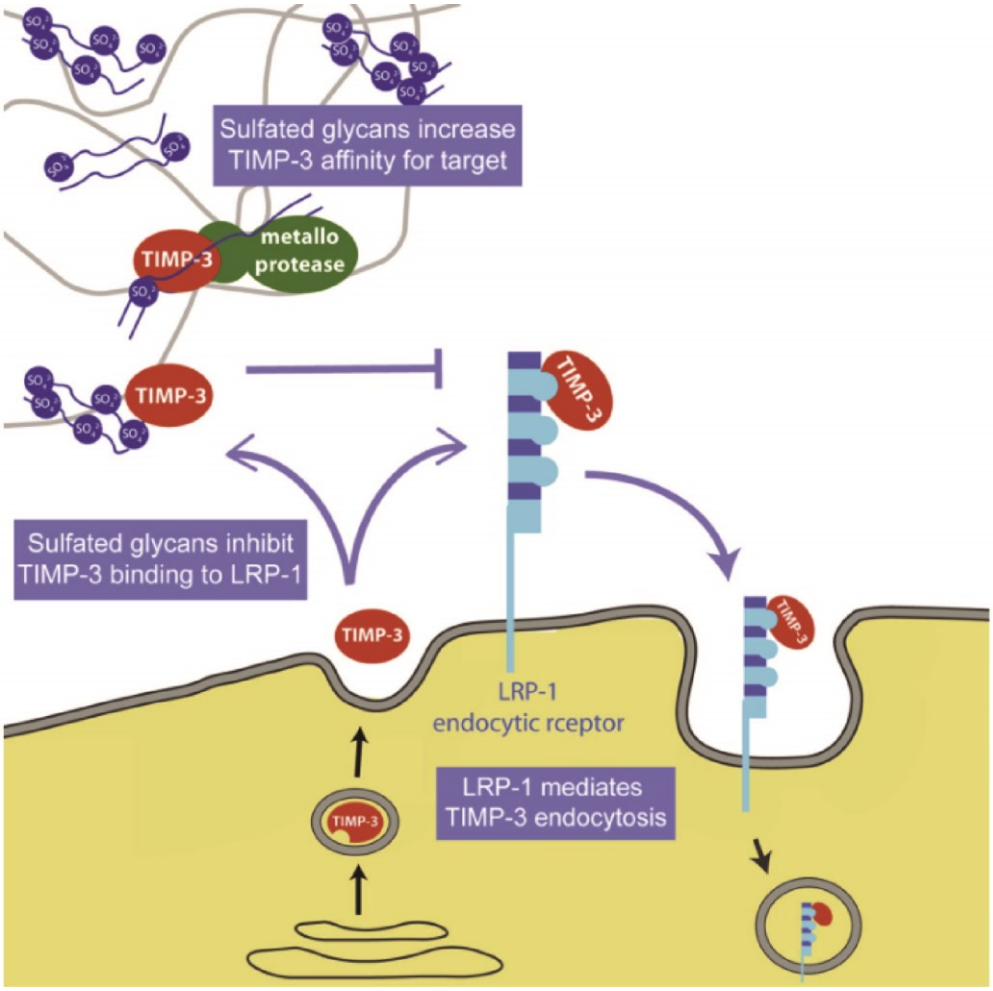


Figure 13: Extracellular levels of TIMP-3 are regulated by the equilibrium between binding to LRP-1 and the ECM.

TIMP-3 trafficking is a dynamic system, regulated by the competition between its binding to the ECM and its endocytosis by LRP-1. Overlapping binding sites are thought to mediate LRP-1 and ECM binding. ECM binding additionally increases affinity for target metalloproteinases that are able to bind to sulfated GAGs, though formation of a high affinity tri-molecular complex.

1.5 Low-density lipoprotein receptor-related protein (LRP-1)

LRP-1 is a member of the low-density lipoprotein receptor (LDLR) super-family and is a scavenger receptor that internalises more than 40 known ligands, leading to activation of signaling pathways and modulation of gene expression.

1.5.1 History of LRP-1

Brown and Goldstein (Goldstein and Brown, 1973) identified the original low-density lipoprotein receptor (LDLR) in 1973 during their search to identify the molecular basis of Familial Hypercholesterolemia. This receptor is the founding member of what is now referred to as the LDLR super family. In 1988, a novel, large human glycoprotein was cloned and found to contain structural features consistent with the LDL receptor (Herz et al., 1988). This protein was originally referred to as LDL receptor-related protein (LRP), but is now known as LRP-1 due to the subsequent identification of other family members. LRP-1 is expressed widely, with highest levels in the liver, lung, intestine and muscle. Macrophages and chondrocytes have also been shown to express high levels of LRP-1. Subsequent work by Herz et al. demonstrated that the 600 kDa LRP-1 precursor underwent cellular processing to generate an 85 kDa C-terminal membrane-spanning β-subunit (601 residues) and a non-covalently attached 515 kDa N-terminal α-subunit (3920 residues)(Herz et al., 1990). This processing is now known to be mediated by the proprotein convertase furin in the trans-Golgi network.

Moestrup et al. and Ascomb et al. (Ashcom et al., 1990; Moestrup and Gliemann, 1989) separately demonstrated that a complex of the proteinase inhibitor α_2-macroglobulin (α_2M) with one of its target proteases could be cleared from the circulation by a receptor expressed in the liver referred, to as the α_2-macroglobulin receptor (α_2MR). The inhibitiory range of α_2M is very broad including almost all known endopeptidases including MMPs (Nagase et al., 1994b), (Enghild et al., 1989). Kristensen et al. (Kristensen et al., 1990) demonstrated that the “liver receptor” α_2MR and the “novel” LRP-1 were in fact

the same receptor. α_2MR isolated from rat liver and human placenta was seen to comprise 3 component species on SDS-PAGE gels (Ashcom et al., 1990; Jensen et al., 1989; Moestrup and Gliemann, 1989), migrating at 440-500 kDa or larger, at 70-85 kDa, and at 40 kDa (Jensen et al., 1989). Kristensen et al. showed that the 500 kDa species of the α_2MR was in fact the LRP-1 α-subunit and that the 85 kDa species of the α_2MR was the LRP-1 β-subunit (Kristensen et al., 1990) It was further determined that the remaining 40 kDa protein co-purified with α_2MR /LRP-1 was not a component of the receptor, and is now known to be receptor-associated protein (RAP), a molecular chaperone of LRP-1 with high affinity for the receptor.

1.5.2 LRP-1 structure

LDL receptors are now referred to as a superfamily consisting of 7 closely related members, namely LRP-1, LRP-1b, LRP-2/megalin, very low-density lipoprotein receptor (VLDL receptor), LRP-4/MEGF7 and LRP-8/apolipoprotein E receptor 2. As shown in Figure 14, these receptors are structurally homologous and are composed of repeating domains. The common domains include the cysteine–rich complimentary repeats (CRs), epidermal growth factor (EGF) repeats, β-propeller domains, as well as transmembrane and cytoplasmic domains which include NPxY motifs and dileucine repeats which play a role in intracellular signaling.

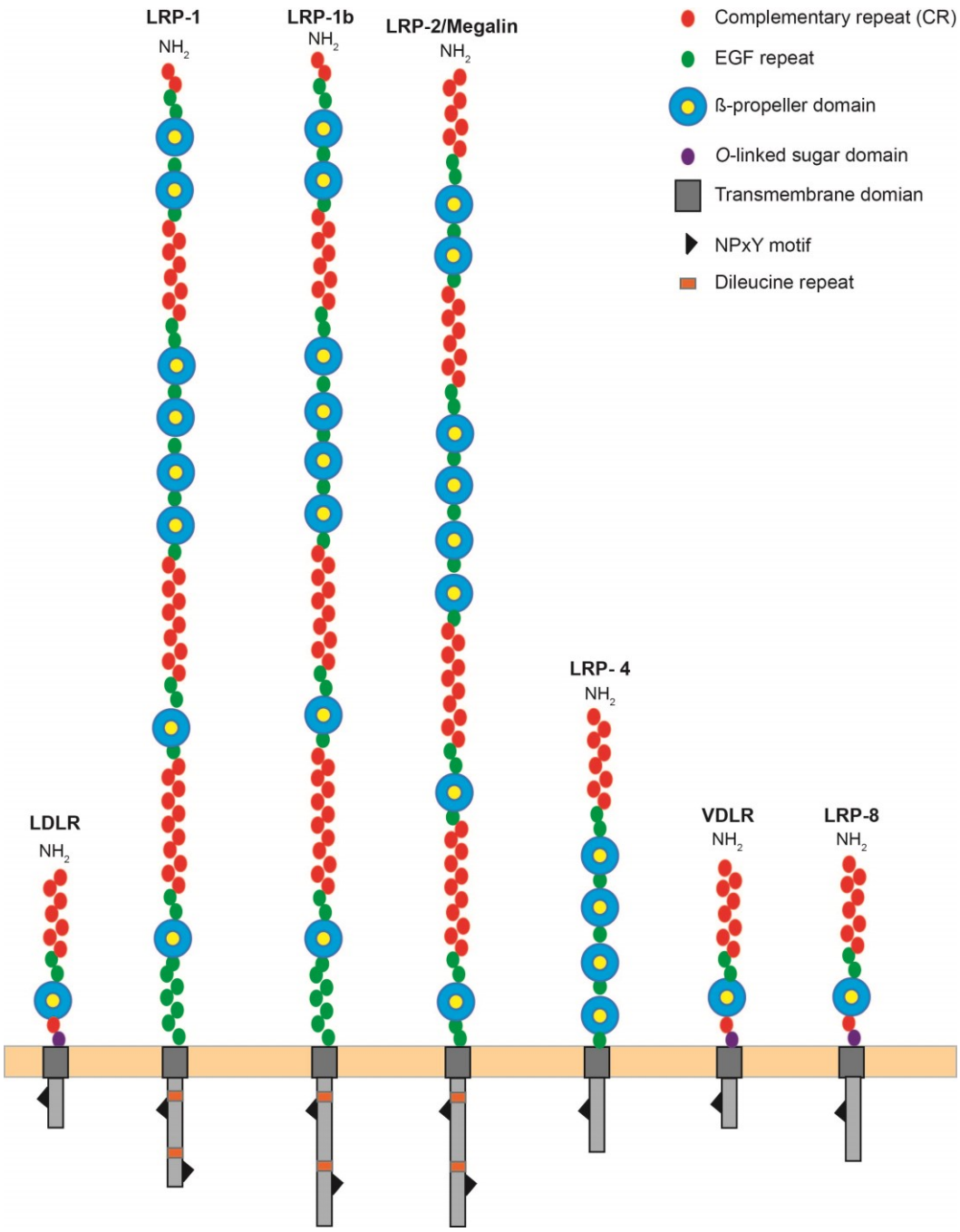


Figure 14: LDL receptors are structurally homologous and composed of repeating subunits.

The common domain structures of LDLRs include the cysteine–rich complimentary repeats (CRs), epidermal growth factor (EGF) repeats, β-propeller domains, transmembrane domains.

1.5.3 LRP-1 ligands and biological function

LRP-1 is a scavenger receptor that has been shown to internalise more than 40 known ligands, including apolipoprotein E (Willnow, 1999), lipoprotein lipase (Knauer et al., 1996), heat shock protein-96, MMPs such as MMP-2, MMP-9 and MMP-13, ADAMTS-5 and TIMP-1, TIMP-2 and TIMP-3 (Scilabra et al., 2013; Thevenard et al., 2014; Troeberg et al., 2008; Yamamoto et al., 2013). MMP-1 does not bind directly to LRP-1, however when in complex with TIMP-3, the inhibitor bridges binding to LRP-1 and the enzyme-inhibitor complex is then endocytosed (S. D. Scilabra and H. Nagase, personal communication). It functions in a range of cellular activities including protein processing, cholesterol homeostasis, and signal transduction, as shown in Figure 15.

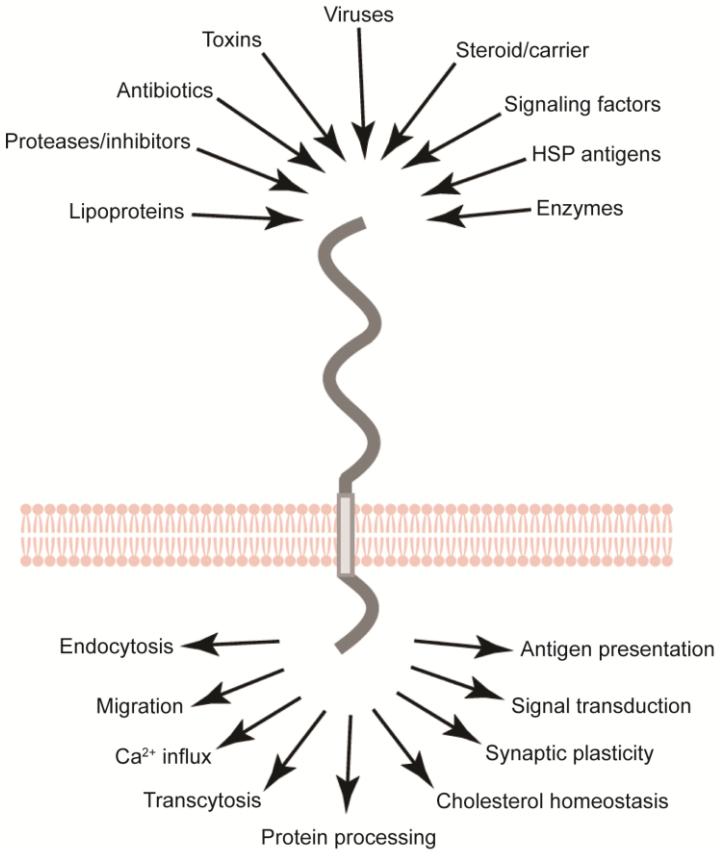


Figure 15: Classes of identified LRP-1 ligands and their proposed intracellular effects.

The extracellular region of LRP-1 is involved in binding to more than 40 known ligands of differing functions, including proteases and their inhibitors, signaling factors and lipoproteins. The intracellular region of LRP-1 mediates signal transduction, protein processing and migration. Adapted from Nykjaer and Willnow (Nykjaer and Willnow, 2002).

It is not fully understood how LRP-1 facilitates the binding of in excess of 40 ligands of such a diverse function and structure. Initially, this ability was thought to be related to the high number (31) of CRs on LRP-1 (see Figure 14). However, this alone cannot account for the diversity of LRP-1 ligands. It has been proposed that LRP-1 utilises differing modes of binding for individual ligands, including direct and indirect binding.

Direct binding has been observed for molecules including activated α_2M, tissue type plasminogen activator (tPA) and α1-antitrypsin. However, other ligands are thought to have an indirect binding strategy. Cell surface heparan sulfate proteoglycans (HSPGs) have been implicated in LRP-1-mediated endocytosis of proteins including amyloid-β-peptides, prion protein and factor VIII (fVIII). These proteins are thought to bind with low affinity to the HSPG GAG side chains before being passed to LRP-1 for internalisation (Kanekiyo et al., 2011; Nykjaer and Willnow, 2002; Sarafanov et al., 2001).

The mechanism of indirect binding to LRP-1 has been best studied for fVIII, which is endocytosed in complex with von Willebrand Factor (vWF). It has been proposed that fVIII initially binds to a HSPG on the cell surface before being scavenged by LRP-1 for endocytosis (Sarafanov et al., 2001). The fVIII-vWf complex was added to LRP-1-expressing or LRP-1-deficient mouse embryonic fibroblasts, incubated for 6 hours in the presence or absence of heparin or RAP, and surface binding of fVIII-vWf determined. The levels of cell surface fVIII-vWf were found to be similar for both LRP-1-expressing and -

deficient cells, and addition of RAP had no significant inhibitory effect on binding of the complex to LRP-1-expressing cells. This suggested that a receptor other than LRP-1 was responsible for binding of fVIII-vWf to the cell surface. Using solid phase binding assays, heparin was shown not to interfere with fVIII-vWf binding to LRP-1, demonstrating that heparin and LRP-1 did not have overlapping binding sites for fVIII-vWf. In vivo studies further supported the conclusion that both LRP-1 and HSPGs are involved in fVIII-vWf clearance (Sarafanov et al., 2001).

A third mode of binding has also been proposed. Glypican-3 (GPC3), a GPI-anchored heparan sulfate proteoglycan, has been shown to participate in a different mechanism in promoting LRP-1-mediated endocytosis of hedgehog (Shh). Shh first binds to GPC3 with high affinity, and the GPC3-Shh complex then binds to LRP-1 via its GAG side chains, and the entire complex is endocytosed (Capurro et al., 2012). This differs from the indirect binding described for fVIII-vWf, which first binds with low affinity to the HSPG before it is passed to LRP-1 for internalization.

1.5.4 Receptor associated protein (RAP)

The study of LRP-1 is intrinsically linked with receptor-associated protein (RAP), the 40 kDa protein co-purified with α_2MR/LRP-1 (Section 1.5.1). As previously mentioned, LRP-1 has in excess of 40 ligands and as such, a mechanism exists to prevent the nascient LRP-1 molecule from prematurely binding with ligands within the endoplasmic reticulum. RAP is a molecular chaperone of LRP-1 and a high affinity antagonist of ligand binding to LRP-1 at neutral pH (Herz et al., 1991; Williams et al., 1992). On guiding LRP-1 from

the ER to the Golgi apparatus, RAP dissociates from LRP-1 by protonation of RAP domain 3 histidine residues in the lower pH environment of the Golgi apparatus (Lee et al., 2006). Due its high affinity binding to LRP-1 at neutral pH, RAP is commonly used as a model for ligand binding to LRP-1 (Fisher et al., 2006; Jensen et al., 2006; Jensen et al., 2009b; van den Bigglelaar et al., 2011).

1.5.5 LRP-1 expression

LRP-1 is ubiquitously expressed, with highest expression in the liver, lung, brain and skeletal muscle (Herz et al., 1988). However, this expression is strongly cell-type specific, with LRP-1 being expressed in gastrointestinal tract epithelial cells, ovary cells, hepatocytes, fibroblasts, neurons and macrophages (Moestrup et al., 1992).

Deletion of the *lrp1* gene in mice resulted in failure of blastocyst implantation and embryonic lethality at around day 10 (Herz et al., 1992). Conditional knockouts are thus widely studied.

Overton et al. (Overton et al., 2007) developed a macrophage LRP-1-deficient mouse model and showed that macrophage LRP-1 deletion increased MMP-9 levels, which was in turn associated with an increase in the frequency of rupture of the blood vessel elastic lumina, and was thought to impact on plague vulnerability. This deletion also led to an increase in inflammatory responses, with an increase in cytokine production. Overton et al. suggested that these studies provided evidence for an atheroprotective function of macrophage LRP-1. In a separate study, LRP-1 has been shown to have a major role in controlling vascular smooth muscle cell proliferation (Boucher et al., 2003). Mice lacking vascular smooth muscle cell LRP-1 demonstrated

hyperplasia of the aortic wall, and as found in the Overton study, disruption of the elastic layer and increased susceptibility to development of atherosclerotic lesions. These lesions were characterized by rapid and extensive foam cell formation, leading to aortic occlusion and ultimately death.

1.5.6 LRP-1 ligand-binding interface

As mentioned in Section 1.5.2, the CRs of LRP-1 mediate ligand binding (Herz and Strickland, 2001). LRP-1 contains 31 CRs arranged into 4 ligand-binding clusters named I, II, III and IV from the N-terminal domain of the α-subunit (Neels et al., 1999). Three aspartic acid residues in each CR form an acidic pocket that interacts with a lysine residue of the ligand (Figure 16). LRP-ligand interactions are highly electrostatic in nature. The crystal structure of RAP domain III bound to a CR of LRP-1 indicates that the minimal binding unit consists of 2 lysine residues that interact with 2 adjacent CRs of LRP-1 (Jensen et al., 2009b). These lysine residues are 21 Å apart and are exposed on the surface of RAP (Fisher et al., 2006; Jensen et al., 2006; Jensen et al., 2009b; van den Bigglelaar et al., 2011). In the case of RAP-LRP-1 binding, mutation of either lysine 256 to alanine (K256A) or lysine 270 to alanine (K270A) reduced RAP binding to LRP-1 by 20-fold (van den Bigglelaar et al., 2011). Mutation of both lysine residues completely abolished binding and endocytosis.

RAP, activated α_2M, uPA/PAI1, apolipoprotein E and lipoprotein lipase and serpin/proteinase nexin-1 have all been experimentally shown to have the same minimal LRP-1 binding unit consisting of 2 lysine residues separated by 21Å, projecting outwards from the structure (Fisher et al., 2006; Jensen et al., 2006; Jensen et al., 2009b; van den Bigglelaar et al., 2011).

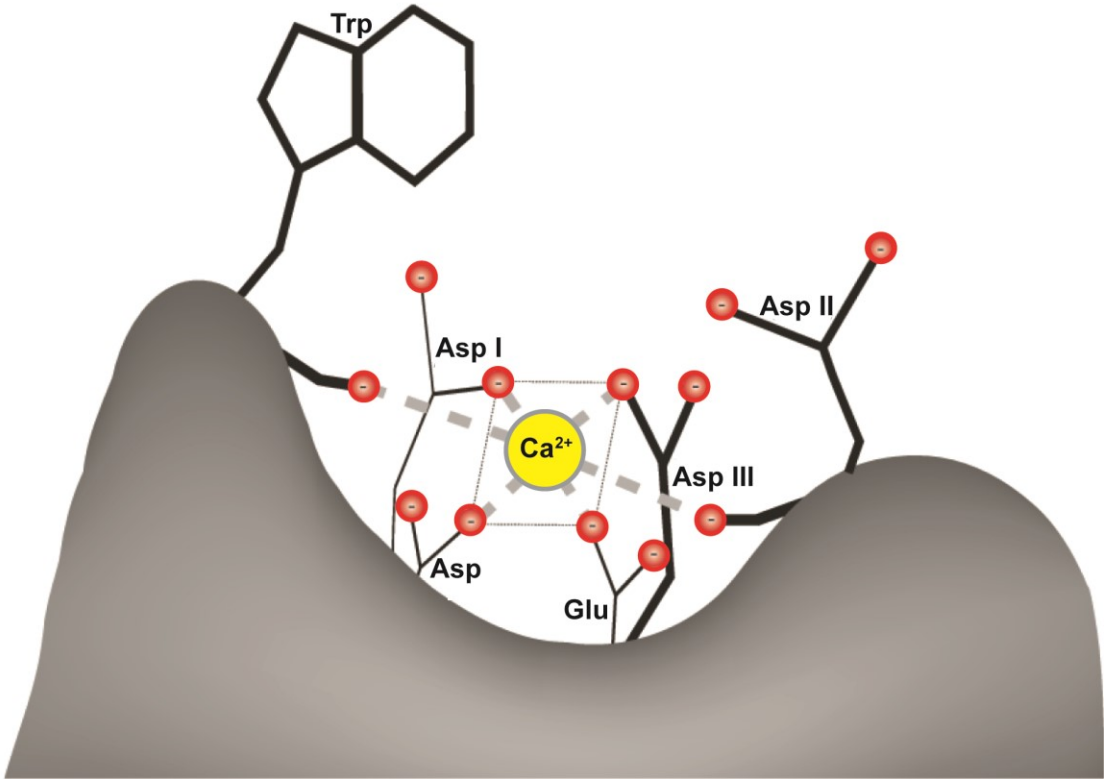


Figure 16: Structure of cysteine–rich complimentary repeats of LRP-1.
The cysteine–rich complimentary repeats (CRs) contain a highly conserved Ca^{2+} ion that is octahedrally coordinated by 3 salt bridges, generated by the interaction of aspartic acid residues, and giving an overall acidic binding pocket. The CR interacts with one lysine residue of a di-lysine pair on the LRP-1 ligand to mediate binding. Adapted from Fisher et al. (2006).

All LDL family members contain one or more regions that are homologous to the EGF precursor, which consists of 2 cysteine-rich EGF repeats, followed by YWTD repeat folds and a β-propeller domain followed by a third cysteine-rich EGF repeat (see Figure 14). It was found that on deletion of the EGF-EGF-β-propeller–EGF region, receptors no longer released their ligands in the low pH environment of the endosomal compartments (Davis et al., 1987; Mikhailenko et al., 1999).

1.5.7 LRP-1-mediated signaling

The LDL receptors are single-pass type I transmembrane proteins and LRP-1. The cytoplasmic domain of LRP-1 consists of approximately 100 residues and includes 2 NPxY motifs and 2 dileucine repeats which are involved in intracellular signaling (Lillis et al., 2008). The transmembrane region has been shown to undergo regulated intra-membrane proteolysis (May et al., 2002), with the resulting intracellular domain being translocated to the nucleus where it mediates transcriptional regulation (Kinoshita et al., 2003).

A large number of intracellular proteins interact with the cytoplasmic tail of LRP-1, linking it with several different signaling pathways. LRP-1 contains 2 NPxY motifs in its cytoplasmic tail, with phosphorylation of the tyrosine residue in the NPxY motif in response to ligand binding to the extracellular region of LRP-1 enabling modulation of signaling pathways, including the mitogen-activated protein kinase (MAPK) pathway (Abbaszade et al., 1999; Barnes et al., 2003; Barnes et al., 2001; Hu et al., 2006; Newton et al., 2005). Of the 2 LRP-1 NPxY motifs, the tyrosine of the C-terminal motif is phosphorylated in response to platelet-derived growth factor (PDGF) (Loukinova et al., 2002) and connective tissue growth factor (CTGF) (Yang et al., 2004).

The intramembrane domain of LRP-1 can undergo regulated intramembrane proteolysis (RIP), with γ-secretase thought to play a central role in this process (Kinoshita et al., 2003). Based on previous RIP studies with Notch, amyloid precursor protein (APP) and LRP-6, the RIP mechanism involves 2 sequential cleavage events (De Strooper et al., 1999; Mi and Johnson, 2007), the first of which occurs in the extracellular region of LRP-1 close to the plasma membrane and results in the shedding of LRP-1

ectodomain. This is mediated in different cell types by MMPs including MT1-MMP (Rozanov et al., 2004; Selvais et al., 2011), ADAM-10 and ADAM-17 (Liu et al., 2009) or by the β-secretase beta-site amyloid precursor protein cleaving enzyme 1 (BACE1) (von Arnim et al., 2005). The resulting transmembrane domain is then further cleaved by γ-secretase (Hass et al., 2009), releasing the intracellular domain to the cytosol, where it translocates to the nucleus and modulates gene transcription (Kinoshita et al., 2003; May et al., 2002; von Arnim et al., 2005; Zurhove et al., 2008). It is not known how such RIP events are regulated or if they occur in response to binding of all ligands.

In their study of LRP-1 function in neurons, Mantuano et al. (Mantuano et al., 2013) demonstrated that LRP-1 is able to assemble unique co-receptor systems to initiate independent cell signaling events in response to binding of different ligands. Binding of tissue-type plasminogen activator (tPA) to LRP-1 was found to initiate ERK1/2 signaling via a LRP-1 and the N-methyl-D-aspartate receptor and the tyrosine receptor kinase TrK, while myelin-associated glycoprotein initiated signaling via the neutrotrophin receptor p75NTR, but not via TrK. Such ligand-dependent signaling outcomes have not yet been investigated in cartilage.

1.5.8 LRP-5 and -6

LDL receptors are known to play a role in Wnt signaling. Wnts are secreted glycoproteins that play a central role in cell signaling, tissue development and homeostasis (Moon et al., 1997; Polakis, 2000; Wodarz and Nusse, 1998). In the canonical pathway, Wnt binds to its receptor Frizzled, activating Dishevelled, which then inactivates β-catenin degradation (Salic et

al., 2000). The stabilised β-catenin accumulates in the nucleus and interacts with T-cell factor (TCF) transcription factor family members, activating expression of Wnt target genes that trigger cell proliferation, oncogenic transformation and inhibition of apoptosis (Behrens, 2000; Polakis, 2001). In vertebrates, LRP-5 and -6 interact with Frizzled and act as Wnt co-receptors in canonical Wnt signaling (Tamai et al., 2000).

The structure of LRP-5 and -6 is sufficiently different to that of LRP-1 that they are classed as belonging to a different subfamily of LRPs. The extracellular regions of LRP-5 and -6 contain the same structural motifs as those found in LRP-1, but they are arranged in reverse order, with the β-propeller domain and EGF repeats at the N-terminus and the CRs located immediately adjacent to the plasma membrane (Howell and Herz, 2001). Zilerberg et al. (Zilberberg et al., 2004) demonstrated that, in contrast to LRP-5 and LRP-6, LRP-1 does not interact with Frizzled or act as a co-receptor in the transmission of Wnt signaling. It was further demonstrated that binding and internalising of Frizzled by LRP-1 prevented formation of Frizzled/LRP-5 or Frizzled/LRP-6 complexes, thereby repressing canonical Wnt signaling.

1.6 Hypothesis and aims of study

TIMP-3 is the only endogenous tissue inhibitor of cartilage-degrading metalloproteinases and aggrecanases, and the decreased levels of TIMP-3 observed in OA are associated with the increased ECM degradation characteristic of the disease.

We therefore hypothesise that an endocytosis-resistant TIMP-3 mutant will have an increased half-life in cartilage, thereby providing improved protection against cartilage breakdown in OA.

We therefore aim to generate an endocytosis-resistant mutant of TIMP-3 that retains comparable affinity for target metalloproteinases and ECM binding as Wild-type TIMP-3. We predict that such a TIMP-3 mutant will show increased chondroprotective activity compared to Wild-type TIMP-3 and contribute to the development of a disease-modifying osteoarthritis drug.

Chapter 2: Material and Methods

2.1 Reagents

2.1.1. Cultured cells

HTB94 human chondrosarcoma and HEK-293-EBNA human embryonic kidney epithelial cells were acquired from laboratory stocks. HEK-293-EBNA cells transfected with C-terminally FLAG tagged pCEP4-TIMP-3 (Troeberg et al., 2009), pCEP4-ADAMTS-5 lacking the C-terminal thrombospondin domain (Gendron et al., 2007), pCEP4-ADAMTS-4 lacking the C-terminal spacer domain (Kashiwagi et al., 2004) and pCEP4-MMP-13 (R. Visse and H. Nagase, unpublished data) were obtained from frozen cell stocks prepared by Dr Linda Troeberg, Dr Christi Gendron and Dr Robert Visse respectively.

2.1.2. Cell culture reagents

Cell culture reagents were purchased from the suppliers listed in Table 4.

2.1.3. Protein biochemistry reagents

Recombinant purified MMP-1 catalytic domain (MMP-1ΔC) was obtained from Dr Robert Visse in this laboratory (Chung et al., 2000), MMP2ΔC, MMP3ΔC, ADAMTS-4 lacking the C-terminal spacer domain, ADAM-17 ectodomain, and ADAMTS-5 lacking the C-terminal thrombospondin domain were obtained from Dr Linda Troeberg also of this laboratory (Gendron et al., 2007).

2.1.4. SDS-PAGE and immunoblotting reagents

SDS-PAGE and immunoblotting reagents were purchased from the suppliers detailed in Table 5.

Table 4: Suppliers of cell culture reagents.

Reagent	Supplier
Dulbecco's modified Eagle's medium (DMEM) Penicillin/streptomycin 4-(2-hydroxyethyl)-1-piperazineethanesulfonic acid (HEPES) Trypsin-ethylenediaminetetracetic acid (EDTA)	Lonza (Slough, UK)
Amphotericin B Sodium chlorate Heparin (porcine) Heparan sulfate (human) Chondroitin-4-Sulfate (Bovine)	Sigma-Aldrich (Dorset, UK)
Hygromycin B (*Streptomyces* sp.)	Calbiochem (Nottingham, UK)
Collagenase (*Clostridium histolyticum*)	Worthington (Lakewood, USA)
Fetal calf serum (FCS)	Gibco (Paisley, UK)
Trypan Blue stain 0.4%	NanoEntek (Seoul, South Korea)
E. coli BL21(DE3)	Laboratory stocks
Dimethyl sulfoxide (DMSO)	Santa Cruz Biotechnology (Dallas, USA)

Table 5: Suppliers of SDS-PAGE and immunoblotting reagents.

Reagent	Supplier
30 % (w/v) acrylamide/bis-acrylamide	Severn Biotech (Worcestershire, UK)
2-amino-2-methyl-1,3-propanediol N,N,N′,N′-tetramethylethylenediamine (TEMED) Ammonium persulfate (APS) Trichloroacetic acid (TCA)	Sigma-Aldrich (Dorset, UK)
PageRuler Plus prestained protein ladder for SDS-PAGE	Fisher Scientific (Loughborough, UK)
Trans-Blot Turbo Transfer System	Bio-Rad Laboratories (Hertfordshire, UK)
Western Blue Stabilised Substrate for Alkaline Phosphatase	Promega UK (Southampton, UK)
Amersham ECL Prime Western Blotting detection reagent	GE Healthcare Life Sciences (Buckinghamshire, UK)
KPL Peroxidase Substrate	KPL Inc. (Gaithersburg, MA, US)
Trans-Blot Turbo Transfer System	Bio-Rad (Hertfordshire, UK)

2.1.5. Antibodies

Antibodies were used in enzyme-linked immunosorbent assays (ELISA) and immunoblotting for the detection of proteins. The specificity of the antibody-antigen interaction enables a target protein to be identified in the midst of a complex protein mixture. Proteins are separated by gel electrophoresis and then transferred to a nitrocellulose or polyvinylidene fluoride (PVDF) membrane in immunoblotting, or in an ELISA the antigen of interest is coated onto a 96-well plate. Both are then incubated with an antibody specific to the protein of interest, referred to as the primary antibody.

Bound primary antibodies are subsequently detected using species-specific secondary antibodies conjugated to an enzyme such as alkaline

phosphatase (AP) or horseradish peroxidase (HRP). In immunoblotting the most commonly used secondary antibodies are conjugated to AP or HRP. In ELISA, the secondary antibodies are commonly conjugated to HRP.

In this study, a mouse monoclonal anti-FLAG M2 primary antibody (Sigma-Aldrich, Dorset, UK) was used for the detection of Wild-type and mutant TIMP-3 in both immunoblotting and ELISA. Alternatively, a rabbit polyclonal antibody against TIMP-3 was used (AB6000, Millipore, Watford UK). Anti-mouse and anti-rabbit IgG secondary antibodies conjugated to AP (Promega UK, Southampton, UK) were used as detection antibodies for immunoblotting. Anti-mouse secondary antibody conjugated to HRP (DAKO UK Ltd, Cambridgeshire, UK) was used for detection of Wild-type and mutant TIMP-3 by ELISA.

An anti-AGEG primary neo-epitope antibody generated in-house (Troeberg et al., 2008) was used with an anti-rabbit IgG AP-conjugated secondary antibody (Promega UK, Southampton, UK) for the detection of ADAMTS-5-mediated aggrecan cleavage by immunoblotting.

2.1.6. Molecular biology reagents

All TIMP-3 mutant constructs were generated using the QuikChange site-directed mutagenesis kit (Agilent Technologies, Cheshire, UK). Bacterial cultures were grown in Luria Bertani (LB) media (Life Technologies, Paisley, UK) with carbenicillin (Merck Millipore, Hertfordshire, UK) (100 µg/mL) and DNA extracted using QIAGEN Plasmid Plus Midi Kits (Qiagen Ltd, Manchester, UK).

TIMP-3 and RAP DNA restriction digests were conducted using *Xho*I, *Nde*I and *Kpn*I restriction enzyme (Life Technologies, Paisley, UK) and

products visualised on agarose gels using Ultrapure Agarose (Qiagen Ltd, Manchester, UK), 10x FastDigest green buffer and Gel Red (Biotium, Cambridge Bioscience, Cambridge, UK).

2.2. Methods

2.2.1. Cell culture

2.2.1.1. Bacterial cell culture

E. coli XLI-Blue electro-competent bacteria were used for DNA extraction. DNA was electroporated into *E. coli* XLI-Blue cells using a BTX Electrocell Manipulator 630 (Holliston, MA, USA) with settings of 2250 V, 200 Ω and 25 μF. After electroporation, LB without carbenicillin (800 μl, 37 ºC) was added to the cells and the culture shaken (37 ºC, 1 h, 200 rpm). Bacteria were then plated on LB-carbenicillin agar (10, 50 and 100 μL) and incubated overnight (37 ºC). Colonies were selected and cultured overnight (37 ºC, 225 rpm) in LB media (100 mL) supplemented with 100 μg/mL carbenicillin and DNA extracted using QIAGEN Plasmid Plus Midi Kits (Qiagen Ltd, Manchester, UK).

E. coli BL21-DE3 heat-shock competent bacteria were used for protein expression. DNA was added to *E. coli* BL21-DE3 cultures (50 μl) in round-bottomed tubes and incubated on ice (30 min), before being exposed to 42 ºC for 45 s and returned to ice for a further 2 min. Warmed LB without carbenicillin (800 μl, 37 ºC) was added and the culture shaken (37 ºC, 1 h, 200 rpm). Cultures (10, 50 and 100 μL) were plated on LB-carbenicillin agar and incubated at 37 ºC overnight. Colonies were selected and cultured overnight in LB media supplemented with 100 μg/mL carbenicillin (37 ºC, 225 rpm) at volumes required for protein purification.

2.2.1.2. Mammalian cell line culture

HEK-293-EBNA and HTB94 were cultured in DMEM supplemented with 100 U/mL penicillin, 100 µg/mL streptomycin and 10 % FCS [5 % (v/v) CO_2, 37 ^oC]. HEK-293-EBNA cells transfected with pCEP4-TIMP-3 constructs were cultured in DMEM supplemented with 100 U/mL penicillin, 100 µg/mL streptomycin, 10 % FCS and 800 µg/mL hygromycin B. Cells were passaged every 2-3 days by trypsinisation. Briefly culture media was removed and cells washed in trypsin-EDTA. Sufficient fresh trypsin-EDTA solution was then added to the culture plate to completely cover the cell monolayer (2.5 mL/10 cm plate). The plate was placed in the incubator [5 % (v/v) CO_2, 37 ^oC] for approximately 5 minutes. When cells were observed to have detached from the plate, DMEM supplemented with10 % FCS was added (7.5 mL/10 cm plate) and cells resuspended and centrifuged (5 min, 1500 rpm). The supernatant was discarded, and the cell pellet resuspended in DMEM containing 10 % FCS and hygromycin B if required. Cells were plated at the density required for subsequent experiments.

2.2.1.3. Primary chondrocyte isolation and culture

Articular cartilage was dissected from the metacarpophalangeal joints of 3-9 month old pigs. Porcine chondrocytes were isolated from the cartilage by treatment with bacterial collagenase (*Clostridium histolyticum*, Worthington, Lakewood, USA) (1 mg/ml) in cartilage growth medium (DMEM supplemented with 10 % FCS, 100 U/mL penicillin, 100 mg/mL streptomycin, 2 mg/mL amphotericin B and 10 mM HEPES)(overnight at 37 ºC, with shaking at 250 rpm). Cells were passed through a cell strainer to remove any undigested tissue, washed three times in cartilage growth medium supplemented with 10

% FCS. Chondrocytes were then counted using an Eve Automated Cell Counter (NanoEnTek, Seoul, South Korea) and plated at required cell density (overnight, 37 ºC, 5 % CO_2).

2.2.2. TCA precipitation

Trichloroacetic acid (TCA) precipitation is an efficient means of concentrating proteins by precipitating them from dilute solutions by reducing the pH of the medium. Low pH disrupts the three dimensional structure of proteins by disturbing electrostatic interactions between charged residues. The denatured protein has reduced solubility and precipitates out of solution. Proteins were precipitated by addition of TCA to a final concentration of 5 % (v/v), vortexing the solution and incubating it at 4 ºC overnight. The solution was centrifuged (13000 rpm, 10 min, 4 ºC) and the resulting pellet resuspended in 2x SDS-PAGE loading buffer for separation by SDS-PAGE. Commonly, this method was used to concentrate 10 mL of conditioned medium to approximately 30 □l.

2.2.3. SDS-PAGE and immunobloting

Sodium dodecyl sulfate-polyacrylamide gel electrophoresis (SDS-PAGE) was formulated as per Laemmli et al (Laemmli, 1970). Samples are mixed with sodium dodecyl sulfate (SDS), an anionic detergent that binds to proteins, giving them a net negative charge. A constant number of SDS molecules binds to a protein per unit length, thus giving proteins a constant charge-to-mass ratio, with the charge being dependent on the protein's size. Proteins are then separated in an electric field, where their velocity is directly proportional to the field strength and the charge on the molecule, and is inversely proportional to the size of the molecule and the viscosity of the medium. Adding a gel with

sieving properties increases the differences in mobility between proteins of different molecular weights, giving the basis of separation by SDS-PAGE.

2.2.3.1. Ammediol SDS-PAGE

Ammediol SDS-PAGE gels were chosen for their high resolution (Wyckoff et al., 1977). Buffers for this gel system are detailed in

Table 6, while Table 7 outlines the quantities of reagents required to cast four 10% gels using the Hoefer Four Gel Caster (for 10 x 8 cm gels) (Massachusetts, USA). The lower gels were cast first, with APS and TEMED added last. The gel solution was added to the gel caster (approximately 10 mL/gel), leaving sufficient space to accommodate the upper gel (approximately 2.5 cm). Oxygen was excluded by adding H_2O-saturated butanol (1 mL/gel) to facilitate polymerisation and gels left to set for 1 h at room temperature. Upper gels were made using the recipe in Table 7, with APS and TEMED again added last and the solution quickly added to the gel caster (approximately 3 mL/gel) and well combs fitted. Gels were set for 1 h at room temperature, and stored wrapped in plastic to prevent dehydration at 4 ^{o}C for up to 2 weeks.

Gels were secured in the SDS-PAGE running tank, and ammediol lower running buffer (anode buffer) added to the lower chamber and ammediol upper running buffer (cathode buffer) added to the upper chamber. Samples were mixed with an equal volume of 2x ammediol sample loading buffer and a current of 150-200 V applied for for up to 70 min, or until the bromophenol blue marker reached the bottom of the gel.

Table 6: Buffers for ammediol SDS-PAGE.

SDS sample buffer (2x)	2 % SDS 5.0 mL ammediol Upper gel buffer 0.1 % (w/v) bromophenol blue 50 % (w/v) glycerol +/- 1 % (v/v) β-mercaptoethanol 0.01 % (w/v) sodium azide
Ammediol upper gel buffer	84 mM ammediol 62 mM HCl 0.02% NaN_3
Ammediol lower gel buffer	110 mM ammediol 47 mM HCl 0.02% NaN_3
Ammediol upper running buffer	10 mM ammediol 10 mM glycine 0.01% SDS
Ammediol lower running buffer	16 mM ammediol 12.5 mM HCl
Sucrose solution	50 % (w/v) sucrose 50 % (v/v) dH_2O
Ammonium persulfate (APS)	10 % (w/v) ammonium persulfate 90 % (v/v) dH_2O

Table 7: Composition of 10 % Ammediol SDS-PAGE gels.

Reagents	**Lower gel**	**Upper gel**
30 % (w/v) acrylamide/bis-acrylamide	13.00 mL	1.6 mL
Lower gel buffer	9.8 mL	n/a
Upper gel buffer	n/a	3.2 mL
50 % Sucrose	8.4 mL	3.2 mL
dH_2O	7.9 mL	4.8 mL
APS	137 µl	156 µl
TEMED	14 µl	34 µl

2.2.3.2. Tris-glycine SDS-PAGE

Tris-glycine SDS-PAGE was used for aggrecan immmunoblots. Buffers for this gel system are outlined in Table 8.

Table 8: Buffers for the Tris-glycine SDS-PAGE system.

Tris-glycine sample buffer	2 % SDS 0.125 mM Tris-HCl 0.1 %(w/v) bromophenol blue 50 % (w/v) glycerol +/- 1 %(v/v) β-mercaptoethanol 0.01 % (w/v) sodium azide
Tris-glycine running buffer	25 mM Tris-HCl 190 mM glycine 1 % SDS

Table 9 outlines the quantities of reagents required to make four 6% Tris-glycine gels using the Hoefer Four Gel Caster (for 10 x 8 cm gels) (Massachusetts, USA) as per manufacturers guidelines.

The lower gels were cast first, ensuring that APS and TEMED were added last. The gel solution was added to the gel caster (approximately 10 mL/gel), leaving sufficient space to accommodate the upper gel (approximately 2.5 cm). Oxygen was excluded by adding H_2O-saturated butanol (1 mL/gel) to facilitate polymerization and lower gels left to set for 1 h at room temperature. Upper gels were made using the recipe in Table 9, with APS and TEMED again being added last and the solution quickly added to the gel caster (approximately 3 mL/gel) and well combs fitted. Gels were allowed to set for 1 h at room temperature, wrapped in plastic to prevent dehydration, and stored at 4 ^oC for up to 3 weeks.

Gels were secured in the SDS-PAGE running tank, and Tris-glycine running buffer added to both upper and lower chambers. Samples were mixed

with equal volumes of 2x Tris-glycine sample loading buffer and a current of 150 V applied for up to 70 min, or until the bromophenol blue marker reached the bottom of the gel.

Table 9: Composition of 6% Tris-glycine gels.

Reagents	Lower gel	Upper gel
30 % (w/v) acrylamide/ bis-acrylamide	8 mL	1.6 mL
Tris-glycine pH 8.8	10 ml	n/a
Tris-glycine pH 6.8	n/a	1 mL
10 % SDS	400 µl	80 uL
dH_2O	21.2 ml	5.5 mL
APS	400 µl	80 µl
TEMED	32 µl	8 µl

2.2.3.3. Immunoblotting

Immunoblotting (also called Western blotting) was developed by Towbin and colleagues (Towbin et al., 1979), and enables identification of a target protein in a complex protein mixture, on the basis of the protein's molecular mass and its reactivity with a specific antibody. The protein mixture is separated by SDS-PAGE and then transferred to a PVDF or nitrocellulose membrane, which is then incubated with primary antibodies specific to the protein of interest. Unbound antibody is washed off, leaving only the antibody specifically bound to the protein of interest. This bound primary antibody is detected using secondary antibodies, which recognised the conserved regions of the primary antibody in a species-dependent manner, and facilitate detection because they are conjugated to a fluorophore or an enzyme such as AP or HRP. Upon addition of a substrate for the enzyme, either a colored precipitate is deposited on the blot (colorimetric detection) or a chemiluminescent or

fluorescent product is formed and the light signal captured on film or CCD camera.

Here, following separation by SDS-PAGE, proteins were transferred to a PVDF membrane using the Trans-Blot Turbo Transfer System system (BioRAd, Hertfordshire, UK). The membrane was blocked in 5 % dry skimmed milk in phosphate buffered saline (PBS) (1 h, room temperature) and membranes incubated with primary antibodies at the required concentrations overnight in 5 % dry skimmed milk in PBS at 4 ^{o}C. The membrane was then washed 3 times in PBS containing 0.1 % Tween-20, and incubated with the required concentration of AP-conjugated secondary antibody at room temperature for 5 hours. The membrane was washed 3 times in PBS containing 0.1 % Tween-20 and the incubated in Western blue stabilised substrate for AP (Promega Southampton, UK) to visualise bands. The reaction was stopped using AP stop (20 mM Tris-HCl pH 7.5 and 10 mM EDTA). Gels were then scanned using a Canon CanoScan LiDE 210 flatbed high-resolution scanner at a resolution of 600 dpi.

2.2.3.4. Coomassie staining

Some SDS-PAGE gels were stained in Coomassie blue stain [0.1 % (w/v) Coomassie Brilliant Blue R-250, 50 % (v/v) methanol, 20 % (v/v) acetic acid, 30 % (v/v) dH_2O] for 15 min to visualise protein bands. The gels were then washed in de-stain solution [30 % (v/v) methanol, 1 % (v/v) formic acid, 69 % (v/v) dH_2O] for 3 washes of 15 min each. The de-stain washes were repeated until Coomassie blue stain was removed from the gel background and protein bands were well defined. Gels were then scanned using a Canon CanoScan LiDE 210 flatbed high-resolution scanner at a resolution of 600 dpi.

2.2.3.5. Densitometry

Phoretix 1D software (TotalLab, Newcastle-upon-Tyne, UK) was used to quantify the pixel volume or intensity of bands in images of gels and blots. For quantitative analysis, it was essential that band intensity be within the linear range of detection. Weaker bands were thus routinely selected for quantification. Background subtraction and quantification was perfumed according to the manufacturer's instructions.

2.2.4. Generation of stable cell lines

2.2.4.1. Liposome transfection

HEK-293-EBNA cells were seeded overnight (8 x 10^5 cells per well in a 12-well plate) in DMEM supplemented with 100 U/mL penicillin, 100 µg/mL streptomycin, 10 % FCS [37 ^oC, 5% (v/v) CO_2]. Wells were transfected with 3 µg of pCEP-4 mammalian expression vector encoding C-terminally FLAG-tagged TIMP-3 mutant using Lipofectamine 2000 transfection reagent (Invitrogen/ThermoFisher Scientific, Paisley, UK) as per the manufacturer's instructions. Control wells were mock transfected.

2.2.4.2. Hygromyin B selection

Hygromycin B was added to both transfected and untransfected HEK-293-EBNA cells at 100, 400 and 800 µg/mL. Media was changed every 2 days and the cells visually examined for toxicity. Untransfected cells, not having received the hygromycin B selection marker, died within 7-9 days. Within the population of transfected cells, cells transfected with the selection marker grew, while those that were not successfully transfected, died. Over time, the entire cell population thus consisted of transfected cells at a particular antibiotic dose.

Following expansion of each stable line, the expression of the target protein was tested by adding 10 mL of serum-free DMEM [DMEM supplemented with 100 U/mL penicillin, 100 µg/mL streptomycin] and incubating the cells at 37 ^{o}C and 5% (v/v) CO_2 for 2 days. For each cell line, 100, 300 and 500 µL of conditioned medium was diluted to 1 mL in DMEM containing 0.1 % FCS and TCA precipitated overnight. The sample was then resuspended in 30 µL of reducing 2x SDS buffer and 15 µL loaded analysed by electrophoresis on 10 % ammediol SDS-PAGE gels (Section 2.2.3.1) and immunoblotting (Section 2.2.3.3) with an anti-FLAG antibody. Those cell lines showing the highest expression of target protein were expanded further and frozen down.

2.2.4.3. Freezing down cell lines

Cell lines were grown to confluence in selection conditions [DMEM supplemented with 100 U/mL penicillin, 100 µg/mL streptomycin and 10 % (v/v) FCS]. For Wild-type TIMP-3, cells were selected in 800 µg/mL hygromycin B, while TIMP-3 mutant stable lines were selected in 100 µg/mL hygromycin B. The media were removed, cells trypsinised (Section 2.2.1.2) and centrifuged (5 min, 1500 rpm, room temperature). Cells were then resuspended in cryoprotectant buffer [10 % (v/v) cell-culture grade DMSO, 45 % (v/v) DMEM and 45 % (v/v) fetal bovine serum] and aliquoted at 1 mL per 1.2 mL Cryovial (Simport, Thermoscientific, Paisley, UK) and stored at -80 ^{o}C for 48 h before being moved to liquid nitrogen for long-term storage.

2.2.5. Protein purification

2.2.5.1. Purification of TIMP-3 for in vitro analysis

Recombinant C-terminally FLAG-tagged TIMP-3 was purified as per the procedure described by Troeberg et al (Troeberg et al., 2009). HEK-293-EBNA cells stably transfected with pCEP4-TIMP-3 construct were grown to confluence in DMEM supplemented with 100 U/mL penicillin, 100 µg/mL streptomycin, 10 % FCS, 800 µg/mL hygromycin B and 30 mM $NaClO_3$. Conditioned media were harvest after 48 h, centrifuged to remove cell debris, and passed over a 2 mL anti-FLAG M2-agarose resin equilibrated in TNC buffer [50 mM Tris-HCl (pH 7.5), 150 mM NaCl, 10 mM $CaCl_2$] at room temperature. To remove any non-specifically bound protein, the column was washed with 10 column volumes of high salt TNC buffer [50 mM Tris-HCl (pH 7.5), 1 M NaCl, 10 mM $CaCl_2$] and a further 5 columns volumes of TNC buffer. TIMP-3 was eluted in 5 mL fractions of 200 µg/mL FLAG peptide in TNC buffer and samples immunoblotted (Section 2.2.3.3) with anti-FLAG antibody. The active concentration of the eluted TIMP-3 was determined by titration against a known concentration of MMP-1ΔC, using the Mca-Pro-Leu-Gly-Leu-Dap(Dnp)-Ala-Arg-NH_2 substrate (Knight et al., 1992).

2.2.5.2. Purification of TIMP-3 and mutants for cell culture analysis

HEK-293-EBNA cells stably transfected with pCEP4-TIMP-3 and TIMP-3 mutant constructs were grown to confluence in DMEM supplemented with 100 U/mL penicillin, 100 µg/mL streptomycin, 10 % FCS and 30 mM $NaClO_3$, with 800 µg/mL and 100 µg/mL hygromycin B for TIMP-3 and TIMP-3 mutants, respectively. Conditioned media were harvest after 48 h, centrifuged to remove cell debris, and passed over a 2 mL anti-FLAG M2-agarose resin equilibrated

at room temperature in serum-free DMEM with 100 U/mL penicillin and 100 µg/mL streptomycin. The column was washed in 10 column volumes of serum-free DMEM with 100 U/mL penicillin and 100 µg/mL streptomycin, followed by 5 column volumes of high salt serum-free DMEM (500 mM NaCl, 100 U/mL penicillin, 100 µg/mL streptomycin) to remove any non-specifically bound proteins. The column was washed again in 10 column volumes of serum-free DMEM with 100 U/mL penicillin and 100µg/mL streptomycin. TIMP-3 and TIMP-3 mutants were eluted in 5 mL fractions using 200 µg/mL FLAG peptide in serum-free DMEM with 100 U/mL penicillin and 100 µg/mL streptomycin, and samples immunoblotted with anti-FLAG antibody. The active concentration of the eluted TIMP-3 and TIMP-3 mutants was determined by titration against a known concentration of MMP-1ΔC, using Mca-Pro-Leu-Gly-Leu-Dap(Dnp)-Ala-Arg-NH_2 substrate (Knight et al., 1992)

2.2.5.3. Purification of RAP

E. coli BL21-DE3 (heat-shock competent) were transformed with pET3a-RAP construct (Yamamoto et al., 2013) and plated on LB-carbenicillin agar. Selected colonies were cultured in LB media supplemented with 100 µg/mL carbenicillin.

Transformed BL21-DE3 (3 mL) were cultured at 37 ^{o}C, 225 rpm for 4 h, before the culture volume was increased to 20 mL and incubated overnight at 37 ^{o}C, 225 rpm. The 20 mL culture was used to inoculate 1L of LB and incubated at 37 ^{o}C, 225 rpm until an OD_{600} of 0.6 was reached. IPTG (1 mM) was added to induce expression. The culture was left to express overnight at 25 ^{o}C and 150 rpm, and cells harvested by centrifugation (8000 rpm, 15 min).

The pellet was resuspended in equilibration buffer (50 mM NaH_2PO_4 pH 8.0, 200 mM NaCl, 0.02 % NaN_3) then lysed on a French press (4 cycles, 10000 psi). The soluble fraction was loaded onto a Ni-NTA column equilibrated in equilibration buffer at a rate of 1mL/min using a peristaltic pump. The resin was sequentially washed with equilibration buffer containing 20 mM and then 50 mM imidazole to remove contaminants. Bound protein was eluted in equilibration buffer containing 250 mM imidazole and samples analysed by SDS-PAGE on a 10 % acrylamide ammediol gel (Section 2.2.3.1.)

2.2.6. Calculation of apparent equilibrium constant, $K_{i(app)}$

2.2.6.1. Calculation of TIMP-3 affinity for MMP-1

Human MMP-1ΔC was expressed in *E. coli* and purified as previously described (Chung et al., 2000). The protein was obtained as a gift from Dr Robert Visse, University of Oxford. The active concentration of MMP-1ΔC was determined by titration against a known concentration of the synthetic inhibitor GM6001. The enzyme assays were conducted in TNC buffer (50 mM Tris-HCl, pH 7.5, 150 mM NaCl, 10 mM $CaCl_2$, 0.05 % Brij-35 and NaN_3) at 37 ^oC, using a Gemini microplate spectrofluorometer. MMP-1ΔC (1.5 nM) was incubated with Wild-type and mutant TIMP-3 (0.5-10 nM) for 1 h at 37 ^oC and residual activity against Knight's fluorescent peptide substrate (Knight et al., 1992) [Mca-Pro-Leu-Gly-Leu-Dap(Dnp)-Ala-Arg-NH_2, 1.5 μM, λ_{ex} 325 nm, λ_{em} 393 nm] determined. Prism software (GraphPad, La Jolla, CA, USA) was used to fit the data to the tight-binding equation (Bieth, 1995a):

$$\frac{v_s}{v_o} = 1 - \frac{(E_o + I_o + K_{i(app)} - [(E_o + I_o + K_{i(app)})^2 - 4E_oK_{i(app)}]^{\frac{1}{2}}}{2E_o}$$

where v_s is the steady state velocity, v_o is the equilibrium rate of substrate hydrolysis in the absence of inhibitor, E_o is the total enzyme concentration, I_o is the total inhibitor concentration and $K_{i(app)}$ is the apparent inhibition constant. $K_{i(app)}$ was calculated using the known enzyme concentration and is shown with the error on the fit.

2.2.6.2. Calculation of TIMP-3 affinity for MMP-2

MMP-2 catalytic domain (MMP-2ΔC, lacking hemopexin-domain residues 466 to 660) was a gift from Dr Linda Troeberg, University of Oxford. The protein was expressed in HEK293-EBNA cells using a pCEP4-based expression vector (Troeberg et al., 2009). The active concentration of MMP-2ΔC was determined by titration against a known concentration of N-TIMP-3. Enzyme assays were conducted in TNC buffer (50 mM Tris-HCl, pH 7.5, 150 mM NaCl, 10 mM CaCl2, 0.05 % Brij-35 and NaN_3) at 37 ºC, using a Gemini microplate spectrofluorometer. MMP-2ΔC (1 nM) was incubated with Wild-type and mutant TIMP-3 (0.5-10 nM) and residual activity against Knight's fluorescent peptide substrate (Knight et al., 1992) [Mca-Pro-Leu-Gly-Leu-Dap(Dnp)-Ala-Arg-NH_2], 1.5 μM, with λ_{ex} 325 nm, λ_{em} 393 nm) determined (1 h, 37 ºC). Data were analysed as for MMP-1 in Section 2.2.6.1.

2.2.6.3. Calculation of TIMP-3 affinity for MMP-3

Human MMP-3ΔC was expressed in *E. coli* (Suzuki et al., 1998) was a gift from Dr Linda Troeberg, University of Oxford. Enzyme assays were conducted in TNC buffer (50 mM Tris-HCl, pH 7.5, 150 mM NaCl, 10 mM $CaCl_2$, 0.05 % Brij-35 and 0.02 % NaN_3) at 37 ºC, using a Gemini microplate spectrofluorometer. MMP-3ΔC (1 nM) was incubated with Wild-type or mutant

TIMP-3 (0.5-10 nM) for 1 h at 37 ^{o}C and residual activity against NFF-3 substrate (Nagase et al., 1994a) [Mca-Arg-Pro-Lys-Pro-Tyr-Ala-Nva-Trp-Met-Lys(Dnp)-NH_2, 1.5 μM, λ_{ex} 325 nm, λ_{em} 393 nm] determined (1 h, 37 ^{o}C). Data were analysed as for MMP-1 in Section 2.2.6.1.

2.2.6.4. Calculation of TIMP-3 affinity for ADAMTS-4

ADAMTS-4 lacking the C-terminal spacer domain was a gift from Dr Linda Troeberg, University of Oxford. ADAMTS-4 (0.5 nM) was incubated with Wild-type or mutant TIMP-3 (0.5-10 nM) for 1 h at 37 ^{o}C and residual activity against GSK substrate (carboxyfluorescein-Ala-Glu-Leu-Asn-gly-Arg-Pro-Ile-Ser-Ile-Ala-Lys-N,N,N',N'-tetramethyl-6-carboxyrhodamine, 0.5 μM) (Wayne et al., 2007) determined (1 h, 37 ^{o}C). Fluorescence was quantified using a Gemini microplate spectrofluorometer with λ_{ex} 485 nm, λ_{em} 538 nm. Data were analysed as for MMP-1 in Section 2.2.6.1.

2.2.6.5. Calculation of TIMP-3 affinity for ADAMTS-5

ADAMTS-5 lacking the C-terminal thrombospondin domain was a gift from Dr Linda Troeberg, University of Oxford. The protein was expressed and purified in accordance with published methods (Gendron et al., 2007). ADAMTS-5 (0.5 nM) was incubated with Wild-type or mutant TIMP-3 (0.5-10 nM), for 1 h at 37 ^{o}C and residual activity against a brevican-based substrate (Matthews et al., 2000; Nakamura et al., 2000) (ortho-aminobenzoyl-Thr-Glu-Ser-Glu-Ser-Arg-Gly-Ala-Ile-Tyr-(N-3-[2,4-dinitrophrenyl]-L-2,3-diamiopropionyl)-Lys-Lys-NH_2, 20 μM, λ_{ex} 300 nm, λ_{em} 430 nm) determined (18 h, 37 ^{o}C). Data were analysed as for MMP-1 in Section 2.2.6.1.

2.2.6.6. Calculation of TIMP-3 affinity for ADAM-17

ADAM-17 was a gift from Prof Gillian Murphy (University of Cambridge), and was expressed and purified in accordance with published methods (Milla et al., 1999). Briefly, the mature recombinant TACE ectodomain (Arg^{215}-Agr^{651}) was expressed in baculovirus-infected sf9 cells and purified by gel chromatography from concentrated cell culture media.

ADAM-17 (1 nM) was incubated with Wild-type or mutant TIMP-3 (0-25 nM) for 1 h at 37 ^{o}C in a modified TNC buffer (50 mM Tris-HCl, pH7.5, 25 mM NaCl, 10 mM $CaCl_2$, 0.05 % Brij-35 and 0.02 % NaN_3) and residual activity against fluorogenic TACE substrate IV (Abz-Leu-Ala-Gln-Ala-Val-Arg-Ser-Ser-Ser-Arg-Dpa, 20 μM) (Jin et al., 2002) determined (1 h, 37 ^{o}C). Fluorescence was quantified using a Gemini microplate spectrofluorometer with λ_{ex} 320 nm, λ_{em} 420 nm. Data were analysed as for MMP-1 in Section 2.2.6.1.

2.2.7. Endocytosis assays

2.2.7.1. Immunoblot analysis of TIMP-3 endocytosis from culture medium

HTB94 cells were seeded at 8 x 10^5 per well in a 12-well plate and incubated overnight (37 ^{o}C, 5 % (v/v) CO_2) in DMEM supplemented with 100 U/mL penicillin,100 μg/mL streptomycin and 10 % FCS. Cells were washed with serum-free DMEM 3 times before dialysed conditioned medium containing Wild-type or mutant TIMP-3 was added in a final volume of 1 mL DMEM supplemented 0.1 % FCS, 100 U/mL penicillin and 100 μg/mL streptomycin. Samples were harvested at time points (0 – 24 h) and TCA precipitated [5 % (v/v), 4 ^{o}C, overnight]. Following centrifugation (13000 rpm, 15 min, 4 ^{o}C), precipitated samples were resuspended in 30 μL of 2x ammediol SDS-PAGE

loading buffer and 15 µL analysed by immunoblotting using an anti-FLAG-M2 antibody (Section 2.2.3.1). Band intensity was quantified using Phoretix software (Section 2.2.3.5) and results represented as a percentage of pixel volume at time =0.

2.2.8. LRP-1 binding ELISA

Binding of Wild-type and mutant TIMP-3 to LRP-1 was evaluated by ELISA. Full-length LRP-1 (5 nM in HEPES, pH 7.4, 0.05 % Brij-35, BioMac, Leipzig, Germany) was coated onto a medium-binding ELISA plate (overnight, 4 ^{o}C). Wells were blocked (10 % BSA in TNC buffer, 1 h, room temperature) and incubated with doubling dilutions of Wild-type or mutant TIMP-3 in 5 % BSA in TNC buffer (3 h, room temperature). Bound TIMP-3 was detected using an M2 anti-FLAG antibody (1:5000 dilution in 5 % BSA in TNC buffer, 2 h, room temperature) followed by an anti-mouse secondary antibody conjugated with HRP (1:1000 dilution in 5 % BSA in TNC buffer, 1 h, room temperature). Tetramethylbenzidine HRP-substrate was added to quantify binding, the reaction stopped with 2N H_2SO_4 and absorbance at 450 nm measured using a FLUOstar OMEGA microplate reader (BMG Labtech, Buckinghamshire, UK).

2.2.9. Heparin binding ELISA

Heparin-binding plates (BD Biosciences, Oxford, UK) were coated with 10 µg/mL heparin or heparan sulfate in PBS overnight. Wells were blocked using 0.2 % gelatin in PBS (1 h, 37 ^{o}C) and washed in TBS containing 0.1 % (v/v) Tween-20 after this and every subsequent step. Wells were then incubated with doubling dilutions of Wild-type or mutant TIMP-3 in blocking solution. Bound TIMP-3 was detected by incubation of wells with an M2 anti-FLAG antibody (3 h, 37 ^{o}C) and then with an anti-mouse secondary antibody

conjugated with HRP (1 h, 37 °C) (DAKO UK Ltd, Cambridgeshire, UK). Hydrolysis of tetramethylbenzidine substrate (KPL Peroxidase Substrate Gaithersburg, MA, US) was stopped with 2N H_2SO_4 and measured at 450 nm using a FLUOstar OMEGA microplate reader (BMG Labtech, Buckinghamshire, UK).

2.3. Measuring GAG release from cartilage

2.3.1. Cartilage explant dissection

Porcine explants were harvested from the metacarpophalangeal joints of 3-9 month old pigs using a 4 mm biopsy punch. Explants were rested in cartilage growth medium (DMEM supplemented with 10 % FCS, 100 U/mL penicillin, 100 mg/mL streptomycin, 2 mg/mL amphotericin B and 10 mM HEPES), with one explant per well in a 48 well plate (48 h, 37 °C). Explants were washed 3 times in serum-free cartilage growth medium (DMEM with 100 U/mL penicillin, 100 mg/mL streptomycin, 2 mg/mL amphotericin B and 10 mM HEPES) and treated with reagents according to the experimental design. The conditioned medium was harvested after 24-72 h and GAG release quantified by dimethylmethylene blue assay (DMMB assay) or immunoblotting.

2.3.1.1. Generation of DMMB assay standard curve

GAG released by cartilage or chondrocytes into the conditioned medium was measured using the dimethylmethylene blue (DMMB) assay (Farndale et al., 1982). Bovine chondroitin-4-sulfate (0-10 µg) (Sigma-Aldrich, Dorset, UK) was added to a 96-well plate and mixed with DMMB dye (16 mg DMMB, 3.04 g glycine, 1.6 g NaCl , 95 ml of 0.1 M Acetic Acid per L). Addition of DMMB dye caused a shift in the absorption spectrum, which was measured in triplicate at

525 nm. Data were plotted in GraphPad Prism software (San Diego, CA, USA) and a standard curve generated by linear regression. Absorbance at 525 nm correlates with GAG content when absorption values fall within the linear range of the DMMB standard curve (Figure 17). This equation was then used to determine the amount of GAG present in conditioned media samples.

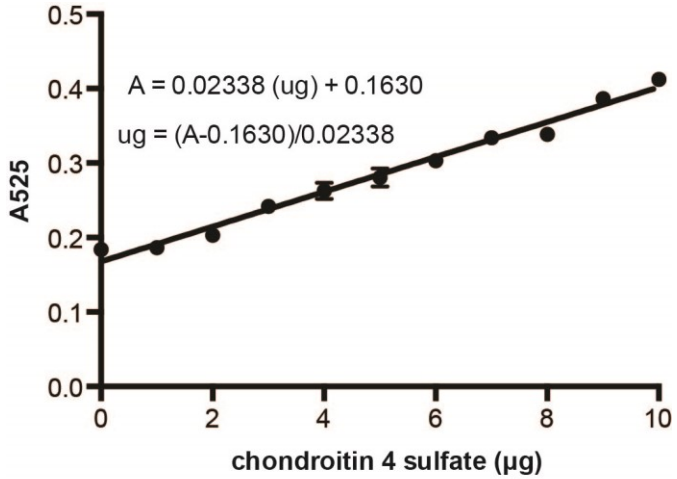


Figure 17: DMMB standard curve using chondroitin-4-sulfate.
Bovine chondroitin-4-sulfate (0-10 µg)(Sigma-Aldrich) was added to wells of a 96-well plate and DMMB dye added. Absorbance at 525 nm was measured in triplicate and values plotted in GraphPad Prism software (San Diego, CA, USA). Linear regression used to fit an equation to the data. Absorbance at 525 nm correlates with GAG content when absorption values are within the linear range of the DMMB standard curve.

2.3.1.2. Analysis of GAG release by DMMB assay

GAG released into the conditioned medium was measured in triplicate using the DMMB assay (Farndale et al., 1982). Fresh serum-free cartilage growth medium (DMEM with 100 U/mL penicillin, 100 mg/mL streptomycin, 2 mg/mL amphotericin B and 10 mM HEPES) was added to the rested explants at 250 µL per well with or without 10 ng/mL recombinant IL-1α (kindly provided by Prof. J. Saklatvala, University of Oxford) and increasing concentrations of Wild-type or mutant TIMP-3. The conditioned medium was harvested after 48 h and GAG release quantified by DMMB assay. In a 96-well plate, DMMB dye

(200 µL) was added to the conditioned media samples (1-3 µL) and absorbance at 525 nm measured in triplicate. The equation generated by the standard curve (Section 2.3.1.1) was used to determine the amount of GAG present for absorbance values that fell within the linear range of the standard curve.

2.3.2. Analysis of GAG release by immunoblotting

GAG released into the conditioned medium was visualised by applying samples to a 6 % Tris-glycine gel (Section 2.3.2). Samples were first deglycosylated by adding an equal volume of 2x GAG buffer (200 mM sodium acetate, 100 mM Tris-HCl pH 8, 100 mM EDTA) before adding chondroitinase ABC (0.05 U, Sigma-Aldrich, Dorset, UK) and keratanase (0.05 U, Seikagaku, Tokyo, Japan) overnight at 37 ^{o}C. Ice-cold acetone (1 mL) was then added and the mixture incubated at -20 ^{o}C overnight. Samples were centrifuged (13000 rpm, 10 min, 4 ^{o}C), resuspended in 2x Tris-glycine SDS loading buffer and separated on a 6 % SDS-PAGE Tris-glycine gel before being transferred to a PVDF membrane (Section 2.2.3.3). Bands were detected using an anti-AGEG primary antibody (1:1000 dilution of anti-serum) and an anti-rabbit IgG conjugated antibody (1:5000). Bands were quantified by densitometry (Section 2.2.3.5).

Chapter 3: Design of an endocytosis-resistant TIMP-3

3.1 Introduction

The molecular mechanisms of ligand binding to LRP-1 has been investigated using various LRP-1 ligands and also the molecular chaperone RAP. Several studies have indicated that LRP-1 binds to its ligands through interaction between acidic pockets on the complementary repeats (CRs) of LRP-1 and lysine residues on the ligand. RAP associates with LRP-1 during its passage through the secretory pathway, to prevent premature intracellular engagement of LRP-1 with its ligands.

While not a physiological LRP-1 ligand, RAP has high affinity for LRP-1 and it has been widely studied as a prototypic ligand. It has been determined that the interaction between RAP and LRP-1 is electrostatic, mediated by basic lysine residues on RAP and acidic pockets of the CRs on LRP-1 (Fisher et al., 2006). Despite the electrostatic nature of the interaction, arginine residues on the RAP cannot substitute for the lysine residues (Dolmer et al., 2013).

Using differential scanning calorimetry Migliorini and colleagues identified K256 and K270 on RAP as a critical di-lysine pair mediating LRP-1 binding (Migliorini et al., 2003). Further studies using NMR (Jensen et al., 2006), X-ray crystallography (Fisher et al., 2006), alanine scanning mutagenesis, fluorescence isothermal titration calorimetry, surface plasmon resonance (van den Bigglelaar et al., 2011) and isothermal titration calorimetry (Dolmer et al., 2013) supported this finding. The X-ray structure of RAP (domain 3) in complex with 2 sequential CRs (CR3 and CR4) of a low density lipoprotein receptor gave further insight to this binding (Fisher et al., 2006). It was observed that, measuring from α-carbon to α-carbon, that the critical lysine residues were separated by 21 Å (Fisher et al., 2006). Further RAP-LRP-1 binding studies

supported this identification of the ligand-binding motif comprising a di-lysine pair separated by 21 Å.

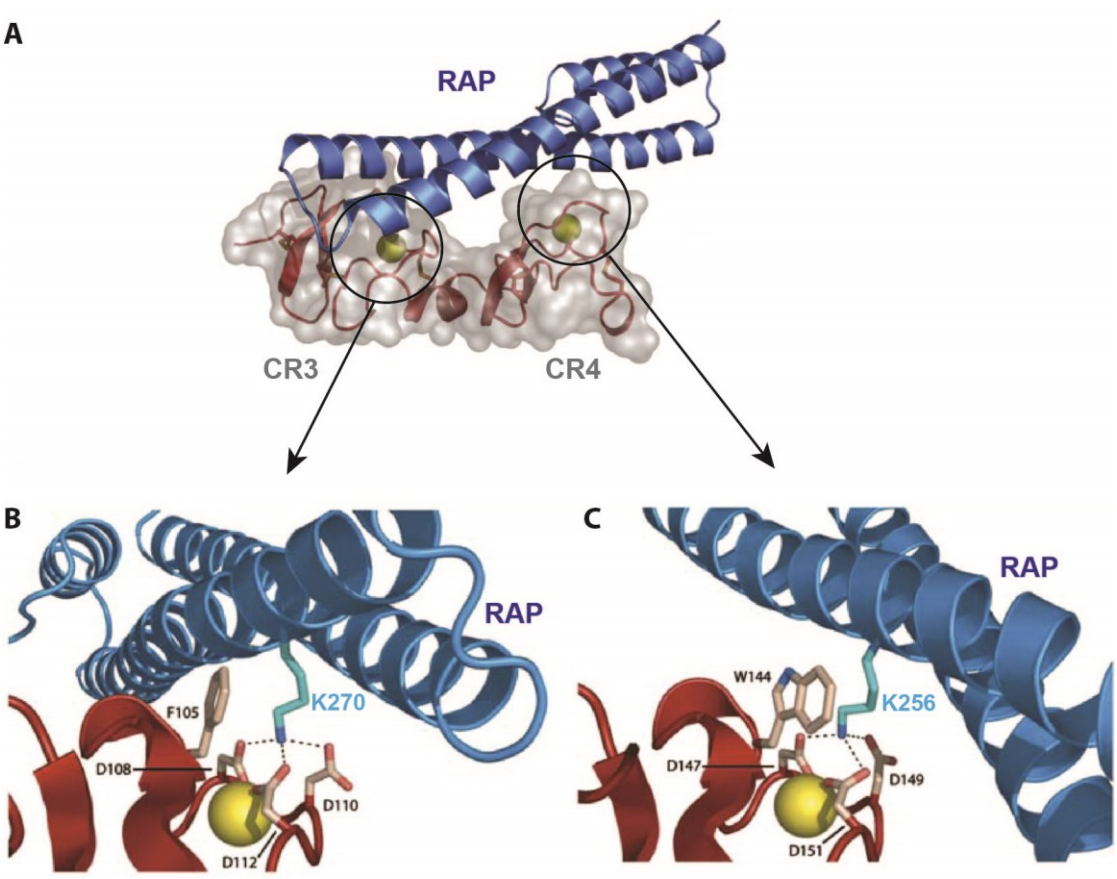


Figure 18: RAP binding to LRP-1 is mediated by a di-lysine pair separated by 21Å.

(**A**) Interaction between LRP-1 CR3 and CR4 (gray) and RAP (blue), showing the electrostatic interaction of K270 (**B**) and K256 (**C**) with the acidic pockets of CR3 and CR4 respectively. Adapted from Fisher et al. (2006).

A quantitative investigation of the contribution of individual lysine residues in RAP to LRP-1 binding was conducted using isothermal titration calorimetry (Dolmer et al., 2013). A range of RAP domain 3 mutants was generated, in which lysine residues were mutated to alanine. In this way 4 lysine residues were identified as being involved in RAP-LRP-1 binding. These 4 lysine residues included the previously identified K256 and K270, as well as K253 and K289. The greatest loss in affinity was observed for K256A where affinity

was reduced 380-fold, followed by K270A with a 44-fold reduction. K253A and K289A demonstrated a 7 and 8-fold reduction in affinity respectively. Multiple di-lysine pairs were generated, including K256/K289, K253/K270 and K253/K289, and all showed further reduced affinity. The relative distance between lysine residues was also quantified, with K256 and K276 being separated 21 Å, the optimal separation identified by Fisher et al. K256 and K289 were shown to be separated by 18 Å, K253 and K270 by 25.3 Å and K253 and K289 by 22.2 Å The difference in separation of the respective lysine residues may have contributed to their differing effect on affinity. It was observed that K289 could compensate for the loss of K270, albeit with a reduced binding affinity.

α_2-macroglobulin (α_2M) is the best studied of the physiological LRP-1 ligands, and it binds to LRP-1 when in complex with target proteases or when it is chemically “activated”, such as by methylamine. Early studies using methylamine modified α_2M showed that one or more lysine residue was required for LRP-1 binding (Noe et al., 2001). Subsequent work using site-directed mutagenesis and ELISA, identified lysine residues 1370 and 1374 as important mediators of binding to LRP-1 (Lochter et al., 1997).

Fluorescence spectroscopy was used to investigate the binding of plasminogen activator inhibitor-1 (PAI1) to LRP-1 (Jensen et al., 2009a). The minimal binding requirements for PAI1 were found to include critical lysine residues projecting outwards from the surface of PAI1, which allowed electrostatic interaction with the binding cleft in the CR. The presence of an additional proximal positive charge was shown to further enhance this electrostatic interaction. The individual lysine residues of the di-lysine pair

required sufficient separation to enable both to engage with 2 successive CR domains (Jensen et al., 2009a). While the distance between interacting lysine residues was not measured in this study, PAI1 was shown to bind to 2 sequential binding domains, CR3 and CR4.

This di-lysine motif was also observed for Apolipoprotein E (ApoE) binding to LRP-1, with mutation of 2 key residues (K143 and K146) impairing binding (Guttman et al., 2010).

We set out to identify the LRP-1 binding motif in TIMP-3 and to ablate this binding using site-directed mutagenesis, thereby generating an endocytosis-resistant TIMP-3 mutant.

3.2 Results

3.2.1 Identification of potential LRP-1 binding motif in TIMP-3

Based on the binding motif identified for the binding of RAP and other ligands to LRP-1, we predict that a similarly spaced di-lysine pair projecting outwards from the surface of TIMP-3 structure will similarly mediate TIMP-3 binding to LRP-1. TIMP-3 has 17 lysine residues (Table 1) and we sought to identify those that fit the criteria for an LRP-binding motif.

3.2.1.1 Model of Wild-type TIMP-3 three-dimensional structure

The crystal structure for full-length TIMP-3 has not been solved, but the crystal structure for the TIMP-3 N-terminal domain (N-TIMP-3) in complex with TACE (Wisniewska et al., 2008) is available, as are the structures of full-length TIMP-1 in complex with the catalytic domain of MMP-3 (Gomis-Ruth et al., 1997) and full-length TIMP-2 (Tuuttila et al., 1998). As TIMP-3 shows high amino acid sequence homology with both TIMP-1 and TIMP-2 (30 % and 38 %

homology repectively) (Pavloff et al., 1992) we were able to construct a model of the TIMP-3 structure. Dr. Deendayal Dinakarpandian in Prof. Hideaki Nagase's laboratory generated a model of the TIMP-3 structure using PyMOL molecular graphics system and the available TIMP structures.

Table 10: Amino acid sequence of FLAG-tagged human TIMP-3.

Signal peptide residues are shown in green, N-terminal domain residues in blue, C-terminal domain residues in black and FLAG-tag residues in purple. The 17 TIMP-3 lysine residues are highlighted in red.

ATG	ACC	CCT	TGG	CTC	GGG	CTC	ATC	GTG	CTC	CTG	GGC	AGC	TGG	AGC	CTG	GGG	GAC	TGG	GGC	GCC	GAG	GCG
M	T	P	W	L	G	L	I	V	L	L	G	S	W	S	L	G	D	W	G	A	E	A
TGC	ACA	TGC	TCG	CCC	AGC	CAC	CCC	CAG	GAC	GCC	TTC	TGC	AAC	TCC	GAC	ATC	GTG	ATC	CGG	GCC	AAG	GTG
C	T	C	S	P	S	H	P	Q	D	A	F	C	N	S	D	I	V	I	R	A	K	V
GTG	GGG	AAG	AAG	CTG	GTA	AAG	GAG	GGG	CCC	TTC	GGC	ACG	CTG	GTC	TAC	ACC	ATC	AAG	CAG	ATG	AAG	ATG
V	G	K	K	L	V	K	E	G	P	F	G	T	L	V	Y	T	I	K	Q	M	K	M
TAC	CGA	GGC	TTC	ACC	AAG	ATG	CCC	CAT	GTG	CAG	TAC	ATC	CAC	ACG	GAA	GCT	TCC	GAG	AGT	CTC	TGT	GGC
Y	R	G	F	T	K	M	P	H	V	Q	Y	I	H	T	E	A	S	E	S	L	C	G
CTT	AAG	CTG	GAG	GTC	AAC	AAG	TAC	CAG	TAC	CTG	CTG	ACA	GGT	CGC	GTC	TAT	GAT	GGC	AAG	ATG	TAC	ACG
L	K	L	E	V	N	K	Y	Q	Y	L	L	T	G	R	V	Y	D	G	K	M	Y	T
GGG	CTG	TGC	AAC	TTC	GTG	GAG	AGG	TGG	GAC	CAG	CTC	ACC	CTC	TCC	CAG	CGC	AAG	GGG	CTG	AAC	TAT	CGG
G	L	C	N	F	V	E	R	W	D	Q	L	T	L	S	Q	R	K	G	L	N	Y	R
TAT	CAC	CTG	GGT	TGT	AAC	TGC	AAG	ATC	AAG	TCC	TGC	TAC	TAC	CTG	CCT	TGC	TTT	GTG	ACT	TCC	AAG	AAC
Y	H	L	G	C	N	C	K	I	K	S	C	Y	Y	L	P	C	F	V	T	S	K	N
GAG	TGT	CTC	TGG	ACC	GAC	ATG	CTC	TCC	AAT	TTC	GGT	TAC	CCT	GGC	TAC	CAG	TCC	AAA	CAC	TAC	GCC	TGC
E	C	L	W	T	D	M	L	S	N	F	G	Y	P	G	Y	Q	S	K	H	Y	A	C
ATC	CGG	CAG	AAG	GGC	GGC	TAC	TGC	AGC	TGG	TAC	CGA	GGA	TGG	GCC	CCC	CCG	GAT	AAA	AGC	ATC	ATC	AAT
I	R	Q	K	G	G	Y	C	S	W	Y	R	G	W	A	P	P	D	K	S	I	I	N
GCC	ACA	GAC	CCC	GAT	TAC	AAG	GAT	GAC	GAC	GAT	AAG	TAG										
A	T	D	P	D	Y	K	D	D	D	D	K	Z										

Figure 19 shows the overlay between the crystal structure of N-TIMP-3 (orange) and the modeled structure for full length TIMP-3 (blue). The proposed structure shows overall good agreement with the published structure for the N-terminal domain, indicating the validity of the model. The model of full-length TIMP-3 was then used as the basis for predicting of endocytosis-resistant TIMP-3 mutants.

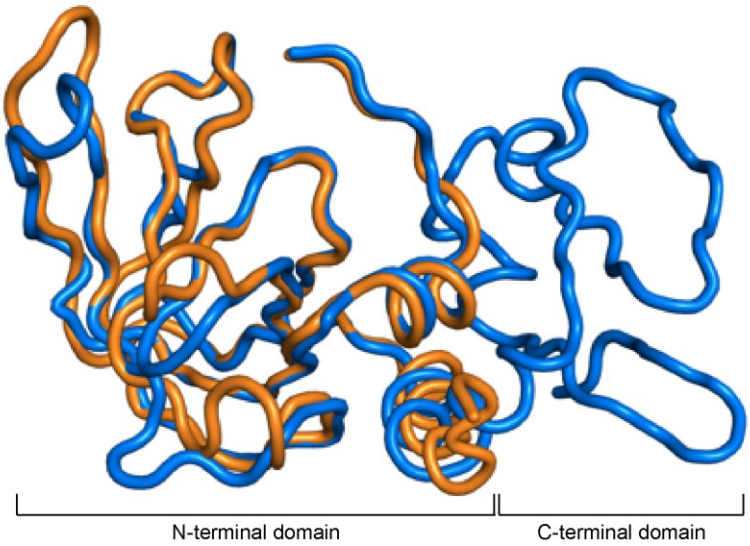


Figure 19: Comparison of N-TIMP-3 crystal structure and proposed model of full-length TIMP-3 structure.

The published N-TIMP-3 stucture (PDB ref 3CKI) is shown in orange and the model of full-length TIMP-3 generated by Dr. Deendayal Dinakarpandian is shown in blue. The structures display good agreement.

3.2.1.2 Potential lysine pairs satisfying the LRP-1 binding motif

Analysis of the TIMP-3 mutant was performed with the help of Dr Robert Visse, University of Oxford. Using the proposed TIMP-3 structure (Figure 20) we identified pairs of lysine residues meeting the LRP-1 binding motif criteria, namely a di-lysine pair with lysine residues projecting outwards from the ligand surface and separated by 21 Å.

Using PyMOL, we established that all 17 TIMP-3 lysine residues are located on the surface of TIMP-3. The distance between the α-carbons of all pairs of lysine residues was measured and pairs of lysine residues approximately 21Å apart were identified (Table 11). We identified 10 di-lysine pairs, comprising 12 single lysine residues that met the desired criteria and were selected for mutation.

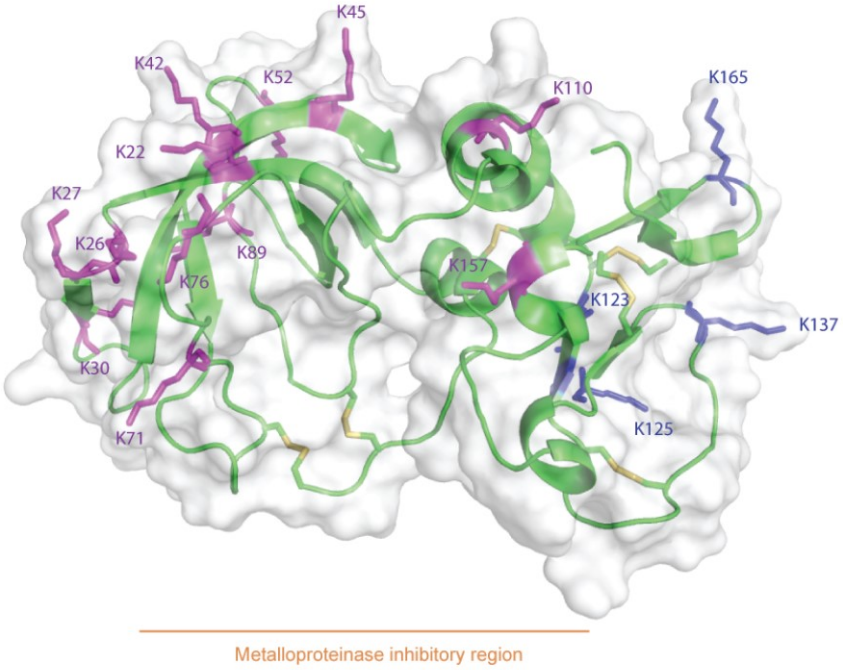


Figure 20: Model of full-length TIMP-3 structure, highlighting lysine residues. Lysine residue side chains are highlighted and numbered. Those compatible with the LRP-1-binding motif are shown as purple sticks and those not meeting the binding-motif criteria are shown in blue. A shortlist of di-lysine pairs meeting the selection criteria was generated using this model.

Table 11: Distance between α-carbons of lysine residues in proposed di-lysine pairs of TIMP-3.

Potential LRP-1-binding di-lysine pair	Distance between lysine residues (Å)
K22A/K110A	16.7
K22A/K157A	22.3
K26A/K45A	19.4
K27A/K45A	23.9
K30A/K52A	23
K30A/K76A	21.2
K42A/K110A	20.6
K42A/K157A	25.9
K45A/K89A	15.6
K71A/K157A	24.6

3.2.2. Generation of TIMP-3 mutants

C-terminally FLAG-tagged TIMP-3 in pCEP4 mammalian expression vector (Troeberg et al., 2009) was used as a template to generate single lysine to alanine mutations at the desired positions in TIMP-3 using Agilent Technologies QuikChange II XL site-directed mutagenesis kit (Agilent Technologies, Cheshire, UK). This kit has been optimised for mutagenesis of large constructs such as the 10.4 kb pCEP4 vector used here and does not require unique restriction sites, or in vitro methylation steps. An overview of the method is shown in Figure 21.

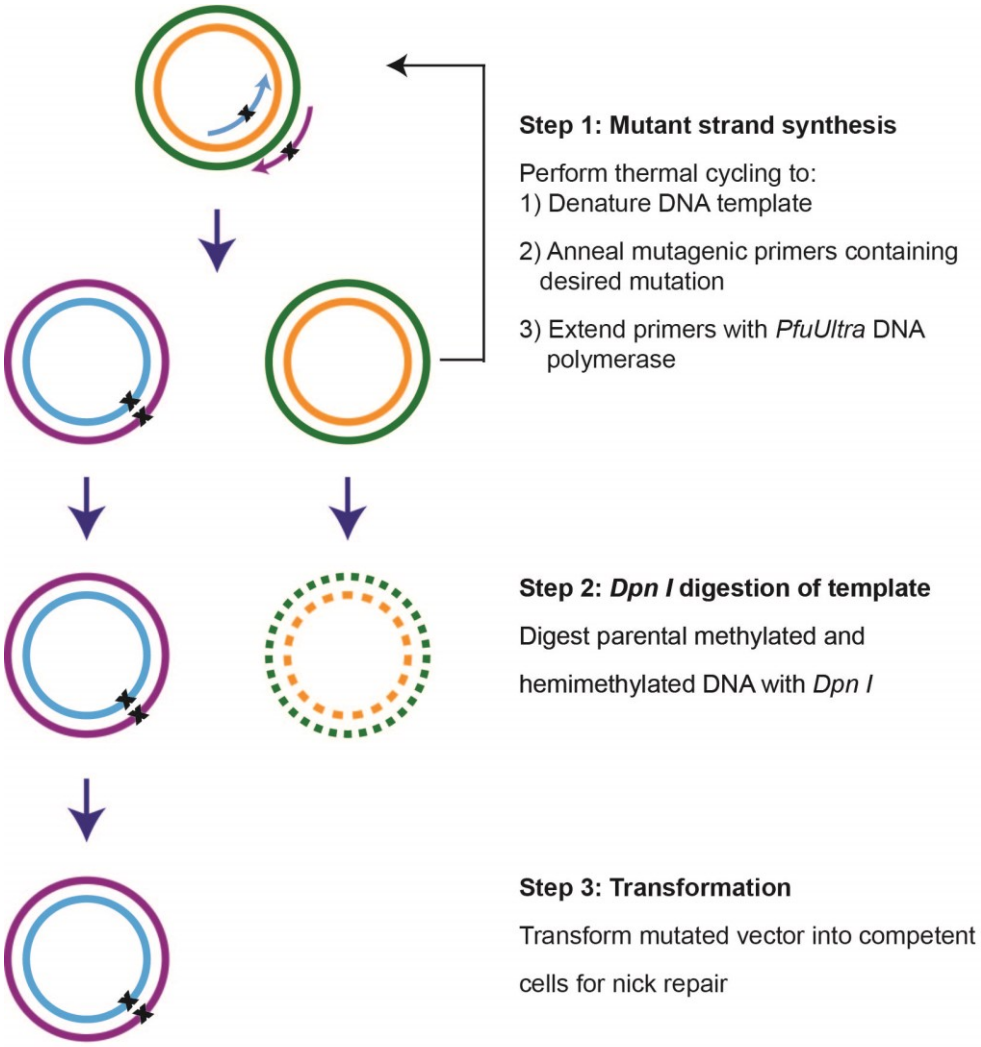


Figure 21: Agilent QuikChange II XL Site-Directed Mutagenesis Strategy. (adapted from Agilent product literature).

TIMP-3 mutants were created by polymerase chain reaction using primers containing the desired mutation, and pCEP4 vector encoding Wild-type TIMP-3 as a template. Use of *Pfu* high-fidelity DNA polymerase reduces the chance of random mutations. Parental methylated DNA is digested by *Dpn I*, the DNA transformed by heat shock into *E. coli* XL 10-Gold Ultracompetent cells and candidate colonies on LB-carbenicillin agar plates screen by restriction digest and sequencing.

3.2.2.1. TIMP-3 mutant primer design

Primers were designed in accordance with Agilent QuikChange II XL site-directed mutagenesis kit guidelines as outlined in Table 12.

Table 12: Agilent QuikChange II XL Site-Directed Mutagenesis kit primer design guidelines.

1.	Both forward and reverse primers must contain the desired mutation and anneal to the same sequence on opposite strands of the plasmid.
2.	Primers must be 25-45 bases in length with a melting temperature (T_m) of ≥ 78 °C Tm = 81.5 + 0.41(% GC)-(675/N)-% mismatch Where N = Primer length in bases % GC = percentage guanine and cytosine in whole numbers % mismatch = percentage mutation in whole numbers
3.	The mutation should be in the middle of the primer, within ~10-15 bases complementary on both sides
4.	The primers should have a minimum GC content of 40 % and should terminate in one or more C or G bases.

Table 13 and Table 14 show design of primers for 2 of the TIMP-3 single mutants following Agilent QuikChange II XL site-directed mutagenesis kit guidelines. The remaining 10 TIMP-3 single mutants were designed the same manner. Primers for all 12 TIMP-3 single mutants are shown in Figure 22.

Table 13: Design of primers for generation of TIMP-3 K22A.

Residue No.	5	16	17	18	19	20	21	22	23	24	25	26	27	28
Residue	S	D	I	V	I	R	A	A	V	V	G	K	K	L
Forward primer	5'-TCC	GAC	ATC	GTG	ATC	CGG	GCC	GCG	GTG	GTG	GGG	AAG	AAG	CTG -3'
Reverse Primer	3'-AGG	CTG	TAG	CAC	TAG	GCC	CGG	CGC	CAC	CAC	CCC	TTC	TTC	GAC -5'
Tm for both forward and reverse = 77 °C								**GC content** for both forward and reverse = 67 %						

Table 14: Design of primers for generation of TIMP-3 K42A

Residue No.	35	36	37	38	39	40	41	42	43	44	45	46	47	48	49
Residue	G	T	L	V	Y	T	I	A	Q	M	K	M	Y	R	G
Forward primer	5' – GGC	ACG	CTG	GTC	TAC	ACC	ATC	GCG	CAG	ATG	AAG	ATG	TAC	CGA	GGC -3'
Reverse Primer	3' – CCG	TGC	GAC	CAG	ATG	TGG	TAG	CGC	GTC	TAC	TTC	TAC	ATG	GCT	CCG -5'
Tm for both forward and reverse = 76 °C								**GC content** for both forward and reverse = 60 %						

Mutant	Primer	T_m (°C)	% GC
K22A	**F** 5'-TCCGACATCGTGATCCGGGCCGCGGTGGTGGGGAAGAAGCTG-3'	77	67
	3'-AGGCTGTAGCACTAGGCCCGGCGCCACCACCCTTCTTCGAC-5' **R**	77	67
K26A	**F** 5'-CGGGCCAAGGTGGTGGGGGCGAAGCTGGTAAAGGAGGGGGCCC-3'	78	71
	3'-GCCCGGTTCCACCACCCCCGCTTCGACCATTTCCTCCCCGGG-5' **R**	78	71
K27A	**F** 5'-CGGGCCAAGGTGGTGGGGAAGGCGCTGGTAAAGGACGGGCCC-3'	78	71
	3'-GCCCGGTTCCACCACCCCTTCCGCGACCATTTCCTGCCCCGGG-5' **R**	78	71
K30A	**F** 5'-GTCGTGGGGAAGAAGCTGGTAGCGGAGGGGCCCTTCGGCACGCTG-3'	78	71
	3'-CAGCACCCCTTCTTCGACCATCGCCTCCCCGGGAAGCCGTGCGAC-5' **R**	78	71
K42A	**F** 5'-GGCACGCTGGTCTACACCATCACGCAGATGAAGATGTACCAGGC-3'	76	60
	3'-CCGTGCGACCAGATGTGGTAGCGCGTCTACTTCTACATGGCTCCG-5' **R**	76	60
K45A	**F** 5'-ACGCTGGTCTACACCATCAAGCAGATGGCGATGTACCGAGGCTTCACC-3'	75	56
	3'-GACCAGATGTGGTAGTTCGTCTGCCGCTACATGGCTCCGAAGTGG-5' **R**	75	56
K52A	**F** 5'-AAGATGTACCGAGGCTTCACCGCGATGCCCCATGTGCAGTACATCCAC-3'	74	56
	3'-TTCTACATGGCTCCGAAGTGGCGCTACGGGGTACACGTCATGTAGGTG-5' **R**	74	56
K71A	**F** 5'-GCTTCCGAGAGTCTCTGTGGCCTTGCGCTGGAGGTCAACAAGTACCAG-3'	75	67
	3'-CGAAGGCTCTCAGAGACACCGGAACGCGACCTCCAGTTGTTCATGCTC-5' **R**	75	67
K76A	**F** 5'-GGCCTTAAGCTGGAGGTCAACGCGTACCAGTACCTGCTGACAGGTCGC-3	76	60
	3'-CCGGAATTCGACCTCCAGTTGCGCATGGTCATGGACGACTGTCCAGCG-5' **R**	76	60
K89A	**F** 5'-GGTCGCGTCTATGATGGCGCGATGTACACGGGGCTGTGC-3'	74	64
	3'-CCAGCGCAGATACTACCGCGCTACATGTGCCCCGACACG-5' **R**	74	64
K110A	**F** 5'-CAGCTCACCCTCTCCCAGCGCGCGGGGCTGAACTATCGGTATC-3'	76	65
	3'-GTCGAGTGGGAGAGGGTCGCGCGCCCCGACTTGATAGCCATAG-5' **R**	76	65
K157A	**F** 5'-GGTTACCCTGGCTACCAGTCCGCGCACTACGCCTGCATCCGG-3'	76	67
	3'-CCAATGGGACCGATGGTCAGGCGCGTGATGCGGACGTAGGCC-5' **R**	76	67

Figure 22: Primers all 12 TIMP-3 single mutants.

Primers for the design of the 12 TIMP-3 single mutants were designed according to the Agilent QuikChange II XL site-directed mutagenesis guidelines.

3.2.2.2. Polymerase chain reaction reagent protocol

All single lysine to alanine TIMP-3 single mutants were first generated using Wild-type TIMP-3 as the DNA template for the Agilent QuikChange mutagenesis reaction. To generate double mutants, QuikChange reactions were carried out using the desired single mutants as templates with the appropriate mutagenic primers. For example, to generate TIMP-3 K42A/K110A, the already generated TIMP-3 K42A single mutant was used as the template with K110A primers.

Polymerase chain reaction (PCR) reagent conditions were used as per Agilent QuikChange II XL site-directed mutagenesis guidelines with some modifications shown in Table 15 (modifications highlighted in red). Due to low colony number of some of the initial mutagenesis reactions, the quantity of DNA template used was increased from 10 ng to 100 ng.

Table 15: PCR mutagenesis reaction components for generation of TIMP-3 mutants using QuikChange II XL-site directed mutagenesis kit.

Reagents	Agilent QuikChange guidelines	Modifications
10x reaction buffer (µL)	5	5
ds DNA template (ng)	10	100
Primer (forward) (ng)	125	100
Primer (reverse) (ng)	125	100
dNTP mix (µL)	1	1
QuikSolution reagent (µL)	3	3
ddH2O (µL)	As required	As required
Final volume (µL)	50	50
PfuUltra High Fidelity polymerase (2.5U/ µL)	1	1

To further improve our success rate, we made some modifications to the Agilent QuikChange site directed mutagenesis PCR conditions (Table 16). The denaturing and annealing steps were extended by 10 s, and the extension time was increased from 60 s/kb of plasmid length to 150 s/kb of plasmid length due to poor efficiency and the use of a large vector (10.4 kb pCEP4 mammalian expression vector). Modifications are highlighted in red in Table 16.

Table 16: PCR parameters for generation of TIMP-3 mutants using QuikChange II XL-site directed mutagenesis kit.

Stage	Cycles	Temperature (°C)		Time (s)	
		Guidelines	Conditions used	Guidelines	Conditions used
1	1	95	95	60	60
2	18	95	95	50	60
		60	60	50	60
		68	68	624*	1435*
3	1	68	68	420	420

60 s/kb of plasmid length, * 150 s/kb of plasmid length

3.2.2.3. Isolation of TIMP-3 mutant DNA

The QuikChange II XL kit was used as outlined in (Section 3.2.2) to mutate 10 lysine residue pairs and their constituent 12 single lysine residues on TIMP-3. The PCR product (50 µL) generated in (Section 3.2.2.2) was digested by *Dpn* I and ethanol precipitated (0.5 µL sodium acetate pH 5.2, 125 µL ultra-pure ethanol added, -20 °C, overnight) and pellets resuspended in nuclease-free water (5 µL), giving a 10-fold concentration. The total volume of precipitated DNA was then transformed into XL10-Gold ultracompetent cells by

heat-shock, plated onto LB-carbenicillin agar (100 µg carbenicillin /mL) plates (250 µL per plate) and incubated overnight (37 °C).

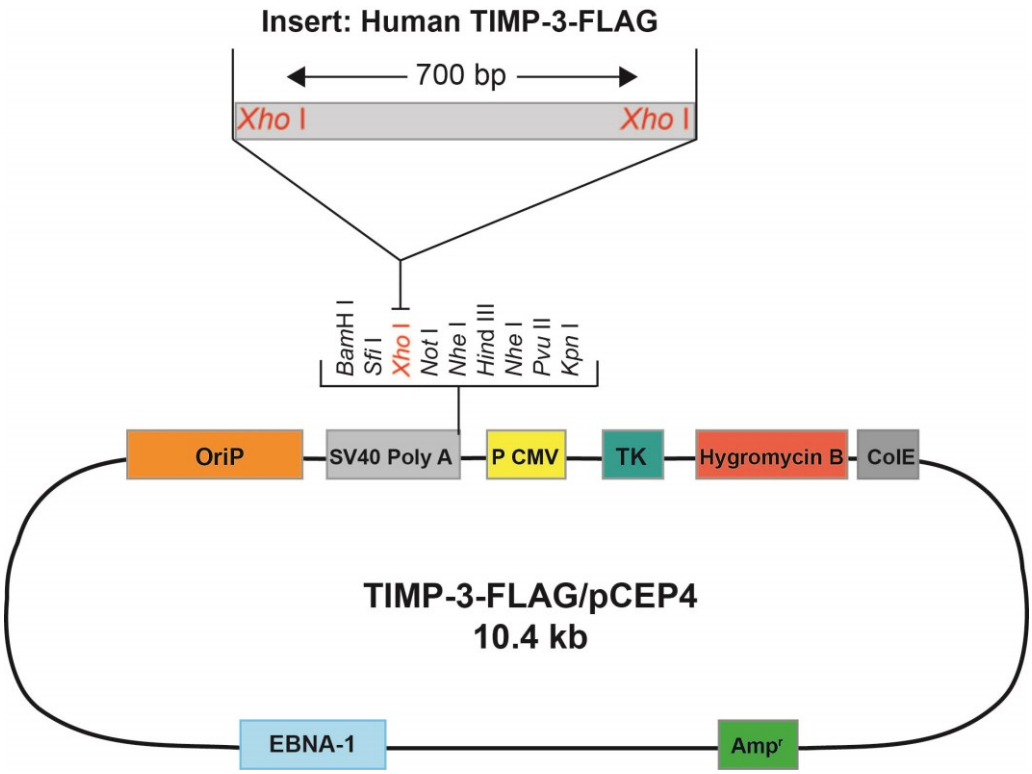


Figure 23: Mammalian expression vector encoding C-terminally FLAG-tagged human TIMP-3

The vector contains a CMV promoter to drive mammalian expression, hygromycin B reistance for mammalian expression and carbenicillin-resistance for bacterial expression.

Colonies visible after 24 h were selected and cultured in LB-carbenicillin overnight (5 mL, 37 °C, 225 rpm). Bacterial DNA was extracted using the alkaline-SDS method. Briefly, cultures were pelleted (13 000 rpm, 1 min), resuspended (100 µL of 25 mM Tris-HCl pH 8.0, 10 mM EDTA pH 8.0), mixed with alkaline-SDS buffer (200 µL of 0.2 N NaOH, 1 % SDS) and rested on ice for 5 min. The suspension was then neutralised (150 µL of 3M CH_3COOK, CH_3COOH), incubated in ice and chloroform added (10 µL) to any precipitate

contaminating proteins from solution. The DNA was precipitated by addition of Ultra-pure-ethanol (800 µL) and centrifuged (13 000 rpm, 5 min). The resulting pellet was washed in 70 % Ultra-pure ethanol (800 µL), centrifugated (3 000 rpm, 10 min). The purified pellet was then resuspended in nuclease-free water (50 µL). To determine whether the expected TIMP-3-encoding insert was present, restriction digests were performed using *Xho*I to generate TIMP-3-FLAG insert bands of ~700 bp in size as shown in Figure 23. The presence of a band at the expected insert size (700 bp) indicated that the insert was present. To determine whether the DNA contained the required mutation, samples with the correct insert bands were sequenced (Eurofins MWG Operon, Ebersberg, Germany).

Figure 24 shows the screening of 2 representative TIMP-3 single mutants, TIMP-3 K110A and TIMP-3 K157A. DNA extracted from candidate colonies, digested with *Xho*I, produced bands of the expected size (700 bp). These 2 colonies were sequenced. On average, 4 DNA samples underwent restriction digest screening per single TIMP-3 mutant. Typically all 4 samples produced bands at the expected size of 700 bp with 2 being sent for sequencing. On average, mutagenesis was successful for 90 % of the TIMP-3 single mutant DNA samples sequenced.

When all single mutants had been successfully generated and sequenced, the QuikChange XL II kit was used to generate the TIMP-3 double mutants. QuikChange reactions were carried out using TIMP-3 single mutants as templates and appropriate mutagenic primers. For example, to generate TIMP-3 K42A/K110A, TIMP-3 K42A was used as the template with K110A primers. Figure 25 shows the screening of 2 representative TIMP-3 double

mutants, K42A/K110A and K42A/K157A. DNA extracted from candidate colonies, digested with *Xho*I produced bands of the expected size (700 bp). These 2 colonies were sequenced. On average, 4 DNA samples underwent restriction digest screening per double TIMP-3 mutant. Typically, 3 of 4 samples produced bands at the expected size of 700 bp with 3 being sent for sequencing. On average, mutagenesis was successful for 66 % of TIMP-3 double mutant DNA samples sequenced.

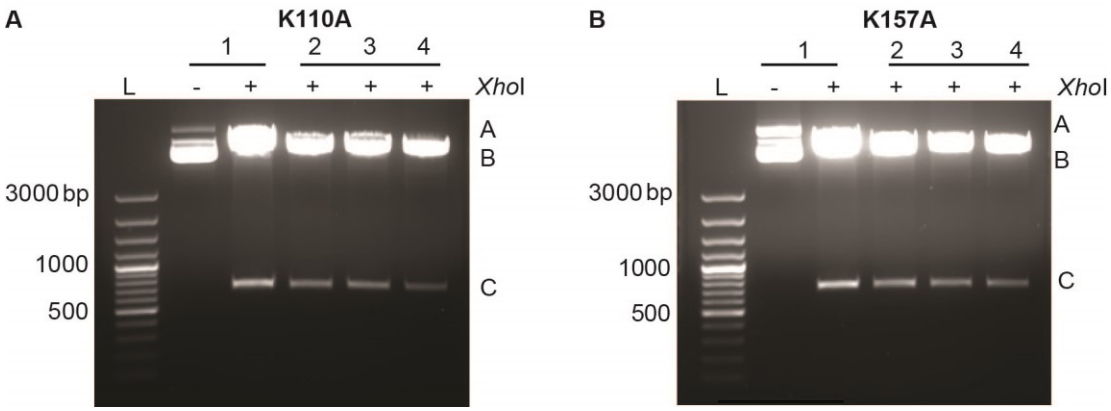


Figure 24: Restriction digest screening of candidate TIMP-3 single mutants K110A and K157A.

Carbenicillin-resistant colonies were picked and cultured in LB-carbenicillin (5 mL) overnight (37 °C, 225 rpm) and DNA isolated using alkaline-SDS DNA extraction. Bacterial cultures were pelleted (13 000 rpm, 1 min), resuspended (100 µL of 25 mM Tris-HCl pH 8.0, 10 mM EDTA pH 8.0) and then lysed with alkaline-SDS buffer (200 µL of 0.2 N NaOH, 1 % SDS, on ice, 5 min). The suspension was neutralised (150 µL of 3M CH_3COOK, CH_3COOH), and protein contaminants precipitated by the addition of chloroform (10 µL). The DNA was precipitated by addition of Ultra-pure ethanol (800 µL) and centrifuged (13 000 rpm, 10 min). The pellet was washed in 70 % Ultra-pure ethanol (1 mL), centrifuged (13 000 rpm, 2 min) and the resulting pellet resuspended in nuclease-free water. DNA samples (1 µl) were then digested (2 µL of 10x digest buffer, 16 µL of ultra-pure water and 1 µl restriction enzyme *Xho*I added, 37 °C, 1 h). Samples were separated on 1 % agarose gel (100 V, 1 h) and stained with ethidium bromide (5 µl/100 mL agarose solution). Bands were visualised under UV light at 302 nm. 3 fragments were produced: (a) corresponds with the uncut pCEP4 vector (10.4 kb), (b) corresponds with digested pCEP4 and (c) corresponds with the TIMP-3 insert (700 bp). (L) represents the 1 kp DNA ladder.

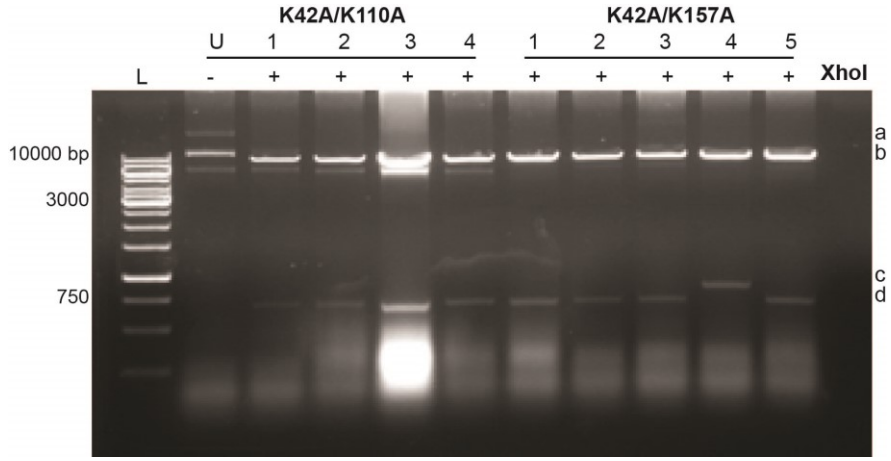


Figure 25: Restriction digest screening of TIMP-3 double mutants K42A/K110A and K42A/K157A.

Carbenicillin-resistant colonies were picked and cultured in LB-carbenicillin (5 mL) overnight (37 °C, 225 rpm) and DNA isolated using alkaline-SDS DNA extraction. Bacterial cultures were pelleted (13 000 rpm, 1 min), resuspended (100 µL of 25 mM Tris-HCl pH 8.0, 10 mM EDTA pH 8.0) and then lysed with alkaline-SDS buffer (200 µL of 0.2 N NaOH, 1 % SDS, on ice, 5 min). The suspension was neutralised (150 µL of 3M CH_3COOK, CH_3COOH), and protein contaminants precipitated by the addition of chloroform (10 µL). The DNA was precipitated by addition of Ultra-pure ethanol (800 µL) and centrifuged (13 000 rpm, 10 min). The pellet was washed in 70 % Ultra-pure ethanol (1 mL), centrifuged (13 000 rpm, 2 min) and the resulting pellet resuspended in nuclease-free water. DNA samples (1 µl) were then digested (2 µL of 10x digest buffer, 16 µL of ultra-pure water and 1 µl restriction enzyme *Xho*I added, 37 °C, 1 h). Samples were separated on 1 % agarose gel (100 V, 1 h) and stained with ethidium bromide (5 µl/100 mL agarose solution). Bands were visualised under light at 302 nm. 4 fragments were produced: (a) corresponds with the uncut pCEP4 vector (10.4 kb), (b) corresponds with the linearised pCEP4, (c) represents an unidentified insert ~ 1000 bp and (d) corresponds with the TIMP-3 insert (700 bp). (L) represents the 1 kp DNA ladder.

3.2.3. Generation of recombinant RAP

3.2.3.1. Introduction

Receptor associated protein (RAP) is a 39 kDa protein was first identified by its co-purification with LRP-1 from human placenta (Jensen et al., 1989). It

has been well documented that RAP binds to LRP-1 with a high affinity of 0.5-1 nM (Iadonato et al., 1993; Moestrup et al., 1993; Willnow et al., 1994a) and it has also been demonstrated that RAP can inhibit the binding and endocytosis of other LRP-1 ligands both in vitro and in vivo (Gliemann et al., 1994; Warshawsky et al., 1994; Willnow et al., 1994b). RAP-LRP-1 ligand binding has been well studied (Dolmer et al., 2013; Fisher et al., 2006; Jensen et al., 2006; Jensen et al., 2009b; van den Bigglelaar et al., 2011) and is used as a tool in the investigation of LRP-1-ligand binding (Jensen et al., 2009a; Mikhailenko et al., 2001). Using a range of methods including site-ditected mutagenesis, surface plasmon resonance and X-ray crystallography, these studies identified that both K256A and K270A residues mediated the binding of RAP to LRP-1. Here we generated Wild-type for use as a control in TIMP-3 endocytosis studies.

3.2.3.2. RAP expression and purification

E. coli BL21-DE3 cells were transformed with Wild-type pET3a-RAP constructs (Yamamoto et al., 2013) and plated on LB-carbenicillin agar. Picked colonies were cultured in LB media (3 mL) supplemented with carbenicillin (100 µg/mL) and were cultured for 4 h (37 ^{o}C, 225 rpm) before being increased to a final volume of 20 mL and incubated overnight (37 ^{o}C, 225 rpm). The 20 mL culture was added to LB (1L) and incubated (37 ^{o}C, 225 rpm), until reaching an OD_{600} of 0.6. IPTG (1 mM) was added, culture temperature reduced to 25 ^{o}C and rpm reduced to 150 rpm and the culture left to express overnight. IPTG induces protein expression by mimicking lactose and binding to the lac repressor on the plasmid. This binding induces a conformational change reducing the affinity of the repressor for DNA. On removal of the lac repressor,

the T7 RNA polymerase binds to the T7 promoter upstream of the gene of interest on the plasmid insert, and initiates transcription of the target gene.

Cells were harvested by centrifugation (10 min, 8000 rpm, 4 ^{o}C) and the pellet resuspended in equilibration buffer (50 mM NaH_2PO_4 pH 8.0, 200 mM NaCl, 0.02 % NaN_3). The cell pellet was lysed on a French press (4 cycles, 10000 psi) and the lysate centrifuged to separate the soluble and insoluble fractions. The soluble fraction was loaded onto Ni-NTA column using a peristaltic pump (1mL/min), washed with 20 mM imidazole in equilibration buffer and then 50 mM imidazole in equilibration buffer. Protein was eluted with 250 mM imidazole in a high salt buffer (50 mM NaH_2PO_4, pH 8.0, 500 mM NaCl, 0.02 % NaN_3). Samples were analysed by SDS-PAGE on a 10 % acrylamide gel and bands visualised with Coomassie blue stain (Figure 26).

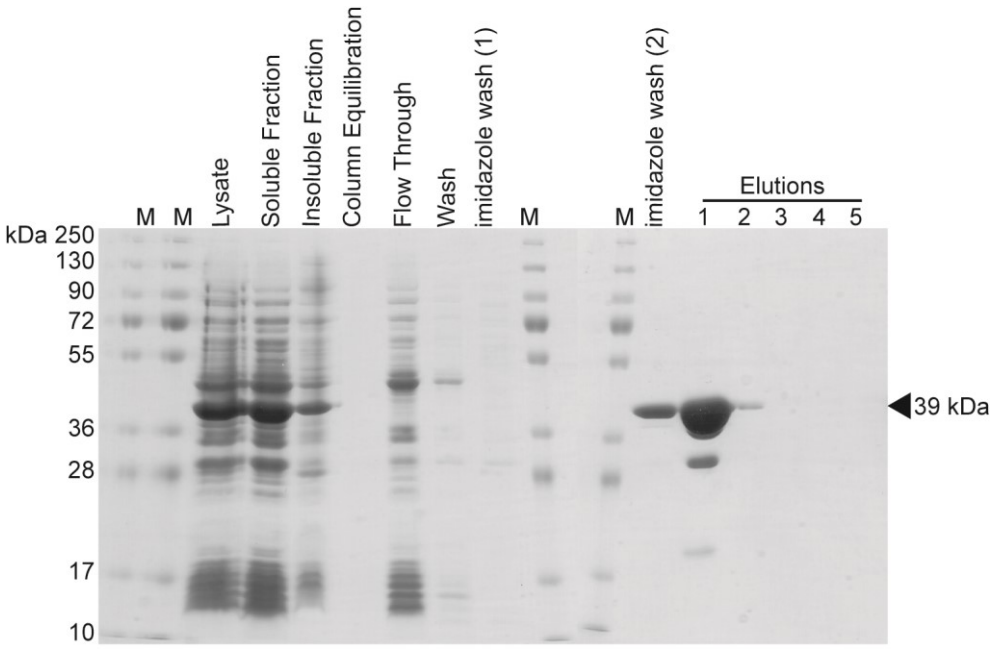


Figure 26: Purification of Wild-type RAP

E. coli BL21-DE3 cells were transformed with Wild-type pET3a-RAP constructs and plated on LB-carbenicillin agar. Picked colonies were cultured in LB media (3 mL) supplemented with carbenicillin (50 µg/mL) and were cultured for 4 h (37 ºC, 225 rpm) before a further 16 mL of LB was added and cultures incubated overnight (37 ºC, 225 rpm). The 20 mL culture was added to LB (1L) and incubated (37 ºC, 225 rpm). On reaching an OD_{600} of 0.6, IPTG (1 mM) was added and culture temperature reduced to 25 ºC and shaking reduced to 150 rpm overnight. Cells were harvested by centrifugation (8000 rpm, 15 min) and the pellet resuspended in equilibration buffer (50 mM NaH_2PO_4 pH 8.0, 200 mM NaCl, 0.02 % NaN_3). The cell pellet was lysed on a French press (4 cycles, 10000 psi) and the lysate centrifuged to separate the soluble and insoluble fractions. The soluble fraction was loaded onto Ni-NTA column using a peristaltic pump (1mL/min), washed with 20 mM imidazole in equilibration buffer and then 50 mM imidazole in equilibration buffer) Protein was eluted with 250 mM imidazole in a 50 mM NaH_2PO_4 pH 8.0, 500 mM NaCl, 0.02 % NaN_3. Samples were analysed by SDS-PAGE on a 10 % acrylamide gel and bands visualised with Coomassie blue stain. Bands corresponding with the predicted mass of RAP (approximately 39 kDa) are indicated with an arrow.

Wild-type RAP was purified to a concentration of 30 µM, with a yield of 1.14mg/mL (Table 17). The protein preparation was dialysed against a sodium

azide-free equilibration buffer (50 mM NaH_2PO_4 pH 8.0, 200 mM NaCl) for use in cell-based assays.

Table 17: Yield of purified Wild-type RAP.

A_{280}	1.103
Extinction co-efficient	36440 $M^{-1}.cm^{-1}$
Molarity	30 µM
Yield	11.4 mg from 1L culture

3.2.3.3. Discussion

An LRP-1 binding motif has previously been identified for a number of LRP-1 ligands, and consists of a pair of lysine residues separated by 21 Å projecting outwards from the surface of the ligand to allow electrostatic interaction with the binding cleft in the binding domains of LRP-1. No crystal structure exists for full-length TIMP-3, so we generated a model of the TIMP-3 structure using the available crystal structures of TIMP-1 and TIMP-2. Overlay of the full-length TIMP-3 model with the N-TIMP-3 structure showed good agreement, lending validity to the use of this model in this study. We shortlisted 10 pairs of lysine residues meeting the selection criteria of 2 lysine residues separated by 21 Å. We then mutated these lysine residues to alanine using the Agilent QuikChange site directed mutagenesis kit, giving 12 single and 10 double TIMP-3 mutants. This proved to be a rapid and easy way of generating the point mutants. The method required some optimization, primarily due to fact that the mammalian expression vector we used (pCEP4) was large (10.4 kb), and required longer extension times during the PCR mutagenesis reactions.

In Chapter 4, we show the assessment of the TIMP-3 mutants generated here for LRP-1-resistance by following their uptake by HTB94 cells from culture media.

Chapter 4: Screening for endocytosis-resistant mutants of TIMP-3 by immunoblotting

4.1 Introduction

Our laboratory has previously shown that TIMP-3 is endocytosed by HTB94 cells human chondrosarcoma cells, primary porcine chondrocytes, HeLa human cervix epithelial adenocarcinoma cells and primary human uterine cervical fibroblasts (Scilabra et al., 2013; Troeberg et al., 2008). This endocytosis is mediated by the membrane-bound endocytic receptor LRP-1 (Scilabra et al., 2013; Troeberg et al., 2008), which is known to mediate the endocytic clearance of more than 40 ligands. Studies of these ligands and an antagonist of LRP-1 binding, RAP, identified a ligand-binding motif of 2 lysine residues on the surface of the ligand, separated by 21 Å (Fisher et al., 2006; Jensen et al., 2009b; van den Bigglelaar et al., 2011).

As discussed Chapter 3, we generated TIMP-3 mutants containing lysine to alanine mutations for the 10 di-lysine pairs meeting the criteria for the ligand-binding motif, and the 12 constituent single lysine residues. In this Chapter, we describe the initial screening of these 22 mutants for endocytosis resistance.

In this preliminary assessment, we used immunoblotting and densitometry analysis to follow clearance of the exogenously-added TIMP-3 mutants from the medium of HTB94 cells over time. Our aim was to generate a shortlist of endocytosis-resistant TIMP-3 mutants that would then be further analysed for their inhibitory activity, extracellular matrix binding and chondroprotective effects in cartilage.

4.2 Results

4.2.1 Transient expression of Wild-type and mutant TIMP-3 in HEK-293-EBNA cell line

We aimed to generate crude conditioned medium containing Wild-type and mutant TIMP-3, and use this medium as a source of TIMP-3 for the endocytosis assays. We transfected HEK-293-EBNA cells with a pCEP-4 mammalian expression vector encoding FLAG-tagged Wild-type and mutant TIMP-3 using Lipofectamine 2000 liposome transfection reagent (Invitrogen/ThermoFisher Scientific, Paisley, UK). The DNA concentration and expression period were first optimised to ensure maximum transfection efficiency.

4.2.1.1 Optimising DNA concentration for transient expression of TIMP-3 in HEK-293-EBNA cells

In accordance with the manufacturer's instructions, HEK-293-EBNA cells were seeded at a density of $1X10^6$ per well in a 6-well plate containing DMEM supplemented with 10 % FCS and incubated overnight [37 ^oC, 5 % (v/v) CO_2]. It was recommended to use 4 µg DNA / 4 mL DMEM medium per well in 6-well plates. Therefore to optimize transfection conditions, a concentration range of 0-5 µg DNA / 4 mL medium was tested. After transfection, cells were incubated in serum-free DMEM in the presence or absence of 30 mM sodium chlorate for 48 hours. Sodium chlorate ($NaClO_3$) is an inhibitor of ATP-sulfurylase, an enzyme required for the biosynthesis of 3'-phosphoadenosine-5'-phosphosulfate (PAPS) a co-substrate for sulfotransferase reactions. $NaClO_3$ treatment therefore blocks sulfation of cell surface glycosaminoglycans and has previously been shown to prevent TIMP-3 endocytosis, resulting in the

accumulation of TIMP-3 in HEK-293-EBNA culture medium (Troeberg et al., 2009). In the absence of $NaClO_3$, TIMP-3 is endocytosed and so was undetectable by immunoblot analysis of control medium.

Two days post-transfection, the conditioned medium (4 mL) was harvested and centrifuged (5000 rpm, 10 min) to eliminate cell debris. Conditioned media for each DNA concentration (in the presence or absence of 30 mM $NaClO_3$) were concentrated by the addition of 5 % (v/v) TCA and incubated at 4 ^{o}C overnight. Precipitated protein was collected by centrifugation (13000 rpm, 4 ^{o}C, 10 mins) and resuspended in 30 µL of 2x SDS-PAGE loading buffer. Samples were analysed by immunoblotting using an anti-FLAG M2 antibody and an anti-mouse IgG AP-conjugated secondary antibody. Bands were visualised using Western blue stabilised substrate for AP and the reaction stopped using AP stop (20 mM Tris-HCl pH 7.5, 10 mM EDTA).

As can be seen in Figure 27, similar transfection efficiency was observed for 1-5 µg of DNA, with 3 µg of DNA showing the highest level of TIMP-3 expression.

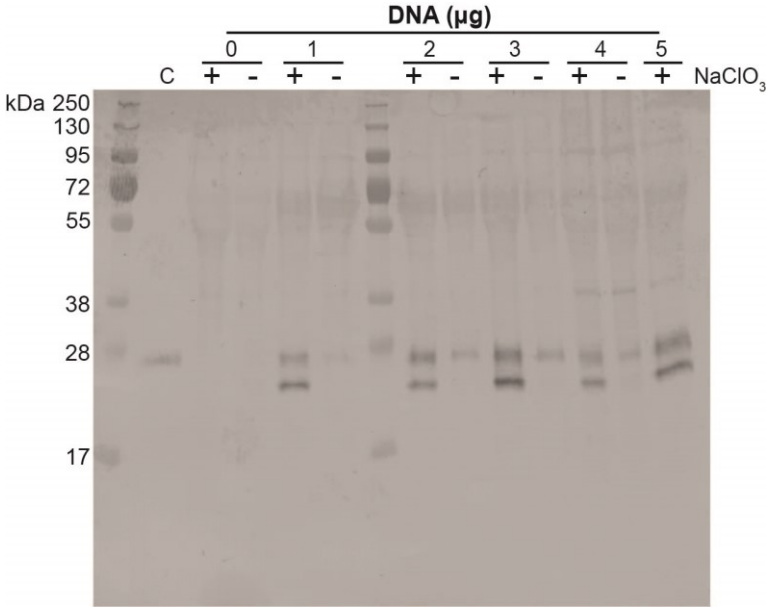


Figure 27: Optimization of DNA concentration for transfection of HEK-293-EBNA cells with TIMP-3.

HEK-293-EBNA cells were transfected with a range of concentrations (0-5 µg) of pCEP-4 mammalian expression vector encoding FLAG-tagged Wild-type TIMP-3. Conditioned media were was harvested 2 days post-transfection. Samples were TCA precipitated [5 % (v/v), 4 ^{o}C, overnight] and pellets resuspended in 30 µL of 2x SDS-PAGE loading buffer. Samples (15 µL) were then analysed by immunoblotting with an anti-FLAG M2 antibody and an anti-mouse IgG AP-conjugated secondary antibody. Bands were visualised using Western blue stabilised substrate for AP and the reaction stopped using AP stop (20 mM Tris-HCl pH 7.5, 10 mM EDTA). Purified TIMP-3 (0.5 nM) was used as a control (C). As expected, TIMP-3 was not detectable in the absence of $NaClO_3$. Transfection with 3 µg of DNA generated the highest TIMP-3 levels.

4.2.1.2 Optimising expression time for transient expression of TIMP-3 in HEK-293-EBNA cells

The optimum expression period was next investigated. HEK-293-EBNA cells were transfected with 3 µg of DNA and left to express for 1-7 days. Samples were TCA precipitated overnight [5 % (v/v), 4 ^{o}C, overnight]. Precipitated protein was collected by centrifugation (13000 rpm, 4 ^{o}C, 10 mins), resuspended in 30 µL of 2x SDS-PAGE loading buffer and analysed by immunoblotting using an anti-FLAG M2 antibody and an anti-mouse IgG AP-

conjugated secondary antibody. Bands were visualised using Western blue stabilised substrate for AP and reaction stopped using AP stop (20 mM Tris-HCl pH 7.5, 10 mM EDTA).

We found that no protein was detected 1 day after transfection, and that expression increased on days 2 and 3 (Figure 28). Expression decreased on day 4, and TIMP-3 was barely detectable 5-7 days after transfection. We identified day 2 as the optimal time for harvesting transiently expressed TIMP-3.

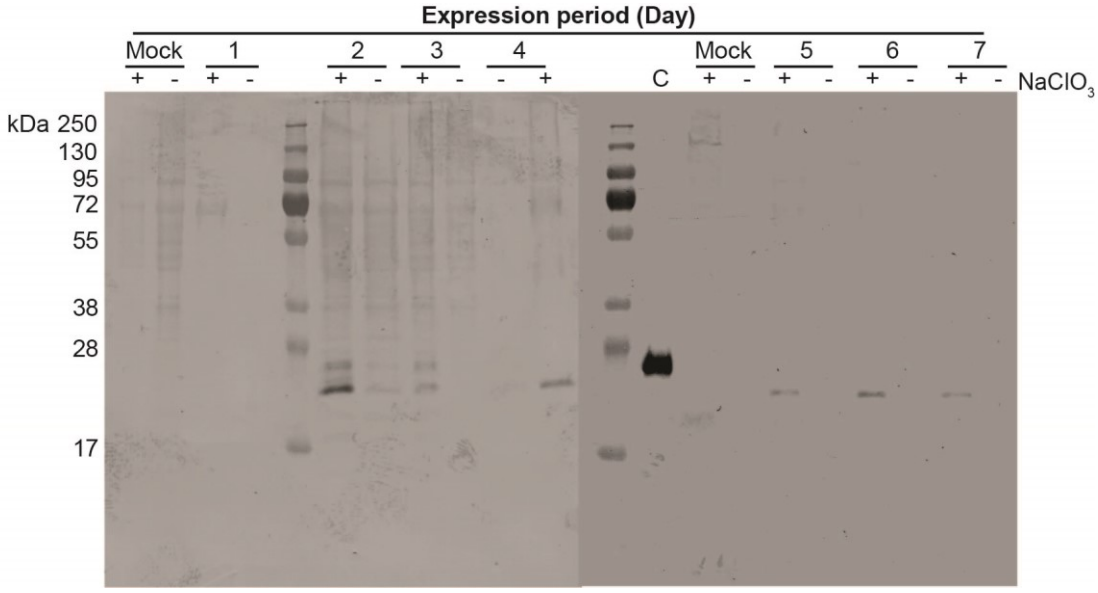


Figure 28: Optimising expression time for transient expression of TIMP-3 in HEK-293-EBNA cells.

HEK-293-EBNA cells were transfected with 3 µg of pCEP-4 mammalian expression vector DNA encoding FLAG-tagged Wild-type TIMP-3 using Lipofectamine 2000 liposome transfection reagent and left to express for 1-7 days as indicated. Samples were TCA precipitated [5 % (v/v), 4 °C, overnight] and pellets were resuspended in 30 µL of 2x SDS-PAGE loading buffer. Samples (15 µL) were then analysed by immunoblotting with an anti-FLAG M2 antibody and an anti-mouse IgG AP-conjugated secondary antibody. Bands were visualised using Western blue stabilised substrate for AP and reaction stopped by using AP stop (20 mM Tris-HCl pH 7.5, 10 mM EDTA). Purified TIMP-3 (0.5 nM) was used as a control (C). TIMP-3 was not detected in the absence of $NaClO_3$ and a 2-day expression time produced the highest level of expression.

4.2.2 Optimising medium volume for screening endocytosis-resistance of Wild-type and mutant TIMP-3 in HTB94 cells

We planned to harvest conditioned medium from HEK-293-EBNA cells transiently expressing TIMP-3 mutants, and follow the endocytosis of these mutants by HTB94 cells over time by immunoblotting. We thus assessed what volume of HEK-293-EBNA conditioned medium was required to detect Wild-type and mutant TIMP-3 by immunoblotting.

4.2.2.1 Detection of Wild-type TIMP-3 in HEK-293-EBNA conditioned medium

HEK-293-EBNA cells were transfected in 6 well plates with 3 µg of Wild-type and mutant TIMP-3 DNA and cells left to express for 2 days. Conditioned medium was harvested and centrifuged (5000 rpm, 10 min) to eliminate cell debris then dialysed against TBS using Slide-A-Lyzer cassettes with a molecular weight cut-off of 3000 Da (500 mL, 4 ^{o}C, overnight). Increasing volumes (100, 200 and 300 µL) were diluted to a final volume of 1 ml in DMEM supplemented with 0.1 % FCS. Samples were TCA precipitated [5 % (v/v), 4 ^{o}C, overnight] and pellets resuspended in 30 µL of 2x SDS-PAGE loading buffer. Resuspended samples (15 µL) were then analysed by immunoblotting with an anti-FLAG M2 antibody and an anti-mouse IgG AP-conjugated secondary antibody. Bands were visualised using Western blue stabilised substrate for AP and reaction stopped using AP stop (20 mM Tris-HCl pH 7.5, 10 mM EDTA).

This experiment showed that Wild-type TIMP-3 was detectable by immunoblotting of 200 µL or more of HEK-293-EBNA conditioned medium (Figure 29).

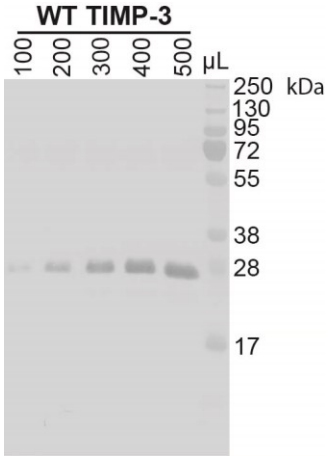


Figure 29: Expression of Wild-type TIMP-3 in HEK-293-EBNA conditioned medium.

HEK-293-EBNA cells were seeded at $1x10^6$ per well in a 6-well plate and transiently transfected (Lipofectamine 2000) with 3 µg of pCEP-4 mammalian expression vector encoding FLAG-tagged Wild-type TIMP-3. Cells were left to express in 4 mL of serum-free DMEM for 48 hours, conditioned medium samples were harvested, centrifuged (5000 rpm, 10 min) and dialysed against TBS (500 mL, 4 °C, overnight, molecular weight cut-off of 3000 Da). Varying volumes (100 µL to 500 µL) were diluted to 1 mL in DMEM supplemented with 0.1 % FCS. Samples were TCA precipitated [5 % (v/v), 4 °C, overnight] and pellets resuspended in 30 µL of 2x SDS-PAGE loading buffer. Resuspended samples (15 µL) were then analysed by immunoblotting with an anti-FLAG M2 antibody and an anti-mouse IgG AP-conjugated secondary antibody. Bands were visualised using Western blue stabilised substrate for AP and the reaction stopped using AP stop (20 mM Tris-HCl pH 7.5, 10 mM EDTA). Wild-type TIMP-3 was detectable by immunoblotting of 200 µL or more of HEK-293-EBNA conditioned medium.

4.2.2.2 Detection of TIMP-3 mutant expression in HEK-293-EBNA conditioned medium

Next we analysed the detectability of the single TIMP-3 mutants in HEK-293-EBNA conditioned medium. HEK-293-EBNA cells were seeded at a density of $1X10^6$ per well in a 6-well plate containing DMEM supplemented with 10 % FCS [37 °C, 5 % (v/v) CO_2]. Cells were transfected with 3 µg of DNA using Lipofectamine 2000 liposome transfection reagent and incubated in

serum-free DMEM in the presence of 30 mM $NaClO_3$ for 2 days. Two days post-transfection, the conditioned medium (4 mL) was harvested and centrifuged (5000 rpm, 10 min) to eliminate cell debris and dialysed against TBS using Slide-A-Lyzer cassettes with a molecular weight cut-off of 3000 Da (500 mL, 4 ^{o}C, overnight). Increasing volumes (100, 300 and 400 µL) were diluted to a final volume of 1 ml in DMEM supplemented with 0.1 % FCS. Samples were TCA precipitated [5 % (v/v), 4 ^{o}C, overnight] and pellets resuspended in 30 µL of 2x SDS-PAGE loading buffer. Resuspended samples (15 µL) were then analysed by immunoblotting with an anti-FLAG M2 antibody and an anti-mouse IgG AP-conjugated secondary antibody. Bands were visualised using Western blue stabilised substrate for AP and reaction stopped using AP stop (20 mM Tris-HCl pH 7.5, 10 mM EDTA).

This experiment showed that all single mutants were detectable, but to differing levels due to differences in their expression efficiency (Figure 30). TIMP-3 single mutants K26A, K27A, K45A, K52A, K71A, K76A and K157A were detectable by immunoblotting of 100 µL of conditioned medium. All mutants were detectable by immunoblotting of 300 µL of HEK-293-EBNA conditioned medium (Figure 30).

Expression of all double mutants was also detectable, but to differing levels due to differences in their expression yields (Figure 31). Only TIMP-3 K42A/K110A, was detectable by immunoblotting 100 µL of HEK-293-EBNA conditioned medium. All mutants except TIMP-3 K71A/K157A were detectable by immunoblotting of 200 µL of conditioned medium and all mutants were detectable by immunoblotting 300 µL of conditioned medium.

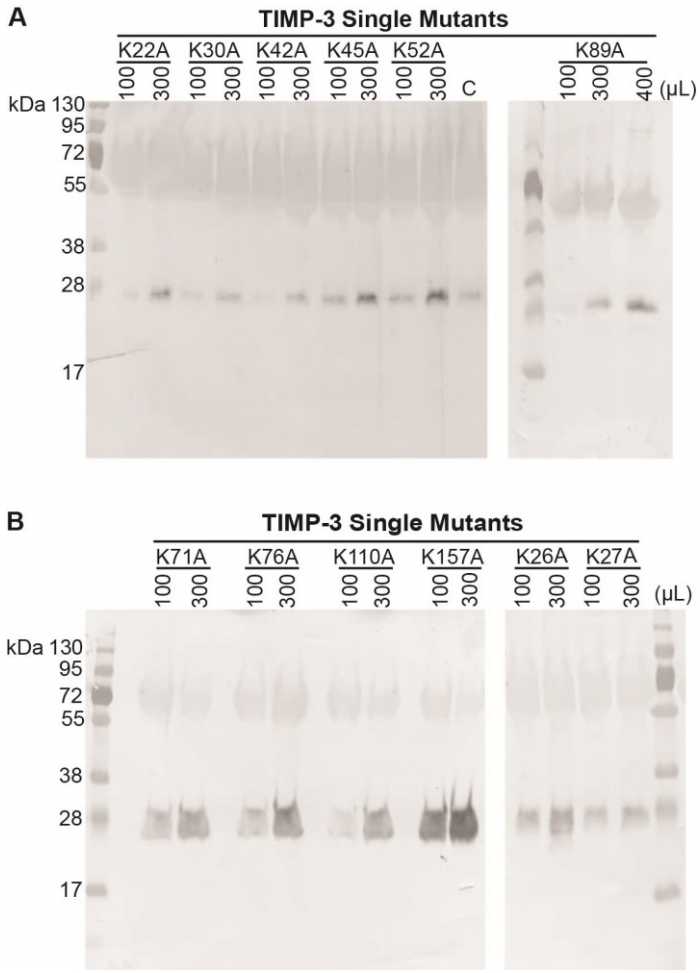


Figure 30: Detection of TIMP-3 single mutant expression in HEK-293-EBNA conditioned medium.

HEK-293-EBNA ($1x10^6$ per well in a 6-well plate) were transfected (Lipofectamine 2000) with 3 µg of pCEP-4 encoding FLAG-tagged single mutant TIMP-3. Cells were left to express in serum-free DMEM (4 mL) for 48 hours, conditioned medium samples harvested, centrifuged (5000 rpm, 10 min) and dialysed against TBS using Slide-A-Lyzer cassettes with a molecular weight cut-off of 3000 Da (500 mL, 4 °C, overnight). Indicated volumes of medium were diluted to 1 mL in DMEM with 0.1 % FCS and TCA precipitated [5 % (v/v), 4 °C, overnight]. Pellets were resuspended in 30 µL of 2x SDS-PAGE loading buffer and analysed (15 µL) by immunoblotting with M2 anti-FLAG antibody and anti-mouse IgG AP-conjugated secondary antibody. Bands were visualised using Western blue stabilised substrate for AP and the reaction stopped using AP stop (20 mM Tris-HCl pH 7.5, 10 mM EDTA). Purified TIMP-3 (0.5 nM) was used as a control (C). TIMP-3 single mutants K26A, K27A, K45A, K52A, K71A, K76A and K157A were detectable by immunoblotting of ≥100 µL conditioned medium. The remaining TIMP-3 mutants were detectable by immunoblotting of 300 µL of conditioned medium.

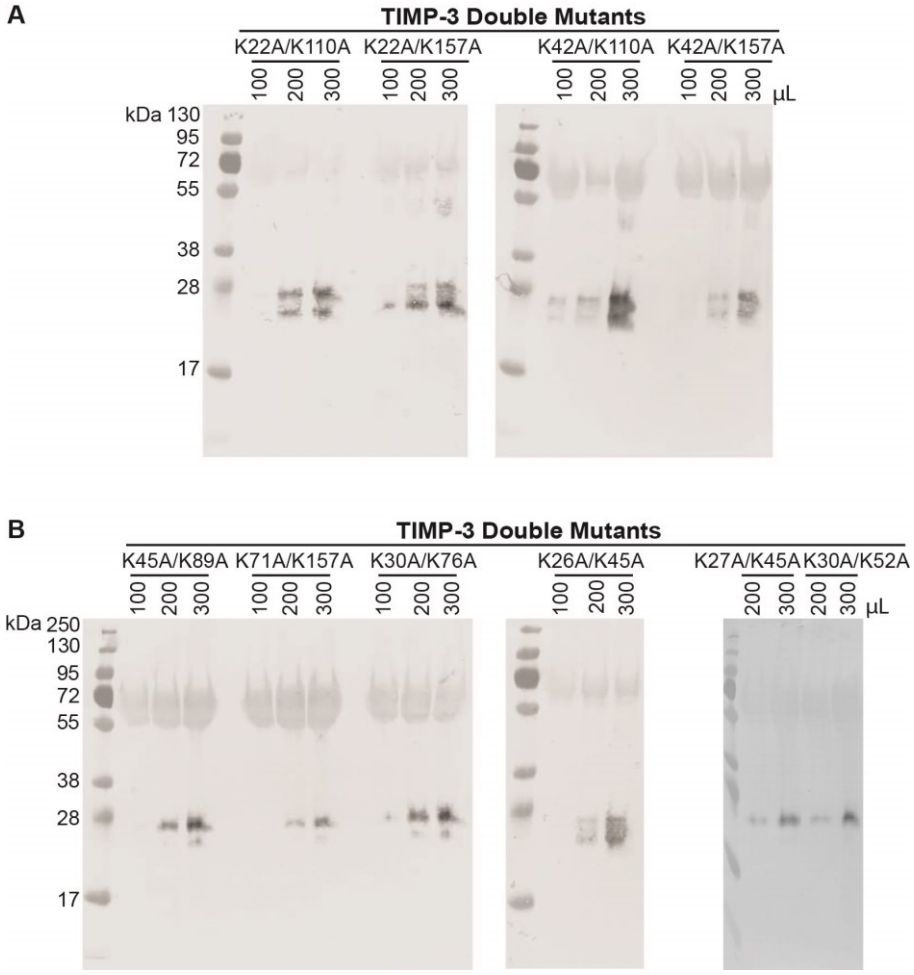


Figure 31: Detection of TIMP-3 double mutant expression in HEK-293-EBNA conditioned medium.

HEK-293-EBNA cells ($1x10^6$ per well in a 6-well plate) were transfected (Lipofectamine 2000) with 3 µg of pCEP-4 encoding FLAG-tagged double TIMP-3 mutants. Cells were left to express in serum-free DMEM (4 mL) for 48 hours, conditioned medium samples harvested, centrifuged (5000 rpm, 10 min) and dialysed against TBS using Slide-A-Lyzer cassettes with a molecular weight cut-off of 3000 Da (500 mL, 4 °C, overnight).. Indicated volumes of medium were diluted to 1 mL in DMEM with 0.1 % FCS and TCA precipitated [5 % (v/v), 4 °C, overnight]. Pellets were resuspended in 30 µL of 2x SDS-PAGE loading buffer and analysed (15 µL) by immunoblotting with M2 anti-FLAG antibody and anti-mouse IgG AP-conjugated secondary antibody. Bands were visualised using Western blue stabilised substrate for AP and the reaction stopped using AP stop (20 mM Tris-HCl pH 7.5, 10 mM EDTA). Purified TIMP-3 (0.5 nM) was used as a control (C). TIMP-3 K42A/K110A was detectable in 100 µL of medium. All mutants except TIMP-3 K71A/K157A were detectable in 200 µL of medium and all TIMP-3 mutants were detectable in 300 µL of medium.

4.2.3 Quantification of the rate of TIMP-3 endocytosis by HTB94 chondrosarcoma cells

Having confirmed that all TIMP-3 mutants could be detected by immunoblotting, expression of the TIMP-3 mutants was expanded to generate sufficient volumes of conditioned medium to follow their endocytosis by HTB94 cells. HEK-293-EBNA cells seeded at 6 x 10^6 cells in a 10 cm plate were transfected (Lipofectamine 2000) with 18 µg of pCEP-4 mammalian expression vector DNA encoding FLAG-tagged mutant TIMP-3. Cells were incubated in 20 mL serum-free DMEM in the presence of 30 mM $NaClO_3$ for 48 hours. Conditioned media were harvested and dialysed (overnight, 4 ^oC) against 1 L Tris-buffered saline (TBS) pH 7.5 using Slide-A-Lyzer cassettes with a molecular weight cut-off of 3000 Da to remove $NaClO_3$. Dialysed conditioned media were aliquoted in 1 mL volumes in low-binding Eppendorf tubes and stored at -20 ^oC.

4.2.3.2 Optimisation of HTB94 cell seeding density for endocytosis assay

We optimised the seeding density of HTB94 cells for the endocytosis assay, using a range of cell densities between 2 and 8 x10^5 per well of a 12-well plate. Cells were seeded overnight, washed 3 times in serum-free DMEM and 1 nM purified recombinant TIMP-3 added (1 mL final volume in DMEM supplemented with 0.1 % FCS). Samples were harvested at the indicated time points and TCA precipitated [5 % (v/v), 4 ^oC, overnight]. Pellets were resuspended in 30 µL of 2x SDS-PAGE loading buffer and samples (15 µL) analysed by immunoblotting with an anti-FLAG M2 antibody and an anti-mouse IgG AP-conjugated secondary antibody. Bands were visualised using Western

blue stabilised substrate for AP and the reaction stopped using AP stop (20 mM Tris-HCl pH 7.5, 10 mM EDTA). Pixel volumes were quantified using Phoretix software (Section 2.2.3.5) and are represented as a percentage of intensity of the band at time zero (t=0).

From Figure 32, it is evident that a seeding density of 8 x10^5 HTB94 cells showed the most linear endocytosis of TIMP-3 over time, with the lower densities giving less consistent results.

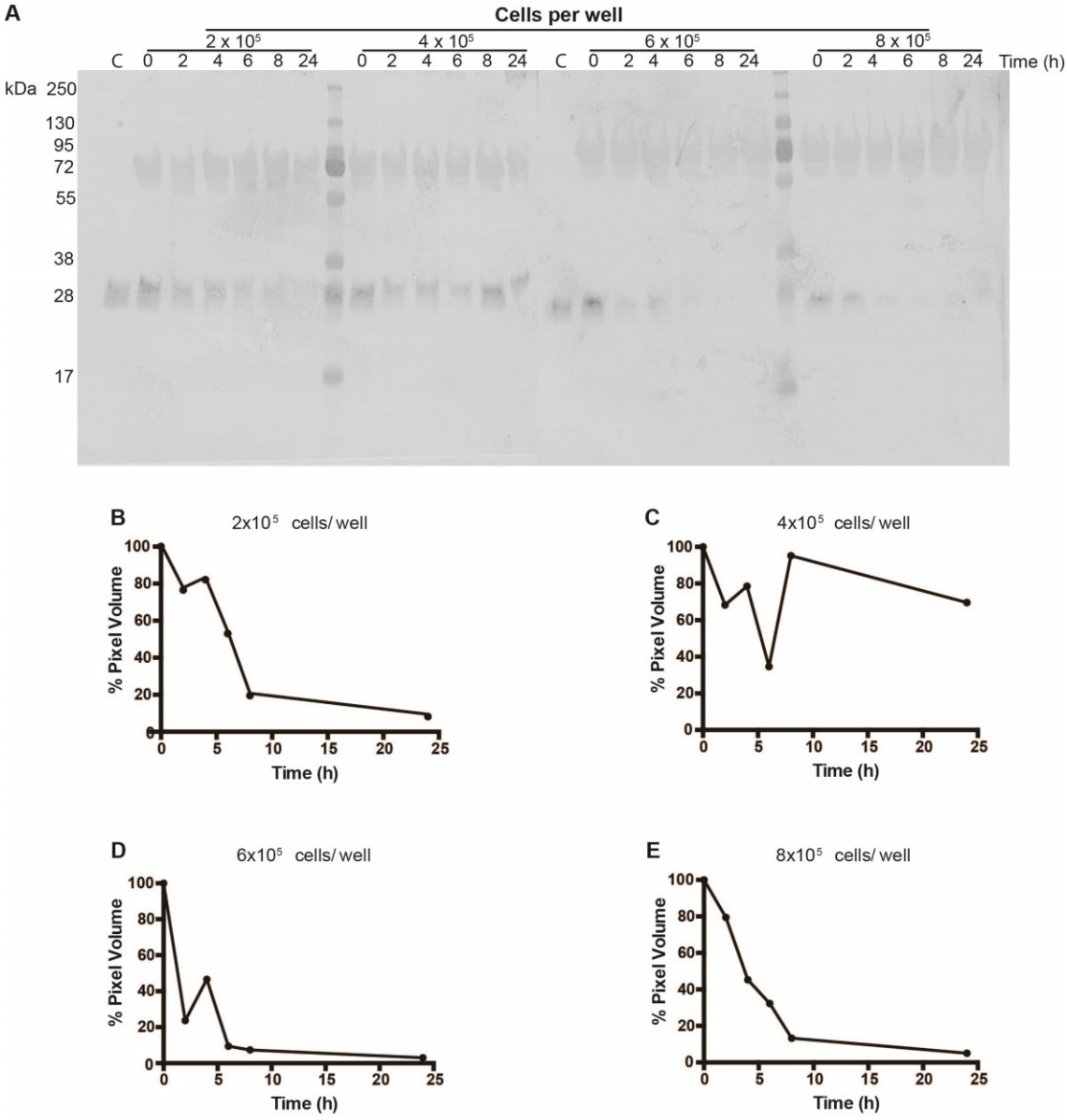


Figure 32: Optimising seeding density of HTB94 cells for endocytosis time course assays.

HTB94 were seeded at the range of densities in a 12-well plate [37 ºC, 5 % (v/v) CO_2, overnight]. Purified TIMP-3 (1 nM) was added in 1 mL DMEM supplemented with 0.1 % FCS and samples harvested the indicated times and TCA precipitated [4 ºC, 5 % (v/v), overnight]. Pellets were resuspended in 30 µL of 2x SDS-PAGE loading buffer and analysed (15 µL) by immunoblotting with M2 anti-FLAG antibody and anti-mouse IgG AP-conjugated secondary antibody. Bands were visualised using Western blue stabilised AP substrate and reaction the stopped using AP stop (20 mM Tris-HCl pH7.5, 10 mM EDTA). Purified TIMP-3 (0.5 nM) was used as a control (C). The immunoblot of endocytosis of Wild-type TIMP-3 over 24 hours is shown in panel **A**, panels **B**-**E** show quantification of band intensity over time for each of the seeding densities used. Band iintensity was quantified using Phoretix ID Gel Analysis software

and expressed as a percentage of pixel volume at t=0. Panels **B**, **C** and **D** show inconsistent results for the amount of protein remaining in the conditioned medium over time. Panel **E** shows Wild-type TIMP-3 endocytosis over time with a half-life of 4 h, in keeping with published data. A density of $8x10^5$ cells per well was thus chosen for further experiments.

4.2.3.3 Evaluating efficiency of dialysis to remove sodium chlorate from HEK-293-EBNA conditioned media

Wild-type TIMP-3 and all mutants were expressed in the presence of the endocytosis inhibitor $NaClO_3$, so we dialysed the crude conditioned medium to remove the $NaClO_3$ before endocytosis was evaluated. The conditioned media were dialysed against TBS using Slide-A-Lyzer cassettes with a molecular weight cut-off of 3000 Da (1 L, 4 ^oC, overnight).

A comparision of the rate of endocytosis of purified recombinant TIMP-3 (Troeberg et al., 2009), dialysed conditioned medium from HEK-293-EBNA cells expressing Wild-type TIMP-3 ($NaClO_3$ removed) and undialysed conditioned medium from HEK-293-EBNA cells expressing Wild-type TIMP-3 ($NaClO_3$ remaining) were assessed by immunoblotting and densitometric analysis. HTB94 cells were seeded at a density of 8×10^5 cells per well of a 12 well plate (Figure 32), grown to confluency [37 ^oC, 5 % (v/v) CO_2, overnight] and washed 3 times with serum-free DMEM. Purified Wild-type TIMP-3 (1.0 nM), dialysed conditioned medium from HEK-293-EBNA cells expressing Wild-type TIMP-3 (300 μL) and undialysed conditioned medium from HEK-293-EBNA cells expressing Wild-type TIMP-3 (300 μL) were diluted to 1 mL in DMEM supplemented 0.1 % FCS. Samples were harvested at the indicated times, TCA precipitated [5 % (v/v), 4 ^oC, overnight] and pellets resuspended in

30 µL of 2x SDS-PAGE loading buffer. Resuspended samples (15 µL) were then analysed by immunoblotting with an anti-FLAG M2 antibody and an anti-mouse IgG AP-conjugated secondary antibody. Bands were visualised using Western blue stabilised substrate for AP and reaction stopped by using AP stop (20 mM Tris-HCl pH 7.5, 10 mM EDTA).

The endocytosis time courses are shown in Figure 33; band intensity was quantified using Phoretix software and is represented as a percentage of band intensity at time zero (t=0). Purified Wild-type TIMP-3 and dialysed conditioned medium from HEK-293-EBNA cells expressing Wild-type TIMP-3 had the same half-life of 4.5 hours ($t_{1/2}$ = 4.5 h) on HTB94 cells, while undialysed conditioned medium from HEK-293-EBNA cells expressing Wild-type TIMP-3 had a longer half-life of 7.5 hours ($t_{1/2}$ = 7.5 h) (Figure 33). This indicates that dialysis had successfully removed the $NaClO_3$ from the medium. Dialysed conditioned medium from HEK-293-EBNA cells expressing Wild-type TIMP-3 was used as a control for further analysis of mutant TIMP-3 endocytosis.

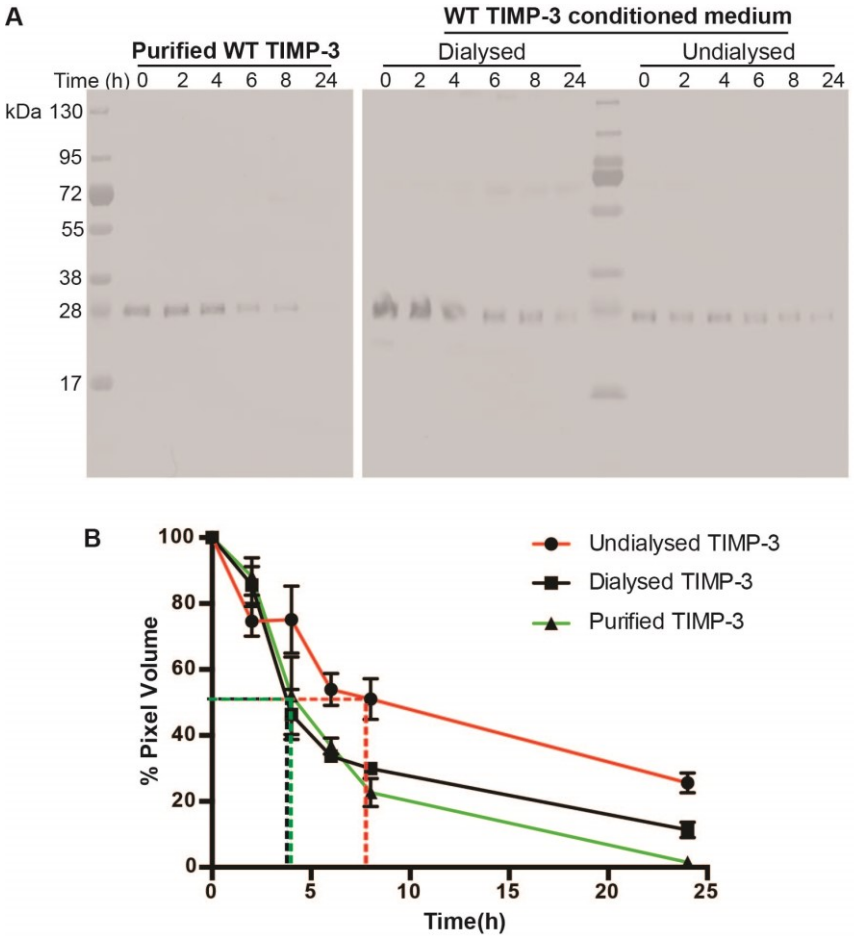


Figure 33: Purified Wild-type TIMP-3 and dialysed Wild-type TIMP-3 conditioned medium have the same half-life on HTB94 cells.

Purified TIMP-3 (1 nM) and dialysed and undialysed medium from HEK-293-EBNA cells expressing Wild-type TIMP-3 (300 µL) were added to HTB94 cells in 1 mL of DMEM with 0.1 % FCS. Samples were harvested at the indicated times, TCA precipitated [4 °C, 5 % (v/v), overnight] and resuspended in 30 µL of 2x SDS-PAGE loading buffer. (**A**) Resuspended samples (15 µL) were analysed by immunoblotting with M2 anti-FLAG antibody and anti-mouse IgG AP-conjugated secondary antibody, with . Bands were visualised using Western blue stabilised substrate for AP and the reaction stopped using AP stop (20 mM Tris-HCl pH 7.5, 10 mM EDTA). (**B**) Band intensity was quantified using Phoretix ID Gel Analysis software and expressed as a percentage of pixel volume at time = 0. Purified TIMP-3 *(n=14)* had a $t_{1/2}$ of 4 hours, dialysed medium from HEK-293-EBNA cells expressing Wild-type TIMP-3 *(n=4)* had a $t_{1/2}$ of 4 hours and undialysed medium from HEK-293-EBNA cells expressing Wild-type TIMP-3 *(n=5)* had a $t_{1/2}$ of 7.5 hours.

4.2.3.4 Endocytosis of TIMP-3 single mutants by HTB94 cells

HEK-293-EBNA cells seeded at 6 x 10^6 in 10 cm plates were transiently transfected (Lipofectamine 2000) with 18 µg of pCEP-4 mammalian expression vector DNA encoding the 12 FLAG-tagged TIMP-3 single mutants. Cells were incubated [37 ^oC, 5 % (v/v) CO_2, 48 h] in 20 mL of serum-free DMEM in the presence of $NaClO_3$. Conditioned media were harvested, dialysed against TBS (1 L, overnight, 4 ^oC) using Slide-A-Lyzer cassettes with a molecular weight cut-off of 3000 Da to remove $NaClO_3$ and stored at -20 ^oC in 1 mL aliquots in low-binding Eppendorf tubes.

HTB94 cells were grown to confluence [37 ^oC, 5 % (v/v), overnight] in DMEM supplemented with 10 % FCS, and washed with serum-free DMEM 3 times before addition of mutant TIMP-3 conditioned media supplemented with 0.1 % FCS. Samples were harvested at the indicated time points and TCA precipitated overnight. All samples were resuspended in 30 µL of 2x SDS-PAGE loading buffer and analysed by immunoblottting using anti-FLAG M2 antibody. Band intensity was measured using Phoretix software and results represented as a percentage of pixel volume at t=0. Mutants were analysed in groups of 2-5 at a time. Each mutant was analysed in at least 3 independent experiments. Endocytosis of Wild-type TIMP-3 was highly reproducible (*n=14*). For clarity, each mutant time course is shown relative to that of Wild-type TIMP-3 (WT TIMP-3) dialysed conditioned medium. The results are for single TIMP-3 mutants are shown in Figure 34 to Figure 39 and Table 18.

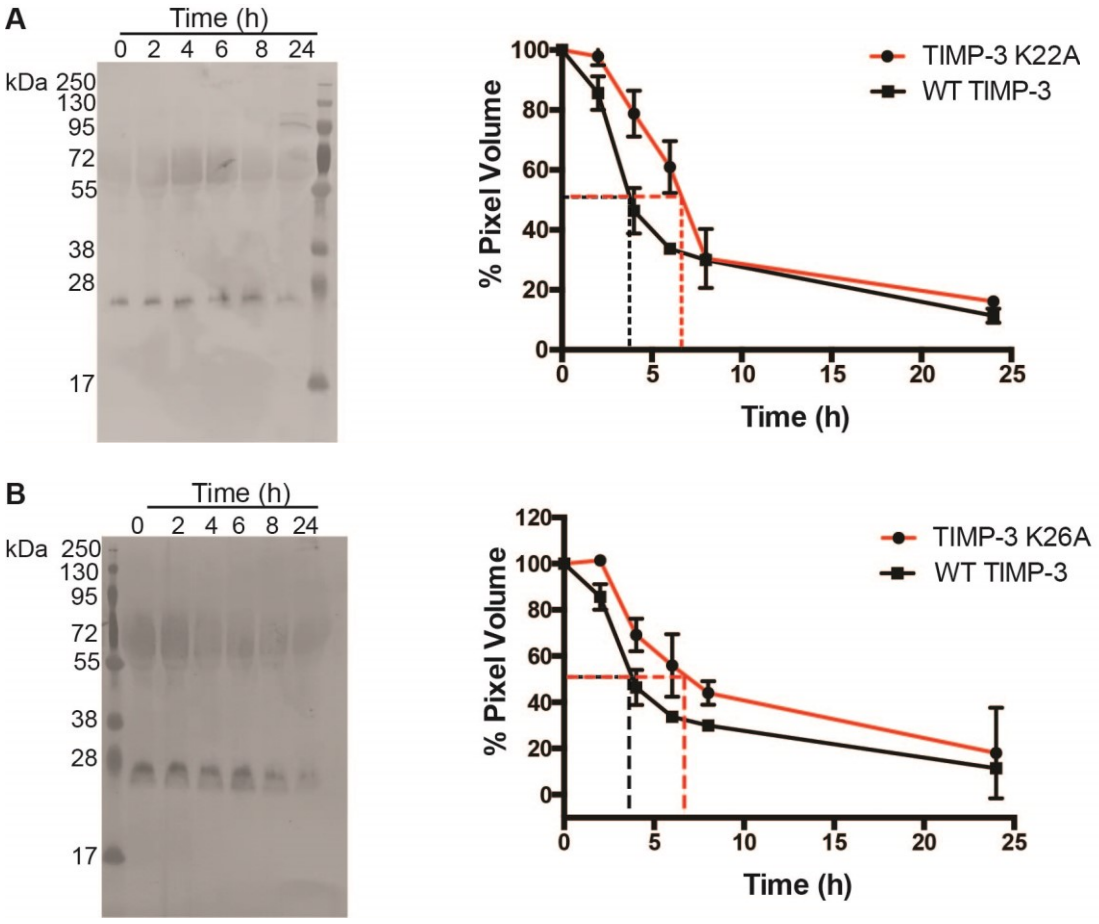


Figure 34: TIMP-3 K22A and TIMP-3 K26A have delayed endocytosis compared to Wild-type TIMP-3.

In a 12-well plate, dialysed conditioned medium (300 µL) from transient expression of TIMP-3 mutants K22A and K26A in HEK-293-EBNA was added to HTB94 cells ($8x10^5$) in 1 mL DMEM supplemented with 0.1 % FCS. Samples were harvested at times indicated, TCA precipitated [5% (v/v), 4 ºC, overnight] and pellets resuspended in 30 µL of 2x SDS-PAGE loading buffer. Resuspended samples (15 µL) were analysed by immunoblotting with an anti-FLAG M2 antibody and an anti-mouse IgG AP-conjugated secondary antibody. Bands were visualised using Western blue stabilised substrate for alkaline phosphatase and the reaction stopped using AP stop (20 mM Tris-HCl pH 7.5, 10 mM EDTA). Band intensity was quantified using Phoretix ID Gel Analysis software and expressed as a percentage of pixel volume at t =0. TIMP-3 K22A (**A**) and TIMP-3 K26A (**B**) had a longer half-life in HTB94 cells (both $t_{1/2}$ of 7 hours, *n=3*) than Wild-type TIMP-3 ($t_{1/2}$ of 4.5 hours).

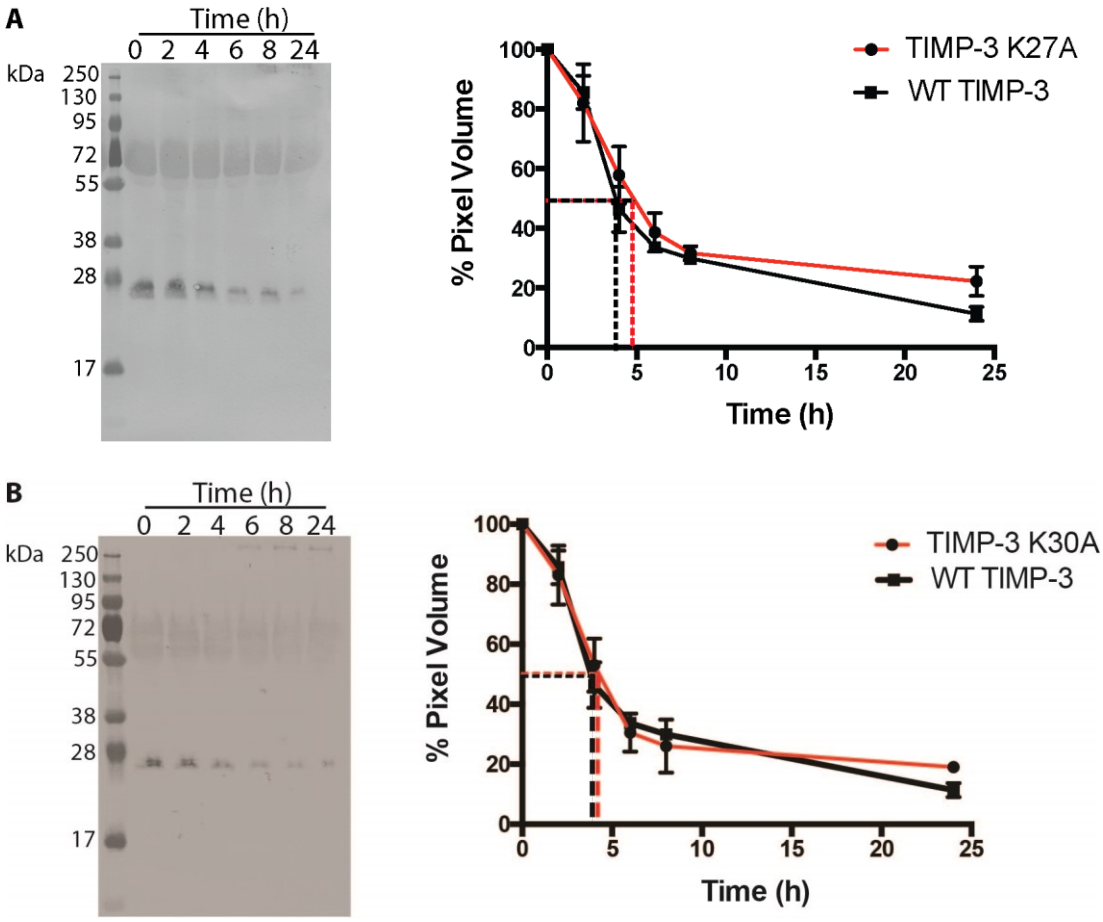


Figure 35: TIMP-3 K27A and TIMP-3 K30A are endocytosed at the same rate as Wild-type TIMP-3.

In a 12-well plate, dialysed conditioned medium (300 µL) from transient expression of TIMP-3 mutants K27A and K30A in HEK-293-EBNA was added to HTB94 cells ($8x10^5$) in 1 mL DMEM supplemented with 0.1 % FCS. Samples were harvested at times indicated, TCA precipitated [5% (v/v), 4 °C, overnight] and pellets resuspended in 30 µL of 2x SDS-PAGE loading buffer. Resuspended samples (15 µL) were analysed by immunoblotting with an anti-FLAG M2 antibody and an anti-mouse IgG AP-conjugated secondary antibody. Bands were visualised using Western blue stabilised substrate for AP and the reaction stopped using AP stop (20 mM Tris-HCl pH 7.5, 10 mM EDTA). Band intensity was quantified using Phoretix ID Gel Analysis software and expressed as a percentage of pixel volume at t =0. Both TIMP-3 K27A (**A**) and TIMP-3 K30A (**B**) have the same half-life in HTB94 cells ($t_{1/2}$ of 4.5 hours, *n=3*) as Wild-type TIMP-3 ($t_{1/2}$ of 4.5 hours).

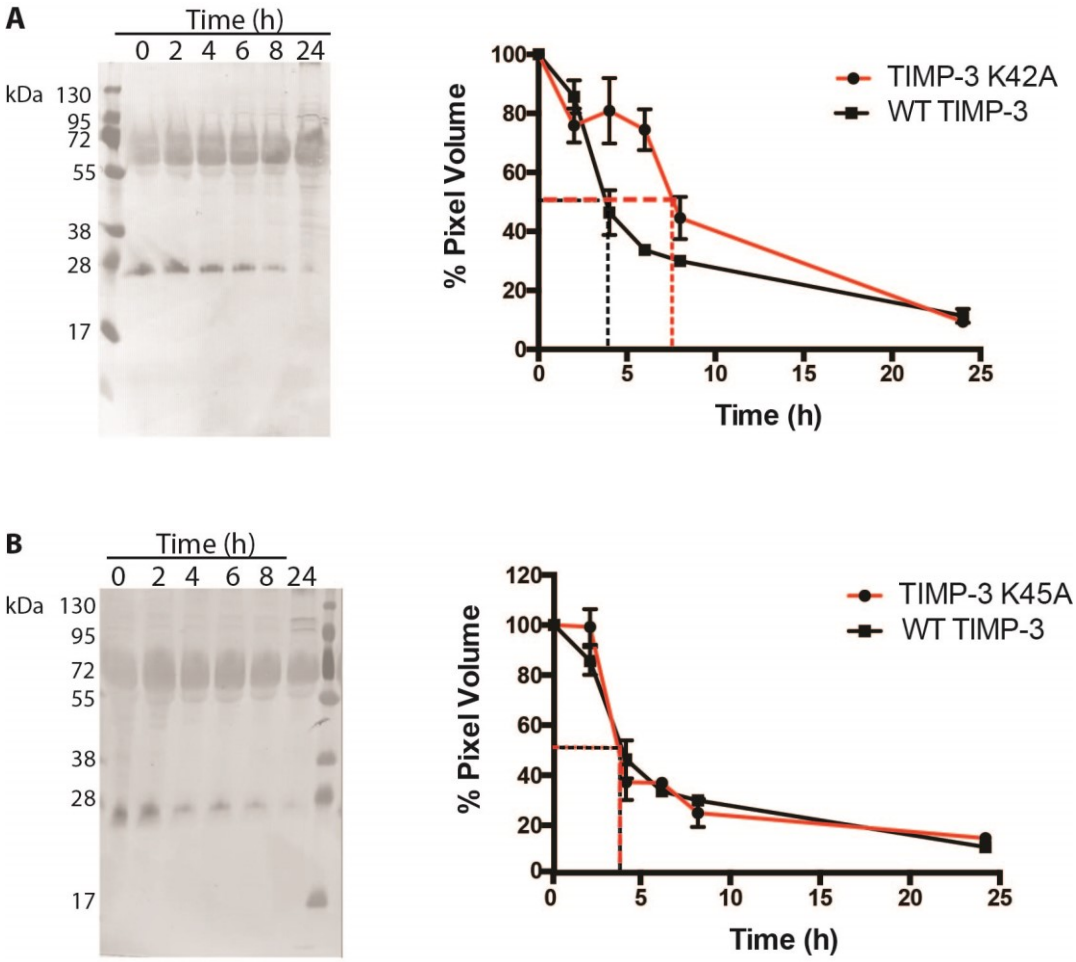


Figure 36: TIMP-3 K42A has delayed endocytosis, but TIMP-3 K45A is endocytosed at the same rate as Wild-type TIMP-3.

In a 12-well plate, dialysed conditioned medium (300 µL) from transient expression of TIMP-3 mutants K42A and K45A in HEK-293-EBNA was added to HTB94 cells ($8x10^5$) in 1 mL DMEM supplemented with 0.1 % FCS. Samples were harvested at times indicated, TCA precipitated [5% (v/v), 4 °C, overnight] and pellets resuspended in 30 µL of 2x SDS-PAGE loading buffer. Resuspended samples (15 µL) were analysed by immunoblotting with an anti-FLAG M2 antibody and an anti-mouse IgG AP-conjugated secondary antibody. Bands were visualised using Western blue stabilised substrate for AP and the reaction stopped using AP stop (20 mM Tris-HCl pH 7.5, 10 mM EDTA). Band intensity was quantified using Phoretix ID Gel Analysis software and expressed as a of percentage pixel volume at t =0. TIMP-3 K42A (**A**) had a longer half-life in HTB94 cells ($t_{1/2}$ = 8 h, *n=3*) than Wild-type TIMP-3 ($t_{1/2}$ of 4.5 hours). TIMP-3 K45A (**B**) had the same half-life as Wild-type TIMP-3 ($t_{1/2}$ of 4.5 hours, *n=3*) in HTB94 cells ($t_{1/2}$ of 4.5 hours, *n=3*).

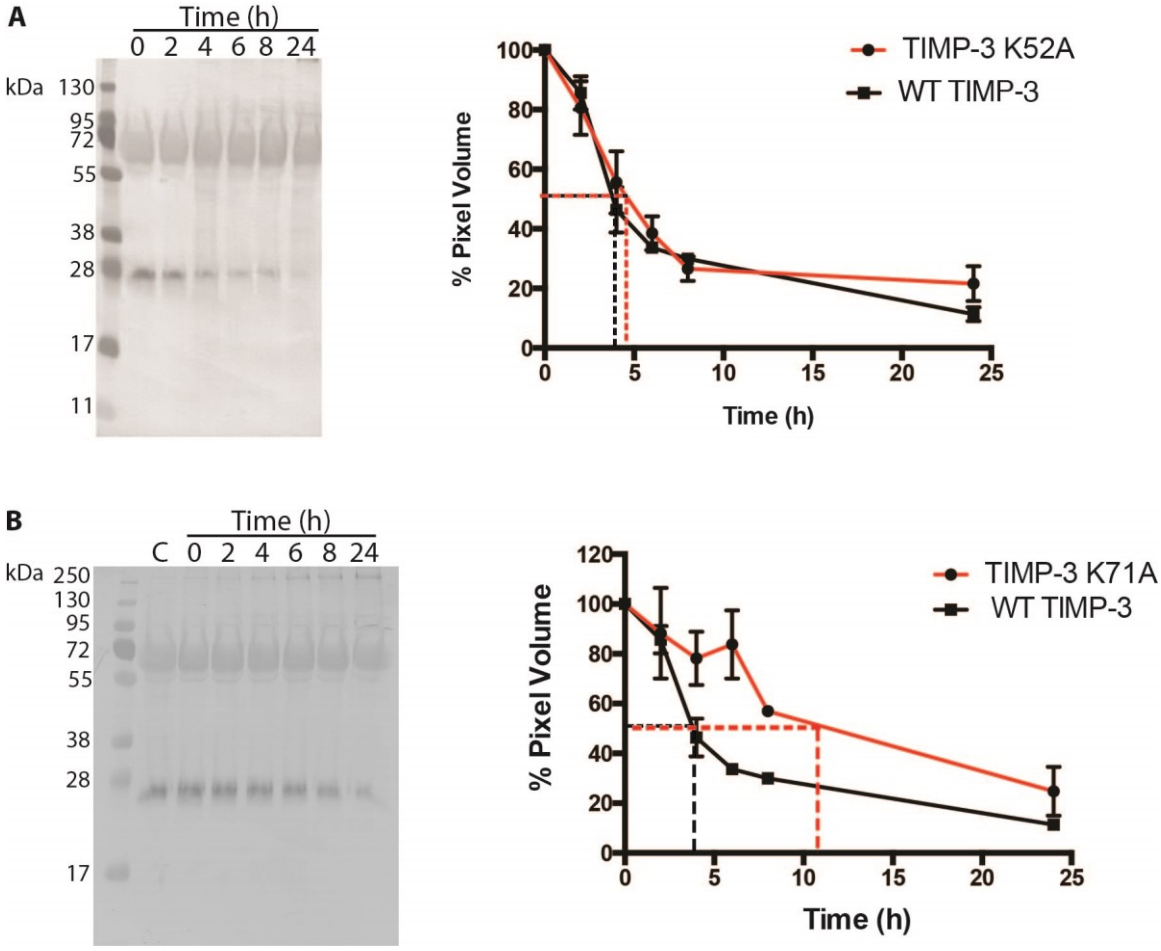


Figure 37: TIMP-3 K52A is endocytosed at the same rate as Wild-type TIMP-3 but TIMP-3 K71A has delayed endocytosis.

In a 12-well plate, dialysed conditioned medium (300 µL) from transient expression of TIMP-3 mutants K52A and K71A in HEK-293-EBNA was added to HTB94 cells ($8x10^5$) in 1 mL DMEM supplemented with 0.1 % FCS. Samples were harvested at times indicated, TCA precipitated [5% (v/v), 4 °C, overnight] and pellets resuspended in 30 µL of 2x SDS-PAGE loading buffer. Resuspended samples (15 µL) were analysed by immunoblotting with an anti-FLAG M2 antibody and an anti-mouse IgG AP-conjugated secondary antibody. Bands were visualised using Western blue stabilised substrate for AP and the reaction stopped using AP stop (20 mM Tris-HCl pH 7.5, 10 mM EDTA). Band intensity was quantified using Phoretix ID Gel Analysis software and expressed as a percentage of pixel volume at t =0. TIMP-3 K52A (**A**) had the same half-life as Wild-type TIMP-3 ($t_{1/2}$ of 4.5 hours, *n=3*) in HTB94 cells. TIMP-3 K71A (**B**) had a longer half-life in HTB94 cells ($t_{1/2}$ = 11 h, *n=4*) relative to Wild-type TIMP-3 ($t_{1/2}$ of 4.5 hours).

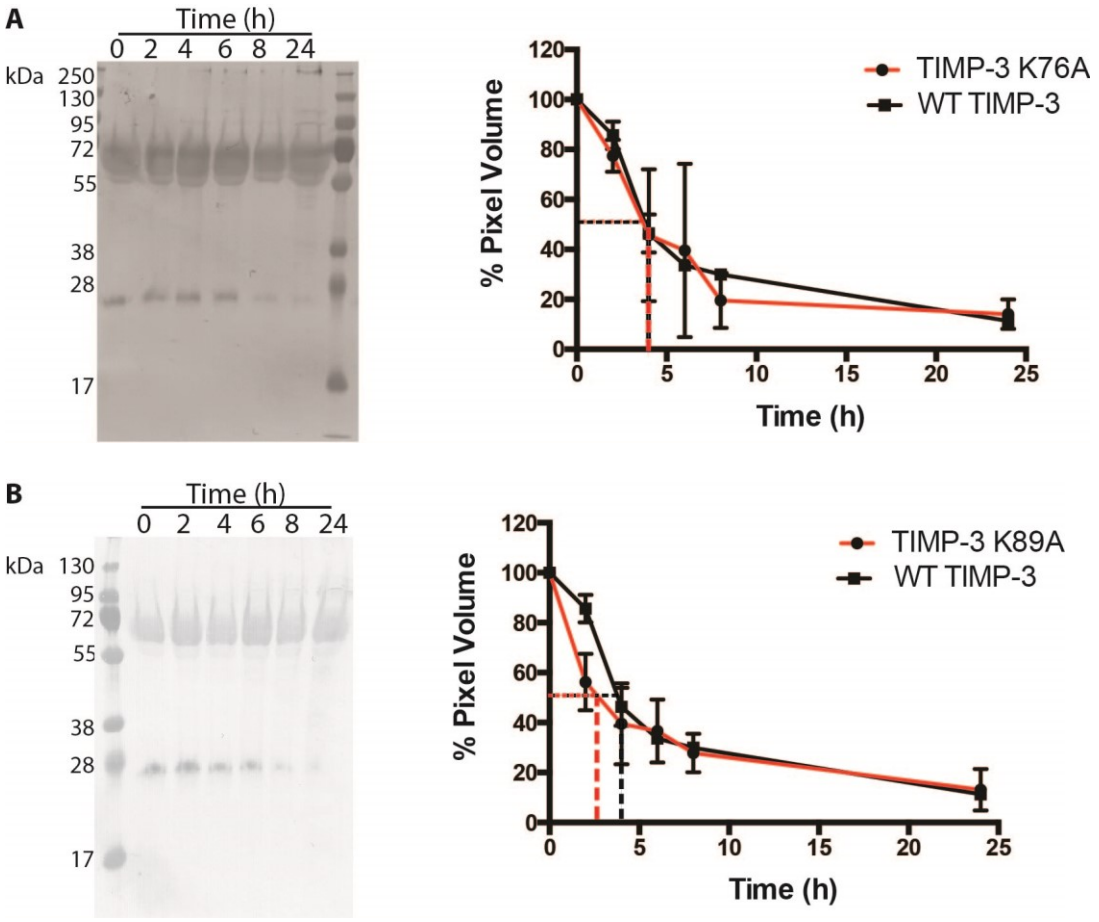


Figure 38: TIMP-3 K76A is endocytosed at the same rate as Wild-type TIMP-3, but TIMP-3 K89A has an increased rate of endocytosis.

In a 12-well plate, dialysed conditioned medium (300 µL) from transient expression of TIMP-3 mutants K76A and K89A in HEK-293-EBNA was added to HTB94 cells ($8x10^5$) in 1 mL DMEM supplemented with 0.1 % FCS. Samples were harvested at times indicated, TCA precipitated [5% (v/v), 4 °C, overnight] and pellets resuspended in 30 µL of 2x SDS-PAGE loading buffer. Resuspended samples (15 µL) were analysed by immunoblotting with an anti-FLAG M2 antibody and an anti-mouse IgG AP-conjugated secondary antibody. Bands were visualised using Western blue stabilised substrate for AP and the reaction stopped using AP stop (20 mM Tris-HCl pH 7.5, 10 mM EDTA). Band intensity was quantified using Phoretix ID Gel Analysis software and expressed as a percentage of pixel volume at t =0. TIMP-3 K76A (**A**) had the same half-life ($t_{1/2}$ of 4.5 hours, *n=4*).as Wild-type TIMP-3 ($t_{1/2}$ of 4.5 hours, *n=3*) in HTB94 cells. TIMP-3 K89A (**B**) has a slightly decreased half-life ($t_{1/2}$ of 3 hours, *n=3*).

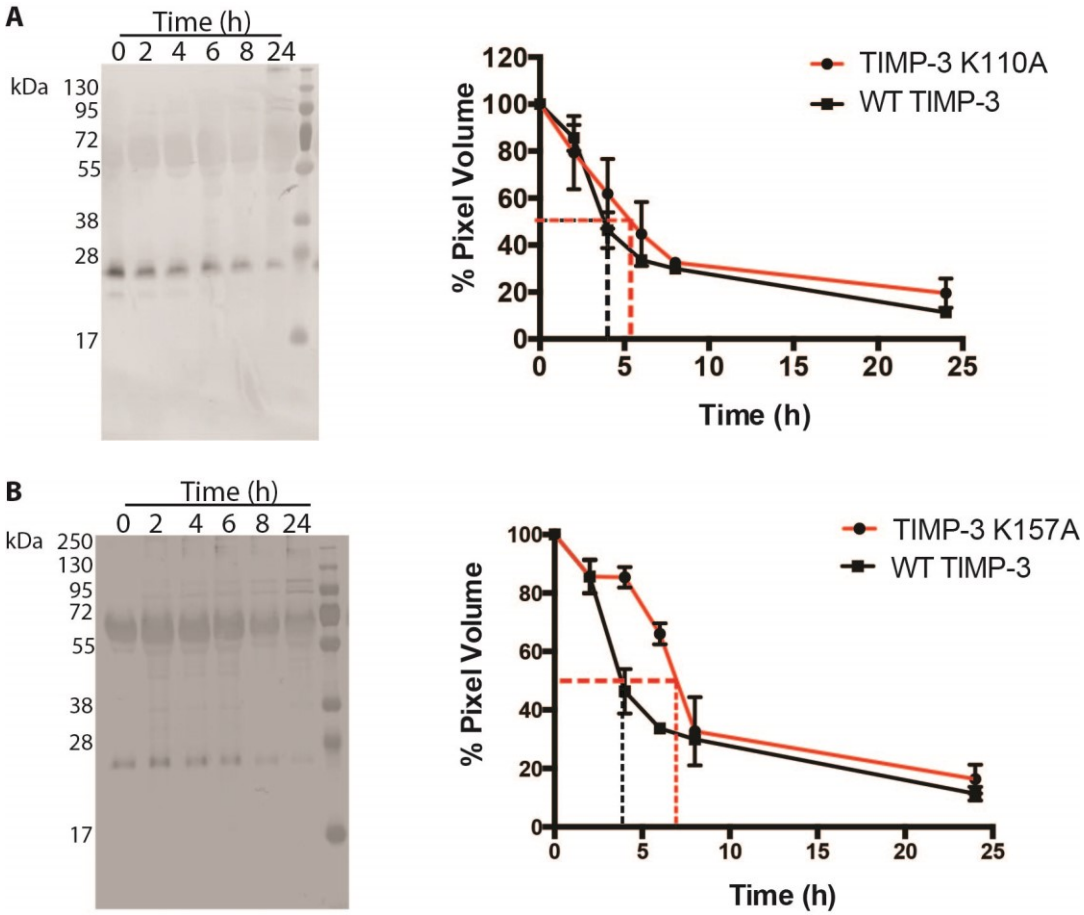


Figure 39: TIMP-3 K110A and TIMP-3 K157A have delayed endocytosis compared to Wild-type TIMP-3.

In a 12-well plate, dialysed conditioned medium (300 µL) from transient expression of TIMP-3 mutants K110A and K157A was added to HTB94 cells ($8x10^5$) in 1 mL DMEM supplemented with 0.1 % FCS. Samples were harvested at times indicated, TCA precipitated [5% (v/v), 4 °C, overnight] and pellets resuspended in 30 µL of 2x SDS-PAGE loading buffer. Resuspended samples (15 µL) were analysed by immunoblotting with an anti-FLAG M2 antibody and an anti-mouse IgG AP-conjugated secondary antibody. Bands were visualised using Western blue stabilised substrate for AP and the reaction stopped using AP stop (20 mM Tris-HCl pH 7.5, 10 mM EDTA). Band intensity was quantified using Phoretix ID Gel Analysis software and expressed as a percentage of pixel volume at t =0. TIMP-3 K110A (**A**) and TIMP-3 K157A (**B**) had longer half-lives in HTB94 cells than Wild-type TIMP-3 ($t_{1/2}$ of 4.5 hours). The increase in half-life for TIMP-3 K157A ($t_{1/2}$ of 7 hours, *n=3*) was more substantial than that for TIMP-3 K110A, ($t_{1/2}$ of 5 hours, *n=3*).

The single mutants showed 3 categories of results. (i) no change in their rate of endocytosis by HTB94 cells, (ii) a slight delay, or (iii) an increase in their rate of endocytosis. No single mutation ablated endocytosis. This was expected, as it has previously been shown for other LRP-1 ligands that a mutation of one lysine residue in the di-lysine pair was not sufficient to prevent LRP-1 binding. The results are summarized in Table 18.

Table 18: Half-life of TIMP-3 single mutants in HTB94 cells.

TIMP-3 single mutants	$t_{1/2}$ (h)	$\Delta t_{1/2}$ (h) between Wild-type & mutant TIMP-3
Wild-Type TIMP-3	4.5	0
K22A	7	+ 2.5
K26A	7	+ 2.5
K27A	4.5	0
K30A	4.5	0
K42A	8	+ 3.5
K45A	4.5	0
K52A	4.5	0
K71A	11	+ 6.5
K76A	4.5	0
K89A	3	-1.5
K110A	5	+ 0.5
K157A	7	+ 2.5

4.2.3.5 Endocytosis of TIMP-3 double mutants from the medium of HTB94 cells

In keeping with literature, no single mutation ablated TIMP-3 endocytosis, so the TIMP-3 double mutants were next investigated. HEK-293-EBNA cells seeded at 6 x 10^6 in a 10 cm plate were transiently transfected (Lipofectamine 2000) with 18 µg of pCEP-4 mammalian expression vector DNA encoding the

10 FLAG-tagged TIMP-3 double mutants. Cells were incubated [37 ^{o}C, 5 % (v/v) CO_2] in 20 mL serum-free DMEM in the presence of $NaClO_3$ for 48 hours. Conditioned media samples were harvested, dialysed in a Slide-A-Lyzer cassette with a molecular weight cut-off of 3000 Da against TBS (1 L, overnight, 4 ^{o}C) to remove $NaClO_3$ and stored at -20 ^{o}C in 1 mL aliquots in low-binding Eppendorf tubes.

HTB94 cells were grown to confluence in DMEM supplemented with 10% FCS [37 ^{o}C, 5 % (v/v), overnight], and washed with serum-free DMEM 3 times before addition of mutant TIMP-3 conditioned media supplemented with 0.1 % FCS. Samples were harvested at the indicated time points and TCA precipitated [4 ^{o}C, 5 % (v/v), overnight]. All pellets were resuspended in 30 µL of 2x SDS-PAGE loading buffer and analysed by immunoblottting using anti-FLAG M2 antibody. Band intensity was measured using Phoretix software and results represented as a percentage of pixel volume at t=0. The band intensity for TIMP-3 K30A/K76A (Figure 42B) was quantified using upper bands only, the lower bands present at t=0 and t=24 were not included . Mutants were analysed in groups of 2-5 at a time. Each mutant was analysed in at least 3 independent experiments. Endocytosis of Wild-type TIMP-3 was highly reproducible (*n=14*). For clarity, endocytosis of each mutant is shown relative to that of Wild-type TIMP-3 dialysed conditioned medium. The results for TIMP-3 double mutants are shown in Figure 40 to Figure 44 and summarized in Table 19.

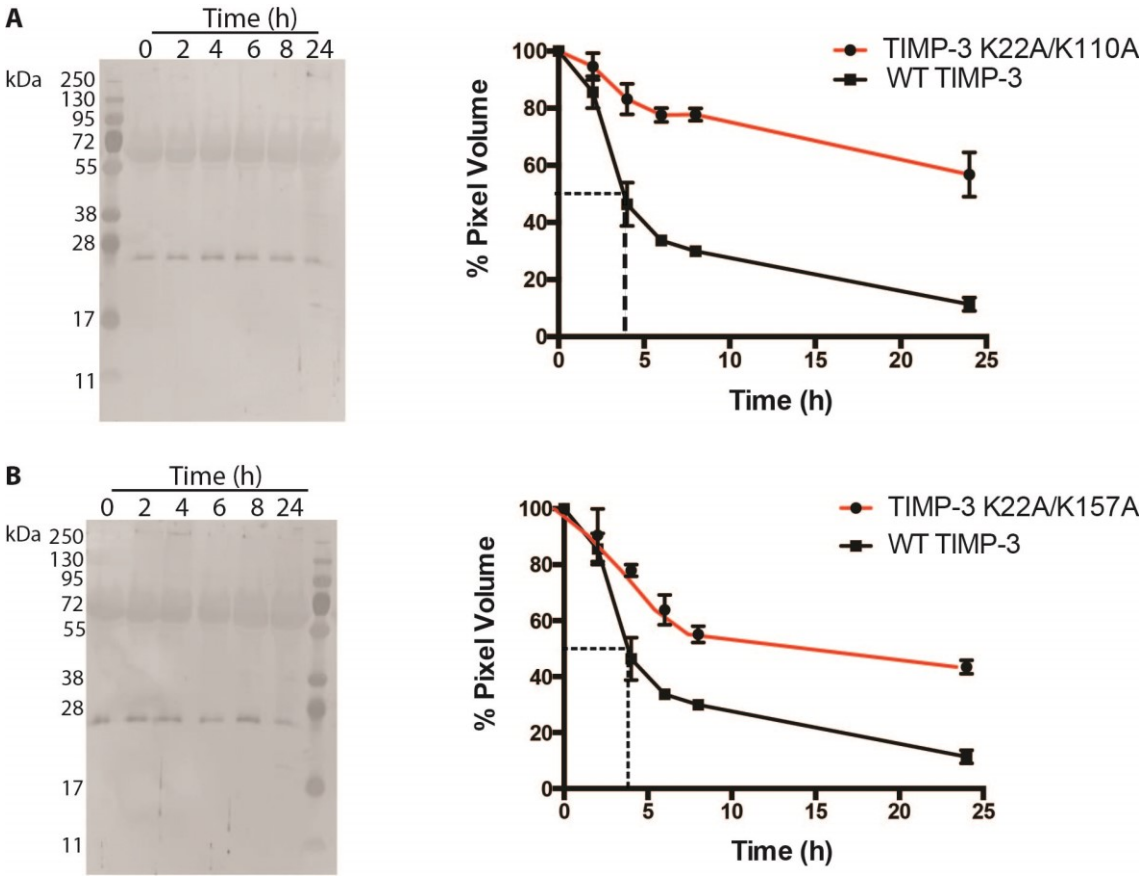


Figure 40: TIMP-3 K22A/K110A and TIMP-3 K22A/K157A are not endocytosed by HTB94 cells within 24 hours.

In a 12-well plate, dialysed conditioned medium (300 µL) from transient expression of TIMP-3 mutants K22AK110A and K22AK157A in HEK-293-EBNA was added to HTB94 ($8x10^5$ cells) in 1 mL DMEM supplemented with 0.1 % FCS. Samples were harvested at times indicated, TCA precipitated [5% (v/v), 4 °C, overnight] and pellets resuspended in 30 µL of 2x SDS-PAGE loading buffer. Resuspended samples (15 µL) were analysed by immunoblotting with an anti-FLAG M2 antibody and an anti-mouse IgG AP-conjugated secondary antibody. Bands were visualised using Western blue stabilised substrate for AP and the reaction stopped using AP stop (20 mM Tris-HCl pH 7.5, 10 mM EDTA). Band intensity was quantified using Phoretix ID Gel Analysis software and expressed as a percentage of pixel volume at t =0. Levels of (**A**) TIMP-3 K22A/K110A (*n=4*) and (**B**) TIMP-3 K22A/K157A (*n=3*) in the conditioned medium dId not decrease to below 50 % within the 24 h analysis period. Approximately 60 % of TIMP-3 K22A/K110A and 50 % of TIMP-3 K22AK157A remained in the conditioned medium after 24 hours.

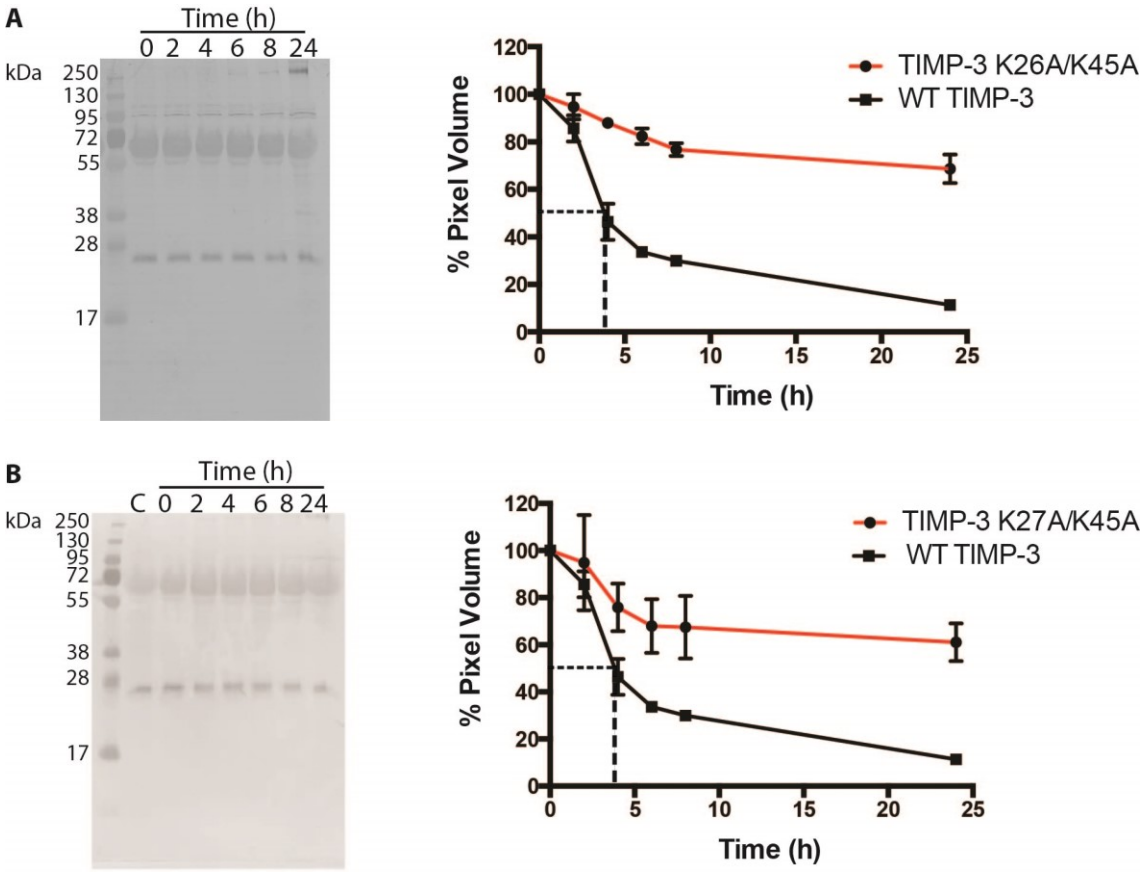


Figure 41: TIMP-3 K26A/K45A and TIMP-3 K27A/K45A are not endocytosed by HTB94 cells within 24 hours.

In a 12-well plate, dialysed conditioned medium (300 µL) from transient expression of TIMP-3 mutants K26A/K45A and K27A/K45 in HEK-293-EBNA was added to HTB94 ($8x10^5$ cells) in 1 mL DMEM supplemented with 0.1 % FCS. Samples were harvested at times indicated, TCA precipitated [5% (v/v), 4 ^oC, overnight] and pellets resuspended in 30 µL of 2x SDS-PAGE loading buffer. Resuspended samples (15 µL) were analysed by immunoblotting with an anti-FLAG M2 antibody and an anti-mouse IgG AP-conjugated secondary antibody. Bands were visualised using Western blue stabilised substrate for AP and the reaction stopped using AP stop (20 mM Tris-HCl pH 7.5, 10 mM EDTA). Band intensity was quantified using Phoretix ID Gel Analysis software and expressed as a percentage of pixel volume at t =0. Levels of (**A**) TIMP-3 K26A/K45A and (**B**) TIMP-3 K27A/K45 in the conditioned medium did not decrease to below 50 % within the 24 h analysis period. Approximately 70% of TIMP-3 K26A/K45A and 65% of TIMP-3 K27A/K45 remained in the conditioned medium after 24 hours

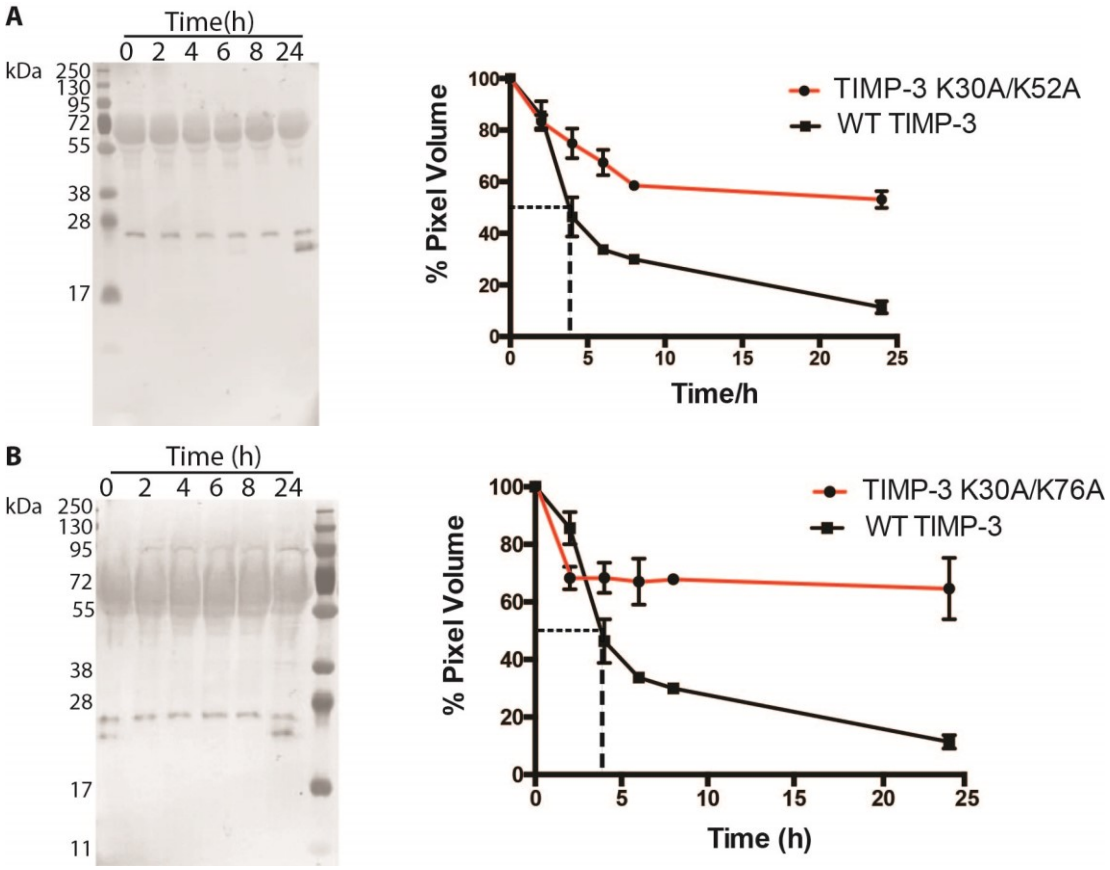


Figure 42: TIMP-3 K30A/K52A and TIMP-3 K30A/K76A are not endocytosed by HTB94 cells within 24 hours.

In a 12-well plate, dialysed conditioned medium (300 µL) from transient expression of TIMP-3 mutants K30A/K52A and K30A/K76A in HEK-293-EBNA was added to HTB94 cells ($8x10^5$) in 1 mL DMEM supplemented with 0.1 % FCS. Samples were harvested at times indicated, TCA precipitated [5% (v/v), 4 °C, overnight] and pellets resuspended in 30 µL of 2x SDS-PAGE loading buffer. Resuspended samples (15 µL) were analysed by immunoblotting with an anti-FLAG M2 antibody and an anti-mouse IgG AP-conjugated secondary antibody. Bands were visualised using Western blue stabilised substrate for AP and the reaction stopped using AP stop (20 mM Tris-HCl pH 7.5, 10 mM EDTA). Band intensity was quantified using Phoretix ID Gel Analysis software and expressed as a percentage of pixel volume at t =0. Band intensity over time for TIMP-3 K30A/K76A (**B**) was quantified using upper bands only. Levels of (**A**) TIMP-3 K30A/K52A *(n=3)* and (**B**) TIMP-3 K30A/K76A *(n=3)* in the conditioned medium do not decrease to below 50 % within 24 h analysis period. Approximately 55 % of TIMP-3 K30A/K52A and 65% of TIMP-3 K30A/K76A remained in the conditioned medium after 24 hours.

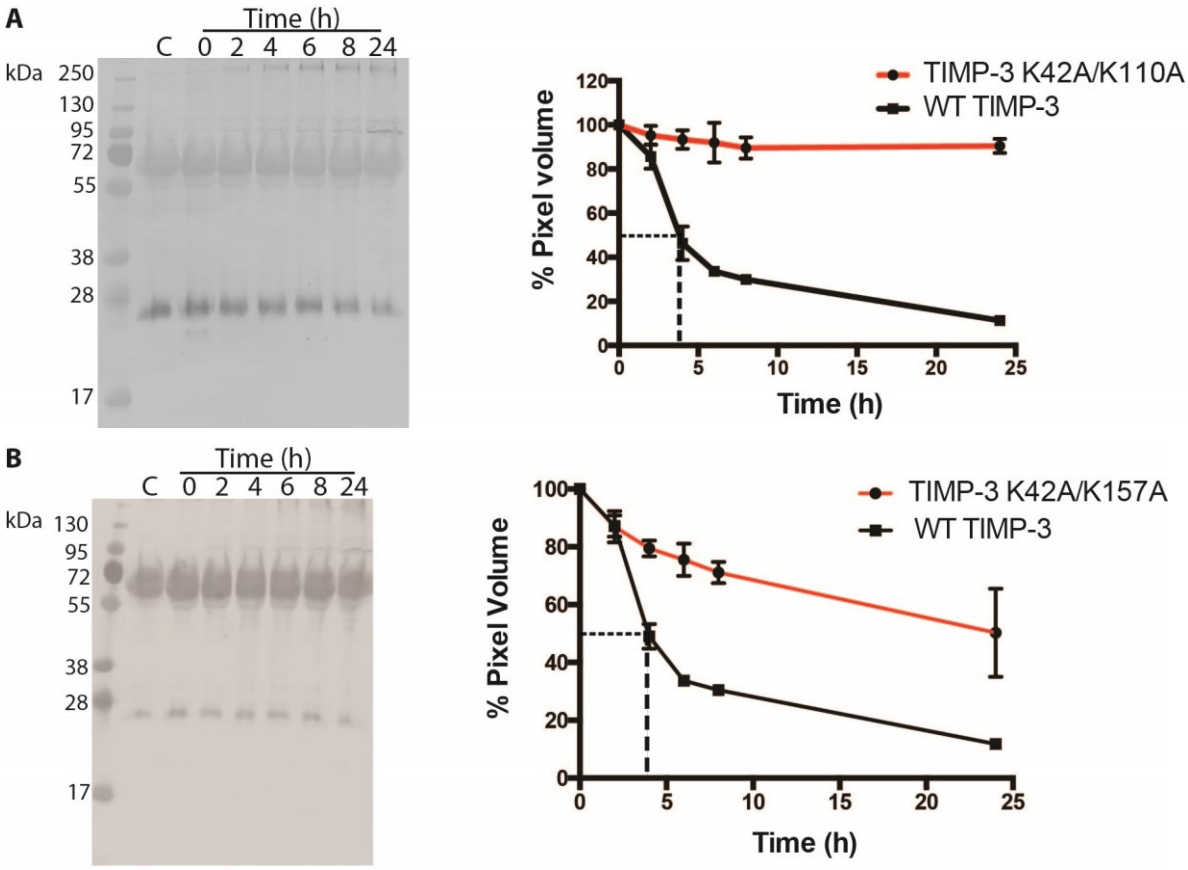


Figure 43: TIMP-3 K42A/K110A and TIMP-3 K42A/K157A are not endocytosed by HTB94 cells within 24 hours.

In a 12-well plate, dialysed conditioned medium (300 µL) from transient expression of TIMP-3 mutants K42A/K110A and K42A/K157A in HEK-293-EBNA was added to HTB94 ($8x10^5$) cells in 1 mL DMEM supplemented with 0.1 % FCS. Samples were harvested at times indicated, TCA precipitated [5% (v/v), 4 ºC, overnight] and pellets resuspended in 30 µL of 2x SDS-PAGE loading buffer. Resuspended samples (15 µL) were analysed by immunoblotting with an anti-FLAG M2 antibody and an anti-mouse IgG AP-conjugated secondary antibody. Bands were visualised using Western blue stabilised substrate for AP and the reaction stopped by using AP stop (20 mM Tris-HCl pH 7.5, 10 mM EDTA). Band intensity was quantified using Phoretix ID Gel Analysis software and expressed as a percentage of pixel volume at t =0. Levels of (**A**) TIMP-3 K42A/K110A and (**B**) TIMP-3 K42A/K157A in the conditioned medium did not decrease to below 50 % within 24 h. Approximately 90 % of K42AK110A and 50 % of K42A/K157A remained in the conditioned medium after 24 hours.

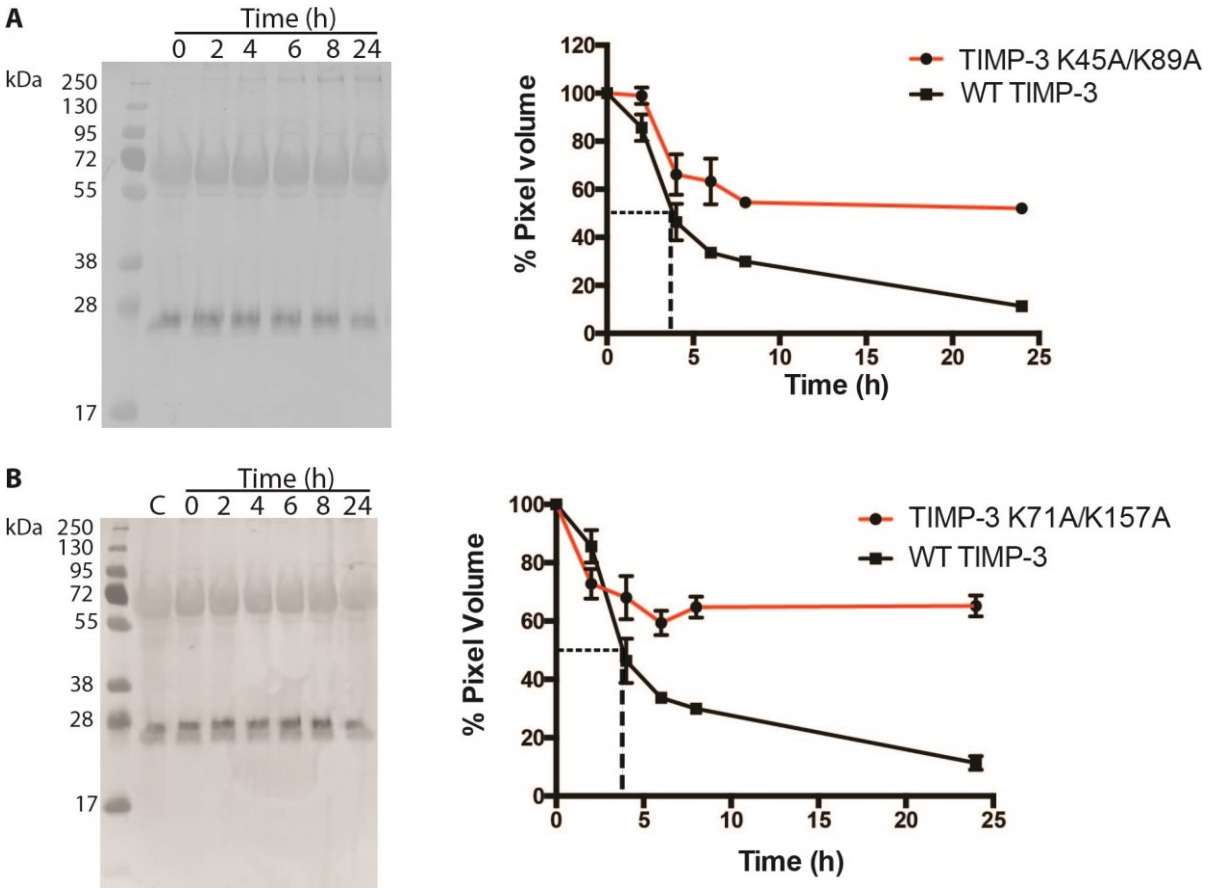


Figure 44: TIMP-3 K45A/K89A and TIMP-3 K71A/K157A are not endocytosed by HTB94 cells within 24 hours.

In a 12-well plate, dialysed conditioned medium (300 µL) from transient expression of TIMP-3 mutants K45AK89A and K71AK157A in HEK-293-EBNA was added to HTB94 cells ($8x10^5$) in 1 mL DMEM supplemented with 0.1 % FCS. Samples were harvested at times indicated, TCA precipitated [5% (v/v), 4 °C, overnight] and pellets resuspended in 30 µL of 2x SDS-PAGE loading buffer. Resuspended samples (15 µL) were analysed by immunoblotting with an anti-FLAG M2 antibody and an anti-mouse IgG AP-conjugated secondary antibody. Bands were visualised using Western blue stabilised substrate for AP and the reaction stopped by using AP stop (20 mM Tris-HCl pH 7.5, 10 mM EDTA). Band intensity was quantified using Phoretix ID Gel Analysis software and expressed as a percentage of pixel volume at t =0. Levels of (**A**) TIMP-3 K45A/K89A and (**B**) TIMP-3 K71A/K157A in the conditioned medium did not decrease to below 50 % within the 24 h analysis period. Approximately 60 % of TIMP-3 K45A/K89A and 65 % of TIMP-3 K71A/K157A remained in the conditioned medium after 24 hours.

All of the double mutants tested showed resistance to endocytosis by HTB94 cells over 24 hours (Table 19). This is in keeping with other LRP-1

ligand studies, which showed that a di-lysine pair is required to mediate ligand binding to LRP-1.

Table 19: Resistance of TIMP-3 di-lysine mutants to LRP-1-mediated endocytosis by HTB94 cells.

TIMP-3 double mutants	Resistance to endocytosis by HTB94 cells In 24 hours	% of mutant remaining in HTB94 cell medium after 24 hours
K22A/K110A	□	60
K22A/K157A	□	50
K26A/K45A	□	70
K27A/K45A	□	65
K30A/K52A	□	55
K30A/K76A	□	65
K42A/K110A	□	90
K42A/K157A	□	50
K45A/K89A	□	60
K71A/K157A	□	65

4.2.4. Evaluation of the effect of Wild-type and mutant TIMP-3 on HTB94 cell viability

TIMP-3 has been shown to induce apoptosis in a variety of cell types. For example, conditioned media from a TIMP-3-expressing colon carcinoma cell line has been shown to activate cell death in fibroblasts (Smith et al., 1997) and infection of melanoma cells with adenoviruses encoding TIMP-3 induced apoptosis in melanoma cells (Ahonen et al., 1998). Exogenously added TIMP-3 (50 nM) was also shown to induce apoptosis in a melanoma cell line by stabilizing cell death receptors (Ahonen et al., 2003). We therefore assessed the viability of HTB94 cells in the presence and absence of Wild-type TIMP-3 and TIMP-3 mutants K26A/K45A and K42A/K110A.

Viable cell number was assessed using the 3-(4,5-dimethylthiazol-2-yl)-5-(3-carboxymethoxyphenyl)-2-(4-sulfophenyl)-2H-tetrazolium (MTS) assay, in which a tetrazolium active compound is reduced to a coloured formazan product that is soluble in culture medium. The production of this formazan product detects mitochondrial activity and therefore absorbance at 490 nm is proportional to the metabolic activity of the cells in the culture. This assay was used as it was a quick, convenient, non-radioactive and safe means to estimate cell viability. The limitation of this assay is that detection of metabolic activity does not necessarily reflect live cell number as a small but very active subgroup of cells may be present.

HTB94 cells (10^4 cells per well) were cultured in a 96-well plate in DMEM supplemented with 10 % (v/v) FCS for 24 h (37 ^oC, 5 % CO_2). After washing in serum-free DMEM, HTB94 cells were incubated in triplicate with or without Wild-type TIMP-3, TIMP-3 K26A/K45A or TIMP-3 K42A/K10A (50 or 100 nM) or sodium nitroprusside (SNP, 10 mM) in DMEM supplemented with 0.1 % v/v FCS. After 24 h incubation, culture media were removed and a mixture of fresh DMEM (100 µL, supplemented with 0.1 % v/v FCS) and MTS reagent (20 µL) were added. Cell number was evaluated by quantifying the coloured formazan product after incubation for 45 min (37 ^oC, 5 % CO_2) by measuring the absorbance at 490 nm.

Figure 45 shows a comparison of HTB94 cell number after treatment with or without Wild-type TIMP-3, TIMP-3 mutants K26A/K45A and K42A/K110A or SNP. SNP induces apoptotic cell death by production of hydrogen peroxide (Yamada et al., 1996) and was used here as a control for cell death, while cells treated with neither TIMP-3 nor SNP served as untreated controls.

HTB94 cells treated with 50 or 100 nM Wild-type TIMP-3 for 24 h (the duration of TIMP-3 endocytosis-resistance assays in the current Chapter and Section 5.2.3), showed no decrease in absorbance at 490 nm relative to untreated cells, indicating that, at concentrations up to 100 nM, TIMP-3 caused no cell death in these cells. Similarly, TIMP-3 K26A/K45A caused no observable cell death over 24 h at 50 or 100 nM. Cells treated with 50 nM K42A/K110A showed no decrease in viability, but a reduced average cell number was measured in the presence of 100 nM of the mutant. The decrease fell within the standard deviation of the replicate values and so was not significant (p-value = 0.1884).

Therefore neither TIMP-3 nor TIMP-3 mutant treatment at the concentrations used in the endocytosis assays, caused a reduction in metabolic activity associated with cell death. Therefore the observed accumulation of TIMP-3 K26A/K45A and TIMP-3 K42A/K110A in culture media was unlikely to be related to TIMP-3-induced apoptosis.

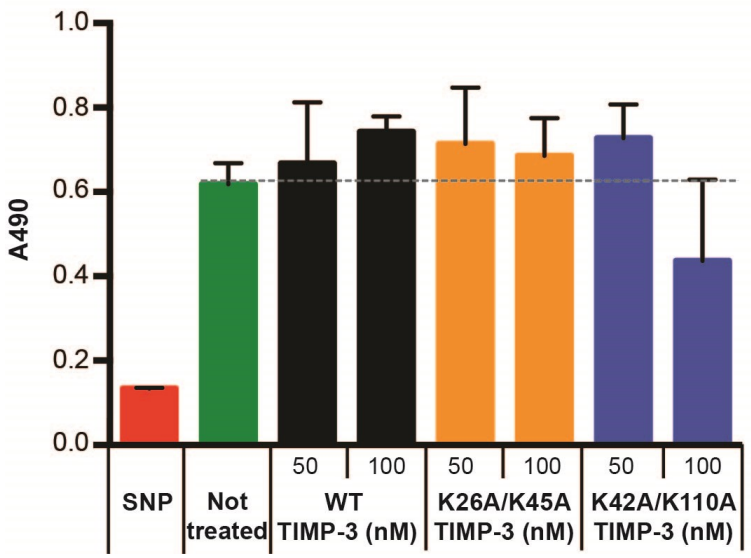


Figure 45: The effect of TIMP-3 and mutants on HTB94 cell viability.

HTB94 cells were seeded (10^4 per well) in a 96-well plate in DMEM supplemented with 10 % (v/v) FCS for 24 h (37 ^oC, 5 % CO_2). Cells were then washed once with serum-free DMEM and incubated with or without SNP (10 mM), Wild-type TIMP-3, TIMP-3 K26A/K45A or TIMP-3 K42A/K10A (50 or 100 nM) in DMEM supplemented with 0.1 % (v/v) FCS. After 24 h, culture media were removed and fresh DMEM supplemented with 0.1 % (v/v) FCS (100 µL) and MTS reagent (20 µL) added, and cell number evaluated by quantification of the formazan reaction product at 490 nm after 45 mins.

4.3 Discussion

Based on the previously identified LRP-1 ligand binding motif (Arandjelovic et al., 2005; Skeldal et al., 2006; van den Bigglelaar et al., 2011), we generated 22 TIMP-3 mutants in which single lysine residues and pairs of lysine residues were mutated to alanine in order to generate an LRP-1-resistant mutant of TIMP-3. We anticipated that such a TIMP-3 mutant would have a longer half-life and increased chondroprotective effect in cartilage.

In this Chapter, we set out to perform an initial screen of these mutants to identify candidates for further evaluation. We assessed the mutants by quantifying the clearance of each mutant from the medium of HTB94 chondrosarcoma cells over time. We required cells that expressed the LRP-1 receptor and endocytosed TIMP-3, and that remained adherent during the washing steps required by the experimental protocol. We found that the HTB94 chondrosarcoma cell line met with all of our requirements. While HTB94 cells do not retain all the features of primary chondrocytes, they were an amenable in vitro model for this initial screen.

Previous LRP-1 ligand binding studies have used NMR (Jensen et al., 2006), X-ray crystallography (Fisher et al., 2006), fluorescence spectrometry (Jensen et al., 2009c), surface plasmon resonance and mutagenesis (van den

Bigglelaar et al., 2011) to identify the critical binding motif. However, as the work presented here was our initial assessment of the mutants, we required a methodology that was easily optimised, quantifiable and suitable for rapid and reproducible assessment of multiple mutants. We choose to use immunoblotting and densitometry analysis to generate a shortlist of mutants exhibiting endocytosis-resistance in a 24 h period.

In their study of α_2M, Arandjelovic et al. (2005) used site-directed mutagenesis and radiochemistry to determine that mutation of lysine 1370 of the predicted di-lysine pair K1370/K1373 almost entirely blocked binding to RAW264.7 cells via LRP-1. This is in contrast with reported studies on a number of other LRP-1 ligands, which found that mutation of a single lysine residue could not ablate binding. For example, Skeldal et al. (2006) identified the binding site of the uPA:PAI-1 complex for LRP-1 by site-directed mutagenesis of lysine residues in PAI-1 and surface plasmon resonance, and found that mutation of a single lysine residue did not ablate receptor binding. In 2011, van den Biggelaar et al. also showed that mutation of a single lysine in the di-lysine pair of RAP was insufficient to ablate LRP-1 binding, while the K256A/K289A double mutant showed only minimal binding.

Our findings were in keeping with the Skeldal and van den Biggelaar studies, in that we found that mutation of a single lysine residue did not prevent TIMP-3 endocytosis. We found that such single mutations had 3 kinds of effects: of the 12 single mutants assessed, 7 showed delayed endocytosis, 4 showed no change in the rate of endocytosis and surprisingly 1 had an increased rate of uptake. Those with delayed endocytosis showed an increase

in half-life ranging from 2.5 – 6.5 hours. The single mutant showing an increased rate of endocytosis (K89A) had a reduction in half-life of 1.5 hours.

Interestingly, all of the double mutants showed resistance to endocytosis by HTB94 cells in the 24-hour time frame assessed. This may indicate that the TIMP-3 binding site for LRP-1 is more extended than we anticipated. The degree to which the TIMP-3 mutants remained in the HTB94 cell medium varied. Of the 10 double TIMP-3 mutants tested, 9 were found to have 50 % to 70 % remaining in the HTB94 conditioned medium after 24 hours, with 90 % of 1 double mutant (K42A/K110A), remaining in the conditioned medium after 24 hours.

Exogenously added TIMP-3 has been shown to induce apoptosis in a variety of cells, raising the question as to whether TIMP-3 mutants remained in the culture media due to endocytosis resistance or due to TIMP-3-induced cell death. It was therefore necessary to eliminate TIMP-3-induced apoptosis as a contributing factor in the observed accumulation of mutant TIMP-3 in HTB94 conditioned media. The metabolic activity of HTB94 cells exposed to Wild-type or mutant TIMP-3 (50 and 100 nM) over 24 h was quantified by MTS assay. No decrease in metabolic activity was observed for HTB94 cells treated with either Wild-type or mutant TIMP-3. These findings are in agreement with Gendron et al. who previously showed that incubation of primary articular chondrocytes with N-TIMP-3 at concentrations up to 100 nM for 3 days did not induce apoptotic cell death (Gendron et al., 2003). To directly detect evidence of cell death, terminal deoxynucleotidyl transferase dUTP nick end labeling (TUNEL) assay or Live and Dead staining (Invitrogen) would be required. A characteristic of late apoptosis is the generation of DNA double-strand breaks

due to extensive genomic DNA fragmentation. TUNEL assays directly identify apoptotic cells by terminal deoxynucleotidyl transferase-mediated addition of labeled deoxyuridine triphosphate nucleotides to the 3'-OH end of the DNA strand breaks. These can then be visualised by the incorporation of a label. Another method for detection of cell death is Live/Dead cell staining. These assays are based on the reaction of a fluorescent reactive dye with cellular amines. The dye permeates compromised membranes of necrotic cells and reacts with free amines in the cell interior as well as on the cells surface, generating a strong fluorescent signal. Conversely, only cell surface amines of viable cells interact with the fluorescent reactive dye, giving a reduced level of staining

This preliminary assessment identified 10 potential endocytosis-resistant TIMP-3 mutants from our starting list of 22 candidates. These 10 mutants were shortlisted for further analyses including confirmation of reduced LRP-1 binding and assessment of affinity for prototypic target metalloproteinases and sulfated glycosaminoglycans in Chapter 5.

Chapter 5: Bioactivity of TIMP-3 mutants

5.1 Introduction

In Chapter 4, transiently expressed TIMP-3 mutants were assessed for their endocytosis resistance in the HTB94 human chondrosarcoma cell-line. A shortlist of potential endocytosis-resistant TIMP-3 mutants was generated from an original starting list of 22 TIMP-3 mutants. 12 of these mutants contained a single lysine to alanine mutation and the remaining 10 contained 2 lysine to alanine mutations. Of these, only the TIMP-3 mutants containing 2 lysine to alanine mutations (TIMP-3 double mutants) were observed to be resistant to endocytosis by HTB94 cells within the 24 h experimental time frame.

In this chapter, we purified the TIMP-3 double mutants and assessed their bioactivity in order to identify whether the TIMP-3 mutants had improved chondroprotective activity relative to Wild-type TIMP-3. The mutants were assessed in terms of their purification yields, binding to LRP-1, affinity for target metalloproteinases and affinity for sulfated glycosaminoglycans.

5.2 Results

5.2.1 Generation of stable cell lines for expression of shortlisted mutants

Stable cell lines were generated to allow for long term, reproducible expression of the mutants of interest.

HEK-293-EBNA cells, seeded at 8 x 10^5 cells per well of a 12 well plate, were transfected with pCEP4 mammalian expression vector encoding FLAG-tagged TIMP-3 mutants using liposome transfection (Section 2.2.4.1). Cells then underwent hygromycin B selection (100, 400 and 800 µg/mL) (Section 2.2.4.2). Over time, those cells containing the hygromycin B resistance

selection marker divided and expanded to comprise the entire cell population. Cells containing more copies of the episomal pCEP4 vector were able to grow in higher concentrations of hygromycin B. This is thus not a true stable cell line, but rather a stable population of cells.

Expression of mutant TIMP-3 protein by the cell lines was tested. Cells were seeded in a 10 cm plate and incubated in 10 mL of serum-free DMEM (DMEM supplemented with 100 U/mL penicillin, 100 µg/mL streptomycin) for 2 days (37 ^{o}C, 5% CO_2). 300 µL of conditioned medium in a final volume of 1 mL 0.1 % FCS in DMEM was TCA precipitated overnight. The samples were analysed by immunoblotting (Section 2.2.3.3). Briefly, the precipitated sample was resuspended in 30 µL of reducing 2x SDS buffer and 15 µL analysed by immunoblotting with an anti-FLAG M2 antibody and an anti-mouse IgG AP-conjugated secondary antibody. Bands were visualised using Western blue stabilised substrate for AP and the reaction stopped using AP stop (20 mM Tris-HCl pH 7.5, 10 mM EDTA).

As an example, the expression of TIMP-3 mutants K26A/K45A and K27A/K45A selected at different hygromycin concentrations is shown in Figure 46. The blot clearly shows that selection with 100 µg/mL hygromycin B gave a higher expression of both mutants than did selection with 400 µg/mL hygromycin B.

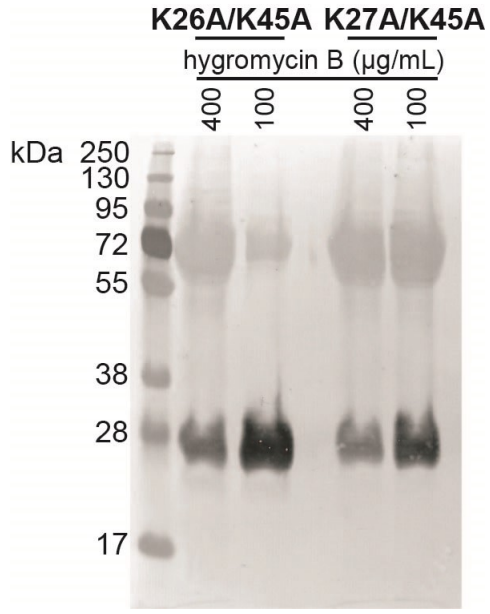


Figure 46: Generation of HEK-293-EBNA stable cell lines expressing TIMP-3 K26A/K45A and K27A/K45A.

HEK-293-EBNA cells were transfected with TIMP-3 K26A/K45A or K27A/K45A using Lipofectamine 2000 and cells selected with either 400 or 100 µg/mL hygromycin B. Subcultures were incubated in serum-free DMEM for 2 days and 300 µL of conditioned medium diluted to 1 mL in DMEM supplemented with 0.1 % FCS. Samples were TCA precipitated [5% (v/v), 4 °C, overnight] and pellets resuspended in 30 µL of 2x SDS-PAGE loading buffer. Resuspended samples (15 µL) were then analysed by immunoblotting with an anti-FLAG M2 antibody and an anti-mouse IgG AP-conjugated secondary antibody. Bands were visualised using Western blue stabilised substrate for AP and reaction stopped using AP stop (20 mM Tris-HCl pH 7.5, 10 mM EDTA).

Of the hygromycin B concentrations used in the generation of TIMP-3 double mutant stable lines (100, 400 and 800 µg/mL), 100 µg/mL was found to be optimum for TIMP-3 double mutant expression. Using this protocol, stable lines for all 10 shortlisted double mutants were successfully generated. The newly generated stable cell lines were expanded for use in larger-scale protein expression.

5.2.2 Purification of TIMP-3 mutants

The stable lines generated in Section 5.2.1 were purified on a large-scale to enable analysis of the inhibitory activity and ECM binding of the shortlisted TIMP-3 mutants both in vitro and ex vivo. Wild-type TIMP-3 has been shown to inhibit aggrecan degradation in cartilage explants at a concentration of 100 nM (Gendron et al., 2003; Lim et al., 2010), therefore a minimal purified concentration of 100 nM was required. Variations in protein expression levels had been observed in the HEK-293-EBNA cells transiently transfected with TIMP-3 mutants using liposome transfection (Section 4.2.1.1). Therefore it was expected that the stably expressed mutants may exhibit variation in their protein expression levels, such that some may not readily express sufficient protein levels required for further analysis.

Culture conditions for protein expression of the stably transfected TIMP-3 mutants were the same as those for the transiently transfected cells, (Section 4.2.1.1) with some modifications. Briefly, the HEK-293-EBNA cells stably transfected with pCEP4-TIMP-3 mutant construct were grown to confluence in a 15 cm plate in DMEM supplemented with 100 U/mL penicillin, 100 µg/mL streptomycin, 10 % FCS, 100 µg/mL hygromycin B. Once confluent, the media were changed to serum-free DMEM containing $NaClO_3$, which has previously been shown to inhibit endocytosis of TIMP-3 (Troeberg et al., 2009) and was added to maximize TIMP-3 levels in the conditioned media. Conditioned media were harvested after 48 h, and centrifuged to remove cell debris and passed over a 2 mL anti-FLAG M2-agarose resin equilibrated in serum-free DMEM at room temperature. The resin was first washed in serum-free DMEM (10 column volumes) with 100 U/mL penicillin, 100 µg/mL streptomycin, followed by a high

salt wash (5 column volumes) in serum-free DMEM containing 500 mM NaCl to remove any non-specifically bound proteins. The column was washed again in serum-free DMEM (10 column volumes) to ensure that all $NaClO_3$ and NaCl had been fully removed before elution. TIMP-3 mutant proteins were then eluted in 5 mL fractions using 200 µg/mL FLAG peptide in serum-free DMEM. Purifications were analysed by immunoblotting with M2 anti-FLAG antibody.

All 10 shortlisted TIMP-3 mutants were successfully purified, albeit with differing yields. From Figure 47, it is clear that TIMP-3 K26A/K45A and K42A/K110A were both purified to a high yield. All 5 elution fractions for both mutants contained detectable levels of mutant protein. As with Wild-type TIMP-3, their concentration was too low to be determined from their absorbance at 280 nm, and was thus determined by titration against MMP-1.

Some TIMP-3 double mutants were purified to yields much lower that those observed for TIMP-3 K26A/K45A and TIMP-3 K42A/K110A. The immunoblots for the purification of TIMP-3 K27A/K45A from 500 mL of conditioned media (Figure 48A) shows that protein was only detectable by anti-FLAG immunoblotting in 1 out of the 5 elution fractions, indicating a poor yield. Purification of TIMP-3 K42A/K157A from 700 mL of conditioned medium (Figure 48B) showed weak bands in elution fractions 1 and 2, with the intensity of these bands greatly reduced compared to those of TIMP-3 K26/K45A and TIMP-3 K42A/K110A.

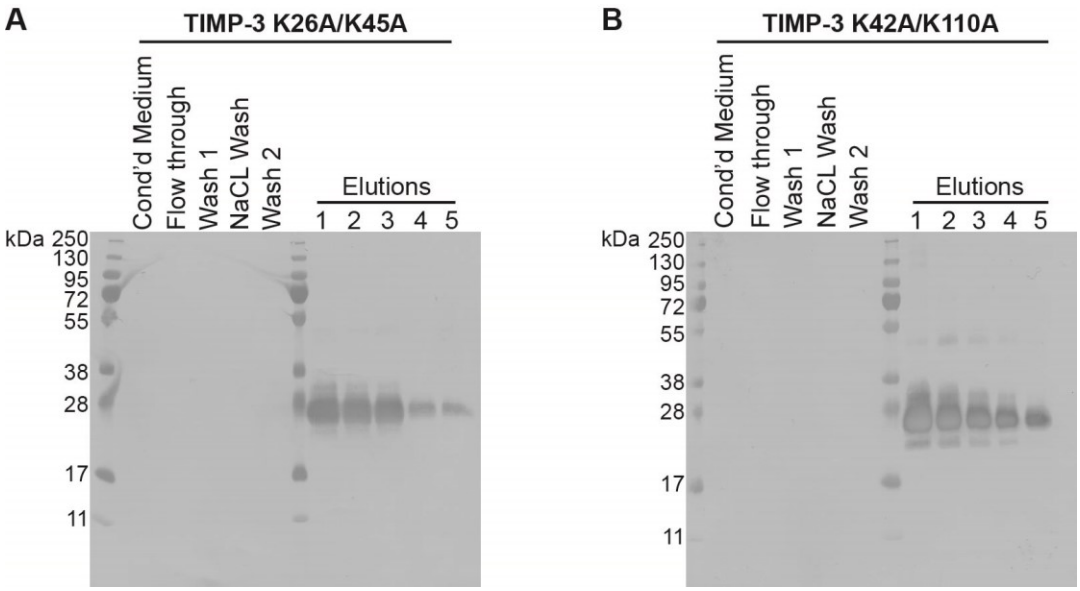


Figure 47: Purification of TIMP-3 K26A/K45A and TIMP-3 K42A/K110A by anti-FLAG affinity chromatography.

HEK-293-EBNA cells stably transfected with pCEP4 encoding TIMP-3 K26A/K45A and TIMP-3 K42A/K110A were grown to confluence in DMEM supplemented with 100 U/mL penicillin, 100 µg/mL streptomycin, 10 % FCS and 100 µg/mL hygromycin B. Once confluent, cells were incubated with serum-free DMEM supplemented with 100 U/mL penicillin, 100 µg/mL streptomycin, 100 µg/mL hygromycin B and 30 mM $NaClO_3$. Conditioned medium (3 and 2.5 L respectively) was harvested after 48 h, and passed over an anti-FLAG M2-agarose column (2 mL) equilibrated in serum-free DMEM. The column was washed in serum-free DMEM, and then in serum-free DMEM containing 500 mM NaCl, and again in serum-free DMEM. TIMP-3 K26A/K45A and TIMP-3 K42A/K110A were eluted in 5 mL fractions using FLAG peptide (200 µg/mL) in serum-free DMEM. Samples (7.5 µL) were diluted in an equal volume of 2x reducing SDS-PAGE loading buffer and analysed by immunoblotting with an anti-FLAG M2 antibody and an anti-mouse IgG AP-conjugated secondary antibody. Bands were visualised using Western blue stabilised substrate for AP and the reaction stopped using AP stop (20 mM Tris-HCl pH7.5, 10 mM EDTA).

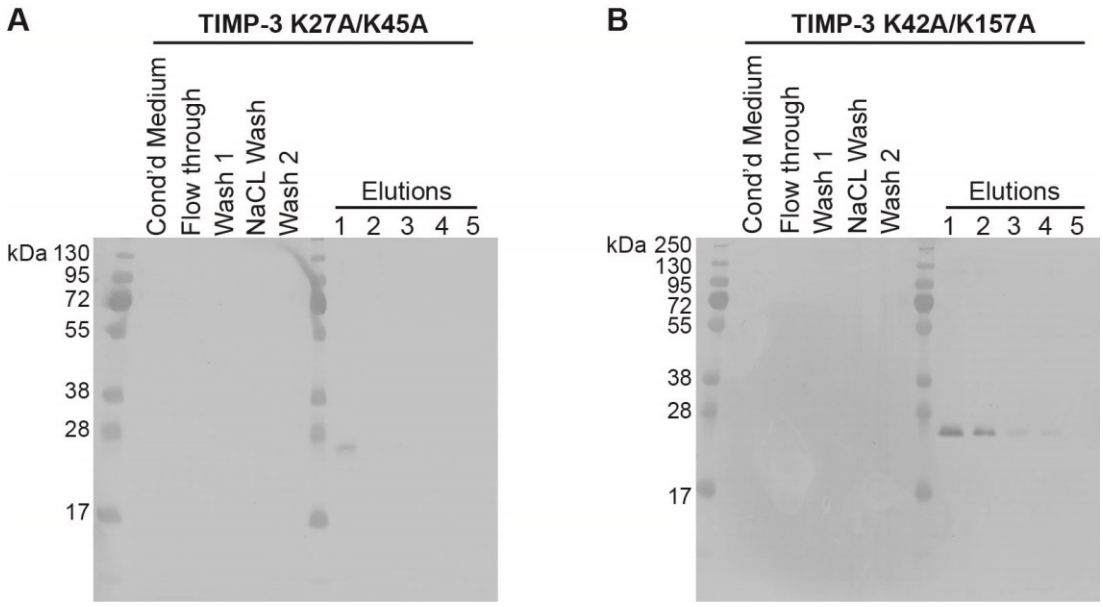


Figure 48: Purification of TIMP-3 K27A/K45A and TIMP-3 K42A/K157A were expressed at low levels by anti-FLAG affinity chromatography.

HEK-293-EBNA cells stably transfected with pCEP4 encoding TIMP-3 K27A/K45A and K42A/K157A were grown to confluence in DMEM supplemented with 100 U/mL penicillin, 100 µg/mL streptomycin, 10 % FCS and 100 µg/mL hygromycin B. Once confluent, cells were incubated with serum-free DMEM supplemented with 100 U/mL penicillin, 100 µg/mL streptomycin, 100 µg/mL hygromycin B and 30 mM $NaClO_3$. Conditioned medium (500 and 700 mL respectively) was harvested after 48 h, and passed over an anti-FLAG M2-agarose column (2 mL) equilibrated in serum-free DMEM. The column was sequentially washed in serum-free DMEM, in serum-free DMEM with 500 mM NaCl, and again in serum-free DMEM. TIMP-3 K27A/K45A and K42A/K157A were eluted in 5 mL fractions using FLAG peptide (200 µg/mL) in serum-free DMEM. Samples (7.5 µL) were diluted in an equal volume of 2x reducing SDS-PAGE loading buffer and analysed by immunoblotting with an anti-FLAG M2 antibody and an anti-mouse IgG AP-conjugated secondary antibody. Bands were visualised using Western blue stabilised substrate for AP and the reaction stopped using AP stop (20 mM Tris-HCl pH7.5, 10 mM EDTA).

The active concentration of the purified TIMP-3 mutants was accurately determined by titration against a known concentration of the catalytic domain of MMP-1 (MMP-1ΔC). The concentration of MMP-1ΔC had previously been determined by titration against the synthetic inhibitor GM6001, which inhibits

MMPs with 1:1 stoichiometry at low nanomolar concentrations. Increasing concentrations of GM6001 were incubated with a constant concentration of MMP-1ΔC (40 nM) in a 96-well plate (37^{o} C, 1 h), and residual enzyme activity measured using Knight's fluorescent peptide substrate Mca-Pro-Leu-Gly-Leu-Dap(Dnp)-Ala-Arg-NH_2 substrate (Knight et al., 1992) The minimum concentration of GM6001 required to completely inhibit MMP-1ΔC activity was determined, thereby determining the concentration of MMP-1ΔC.

The active concentration of purified TIMP-3 mutants was measured by titrating them against a known concentration of MMP-1ΔC. MMP-1ΔC (50 µl of 40 nM) was incubated with doubling dilutions of TIMP-3 (50 µl 1 h, 37 ^{o}C). Knight's fluorescent peptide substrate [Mca-Pro-Leu-Gly-Leu-Dap(Dnp)-Ala-Arg-NH_2, 100 µl, 3 µM,) (Knight et al., 1992) was added and the increase in fluorescence measured (λ_{ex} 325 nm, λ_{em} 393 nm, 1 h). The percentage MMP-1ΔC activity was plotted against the dilution of TIMP-3 and a line of best fit applied to determine the TIMP-3 dilution required to completely inhibit MMP-1ΔC activity. As TIMP-3 inhibits MMP-1ΔC with 1:1 stoichiometry, the TIMP-3 dilution factor multiplied by the starting concentration of MMP-1ΔC, gave the active concentration of the TIMP-3. For example, a 12-fold dilution of TIMP-3 K26A/K45A completely inhibited 40 nM MMP-1ΔC, therefore the active concentration of TIMP-3 K26A/K45A was 480 nM (12 x 40 nM). Similarly, an 11.5-fold dilution of TIMP-3 K42A/K110A completely inhibited 40 nM MMP-1ΔC, therefore the active concentration of TIMP-3 K42A/K110A was 460 nM.

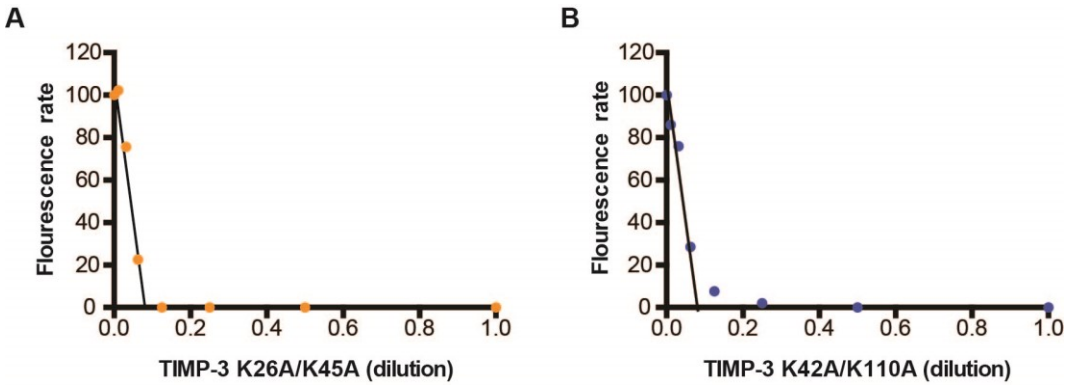


Figure 49: Titration of TIMP-3 K26A/K45A and K42A/K110A against MMP-1ΔC
The active concentration of purified (**A**) TIMP-3 K26A/K45A and (**B**) TIMP-3 K42A/K110A was determined by titration against a known concentration of MMP-1ΔC. MMP-1ΔC (50 µL of 40 nM solution; 10 nM final concentration) was incubated with doubling dilutions of TIMP-3 K26A/K45A or K42A/K110A of unknown concentration (1 h, 37 ºC). Knight substrate Mca-Pro-Leu-Gly-Leu-Dap(Dnp)-Ala-Arg-NH_2 (100 µL of 3 µM) was added and the increase in fluorescence measured at λ_{ex} 325 nm, λ_{em} 393 nm over 60 min. The percentage of MMP-1ΔC activity was plotted against the dilution of TIMP-3 and a line of best fit applied to determine the TIMP-3 concentration that completely inhibited MMP-1ΔC activity.

Table 20 shows a summary of the purification of all 10 shortlisted TIMP-3 double mutants. Only TIMP-3 K26A/K45A and TIMP-3 K42A/K110A were purified to usable concentrations of 480 nM and 460 nM respectively. This is equivalent to a yield of 96.4 µg per Litre of conditioned medium for TIMP-3 K26A/K45A and 110.4 µg per Litre for TIMP-3 K42A/K110A. These yields are lower than that achieved for Wild-type TIMP-3, which was purified with a yield of 288 µg per Litre of conditioned medium.

TIMP-3 mutants K30A/K52A and K30A/K76A were purified at yields of 18 µg and 17.5 µg per Litre of conditioned medium respectively. However the active concentration of these mutants failed to improve with increasing volumes (2 L) of starting conditioned medium. TIMP-3 K22A/K157A, K42A/K157A and K45A/K89A had very low active yields of 7.2, 6 and 5.5 µg per Litre of

conditioned medium as determined by titration against MMP-1ΔC. TIMP-3 K22A/K110A, K27A/K45A and K71A/K157A showed very poor expression levels by anti-FLAG immunoblotting, and were thus not titrated against MMP-1ΔC.

Table 20: Summary of purification of shortlisted TIMP-3 double mutants.

TIMP-3	Purified TIMP-3 [nM]	Elution volume (mL)	Yield (µg/L)
Wild-type	500	12	288
K22A/K110A	*	25	*
K22A/K157A	15	10	7.2
K26A/K45A	475	25	96.4
K27A/K45A	*	25	*
K30A/K52A	75	10	18
K30A/K76A	73	15	17.5
K42A/K110A	466	25	110.4
K42A/K157A	16	15	6
K45A/K89A	15.6	15	5.5
K71A/K157A	*	25	*

* Concentration below anti-FLAG immunoblotting detection limit.

5.2.3 Resistance of purified TIMP-3 double mutants to endocytosis by HTB94 cells

The 10 candidate endocytosis-resistant double mutants of TIMP-3 were shown to be resistant to endocytosis by LRP-1 in HTB94 cells using crude conditioned medium obtained from transiently transfected HEK-293-EBNA cells (Section 4.2.3.5). Here we analysed the endocytosis-resistance of these TIMP-3 mutants after purification from stably transfected cell lines.

Similarly to the transiently expressed TIMP-3 mutants, endocytosis-resistance was determined by quantifying the levels of exogenously added TIMP-3 mutant remaining in the medium of HTB94 cells after 24 h, either in the

presence or absence of RAP. Due to its high affinity binding to LRP-1, RAP is an antagonist of LRP-1 ligand binding (Fisher et al., 2006; Jensen et al., 2006; Jensen et al., 2009b) and is commonly used to demonstrate LRP-1-dependent ligand endocytosis. Our group has previously shown that the addition of RAP to HTB94 cell cultures prevents endocytosis of exogenously added TIMP-3, causing TIMP-3 to accumulate in the conditioned medium (Scilabra et al., 2013; Troeberg et al., 2008).

HTB94 cells were seeded in a 12-well plate, washed in serum-free DMEM and incubated with or without RAP (500 nM, 1h) prior to addition of TIMP-3 or TIMP-3 mutants. Purified Wild-type TIMP-3 and TIMP-3 mutants K26A/K45A, K30A/K76A or K42A/K110A (1 nM) were added to cells in DMEM with 0.1 % FCS and conditioned media harvested at 0 and 24 h. Samples were analysed by immunoblotting with an anti-FLAG M2 antibody and an anti-mouse IgG AP-conjugated secondary antibody. Band intensity was quantified using Phoretix ID Gel Analysis software and expressed as a percentage of pixel volume at t = 0.

As expected, Wild-type TIMP-3 was endocytosed within 24 h in the absence of RAP, but remained in the conditioned medium in the presence of RAP (Figure 50). However TIMP-3 mutants K26A/K45A, K30A/K76A and K42A/K110A were present in the medium at similar levels at 0 and 24 h, both in the presence or absence of RAP. This clearly demonstrates that the TIMP-3 mutants K26A/K45A, K30A/K76A and K42A/K110A were endocytosis-resistant.

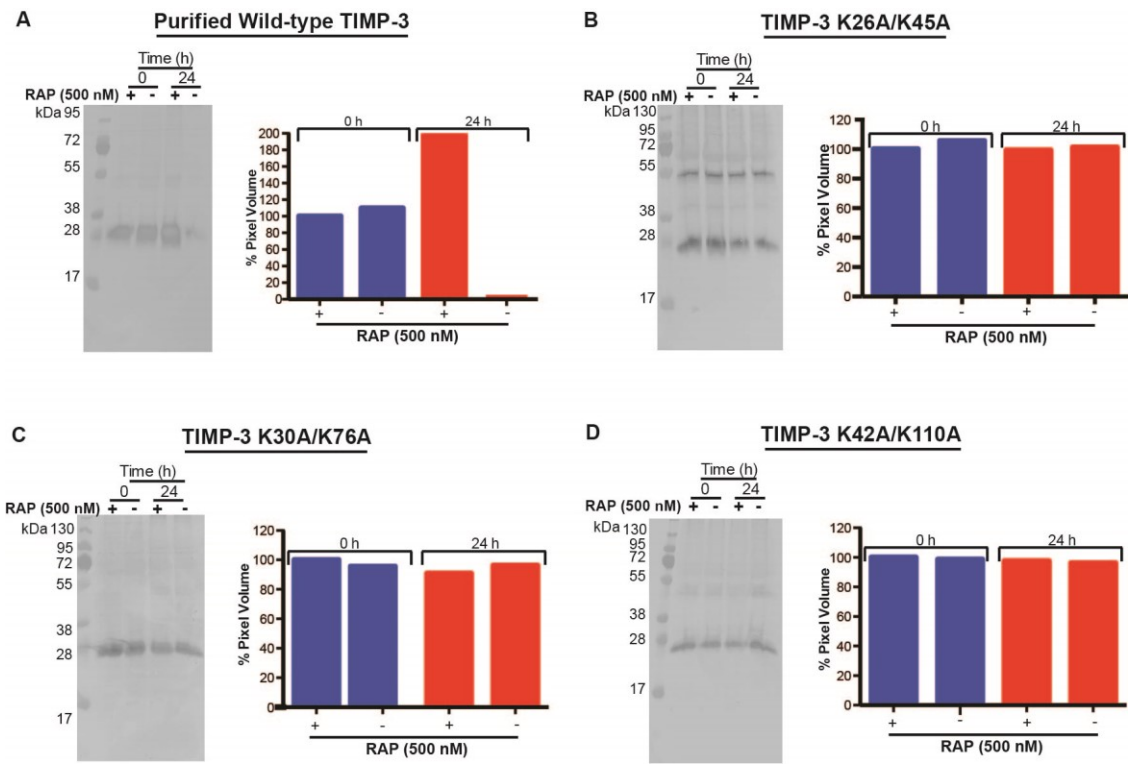


Figure 50: TIMP-3 mutants K26A/K45A, K30A/K76A and K42A/K110A retain endocytosis resistance after purification in HTB94.

HTB94 cells were seeded in a 12-well plate [$8x10^5$ cells, 37 °C, 5 % (v/v) CO_2]. Cells were washed in serum-free DMEM and incubated with or without RAP (500 nM, 1 h). Purified Wild-type TIMP-3 (**A**), TIMP-3 K26A/K45A (**B**), TIMP-3 K30A/K76A (**C**) or TIMP-3 K42A/K110A (**D**) were added (1 nM) to cells in DMEM (1 mL) with 0.1 % FCS with or without RAP (500 nM). Conditioned media samples were harvested at 0 and 24 h, TCA precipitated and pellets resuspended in 30 µL of 2x SDS-PAGE loading buffer. Resuspended samples (15 µL) were analysed by immunoblotting with an anti-FLAG M2 antibody and an anti-mouse IgG AP-conjugated secondary antibody. Bands were visualised using Western blue stabilised substrate for AP and reaction stopped using AP stop (20 mM Tris-HCl pH 7.5, 10 mM EDTA). Band intensity was quantified using Phoretix ID Gel Analysis software and expressed as a percentage of pixel volume at t = 0.

5.2.4 Evaluation of TIMP-3 mutant binding to LRP-1

Of the 10 shortlisted TIMP-3 mutants (Sections 4.2.3.4 and 4.2.3.5), only TIMP-3 K26A/K45A and TIMP-3 K42A/K110A were successfully purified to a concentration in excess of the minimum 100 nM required for analysis of chondroprotective activity (Chapter 6). TIMP-3 K30A/K52A and TIMP-3

K42A/K157A were purified at reduced concentrations, namely 74.8 nM and 16 nM respectively. Here we evaluated the LRP-1 binding affinity of these 4 TIMP-3 mutants and compare them with Wild-type TIMP-3.

LRP-1 binding of Wild-type TIMP-3 and TIMP-3 mutants K26A/K45A, K30A/K52A, K42A/K110A and K42A/K157A was evaluated by ELISA. Full-length LRP-1 (5 nM in 20 mM Hepes, 150 mM NaCl, 5 mM $CaCl_2$, 0.05 % Tween-20, pH 7.4, BioMac, Leipzig, Germany) was coated onto a medium-binding ELISA plate (overnight, 4 ^oC). Wells were blocked (10 % BSA in TNC buffer with 0.05 % Brij-35, 1 h, room temperature) and then incubated with doubling dilutions of Wild-type TIMP-3, TIMP-3 K26A/K45A, TIMP-3 K42A/K110A or TIMP-3 K30A/K52A (0.4 - 50 nM) or TIMP-3 K42A/K157A (0.4 – 6.25 nM) in 5 % BSA in TNC buffer with 0.05 % Brij-35 (3 h, room temperature). Bound TIMP-3 was detected using M2 anti-FLAG antibody (1:5000 dilution in 5 % BSA in TNC buffer with 0.05 % Brij-35, 2 h, room temperature) followed by an anti-mouse secondary antibody conjugated with horseradish peroxidase (1:1000 dilution in 5 % BSA in TNC buffer, with 0.05 % Brij-35, 1 h, room temperature). Tetramethylbenzidine HRP-substrate was added to quantify binding, the reaction stopped with 2N H_2SO_4 and absorbance at 450 nm measured.

Wild-type TIMP-3 showed highest affinity for LRP-1 with TIMP-3 mutants K26A/K45A, K30A/K52A, K42A/K110A and K42A/K157A showing a lower binding affinity (Figure 51). TIMP-3 K42A/K110A and K42A/K157A showed minimal binding to LRP-1, while TIMP-3 K26A/K45A and K30A/K52A bound to LRP-1 with a similar higher affinity, albeit much reduced relative to Wild-type TIMP-3.

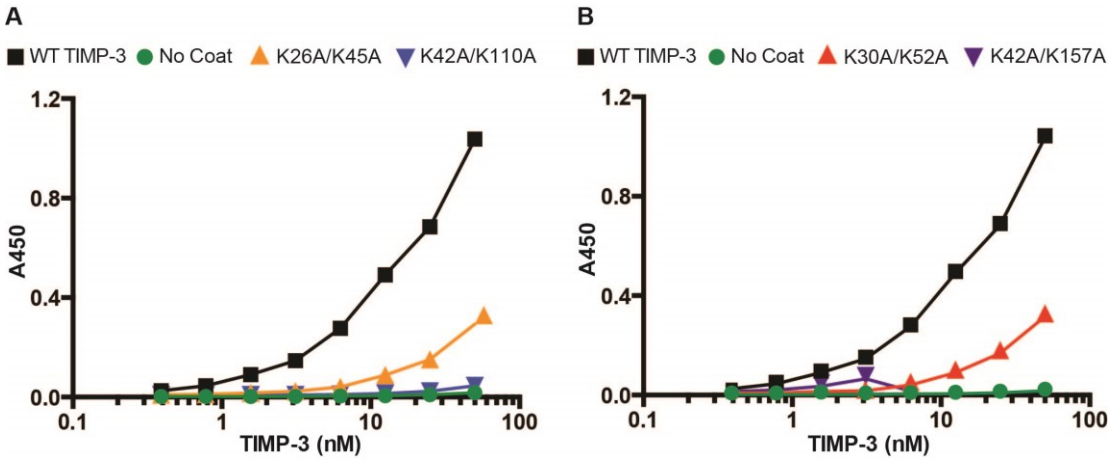


Figure 51: Affinity of TIMP-3 mutants for LRP-1 evaluated by ELISA.
Medium-binding ELISA plates were coated with or without (no coat) 5 nM LRP-1 in HEPES buffer (20 mM Hepes, 150 mM NaCl, 5 mM $CaCl_2$, 0.05 % Tween-20, pH 7.4, overnight, 4 °C). Wells were blocked (200 µL of 10 % BSA in TNC buffer with 0.05 % Brij-35, 1 h, room temperature) and washed three times [3x250 µL TNC containing 0.1 % (v/v) Tween-20] after this and every subsequent step. Wells were then incubated with doubling dilutions of (**A**) Wild-type TIMP-3 (■)(●), TIMP-3 mutants K26A/K45A (▲) or TIMP-3 K42A/K110A (▼) (0.4 - 50 nM) or (**B**) Wild-type TIMP-3 (■)(●) or TIMP-3 mutants K30A/K52A (▲)(0.4 - 50 nM) or TIMP-3 K42A/K157A (▼) (0.4 – 6.25 nM) in 100 µL of 5 % BSA in TNC buffer with 0.05 % Brij-35, (3 h, room temperature). Bound TIMP-3 was detected by M2 anti-FLAG antibody (100 µL, 1:5000 dilution in 5 % BSA in TNC buffer with 0.05 % Brij-35, 2 h, room temperature) and then with anti-mouse-HRP secondary antibody (100 µL, 1:1000 dilution in 5 % BSA in TNC buffer with 0.05 % Brij-35, 1 h, room temperature). Tetramethylbenzidine HRP-substrate was added to quantify binding, the reaction stopped with 2N H_2SO_4 and absorbance at 450 nm measured.

5.2.5 Metalloproteinase inhibitory activity of TIMP-3 mutants

Of the 4 mammalian TIMPs, TIMP-3 has the broadest inhibition profile, as it effectively inhibits MMPs, adamalysins (ADAMs) and ADAMTSs. TIMP-3 is thus unique amongst the TIMPs. Here we compare the ability of TIMP-3 mutants K26A/K45A and K42A/K110A purified in Section 5.2.2 with that of Wild-type TIMP-3 to inhibit representative metalloproteinases from each of

these families, to establish whether TIMP-3 K26A/K45A and K42A/K110A had retained their ability to inhibit target metalloproteinases.

The $K_{i(app)}$ values of Wild-type TIMP-3 and TIMP-3 mutants K26A/K45A and TIMP-3 K42A/K110 for MMP-1, MMP-2, MMP-3, ADAMTS-4, ADAMTS-5 and ADAM-17 were determined under equilibrium kinetic conditions (Bieth, 1995b). Enzymes, at concentrations below their K_i, were preincubated (1 h, 37 ^oC) with excess TIMP-3 to allow formation of an equilibrium complex, and substrate added to determine the equilibrium rate of hydrolysis (v_s) (1- 18 h, 37 ^oC). Prism software (GraphPad, La Jolla, CA, USA) was used to fit the data to the tight-binding equation (Bieth, 1995a):

$$\frac{v_s}{v_o} = 1 - \frac{(E_o + I_o + K_{i(app)} - [(E_o + I_o + K_{i(app)})^2 - 4E_o K_{i(app)}]^{\frac{1}{2}}}{2E_o}$$

where v_s is the equilibrium rate of substrate hydrolysis in the presence of inhibitor, v_o is the equilibrium rate of substrate hydrolysis in the absence of inhibitor, E_o is the total enzyme concentration, I_o is the total inhibitor concentration and $K_{i(app)}$ is the apparent inhibition constant. $K_{i(app)}$ was calculated using the known enzyme concentration and is shown with the error on the fit. All concentrations described in Section 5.2.5.1 to Section 5.2.5.6 are at final concentrations.

5.2.5.1 Affinity of TIMP-3 mutants K26A/K45A and K42A/K110A for MMP-1ΔC

MMP-1 (also known as Collagenase 1 or interstitial collagenase) cleaves collagen types I, II and III at a specific site ¾-length from the N-terminus and ¼ from the C-terminus (Gross and Nagai, 1965). The $K_{i(app)}$ value for Wild-type TIMP-3 inhibition of MMP-1ΔC (catalytic domain of MMP-1) has previously been documented as 1.1 ± 0.6 nM (Troeberg et al., 2009). We set about reproducing this published data by quantifying the $K_{i(app)}$ value of Wild-type TIMP-3 for MMP-1ΔC, and determining the affinity of TIMP-3 mutants K26A/K45A and K42A/K110A for MMP-1ΔC.

Human MMP-1ΔC was expressed in *E. coli* and purified as previously described (Chung et al., 2000). The protein was obtained as a gift from Dr Robert Visse, University of Oxford. The enzyme assays were conducted in TNC buffer (50 mM Tris-HCl, 150 mM NaCl, 10 mM $CaCl_2$, 0.05 % Brij-35 and 0.02 % NaN_3) at 37 °C, using a Gemini microplate spectrofluorometer. MMP-1ΔC (1.5 nM) was incubated with Wild-type TIMP-3 (Figure 52A**,** 0.5-10 nM), TIMP-3 K26A/K45A (Figure 52B**,** 0.5-10 nM) or TIMP-3 K42A/K110A (Figure 52C**,** 0.5-10 nM) for 1 h at 37 °C and residual activity against Knight's fluorescent peptide substrate [Mca-Pro-Leu-Gly-Leu-Dap(Dnp)-Ala-Arg-NH_2, 1.5 μM, λ_{ex} 325 nm, λ_{em} 393 nm] (Knight et al., 1992) determined (1 h, 37 °C).

Wild-type TIMP-3 had a calculated $K_{i(app)}$ value of 0.43 ± 1.18 nM, TIMP-3 K26A/K45A had a $K_{i(app)}$ value of 0.35 ± 0.045 nM and TIMP-3 K42A/K110A had a $K_{i(app)}$ value of 0.40 ± 1.03 nM. Figure 52D shows a comparison of MMP-1ΔC inhibition by Wild-type TIMP-3, TIMP-3 K26A/K45A and TIMP-3 K42A/K110A.

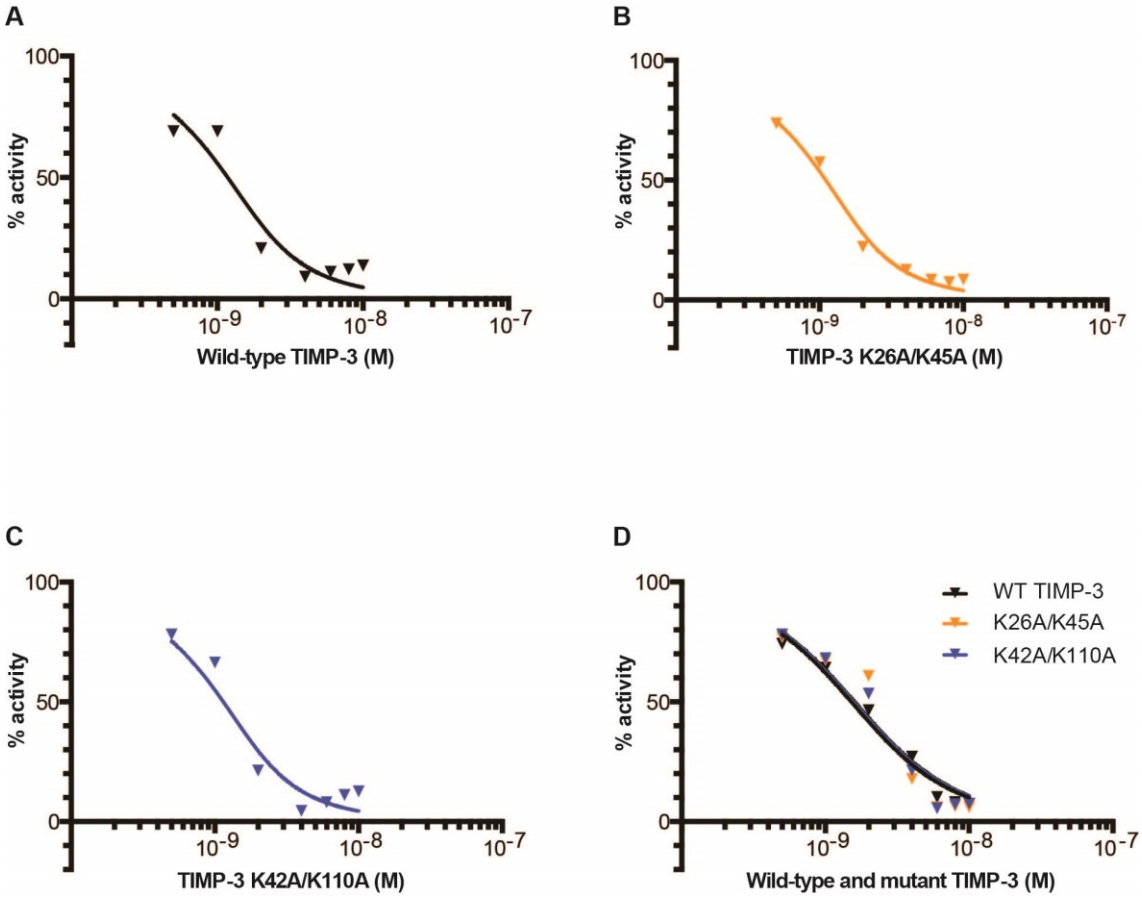


Figure 52: Affinity of Wild-type TIMP-3 and TIMP-3 mutants K26A/K45A and K42A/K110A for MMP-1ΔC.

MMP-1ΔC (1.5 nM) was incubated with Wild-type TIMP-3 (**A,** 0.5-10 nM), TIMP-3 K26A/K45A (**B,** 0.5-10 nM) or TIMP-3 K42A/K110A (**C,** 0.5-10 nM) for 1 h at 37 ºC and residual activity against Knight substrate Mca-Pro-Leu-Gly-Leu-Dap(Dnp)-Ala-Arg-NH_2 (1.5 µM) determined (1 h, 37 ºC). Prism software was used to fit the data to the tight-binding equation. (**D**) Wild-type TIMP-3, TIMP-3 K26A/K45A and TIMP-3 K42A/K110A were shown to have indistinguishable affinity for MMP-1ΔC. $K_{i(app)}$ values of 0.43 ± 1.18 nM, 0.35 ± 0.045 nM and 0.40 ± 1.03 nM were calculated for Wild-type TIMP-3, TIMP-3 K26A/K45A and TIMP-3 K42A/K110A respectively.

5.2.5.2 Affinity of TIMP-3 mutants K26A/K45A and K42A/K110A for MMP-2ΔC

MMP-2 (also known as Gelatinase A) digests gelatin and collagen types, I, II, III and IV, with type IV collagen being an important component of basement membrane (Sato et al., 1992). The $K_{i(app)}$ value for Wild-type TIMP-3 inhibition

of MMP-2ΔC activity has previously been documented as 0.9 ± 0.3 nM (Troeberg et al., 2009). We set about reproducing this published data by quantifying the $K_{i(app)}$ value of Wild-type TIMP-3 for MMP-2ΔC, and determining the affinity of TIMP-3 mutants K26A/K45A and K42A/K110A for MMP-2ΔC.

MMP-2ΔC was a gift from Dr Linda Troeberg, University of Oxford. The pro-form of the human MMP-2 catalytic domain (proMMP-2ΔC, lacking hemopexin-domain residues 466 to 660) was expressed in HEK-293-EBNA cells using a pCEP4-based expression vector (Troeberg et al., 2009). The active form of MMP-2ΔC was prepared by 4-aminophenylmercuric acetate treatment (1 mM, 60 min, 37 °C), followed by an TNC buffer exchange using a PD-10 desalting column. The active concentration of MMP-2ΔC was determined by titration against a known concentration of N-TIMP-3. MMP-2ΔC (1 nM) was incubated with Wild-type TIMP-3 (Figure 53A, 0.5-10 nM), TIMP-3 K26A/K45A (Figure 53B, 0.5-10 nM) or TIMP-3 K42A/K110A (Figure 53C, 0.5-10 nM) for 1 h at 37 °C in TNC buffer and residual activity against Knight's substrate [Mca-Pro-Leu-Gly-Leu-Dap(Dnp)-Ala-Arg-NH_2, 1.5 μM] (Knight et al., 1992) determined (1 h, 37 °C). Fluorescence was quantified using a Gemini microplate spectrofluorometer with λ_{ex} 325 nm, λ_{em} 393 nm.

Figure 53D shows a comparison of MMP-2ΔC inhibition by Wild-type TIMP-3, TIMP-3 K26A/K45A and TIMP-3 K42A/K110A. Wild-type TIMP-3 $K_{i(app)}$ was 0.952 ± 0.085 nM, in agreement with the published value of 0.9 ± 0.3 nM. TIMP-3 mutants K26A/K45A and K42A/K110A had equivalent affinity, with $K_{i(app)}$ values of 1.199 ± 0.13 nM and 1.184 ± 0.1496 nM respectively.

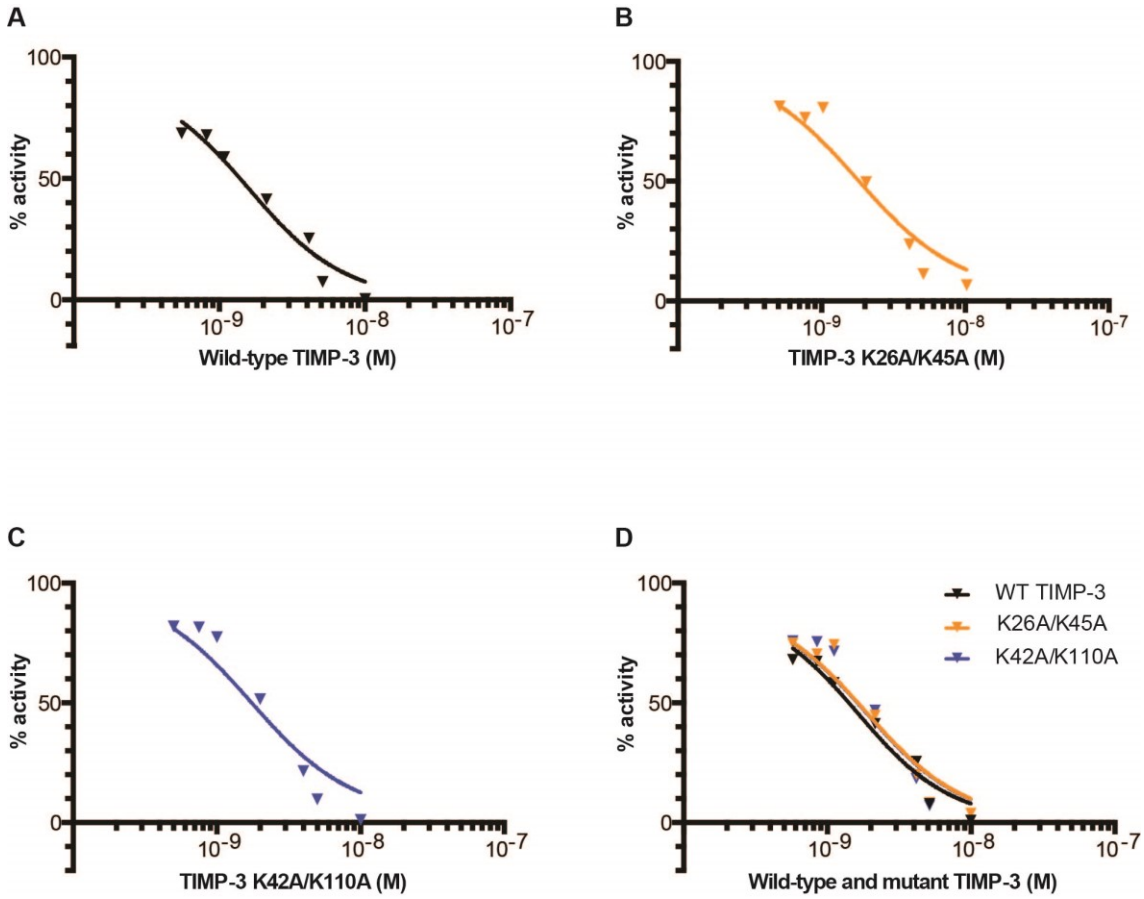


Figure 53: Affinity of Wild-type TIMP-3 and TIMP-3 mutants K26A/K45A and K42A/K110A for MMP-2ΔC.

MMP-2ΔC (1.5 nM) was incubated with Wild-type TIMP-3 (**A,** 0.5-10 nM), TIMP-3 K26A/K45A (**B,** 0.5-10 nM) or TIMP-3 K42A/K110A (**C,** 0.5-10 nM) for 1 h at 37 °C and residual activity against Knight substrate Mca-Pro-Leu-Gly-Leu-Dap(Dnp)-Ala-Arg-NH_2 (1.5 μM) determined (1 h, 37 °C). Prism software was used to fit the data to the tight-binding equation. (**D**) Wild-type TIMP-3, TIMP-3 K26A/K45A and TIMP-3 K42A/K110A were shown to have indistinguishable affinity for MMP-2ΔC. $K_{i(app)}$ values of 0.952 ± 0.085 nM, 1.199 ± 0.13 nM and 1.184 ± 0.15 nM were calculated for Wild-type TIMP-3, TIMP-3 K26A/K45A and TIMP-3 K42A/K110A respectively.

5.2.5.3 Affinity of TIMP-3 mutants K26A/K45A and K42A/K110A for MMP-3ΔC

MMP-3 (also known as stromelysin 1) digests collagen types III, IV, V, VII, IX and X, as well as E-cadherin (Lochter et al., 1997; Noe et al., 2001), plasminogen (Lochter et al., 1997). The $K_{i(app)}$ value of Wild-type TIMP-3 inhibition of MMP-3ΔC (catalytic domain of MMP-3) has previously been

documented as 1.0 ± 0.4 nM (Troeberg et al., 2009). We set about reproducing this published data by quantifying the $K_{i(app)}$ value of Wild-type TIMP-3 for MMP-3ΔC, and then determining the affinity of TIMP-3 mutants K26A/K45A and K42A/K110A for MMP-3ΔC.

Human MMP-3ΔC was expressed in *E. coli* (Suzuki et al., 1998) and was a gift from Dr Linda Troeberg, University of Oxford. MMP-3ΔC (1 nM) was incubated with Wild-type TIMP-3 (Figure 54A, 0.5-10 nM), TIMP-3 K26A/K45A (Figure 54B, 0.5-10 nM) or TIMP-3 K42A/K110A (Figure 54C, 0.5-10 nM) for 1 h at 37 °C in TNC buffer and residual activity against NFF-3 substrate [Mca-Arg-Pro-Lys-Pro-Tyr-Ala-Nva-Trp-Met-Lys(Dnp)-NH_2, 1.5 μM] (Nagase et al., 1994a) determined (1 h, 37 °C). Fluorescence was quantified using a Gemini microplate spectrofluorometer with λ_{ex} 325 nm, λ_{em} 393 nm. Wild-type TIMP-3 had a $K_{i(app)}$ value of 0.978 ± 0.052 nM, in agreement with the published value of 1.0 ± 0.4 nM. TIMP-3 mutants K26A/K45A and K42A/K110A had equivalent affinity, with $K_{i(app)}$ values of 1.023 ± 0.09 nM and 1.095 ± 0.147 nM respectively.

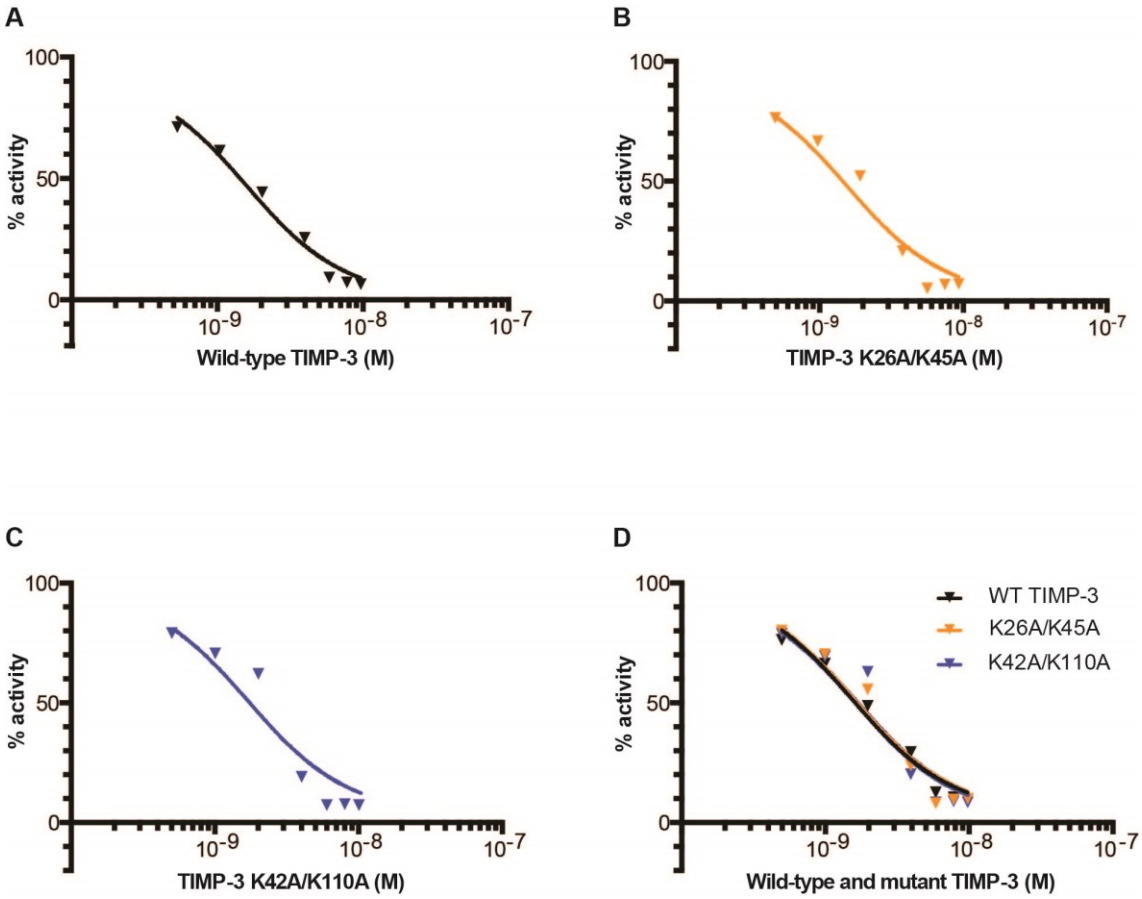


Figure 54: Affinity of Wild-type TIMP-3 and TIMP-3 mutants K26A/K45A and K42A/K110A for MMP-3ΔC.

MMP-3ΔC (1 nM) was incubated with Wild-type TIMP-3 (**A,** 0.5-10 nM), TIMP-3 K26A/K45A (**B,** 0.5-10 nM) or TIMP-3 K42A/K110A (**C,** 0.5-10 nM) for 1 h at 37 °C and residual activity against NFF-3 substrate [Mca-Arg-Pro-Lys-Pro-Tyr-Ala-Nva-Trp-Met-Lys(Dnp)-NH_2, 1.5 μM) determined (1 h, 37 °C). Prism software was used to fit the data to the tight-binding equation. (**D**) Wild-type TIMP-3, TIMP-3 K26A/K45A and TIMP-3 K42A/K110A were shown to have indistinguishable affinity for MMP3-ΔC. $K_{i(app)}$ of values of 0.978 ± 0.052 nM, 1.023 ± 0.09 nM and 1.095 ± 0.147 nM were calculated for Wild-type TIMP-3, TIMP-3 K26A/K45A and TIMP-3 K42A/K110A respectively.

5.2.5.4 Affinity of TIMP-3 mutants K26A/K45A and K42A/K110A for ADAMTS-4

ADAMTS-4 (also known as aggrecanase 1) is considered to be one of the main enzymes involved in aggrecan cleavage in OA. ADAMTS-4 cleaves

aggrecan at several sites, including Glu^{373}-Ala^{374} (Arner et al., 1999) generating the N-terminal ^{374}ARGSV neo-epitope, and at Glu^{1819}-Ala^{1820} generating the ^{1820}AGEG neo-epitope (Kashiwagi et al., 2004). The $K_{i(app)}$ value for Wild-type TIMP-3 inhibition of ADAMTS-4 lacking the C-terminal spacer domain has previously been documented as 0.22 ± 0.7 nM (Troeberg et al., 2009). We set about reproducing this published data by quantifying the $K_{i(app)}$ value of Wild-type TIMP-3 for ADAMT4-2 and then determining the affinity of TIMP-3 mutants K26A/K45A and K42A/K110A for ADAMTS-4.

ADAMTS-4 lacking the C-terminal spacer domain was a gift from Dr Linda Troeberg, University of Oxford. The protein was expressed in HEK-293-EBNA cells and purified using anti-FLAG M2-agarose affinity chromatography and gel filtration (Kashiwagi et al., 2004). ADAMTS-4 (0.5 nM) was incubated with Wild-type TIMP-3 (Figure 55A, 0.5-10 nM), TIMP-3 K26A/K45A (Figure 55B, 0.5-10 nM) or TIMP-3 K42A/K110A (Figure 55C, 0.5-10 nM) for 1 h at 37 ^{o}C and residual activity against carboxyfluorescein-Ala-Glu-Leu-Asn-gly-Arg-Pro-Ile-Ser-Ile-Ala-Lys-N,N,N',N'-tetramethyl-6-carboxyrhodamine (0.5 μM) (Wayne et al., 2007) determined (1 h, 37 ^{o}C). Fluorescence was quantified using a Gemini microplate spectrofluorometer with λ_{ex} 485 nm, λ_{em} 538 nm. Figure 55D shows a comparison of ADAMTS-4 inhibition by Wild-type TIMP-3, TIMP-3 K26A/K45A and TIMP-3 K42A/K110A. Wild-type TIMP-3 $K_{i(app)}$ of 0.11 ± 0.038 nM was comparable to the published value of 0.22 ± 0.07 nM. TIMP-3 mutants K26A/K45A and K42A/K110A had equivalent affinity, with $K_{i(app)}$ values of 0.064 ± 0.018 nM and 0.081 ± 0.015 nM respectively.

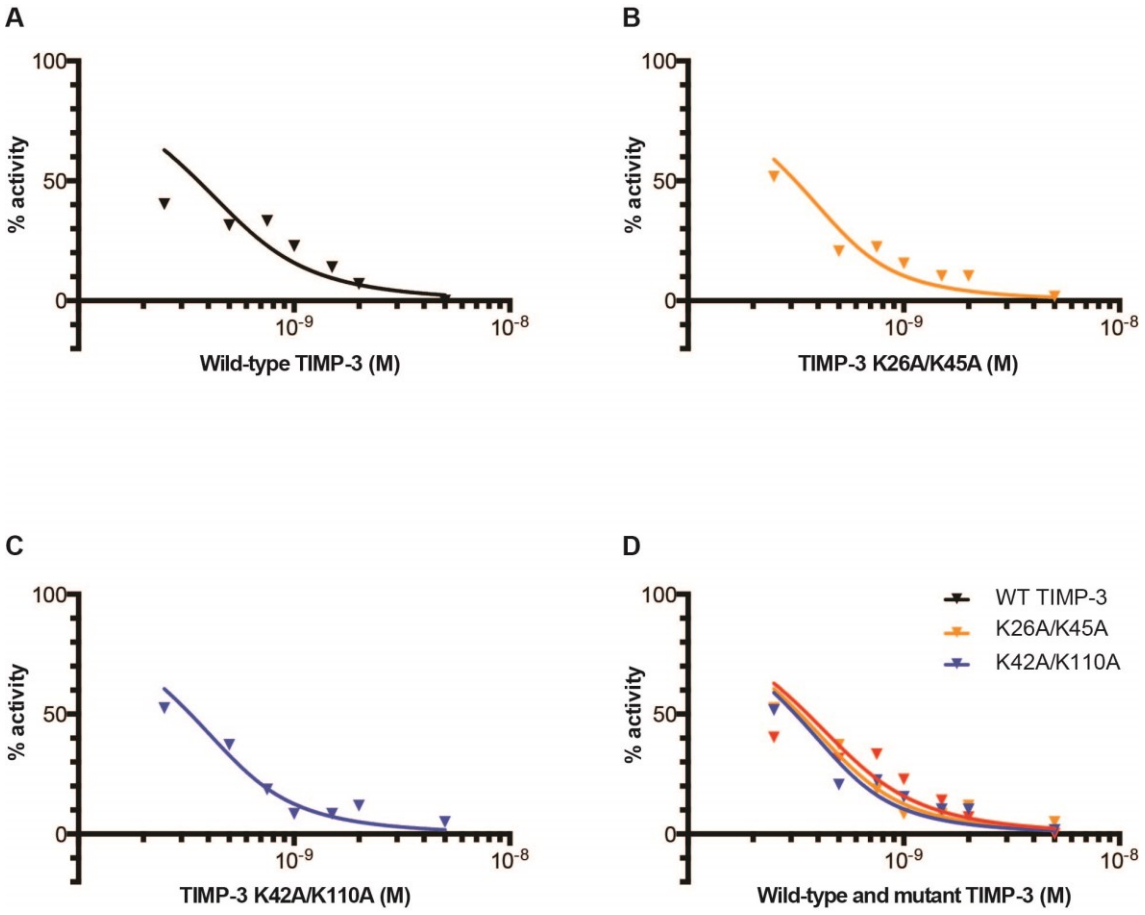


Figure 55: Affinity of Wild-type TIMP-3 and TIMP-3 mutants K26A/K45A and K42A/K110A for ADAMTS-4.

ADAMTS-4 (1 nM) was incubated with Wild-type TIMP-3 (**A,** 0.5-10 nM), TIMP-3 K26A/K45A (**B,** 0.5-10 nM) or TIMP-3 K42A/K110A (**C,** 0.5-10 nM) for 1 h at 37 °C and residual activity against carboxyfluorescein-Ala-Glu-Leu-Asn-Gly-Arg-Pro-Ile-Ser-Ile-Ala-Lys-N,N,N',N'-tetramethyl-6-carboxyrhodamine (0.5 µM) determined (1 h, 37 °C). Prism software was used to fit the data to the tight-binding equation. (**D**) Wild-type TIMP-3, TIMP-3 K26A/K45A and TIMP-3 K42A/K110A were shown to have comparable affinity for ADAMTS-4. $K_{i(app)}$ of values of 0.109 ± 0.038 nM, 0.064 ± 0.018 nM and 0.081 ± 0.0155 nM were calculated for Wild-type TIMP-3, TIMP-3 K26A/K45A and TIMP-3 K42A/K110A respectively.

5.2.5.5 Affinity of TIMP-3 mutants K26A/K45A and K42A/K110A for ADAMTS-5

ADAMTS-5 (also known as aggrecanase 2) is considered to be one of the 2 main enzymes involved in aggrecan cleavage in OA. ADAMTS-5 cleaves

aggrecan at several sites including at Glu^{373}-Ala^{374} in aggrecan (Arner et al., 1999) generating the N-terminal ^{374}ARGSV neo-epitope, and at Glu^{1819}-Ala^{1820} generating the ^{1820}AGEG neo-epitope (Gendron et al., 2007). The $K_{i(app)}$ value for Wild-type TIMP-3 inhibition of ADAMTS-5 lacking the C-terminal thrombospondin domain has previously been documented as 0.72 ± 0.17 nM (Troeberg et al., 2009). We set about reproducing this published data by quantifying the $K_{i(app)}$ value for Wild-type TIMP-3 for ADAMTS-5 and then determining the affinity of TIMP-3 mutants K26A/K45A and K42A/K110A for ADAMTS-5.

ADAMTS-5 lacking the C-terminal thrombospondin domain was a gift from Dr Linda Troeberg, University of Oxford. The protein was expressed and purified in accordance with published methods (Gendron et al., 2007). ADAMTS-5 (0.5 nM) was incubated with Wild-type TIMP-3 (Figure 56A, 0.5-10 nM), TIMP-3 K26A/K45A (Figure 56B, 0.5-10 nM) or TIMP-3 K42A/K110A (Figure 56C, 0.5-10 nM) for 1 h at 37 ^{o}C and residual activity against a brevican-based substrate, ortho-aminobenzoyl-Thr-Glu-Ser-Glu-Ser-Arg-Gly-Ala-Ile-Tyr-(N-3-[2,4-dinitrophrenyl]-L-2,3-diamiopropionyl)-Lys-Lys-NH_2 (20 μM, 18 h, λ_{ex} 300 nm, λ_{em} 430 nm) determined (Matthews et al., 2000; Nakamura et al., 2000). Figure 56D shows a comparison of ADAMTS-5 inhibition of Wild-type TIMP-3, TIMP-3 K26A/K45A and TIMP-3 K42A/K110A. Wild-type TIMP-3 had a $K_{i(app)}$ value of 1.65 ± 0.063 nM, TIMP-3 K26A/K45A had a $K_{i(app)}$ value of 1.5 ± 0.049 nM and TIMP-3 K42A/K110A had a $K_{i(app)}$ value of 3.62 ± 0.055 nM.

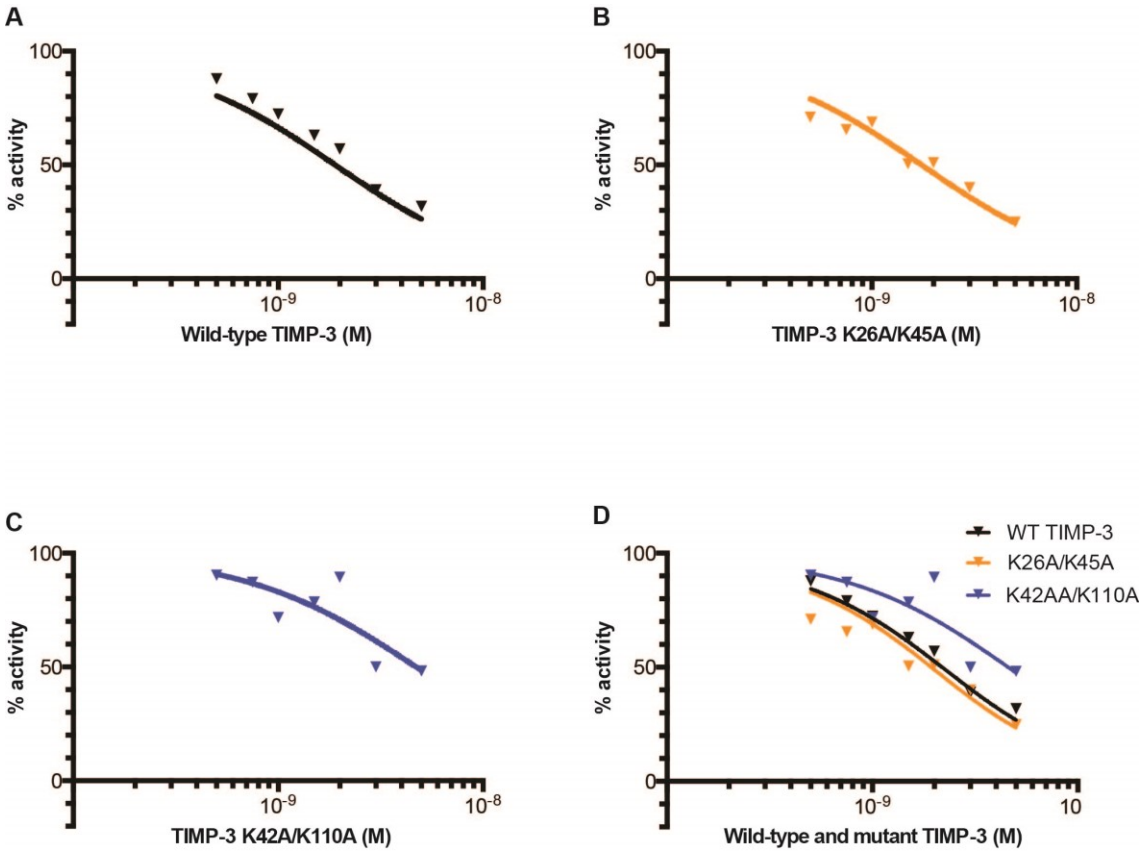


Figure 56: Affinity of Wild-type TIMP-3 and TIMP-3 mutants K26A/K45A and K42A/K110A for ADAMTS-5.

ADAMTS-5 (0.5 nM) was incubated with Wild-type TIMP-3 (**A,** 0.5-10 nM), TIMP-3 K26A/K45A (**B,** 0.5-10 nM) and TIMP-3 K42A/K110A (**C,** 0.5-10 nM) for 1 h at 37 °C and residual activity against the brevican-based substrate ortho-aminobenzoyl-Thr-Glu-Ser-Glu-Ser-Arg-Gly-Ala-Ile-Tyr-(N-3-[2,4-dinitrophrenyl]-L-2,3-diamiopropionyl)-Lys-Lys-NH_2 (20 µM) determined (18 h, 37 °C). Prism software was used to fit the data to the tight-binding equation. (**D**) Wild-type TIMP-3, TIMP-3 K26A/K45A and TIMP-3 K42A/K110A were shown to have indistinguishable affinity for ADAMTS5-2. $K_{i(app)}$ of values of 1.65 ± 0.063 nM, 1.5 ± 0.049 nM and 3.62 ± 0.055 nM were calculated for Wild-type TIMP-3, TIMP-3 K26A/K45A and K42A/K110A respectively.

5.2.5.6 Affinity of TIMP-3 mutants K26A/K45A and K42A/K110A for ADAM-17

ADAM-17 (also known as TNF-α-converting enzyme or TACE) cleaves soluble tumor necrosis factor-α (TNF-α) from its membrane-bound precursor (Black et al., 1997). This facilitates release of this proinflammatory cytokine from activated monocytes and macrophages to induce a protective

inflammatory response (Amour et al., 1998). The $K_{i(app)}$ value for Wild-type TIMP-3 inhibition of ADAM-17 has previously been documented as ranging between 0.74 ± 0.4 nM (Lee et al., 2002) and 13.7 ± 0.2 nM (Wei et al., 2005). We set about reproducing this published data by quantifying the $K_{i(app)}$ value of Wild-type TIMP-3 for ADAM-17, and then determining the affinity of TIMP-3 mutants K26A/K45A and K42A/K110A for ADAM-17.

ADAM-17 was a gift from Prof Gillian Murphy, University of Cambridge. The mature TACE ectodomain (Arg^{215}-Agr^{651}) was expressed in baculovirus-infected sf9 cells and purified by gel chromatography from concentrated cell culture media (Milla et al., 1999). ADAM-17 (1 nM) was incubated with Wild-type TIMP-3 (Figure 57A, 0-25 nM), TIMP-3 K26A/K45A (Figure 57B, 0-25 nM) or TIMP-3 K42A/K110A (Figure 57C, 0-25 nM) for 1 h at 37 ^{o}C in a modified TNC buffer (50 mM Tris-HCl, 25 mM NaCl, 10 mM $CaCl_2$, 0.05 % Brij-35 and 0.02 % NaN_3) and residual activity against fluorogenic TACE substrate IV (Abz-Leu-Ala-Gln-Ala-Val-Arg-Ser-Ser-Ser-Arg-Dpa, 20 μM) (Jin et al., 2002) determined (1 h, 37 ^{o}C). Fluorescence was quantified using a Gemini microplate spectrofluorometer with λ_{ex} 320 nm, λ_{em} 420 nm.

Figure 57D shows a comparison of ADAM-17 inhibition by Wild-type TIMP-3, TIMP-3 K26A/K45A and K42A/K110A. The Wild-type TIMP-3 $K_{i(app)}$ quantified here was 4.83 ± 0.36 nM, within the published range of $K_{i(app)}$ values calculated using 2 differing fluorescent substrates. Lee et al. (2002) used QF-45 (Mca-Ser-Pro-Leu-Ala-Gln-Ala-Val-Arg-Ser-Ser-Ser-Arg-Lys-Dnp-NH_2) while Wei et al. (2005) used TACE substrate III (Mca-Pro-Leu-Ala-Gln-Ala-Val-Dpa-Arg-Ser-Ser-Ser-Arg-NH_2) and the $K_{i(app)}$ value reported here was calculated using fluorgenic TACE substrate IV (Abz-Leu-Ala-Gln-Ala-Val-Arg-

Ser-Ser-Ser-Arg-Dpa) (Hashimoto et al., 2001). It would be expected that ADAM-17 would have different K_m values for hydrolysis of these substrates and so that $K_{i(app)}$ would vary. Wild-type TIMP-3, TIMP-3 K26A/K45A and TIMP-3 K42A/K110A had equivalent affinity for ADAM-17, with $K_{i(app)}$ values of 4.83 ± 0.36 nM, 6.30 ± 0.29 nM and 4.34 ± 0.20 nM respectively. The kinetic parameters determined are summarized in Table 21.

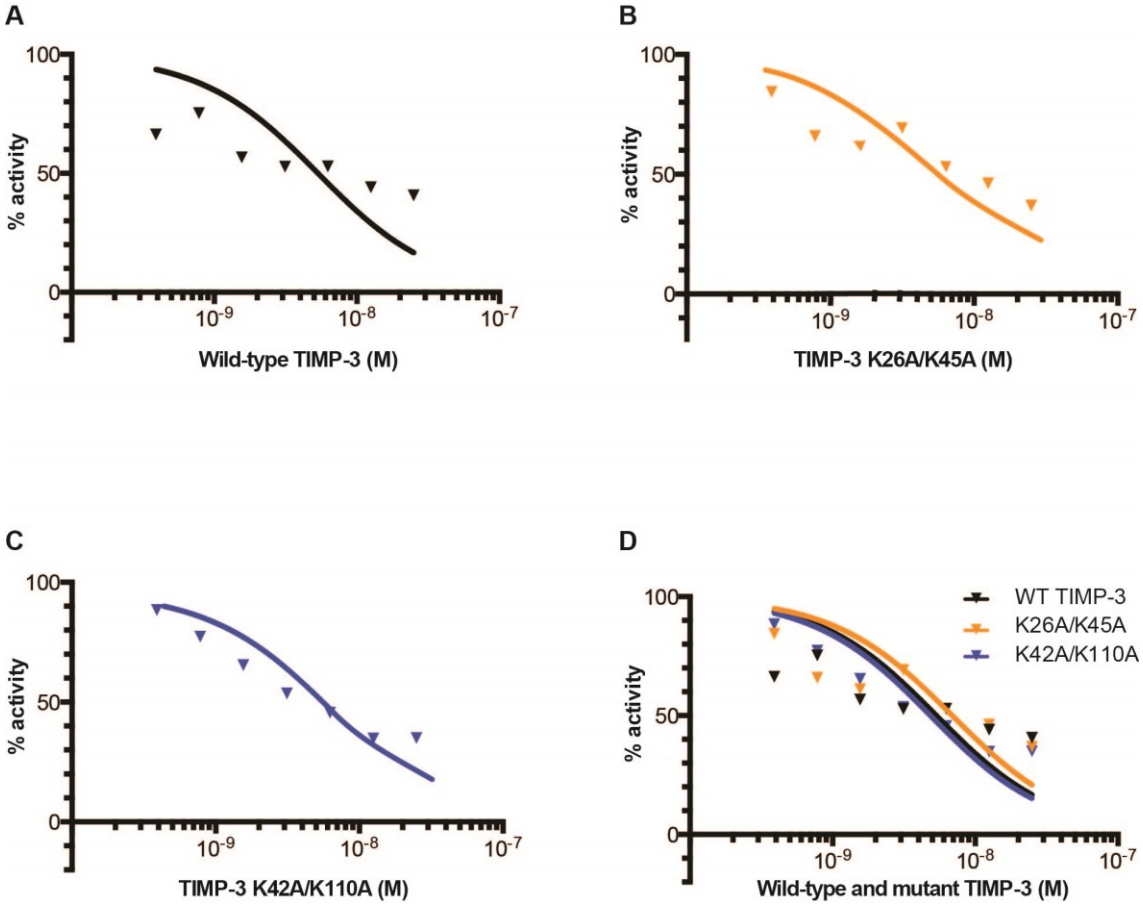


Figure 57: Affinity of Wild-type TIMP-3 and TIMP-3 mutants K26A/K45A and K42A/K110A for ADAM-17.

ADAM-17 (1 nM) was incubated with Wild-type TIMP-3 (**A,** 0-25 nM), TIMP-3 K26A/K45A (**B,** 0-25 nM) or TIMP-3 K42A/K110A (**C,** 0-25 nM) for 1 h at 37 °C and residual activity against the fluorogenic substrate IV (Abz-Leu-Ala-Gln-Ala-Val-Arg-Ser-Ser-Ser-Arg-Dpa) determined (1 h, 37 °C). Prism software was used to fit the data to the tight-binding equation. (**D**) Wild-type TIMP-3, TIMP-3 K26A/K45A and TIMP-3 K42A/K110A were shown to have indistinguishable affinity for ADAMTS-17, with $K_{i(app)}$ of values 4.83 ± 0.36 nM, 6.30 ± 0.29 nM and 4.34 ± 0.20 nM calculated for Wild-type TIMP-3,TIMP-3 K26A/K45A and K42A/K110A respectively.

Table 21: Affinity of Wild-type and mutant TIMP-3 for prototypic TIMP-3 target metalloproteinases.

$K_{i(app)}$ (nM)				
	Published Wild-type TIMP-3	**Measured Wild-type TIMP-3**	**Measured TIMP-3 K26A/K45A**	**Measured TIMP-3 K42A/K110A**
MMP-1ΔC	1.1 ± 0.6‡	0.43 ± 1.2	0.35 ± 0.05	0.40 ± 1.03
MMP-2ΔC	0.9 ± 0.3‡	0.95 ± 0.09	1.2 ± 0.13	1.18 ± 0.15
MMP-3ΔC	1.0 ± 0.4‡	0.98 ± 0.05	1.02 ± 0.09	1.1 ± 0.15
ADAMTS-4	0.22 ± 0.1‡	0.11 ± 0.04	0.64 ± 0.02	0.08 ± 0.02
ADAMTS-5	0.72 ± 0.2‡	1.65 ± 0.06	1.5 ± 0.05	3.6 ± 0.06
ADAM-17	0.74*-13.7°	4.83 ± 0.36	6.3 ± 0.29	4.3 ± 0.20

‡(Troeberg et al., 2009), *(Lee et al., 2002), °(Wei et al., 2005)

5.2.6 Binding of TIMP-3 mutants to sulfated glycosaminoglycans

Of the 4 mammalian TIMPs, only TIMP-3 binds to the ECM where it is thought to bind to sulfated GAGs (Yu et al., 2000). Lee et al. (2007) have previously shown that mutation of 6 basic residues (K26, K27, K30, K76, R163 and K165) on TIMP-3 ablates ECM binding, suggesting that TIMP-3 binds to a strongly negatively charged moiety in the ECM, with GAGs being the most likely binding partners. Our group also has recently shown that sulfated GAGs including heparan sulfate (HS), regulate the trafficking of secreted TIMP-3 by inhibiting LRP-1 binding (Troeberg et al., 2014). Since the strategy used here to engineer an endocytosis-resistant TIMP-3 involved the mutation of positively charged lysine residues to neutral alanine residues, we investigated the affinity of the LRP-1-resistant TIMP-3 mutants for ECM glycans and sulfated GAGs, to determine whether ECM binding may be compromised.

5.2.6.1 Binding of Wild-type TIMP-3, TIMP-3 K26A/K45A and TIMP-3 K42A/K110A to heparin and heparan sulfate

The affinity of Wild-type and mutant TIMP-3 for heparin and heparan sulfate was compared by ELISA. Both heparin and heparan sulfate are linear sulfated polysaccharides constructed from the same monosaccharide building blocks. However their primary structure differs significantly, in that the disaccharide subunits are present in different proportions and that heparin is more highly and regularly sulfated than heparan sulfate. Heparin occurs only in mast cells, while heparan sulfate proteoglycans are present on the cell surface and in the ECM of most mammalian cells. As such, heparan sulfate proteoglycans are more physiologically relevant in cartilage than heparin.

To compare the binding of Wild-type TIMP-3 and TIMP-3 mutants K26A/K45A and K42A/K110A to sulfated GAGs, heparin or heparan sulfate (10 µg/mL) were coated onto a GAG-binding plate in PBS (overnight, room temperature). Wells were blocked with gelatin (0.2 % in PBS, 1 h, 37 ^{o}C) and incubated with doubling dilutions of Wild-type TIMP-3 or TIMP-3 mutants K26A/K45A, K42A/K110A (0.2 - 25 nM) in blocking solution (0.2 % gelatin in PBS). Bound TIMP-3 was detected with an M2 anti-FLAG antibody (1:5000 dilution in blocking solution, 3 h, 37 ^{o}C) followed by an anti-mouse secondary antibody conjugated with HRP (1:500 dilution in blocking solution, 1 h, 37 ^{o}C). Tetramethylbenzidine HRP-substrate was added to quantify binding, the reaction stopped with 2N H_2SO_4 and absorbance at 450 nm measured.

The relative heparin-binding of Wild-type TIMP-3, TIMP-3 K26A/K45A and TIMP-3 K42A/K110A is shown in Figure 58A. Wild-type TIMP-3 showed the highest affinity for heparin, with a K_D value of 3.86 ± 0.29 nM. Both mutants

showed reduced binding to heparin. TIMP-3 K26A/K45A retained higher binding, with a K_D value of 15.17±2.99 nM. TIMP-3 K42A/K110A showed further reduced affinity for heparin, with a K_D value of ~ 30 nM.

The binding of Wild-type and mutant TIMP-3 to heparan sulfate is shown in Figure 58B. Wild-type and mutant TIMP-3 affinity for heparan sulfate was lower than that observed for heparin, in keeping with previous studies (Troeberg et al., 2014) and most likely due to the lower sulfation of heparan sulfate. Overall, heparan sulfate binding followed the same trend to that observed for heparin binding, with Wild-type TIMP-3 showing highest affinity, followed by TIMP-3 K26A/K45A and then by TIMP-3 K45A/K110A.

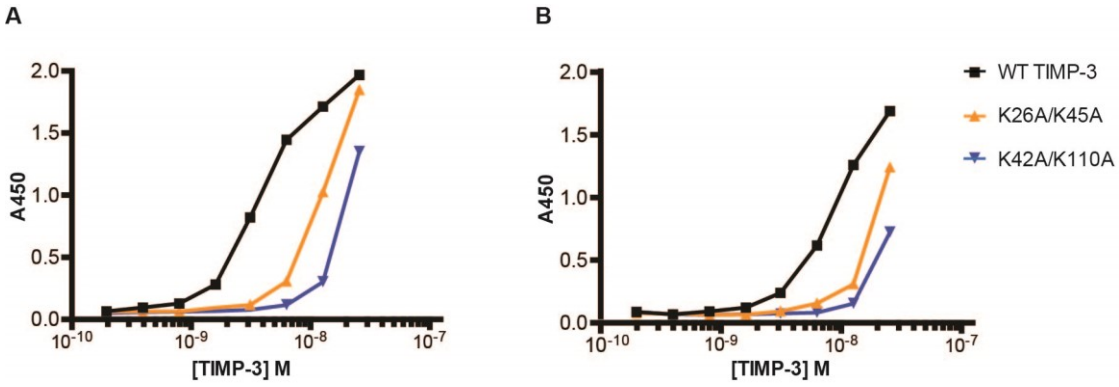


Figure 58: Binding by Wild-type TIMP-3, TIMP-3 K26A/K45A and TIMP-3 K42A/K110A to heparin and heparan sulfate.

Heparin-binding plates were coated with 10 µg/mL heparin (**A**) or heparan sulfate (**B**) in PBS (overnight, room temperature). Wells were blocked (200 µL of 0.2 % gelatin in PBS, 1 h, 37 °C) and washed three times [3x250 µL PBS containing 0.1 % (v/v) Tween 20] after this and every subsequent step. Wells were then incubated with doubling dilutions of Wild-type TIMP-3, TIMP-3 K26A/K45A or TIMP-3 K42A/K110A (0.2 - 25 nM) in blocking solution. Bound TIMP-3 was detected by incubation of wells with M2 anti-FLAG antibody (100 µL, 1:5000 dilution in blocking solution, 3 h, 37 °C) and then with an anti-mouse secondary antibody conjugated with HRP (100 µL, 1:500 dilution in blocking solution, 1 h, 37 °C) Tetramethylbenzidine HRP-substrate was added to quantify binding, the reaction stopped with 2N H_2SO_4 and absorbance at 450 nm measured.

5.2.6.2 Effect of reduced heparin binding on inhibition of ADAMTS-5

Previous studies have shown that TIMP-3 affinity for ADAMTS-5 is increased in the presence of heparin and heparan sulfate, due to the ability of the sulfated GAGs to mediate formation of a high affinity trimolecular complex with the enzyme and inhibitor (Troeberg et al., 2012). Having demonstrated that TIMP-3 K26A/K45A and TIMP-3 K42A/K110A have reduced heparin and heparan sulfate binding, we investigated whether their affinity for ADAMTS-5 could still be increased by addition of heparin. The affinity of Wild-type TIMP-3, TIMP-3 K26A/K45A and TIMP-3 K42A/K110A for ADAMTS-5 was calculated in the presence or absence of heparin (Section 5.2.5.5). ADAMTS-5 (1 nM) was incubated with Wild-type TIMP-3 (Figure 59A, 0.5-10 nM), TIMP-3 K26A/K45A (Figure 59B, 0.5-10 nM) or TIMP-3 K42A/K110A (Figure 59C**,** 0.5-10 nM) in the presence or absence of heparin (100 nM, equivalent to 1.25 µg/mL, for 1 h at 37 ^{o}C) and residual activity against the brevican-based substrate, (Matthews et al., 2000; Nakamura et al., 2000) ortho-aminobenzoyl-Thr-Glu-Ser-Glu-Ser-Arg-Gly-Ala-Ile-Tyr-(N-3-[2,4-dinitrophrenyl]-L-2,3-diamiopropionyl)-Lys-Lys-NH_2, (20 µM, 18 H, λ_{ex} 300 nm, λ_{em} 430 nm) determined.

Wild-type TIMP-3 was calculated to have a $K_{i(app)}$ value of 1.65 ± 0.063 nM affinity for ADAMTS-5. However, in the presence of heparin this value decreased to a $K_{i(app)}$ value too low to be calculated accurately (Figure 59A), as has previously been reported (Troeberg et al., 2014).

For TIMP-3 K26A/K45A (Figure 59B), the calculated $K_{i(app)}$ was 1.5 ± 0.05 nM, while in the presence of heparin this value similarly decreased to a value too low to be determined.

TIMP-3 K42A/K110A showed no meaningful improvement in affinity in the presence of heparin, with a $K_{i(app)}$ value of 3.61 ± 0.06 nM in its absence and 2.46 ± 0.07 nM in its presence (Figure 59C).

Table 22 shows a summary of the calculated values.

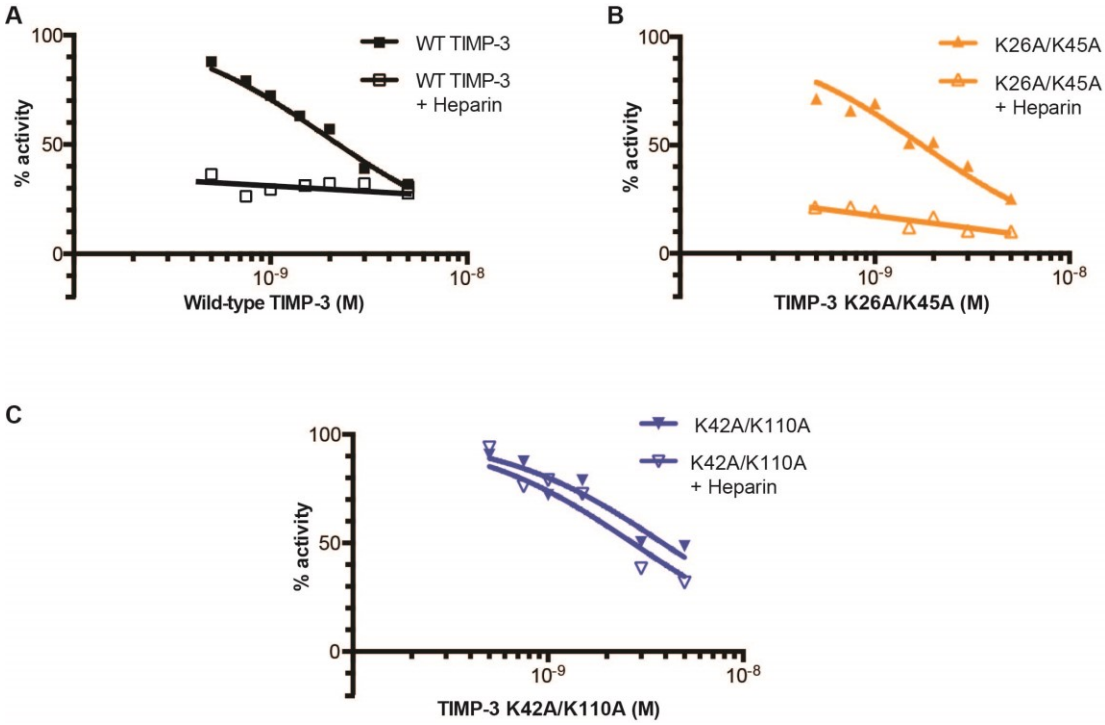


Figure 59: Effect of heparin on affinity of Wild-type TIMP-3 and TIMP-3 mutants K26A/K45A and K42A/K110A for ADAMTS-5.

ADAMTS-5 (1 nM) was incubated with Wild-type TIMP-3 (**A,** 0.5-10 nM), TIMP-3 K26A/K45A (**B,** 0.5-10 nM) or TIMP-3 K42A/K110A (**C,** 0.5-10 nM) in the presence or absence of heparin (1.25 µg/mL) for 1 h at 37 °C and residual activity against ortho-aminobenzoyl-Thr-Glu-Ser-Glu-Ser-Arg-Gly-Ala-Ile-Tyr-(N-3-[2,4-dinitrophrenyl]-L-2,3-diamiopropionyl)-Lys-Lys-NH_2 (20 µM) determined (18 h, 37 °C). Prism software was used to fit the data to the tight-binding equation. (**A**) The $K_{i(app)}$ value of Wild-type TIMP-3 for ADAMTS-5 in the absence of heparin was shown to be 1.65 ± 0.063 nM. In the presence of heparin, the $K_{i(app)}$ was too low to be calculated accurately. (**B**) The $K_{i(app)}$ value of TIMP-3 K26A/K45A for ADAMTS-5 in the absence of heparin was shown to be 1.5 ± 0.05 nM, while the $K_{i(app)}$ value in the presence of heparin was too low to be calculated accurately. (**C**) The $K_{i(app)}$ value for TIMP-3 K42A/K110A for ADAMTS-5 in the absence and presence of heparin was shown to be 3.61 ± 0.06 nM and 2.46 ± 0.07 nM respectively.

Table 22: Effect of heparin on affinity of TIMP-3, TIMP-3 K26A/K45A and TIMP-3 K42A/K110A for ADAMTS-5.

$K_{i(app)}$ (nM)		
	ADAMTS-5	**ADAMTS-5 + Heparin**
TIMP-3 Wild-type	1.65 ± 0.063	Too low to be calculated
TIMP-3 K26A/K45A	1.5 ± 0.05	Too low to be calculated
TIMP-3K42A/K110A	3.61 ± 0.06	2.46 ± 0.07

5.3 Discussion

In Chapter 4, transiently expressed TIMP-3 mutants were assessed for their endocytosis-resistance in the HTB94 human chondrosarcoma cell line. A shortlist of potentially endocytosis-resistant TIMP-3 mutants was generated from an original starting list of 22 mutants. 12 of these TIMP-3 mutants contained a single lysine to alanine mutation, with the remaining 10 containing 2 lysine to alanine mutations. Only the TIMP-3 mutants containing 2 lysine to alanine mutations (TIMP-3 double mutants) were observed to be resistant to endocytosis by HTB94 cells within the 24 h experimental time frame.

In this Chapter, we assessed the bioactivity of these shortlisted TIMP-3 double mutants after purifying them from HEK-293-EBNA cells selected for stable expression of the mutants. In generating the TIMP-3 double mutant expressing stable cell-lines, we identified that the lowest tested hygromycin B concentration (100 µg/mL) gave highest levels of mutant protein expression. This is likely to be due to the toxic effects of higher expression of the TIMP-3 mutants at 400 and 800 µg/mL hygromycin B, potentially through apoptosis. Interestingly, Wild-type TIMP-3 stable lines showed best expression at 800 µg/mL hygromycin B, suggesting that the TIMP-3 mutants may be more toxic due to their reduced endocytosis.

Previous studies of the chondroprotective effect of TIMP-3 have shown that 100 nM Wild-type TIMP-3 is required to inhibit aggrecan degradation in cartilage explants (Gendron et al., 2003; Lim et al., 2010) Thus, only those TIMP-3 mutants purified to this minimum concentration were deemed suitable for further analysis. Of the initial 10 shortlisted TIMP-3 mutants, only TIMP-3 K26A/K45A and TIMP-3 K42A/K110A were successfully purified to a concentration in excess of the minimum required.

The poor expression of mutants such as TIMP-3 K22A/K110A and K27A/K45A may have been due to the toxic effects of expressing high quantities of the proteins over time. As these mutants had yields below the detection limit of anti-FLAG immunoblotting it was unlikely that they would have sufficiently responded to optimisation to improve their yields to the required level.

While mutants TIMP-3 K30A/K52A and K30A/K76A were detected at higher yields than TIMP-3 K22A/K110A and K27A/K45A, their yield did not improve by increasing the volume of the culture medium used for purification. This suggests that the maximum expression limit had been achieved at 18 µg/L and further optimisation would have proven unrewarding. TIMP-3 K22A/K157A, K42A/K157A and K45A/K89A were successfully detected by immunoblotting but had very low active concentrations of 7.2, 6 and 5.5 µg per Litre of starting conditioned medium respectively, as determined by titration against MMP-1ΔC. It may have been possible to purify sufficient TIMP-3 K22A/K157A, K42A/K157A and K45A/K89A by increasing the culture volume or by concentrating the eluted protein, but as 2 mutants of sufficiently high yield had already been identified, this was not deemed necessary at this stage. From

the initial shortlist of 10 TIMP-3 double mutants, 2 were thus successfully purified to a concentration in excess of the minimum required concentration. It should be noted that the remaining 8 displayed good endocytosis-resistance and were omitted from analysis only on the basis of their low yield. Also, while the TIMP-3 mutants showed low yields overall, they were not substantially worse than Wild-type TIMP-3, which has a notoriously low expression yield compared to the other TIMPs, and to recombinant protein expression in general.

The shortlist of endocytosis-resistant TIMP-3 mutants was generated by analysing the uptake of TIMP-3 mutants expressed in crude conditioned media of HEK-293-EBNA by HTB94 cells (Section 4.2.3.5). Following stable expression and purification, the endocytosis of purified TIMP-3 double mutants K26A/K45A, K30A/K76A and K42A/K110A was assessed to ensure they had retained their endocytosis-resistance. Purified Wild-type TIMP-3 was completely endocytosed by HTB94 cells within 24 h, only remaining in culture medium in the presence of RAP, a known antagonist of LRP-1 ligand binding. On the other hand, purified TIMP-3 K26A/K45A and K42A/K110A, as well as TIMP-3 K30A/K76A, remained in cell media after 24 h in the presence or absence of RAP, indicating that they behaved in the same manner when purified as had been observed in crude conditioned media. This validated our initial screening procedure.

Binding of TIMP-3 mutants to LRP-1 was quantified by ELISA to determine whether the accumulation of TIMP-3 mutants in HTB94 cell culture medium correlated with the expected reduction in LRP-1 binding. The LRP-1 affinity of TIMP-3 mutants K30A/K52A and K42A/K157A was quantified along

with the shortlisted TIMP-3 mutants K26A/K45A and K42A/K110A. TIMP-3 mutants K30A/K52A and K42A/K157A had been removed from the endocytosis shortlist due to their low purified concentration. As expected, Wild-type TIMP-3 showed high affinity binding for LRP-1 with TIMP-3 mutants K26A/K45A, K30A/K52A, K42A/K110A and K42A/K157A showing a lower binding affinity (Section 5.2.4). Due to its reduced purified concentration, TIMP-3 K42A/K157A affinity for LRP-1 was quantified from a starting concentration of 6.25 nM and showed similar minimal binding to that observed for TIMP-3 K42A/K110A at these concentrations. It was observed that TIMP-3 K26A/K45A and TIMP-3 K30A/K52A bound to LRP-1 with a similar higher affinity than TIMP-3 K42A/K110A and K42A/K157A. All 4 TIMP-3 mutants tested here display good endocytosis resistance, but TIMP-3 K30A/K52A and TIMP-3 K42A/K110A were not suitable for further use in chondroprotectivity assays due to their low purified concentrations. As TIMP-3 K26A/K45A and TIMP-3 K42A/K157A showed reduced LRP-1 affinity and were successfully purified to yields in excess of the minimum 100 nM required, they were further investigated

At this point, we had successfully determined that TIMP-3 mutants K26A/K45 and K42A/K110A reproducibly displayed the endocytosis-resistance (Section 5.2.3) we had previously observed for crude conditioned media (Section 4.2.3), had reduced binding to LRP-1 and did not induce cell death at the concentrations expected to inhibit cartilage degradation.

The working hypothesis for this study was that LRP-1-resistant TIMP-3 mutants would have increased chondroprotective activity relative to Wild-type TIMP-3 (Chapter 6), so we next established that the acquisition of endocytosis-resistance had not negatively impacted on TIMP-3 inhibitory activity. Wild-type

TIMP-3 has a broad inhibition profile and affinity for representative target metalloproteinases by TIMP-3 K26A/K45A and TIMP-3 K42A/K110A was quantified to confirm retention of prototypic TIMP-3 inhibitory activity. We compared the affinity of TIMP-3 K26A/K45A and TIMP-3 K42A/K110A for MMP-1ΔC, MMP-2ΔC, MMP-3 ΔC, ADAMTS-4, ADAMTS-5 and ADAM-17 with that of Wild-type TIMP-3.

The Wild-type TIMP-3 affinity for MMP-1ΔC, MMP-2ΔC and MMP-3ΔC has previously been documented with $K_{i(app)}$ values of 1.1 ± 0.6 nM, 0.9 ± 0.3 nM and 1.0 ± 0.4 nM respectively reported (Troeberg et al., 2009). We calculated $K_{i(app)}$ values for Wild-type TIMP-3 inhibition of MMP-1ΔC and MMP-2ΔC and MMP-3ΔC as 0.43 ± 1.2 nM, 0.95 ± 0.09 nM and 0.98 ± 0.05 nM respectively. These values were comparable with the published values. $K_{i(app)}$ values for TIMP-3 mutant K26A/K45A inhibition of MMP-1ΔC, MMP-2ΔC and MMP-3ΔC were then similarly quantified and determined to be 0.35 ± 0.05 nM, 1.2 ± 0.13 nM and 1.02 ± 0.09 nM respectively. $K_{i(app)}$ values for TIMP-3 K42A/K110A inhibition of MMP-1ΔC, MMP-2ΔC and MMP-3ΔC were calculated to be 0.40 ± 1.03 nM, 1.18 ± 0.15 nM and 1.01 ± 0.15 nM respectively. The $K_{i(app)}$ values observed for TIMP-3 K26A/K45A and TIMP-3 K42A/K110A were thus comparable to each other and to values for Wild-type TIMP-3. This confirms that TIMP-3 mutants K26A/K45A and K42A/K110A had unaltered affinity for MMP-1, MMP-2 and MMP-3.

Of the 4 mammalian TIMPs, only TIMP-3 inhibits ADAMTS-4 and ADAMTS-5. These enzymes, also known as aggrecanases, degrade aggrecan, the structural component that gives cartilage its resistance to compression. Wild-type TIMP-3 affinities for ADAMTS-4 and ADAMTS-5 have

previously been documented, with $K_{i(app)}$ values of 0.22 ± 0.1 nM and 0.72 ± 0.2 nM respectively reported (Troeberg et al., 2009). In the current study, TIMP-3 K26A/K45A was calculated to have $K_{i(app)}$ values of 0.64 ± 0.02 nM and 1.5 ± 0.05 nM for ADAMTS-4 and ADAMTS-5 respectively. TIMP-3 K42A/K110A was calculated to have $K_{i(app)}$ values of 0.08 ± 0.02 nM and 3.6 ± 0.06 nM for ADAMTS-4 and ADAMTS-5 respectively. The TIMP-3 mutants thus had unaltered affinity for these aggrecanases. This was critically important to the chondroprotective activity of the TIMP-3 mutants, due to the central role that ADAMTS-4 and ADAMTS-5 plays in aggrecan degradation in osteoarthritis.

Wild-type TIMP-3 affinity for ADAM-17 has previously been documented, with $K_{i(app)}$ values ranging between 0.74 ± 0.4 nM (Lee et al., 2002) and 13.7 ± 0.2 nM (Wei et al., 2005). Different ADAM-17 substrates were used in these experiments: Lee et al. used QF-45 (Mca-Ser-Pro-Leu-Ala-Gln-Ala-Val-Arg-Ser-Ser-Ser-Arg-Lys-Dnp-NH_2) while Wei et al. used TACE substrate III (Mca-Pro-Leu-Ala-Gln-Ala-Val-Dpa-Arg-Ser-Ser-Ser-Arg-NH_2). Here we used TACE substrate IV (Abz-Leu-Ala-Gln-Ala-Val-Arg-Ser-Ser-Ser-Arg-Dpa) (Jin et al., 2002). The $K_{i(app)}$ value of Wild-type TIMP-3 calculated here (4.83 ± 0.36 nM) fell within the range of published values. The affinity of TIMP-3 mutants K26A/K45A and K42A/K110A for ADAM-17 was calculated, with $K_{i(app)}$ values of 6.3 ± 0.29 nM and 4.3 ± 0.2 nM respectively. These values are comparable to those calculated here for Wild-type TIMP-3 and to the published values.

We therefore demonstrated that the TIMP-3 mutants K26A/K45A and K42A/K110A had retained unaltered affinity for a range of prototypic TIMP-3 target metalloproteinases. We had expected this to be the case, because Scilabra et al. (2013) have previously shown that TIMP-3 bound to LRP-1

retains its ability to inhibit ADAMTS-4, indicating that residues mediating metalloproteinase inhibition and LRP-1 binding are on opposite faces of the TIMP-3 molecule. Therefore, mutation of residues mediating LRP-1-binding would not have been expected to alter the affinity of a TIMP-3 mutant for target metalloproteinases.

TIMP-3 binds to the ECM and forms a trimolecular complex with target enzymes such as ADAMTS-5 and sulfated matrix GAGs. This increases the affinity of TIMP-3 for the target enzyme by around 1000-fold (Troeberg et al., 2012). The model of the 3D structure of TIMP-3 indicates that the protein has an extended basic patch on the face opposite the inhibitory ridge. It is thought that the TIMP-3 binding to sulfated matrix GAGs is mediated by interaction between the strongly negatively charged GAGs in the ECM and the positive charges on the basic patch of TIMP-3. It has previously been shown that mutation of 6 basic residues in this patch ablates TIMP-3 binding to the ECM (Lee et al., 2007). The strategy used here to generate endocytosis-resistant TIMP-3 mutants involved the mutation of positively charged lysine residues to neutral alanine residues, raising the possibility that the ECM binding of the TIMP-3 mutants might be reduced or ablated. Therefore the binding of TIMP-3 mutants to heparin and heparan sulfate was investigated by ELISA. Due to differences in sulfation patterns between the heparin and heparan sulfate, Wild-type and mutant TIMP-3 bound with higher affinity to heparin than to heparan sulfate. However in both cases, Wild-type TIMP-3 bound with highest affinity, with TIMP-3 K26A/K45A showing an estimated 3-fold reduction in affinity and TIMP-3 K42A/K110A showing an estimated 10-fold reduction in affinity.

We assessed the affect of this reduced heparin and heparan sulfate-binding on the increase in TIMP-3 affinity for ADAMTS-5 in the presence of these GAGs. Heparin increased the affinity of Wild-type TIMP-3 to a value too low to be accurately determined. Heparin similarly increased the affinity of TIMP-3 K26A/K45A for ADAMTS-5 to a value too low to be accurately determined. We thus conclude that TIMP-3 K26A/K45A retained sufficient affinity for sulfated GAGs to display increased inhibitory activity when bound to the ECM. No increase in affinity was observed for TIMP-3 K42A/K110A, which coincided with its greatly reduced heparin binding, so we conclude that ECM glycans will not substantially increase its affinity for GAG-binding TIMP-3 target metalloproteinases.

In this Chapter, we have successfully demonstrated that TIMP-3 mutants K26A/K45A and K42A/K110A are resistant to endocytosis by HTB94 chondrosarcoma cells and that this resistance correlates with their reduced LRP-1 binding and is not due to TIMP-3-induced apoptosis. We have also shown that these TIMP-3 mutants have unaltered inhibitory activity for prototypic TIMP-3 target metalloproteinases, with affinities comparable to that observed for Wild-type TIMP-3. The mutation of 2 lysine residues to alanine residues in the generation of endocytosis resistance did however negatively affect ECM binding. This was particularly observed in the case of TIMP-3 K42A/K110A, which showed no increase in affinity for ADAMTS-5 in the presence of heparin. TIMP-3 K26A/K45A, however, did show increased affinity for ADAMTS-5 in the presence of heparin, albeit to a lesser degree than that observed for Wild-type TIMP-3. Based on these findings, we hypothesized that

TIMP-3 K26A/K45A would be a more effective inhibitor of cartilage breakdown than TIMP-3 K42A/K110A. This hypothesis was tested in Chapter 6.

Chapter 6: Chondroprotective effect of TIMP-3 mutants

6.1. Introduction

As discussed in Chapter 5, the shortlisted endocytosis-resistant TIMP-3 mutants TIMP-3 K26A/K45A and TIMP-3 K42A/K110A were shown to have retained their inhibitory activity against their target metalloproteinases, with comparable affinity to that of Wild-type TIMP-3. In the current Chapter, we investigated whether the TIMP-3 mutants had increased chondroprotective activity relative to that of Wild-type TIMP-3.

The core protein of the proteoglycan aggrecan is composed of composed of 3 globular domains (G1, G2 and G3) separated by 2 interglobular domains (IGDs). G1, the N-terminal globular domain, is attached to hyaluronan by link protein. Chondroitin sulfate and keratan sulfate GAG side chains are covalently bound to the second larger IGD between G2 and the C-terminal G3.

ADAMTS-4 and ADAMTS-5 are considered to be the main enzymes involved in the aggrecan cleavage in OA. ADAMTS-4 and ADAMTS-5 cleave aggrecan at several sites, including at Glu^{373}-Ala^{374} in the first IGD (Arner et al., 1999) generating the N-terminal ^{374}ARGSV neo-epitope, and at Glu^{1819}-Ala^{1820} in the second IGD generating the ^{1820}AGEG neo-epitope. These neo-epitopes can be detectable in vitro using the BC-3 anti-ARGSV antibody and our in-house generated rabbit anti-AGEG antibody respectively.

Aggrecanase-associated GAG release from cartilage can be stimulated by cytokines or retinoic acid (Caterson et al., 2000; Von den Hoff et al., 1993), singly or in combination. Stimulating cytokines include IL-1 (Dingle et al., 1979; Sandy et al., 1991; Smith et al., 1989), TNFα (Arner et al., 1998; Fushimi et al., 2008) and IL-6 (Stanton et al., 2011a). In this study, the relative chondroprotectivity of Wild-type TIMP-3 and TIMP-3 mutants K26A/K45A and

K42A/K110A was assessed by comparing their ability to inhibit IL-1 stimulated GAG release from porcine cartilage explants. Cartilage explants are a physiologically relevant system in which to measure cartilage degradation in vitro, and have been the gold standard in vitro system in the field of cartilage research for decades (Dingle et al., 1979).

The inhibition of GAG release was quantified using the dimethylmethylene methylene blue (DMMB) dye binding assay and neo-epitope immunoblotting. In the DMMB assay (Section 2.3.1.1), sulfated GAGs form a complex with the DMMB dye, causing a shift in the absorption spectrum (Farndale et al., 1982). The absorbance at 525 nm is correlated with GAG content for absorption values that fall within the linear range of the assay. A standard curve was generated by adding DMMB dye to bovine chondroitin-4-sulfate (0-4 µg) in a 96 well plate and measuring the absorbance at 525 nm. Linear regression was used to fit an equation to the data, which was then used to determine the amount of GAG present in experimental samples.

GAG release was also analysed by immunoblotting using neo-epitope antibodies that recognize the new N-termini generated by ADAMTS-4 or ADAMTS-5 aggrecanase activity (Section 2.2.3.3). Samples were first deglycosylated with chondroitinase ABC and keratanase, and then acetone precipitated and separated on a 6% Tris-glycine gel. After immunoblotting onto PVDF, blots were incubated with anti-AGEG neo-epitope antibodies to detect aggrecanase cleavage of aggrecan.

Previous studies have shown that the N-terminal domain of TIMP-3 (N-TIMP-3) inhibits aggrecanase-generated GAG release from porcine and bovine cartilage explants (Gendron et al., 2003; Lim et al., 2010). Gendron et al. (2003)

stimulated bovine nasal cartilage explants with IL-1α (100 ng/mL) and porcine articular cartilage explants with retinoic acid (1 μM). In both cases, GAG release was quantified by DMMB assay and neo-epitope immunoblotting using the anti-ARGSV antibody. Lim et al. (2010) stimulated porcine articular cartilage with a lower concentration of IL-1α (10 ng/mL) and quantified GAG release by DMMB assay. Both studies found that the minimal concentration of N-TIMP-3 required to inhibit GAG release was 100 nM (Gendron et al., 2003; Lim et al., 2010).

We set out to compare the chondroprotective activity of full-length Wild-type TIMP-3 with that of the TIMP-3 mutants K26A/K45A and K42A/K110A, by analyzing their ability to inhibit aggrecanase-dependent GAG release in a cartilage explant system. Based on previous studies (Gendron et al., 2003; Lim et al., 2010), we first optimised a range of variables to ensure that findings were both reproducible and representative.

6.2. Results

6.2.1. Resistance of purified TIMP-3 double mutants to endocytosis by primary porcine chondrocytes

We have previously shown that purified TIMP-3 K26A/K45A, K30A/K76A and TIMP-3 K42A/K110A are resistant to endocytosis by HTB94 cells (Section 5.2.3). Here, we tested whether these purified TIMP-3 mutants were also resistant to endocytosis by primary porcine chondrocytes. Endocytosis resistance was determined by quantifying the levels of exogenously added TIMP-3 mutant remaining in the medium of chondrocytes after 24 h, either in the presence or absence of RAP. Porcine explants were harvested from the metacarpophalangeal joints of 3-9 month old pigs and chondrocytes isolated

by treatment with 1 mg/ml bacterial collagenase in cartilage growth medium (DMEM supplemented 10 % FCS, 100 U/mL penicillin, 100 mg/mL streptomycin, 2 mg/mL amphotericin B and 10 mM HEPES, overnight at 37 ºC, with shaking at 250 rpm)(Section 2.2.1.3). Cells were passed through a cell strainer, washed three times in cartilage growth medium, and counted using an Eve Automated Cell Counter (NanoEnTek, Seoul, South Korea). Chondrocytes were plated overnight in 12-well plates at a density of $8x10^5$ cells per well.

Chondrocytes were washed in serum-free cartilage growth medium and incubated with or without RAP (500 nM) for 1h prior in serum-free cartilage growth medium with 0.1 % FCS. Purified Wild-type TIMP-3 and TIMP-3 mutants K26A/K45A, K30A/K76A or K42A/K110A (1 nM) were added to the wells after 1 h, and media harvested at 0 and 24 h. Samples were analysed by immunoblotting with an anti-FLAG M2 antibody and an anti-mouse IgG AP-conjugated secondary antibody. Band intensity was quantified using Phoretix ID Gel Analysis software and expressed as a percentage of pixel volume at t = 0.

As expected, Wild-type TIMP-3 was endocytosed within 24 h in the absence of RAP, but remained in the conditioned medium in the presence of RAP (Figure 60A). However TIMP-3 mutants K26A/K45A, K30A/K76A and K42A/K110A were present in the medium at similar levels at 0 and 24 h, both in the presence or absence of RAP (Figure 60B-D). This demonstrates that the TIMP-3 mutants K26A/K45A, K30A/K76A and K42A/K110A were resistant to chondrocyte endocytosis, as has been previously observed in HTB94.

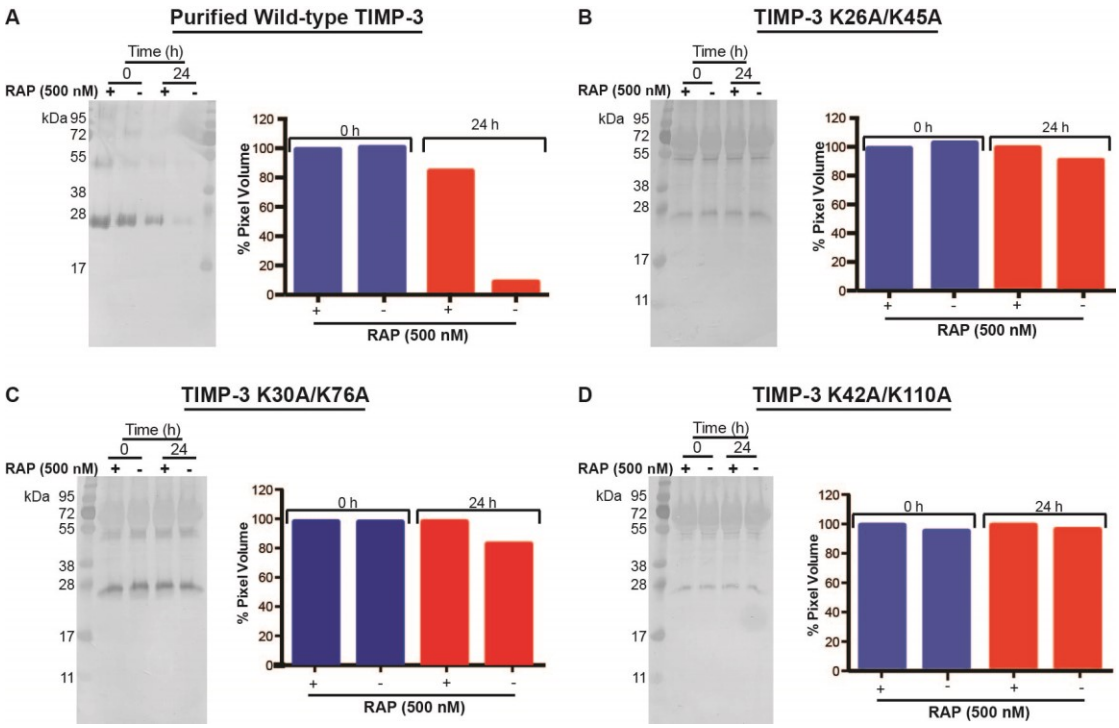


Figure 60: TIMP-3 mutants K26A/K45A, K30A/K76A and K42A/K110A are resistant to endocytosis by primary porcine chondrocytes.

Chondrocytes were seeded overnight in a 12-well plate [8x10^5 cells, 37 °C, 5 % (v/v) CO_2] and washed in serum-free DMEM. Wells were then incubated with or without RAP (500 nM) for 1h, before media were reaplaced with in cartilage growth medium (1 mL) containing 0.1 % FCS with purified Wild-type TIMP-3 (**A**), TIMP-3 K26A/K45A (**B**), TIMP-3 K30A/K76A (**C**) or TIMP-3 K42A/K110A (**D**) (1 nM), with or without RAP (500 nM). Conditioned media were harvested at 0 and 24 h, TCA precipitated and pellets resuspended in 30 µL of 2x SDS-PAGE loading buffer. Resuspended samples (15 µL) were analysed by immunoblotting with an anti-FLAG M2 antibody and an anti-mouse IgG AP-conjugated secondary antibody. Bands were visualised using Western blue stabilised substrate for AP and reaction stopped using AP stop (20 mM Tris-HCl pH 7.5, 10 mM EDTA). Band intensity was quantified using Phoretix ID Gel Analysis software and expressed as a percentage of pixel volume at t = 0.

6.2.2. Optimising quantification of GAG release

A number of factors were optimised to develop an assay comparing the relative chondroprotectivity of the shortlisted TIMP-3 mutants, TIMP-3

K26A/K45A and TIMP-3 K42A/K110A, with that of Wild-type TIMP-3. These factors were:

- method of stimulating GAG release (IL-1 or retinoic acid).
- duration of stimulation (1, 2 or 3 days)
- GAG detection (DMMB assay or neo-epitope immunoblotting)
- culture conditions (12 or 48 well plate, 250 µL or 500 µL medium).

The method of stimulating GAG release and duration of stimulation were particularly important as the conditions producing the largest increase would allow for ease of quantification with minimum error. Each detection method had its own associated limits of specificity, sensitivity and reproducibility.

6.2.2.1. Evaluation of GAG release stimulation method

It has been shown that GAG release from cartilage can be stimulated by addition of RA or cytokines such as IL-1, TNFα or IL-6, either alone or in combination (Arner et al., 1998; Fushimi et al., 2008; Sandy et al., 1991; Smith et al., 1989; Stanton et al., 2011a; Von den Hoff et al., 1993). To investigate the optimum method of stimulating GAG release in cartilage, Flannery et al quantified ADAMTS-1, -2, -3, -4, and -5 mRNA levels in RA-, IL-1- and TNF-α-stimulated human articular cartilage and human cartilage explants cultures. Of the treatments used, only RA caused a marked increase in mRNA levels for any of the ADAMTSs investigated. RA was shown to increase aggrecanase activity without increasing ADAMTS expression (Flannery et al., 1999). It has also been demonstrated that RA down-regulated transcription of the collagen II, suggesting that it also reduces matrix synthesis (Horton et al., 1987). While no direct comparison has been made between the induction of MMPs and

ADAMTS induction following RA treatment, work completed by Gendron et al. suggests that RA induces ADAMTSs more than MMPs (Gendron et al., 2007).

Here, we compared the ability of retinoic acid and IL-1 to stimulate GAG release from porcine cartilage explants and chondrocyte monolayer cultures. The method producing the highest level of GAG release was then used in future experiments to compare the inhibitory activity of TIMP-3 mutants compared to that of Wild-type TIMP-3.

Porcine explants were harvested from the metacarpophalangeal joints of 3-9 month old pigs using a 4 mm biopsy punch (Section 2.3.1). Explants were rested for 2 days in cartilage growth medium (DMEM supplemented with 10 % FCS, 100 U/mL penicillin, 100 mg/mL streptomycin, 2 mg/mL amphotericin B and 10 mM HEPES), with one explant per well in a 12 well plate. They were then washed 3 times in serum-free cartilage growth medium (DMEM supplemented with 100 U/mL penicillin, 100 mg/mL streptomycin, 2 mg/mL amphotericin B and 10 mM HEPES), and stimulated for 2 days with retinoic acid (1 μM) or IL-1 (10 ng/ml) in 500 μL of serum-free DMEM cartilage growth medium. Assays were performed in triplicate.

Alternatively, porcine chondrocytes were isolated from cartilage explants by treatment with 1 mg/ml bacterial collagenase in cartilage growth medium (overnight at 37 ºC, with shaking at 250 rpm)(Section 2.2.1.3). Cells were passed through a cell strainer, washed three times in cartilage growth medium and counted using an Eve Automated Cell Counter (NanoEnTek, Seoul, South Korea). Chondrocytes were plated in 12-well plates at a density of $8x10^5$ cells per well.

GAG release was first quantified using the DMMB assay (Farndale et al., 1982), with measurements performed in triplicate. We optimised the volume of conditioned medium to add to the DMMB dye to ensure readings were on the linear portion of the standard curve (Section 2.3.1.1), and found that 2-3 µL of medium was optimal for most experiments. Using this standard curve, the amount of GAG released into the medium was calculated from the absorbance readings at 525 nm.

Using the DMMB assay, it was observed that retinoic acid and IL-1 both stimulated GAG release from cartilage explants (Figure 61A). Unstimulated cartilage explants released a maximum of 23.69 µg GAG, while retinoic acid-stimulated explants released a maximum of 119.02 µg, and IL-1-treated explants released a maximum of 251.38 µg. Retinoic acid thus stimulated a 5-fold increase in GAG release, while IL-1 stimulated a 10-fold increase. There was good reproducibility between the triplicate repeats of each condition.

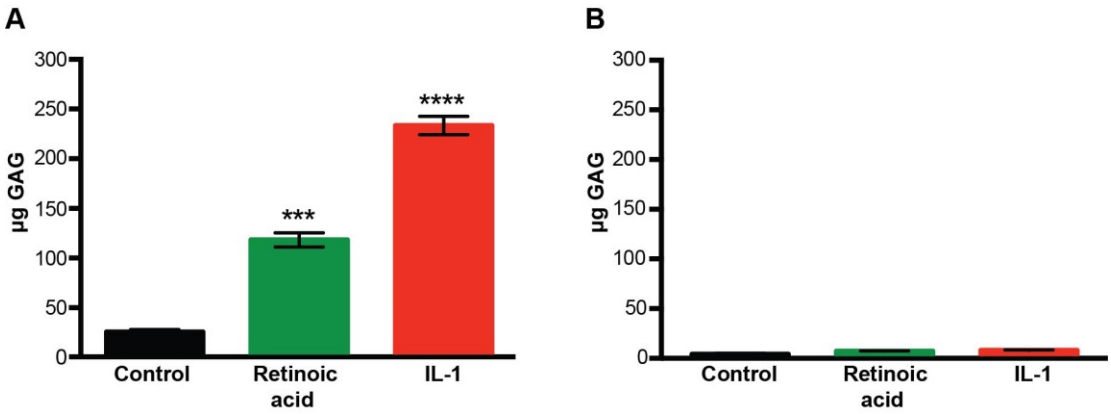


Figure 61: By DMMB assay, IL-1 stimulates highest GAG release from porcine cartilage explants and articular chondrocytes.

(A) Porcine cartilage explants were harvested using a 4 mm biopsy punch and rested for 2 days in a 12-well plate in 500 µL of cartilage growth medium (DMEM supplemented with 10 % FCS, 100 U/mL penicillin, 100 mg/mL streptomycin, 2 mg/mL amphotericin B and 10 mM HEPES). Explants were then washed into serum-free cartilage growth medium (DMEM supplemented with 100 U/mL penicillin, 100 mg/mL streptomycin, 2 mg/mL amphotericin B and 10 mM HEPES) and treated in triplicate with or without retinoic acid (1 µM) or IL-1 (10 ng/mL) for 48 h. Conditioned media were harvested and analysed for GAG content using the DMMB assay. (**B)** Porcine chondrocytes were isolated from cartilage by bacterial collagenase treatment (1 mg/ml) in cartilage growth medium (overnight at 37 ºC, shaking at 250 rpm). Chondrocytes were seeded in a 12-well plate in cartilage growth medium (37 ºC, 5 % CO_2, overnight), washed into serum-free cartilage growth medium and treated in triplicate with or without retinoic acid (1 µM) or IL-1 (10 ng/mL IL-1) for 48 h. Conditioned media were harvested and analysed for GAG content using the DMMB assay. Statistical differences were determined by a One-Way Anova followed by Dunnet's *post-hoc* test, where *** $P \leq 0.001$ and **** $P \leq 0.0001$.

Chondrocyte monolayer cultures, however, released too little GAG to be detected by the DMMB assay (Figure 61B). Future experiments were thus conducted using the cartilage explant cultures only.

Following DMMB analysis, the explant cultures were also analysed by neo-epitope immunoblotting (Section 2.3.2) using the anti-AGEG antibody, which recognises the N-terminal neo-epitope generated by ADAMTS-cleavage of aggrecan at the Glu^{1819}-Ala^{1820} site in the second IGD. This method also showed good reproducibility.

Figure 62 shows that no AGEG-containing aggrecan fragment was detected in unstimulated cultures. Addition of retinoic acid or IL-1 stimulated the accumulation of the aggrecan fragment in the conditioned medium. However, IL-1 stimulated higher release of this fragment than retinoic acid. Control samples had a mean pixel volume of 3880.94, while retinoic acid and IL-1-stimulated samples had mean pixel volumes of 4940.75 and 48295.82

respectively. Retinoic acid thus stimulated a modest 1.5-fold increase in AGEG release, while IL-1 stimulated a 10-fold increase. Retinoic acid thus showed a lower level of stimulation when analysed by neo-epitope immunoblotting than when analysed by DMMB assay.

Both the DMMB assay and neo-epitope immunobloting showed IL-1 to be a better method for stimulating GAG release. This was unexpected, seeing as retinoic acid has previously been shown to stimulate to a comparable level (Gendron et al., 2003). IL-1 was chosen as the method of stimulation for future experiments.

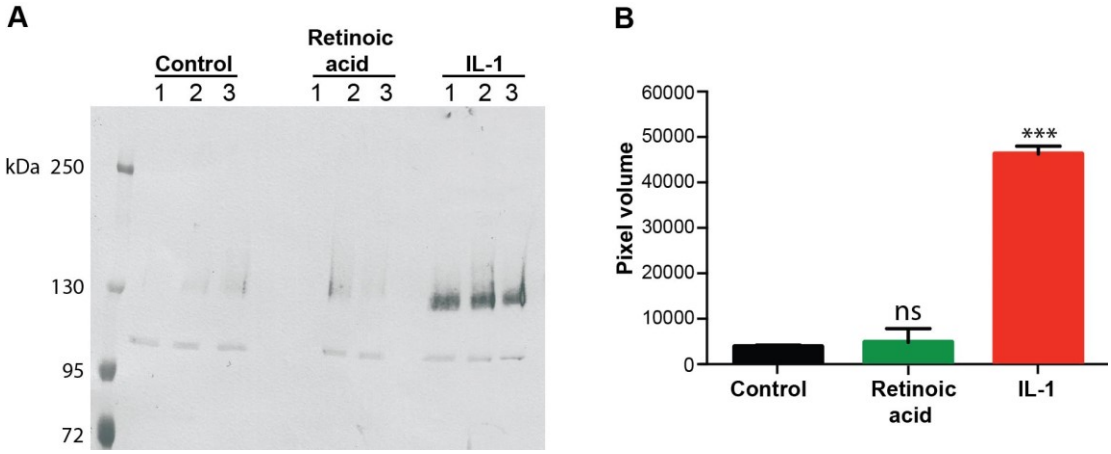


Figure 62: IL-1 and retinoic acid stimulation of AGEG neo-epitope release from porcine cartilage explants by immunoblotting.

Porcine cartilage explants were harvested using a 4 mm biopsy punch and rested for 2 days in a 12-well plate in 500 µL of cartilage growth medium). Explants were then washed into serum-free cartilage growth medium and treated in triplicate with or without retinoic acid (1 µM) or IL-1 (10 ng/mL) for 48 h. Conditioned media were harvested and deglycosylated in 2x GAG buffer (200 mM sodium acetate, 100 mM Tris-HCl pH 8.0, 100 mM EDTA) with 0.05 U each of chondroitinase ABC and keratanase (overnight, 37 ºC) (**A**) Samples (10 µL) were separated on a 6 % Tris-glycine gel and analysed by immunoblotting with an anti-AGEG primary antibody (1/1000 dilution of anti-serum) and an anti-rabbit IgG AP-conjugated antibody (1:5000). Bands were visualised using Western blue stabilised substrate for AP and

the reaction stopped using AP stop (20 mM Tris-HCl pH 7.5, 10 mM EDTA). **(B)** Pixel volume of (**A**) was quantified using Phoretix ID Gel Analysis software. Statistical differences were determined by a One-Way Anova followed by Tukey's *post-hoc* test, where ns $P>0.05$, *** $P\leq0.001$.

6.2.2.2. Evaluation of duration of stimulation period

The optimum time of stimulation was assessed by culturing explants for 1, 2 or 3 days and quantifying GAG release. With increasing exposure to stimulation, it was expected that there would be increasing GAG release, and that this would plateau as the cartilage matrix was degraded.

Porcine cartilage explants were harvested from the metacarpophalangeal joints of 3-9 month old pigs using a 4 mm biopsy punch (Section 2.3.1). Explants were rested for 2 days in cartilage growth medium, at one explant per well in a 12 well plate. Explants were then washed 3 times in serum-free cartilage growth medium and cultured in triplicate in 500 µL of serum-free cartilage growth medium for 24, 48 or 72 h, either with or without IL-1 stimulation (10 ng/mL). Conditioned media were harvested and analysed for release of GAG by DMMB assay and the AGEG neo-epitope fragment of aggrecan by immunoblotting.

From Figure 63, it can be seen that the AGEG neo-epitope GAG fragment was detectable on all days investigated. In the absence of IL-1 stimulation, the intensity of the anti-AGEG neo-epitope in culture medium increased from a pixel volume of 4147 on day 1, to 43895 on day 4, indicating that some non-stimulated degradation of aggrecan occurs in this assay system. However, when explants were exposed to IL-1, levels of anti-AGEG neo-epitope detected in the medium increased from a pixel volume of 311237 on day 1, to 73364 on

day 4. The optimum duration of stimulation was taken as that giving the maximum difference in pixel volume between unstimulated and stimulated explants. Figure 63 shows that 1 day of stimulation gave a 7.5-fold increase in pixel volume, but the band intensity in the unstimulated sample was so low that band quantification may have proved inconsistent. After 2 days of culture, a clear and quantifiable increase in pixel volume was evident, so 2 days was chosen as the optimal stimulation period for future experiments.

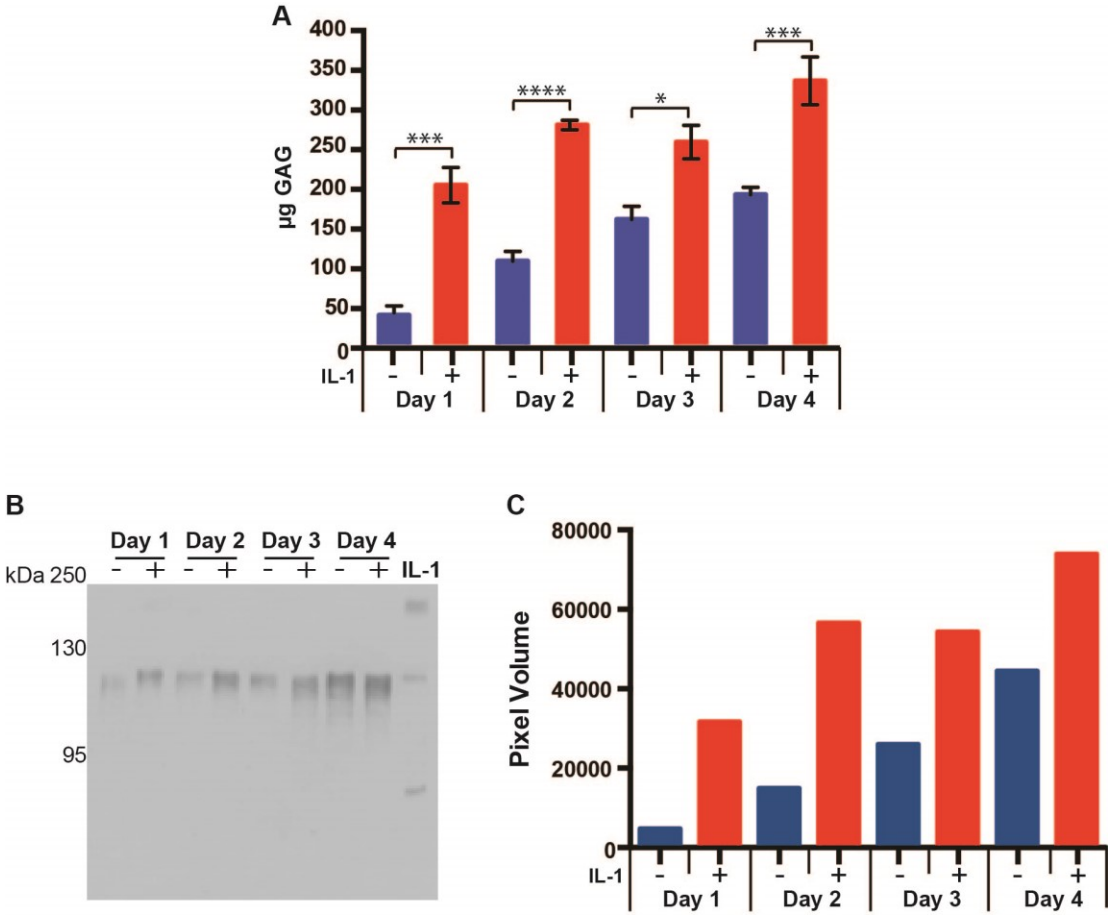


Figure 63: Time course of AGEG neo-epitope release from IL-1-stimulated porcine cartilage explants.

Porcine cartilage explants were harvested using a 4 mm biopsy punch and rested for 2 days in a 12-well plate in 500 µL of cartilage growth medium. Explants were then washed into serum-free cartilage growth medium and treated in triplicate with or without IL-1 (10 ng/mL IL-1) for 24, 48 or 72 h. (**A**) Conditioned media were harvested and analysed for GAG content using the DMMB assay, data represents mean ± SEM. (**B**) and (**C**) and deglycosylated in 2x GAG buffer (200 mM, sodium acetate, 100 mM

Tris-HCl pH 8.0, 100 mM EDTA) with 0.05 U each of chondroitinase ABC and keratanase (overnight, 37 ^{o}C) (**A**) Samples (10 µL) were separated on a 6 % Tris-glycine gel and analysed by immunoblotting with an anti-AGEG primary antibody (1:1000 dilution of anti-serum) and an anti-rabbit IgG AP-conjugated antibody (1:5000). Bands were visualized using Western blue stabilised substrate for AP and the reaction stopped using AP stop (20 mM Tris HCl pH7.5, 10 mM EDTA). **(C)** Pixel volume of (**B**) was quantified using Phoretix ID Gel Analysis software. Statistical differences were determined by a Two-Way Anova followed by Tukey's *post-hoc* test where * $P \leq 0.05$ *** $P \leq 0.001$ and **** $P \leq 0.0001$.

6.2.2.3. Effect of Wild-type and mutant TIMP-3 on chondrocyte viability in IL-1 stimulated porcine cartilage explants

TIMP-3 has been shown to induce apoptosis in a variety of cell types. For example, conditioned media from a TIMP-3-expressing colon carcinoma cell line has been shown to activate cell death in fibroblasts (Smith et al., 1997), infection of melanoma cells with TIMP-3-expressing adenoviruses induced apoptosis in melanoma cells (Ahonen et al., 1998), and exogenously added TIMP-3 (50 nM) induced apoptosis in a melanoma cell line (Ahonen et al., 2003). This necessitated assessment of the viability of chondrocytes in porcine cartilage explants treated with Wild-type TIMP-3 and TIMP-3 mutants K26A/K45A and K45A/K110A.

Viable cell number was assessed using the 3-(4,5-dimethylthiazol-2-yl)-5-(3-carboxymethoxyphenyl)-2-(4-sulfophenyl)-2H-tetrazolium (MTS) assay, in which a tetrazolium active compound is reduced to a coloured formazan product that is soluble in cell culture medium. The production of this formazan product is directly proportional to the number of live cells in the culture, with absorbance a 490 nm correlating positively with cell number.

Porcine cartilage explants were harvested from the metacarpophalangeal joints of 3-9 month old pigs using a 4 mm biopsy punch (Section 2.3.1). Explants were rested for 2 days in cartilage growth medium at one explant per well in a 48 well plate. Explants were then washed 3 times in serum-free cartilage growth medium, and incubated in triplicate in 250 µL with or without Wild-type TIMP-3, TIMP-3 K26A/K45A or TIMP-3 K42A/K10A (50 or 100 nM) or sodium nitroprusside (SNP, 10 mM) in serm-free cartilage growth medium for 48 h, either with or without IL-1 stimulation (10 ng/mL). After 48 h incubation, culture media were removed and fresh DMEM (200 µL, supplemented with 0.1 % v/v FCS) and MTS reagent (40 µL) were added. Cell number was evaluated by quantifying the coloured formazan product after incubation for 35 mins (37 ^{o}C, 5 % CO_2) by measuring the absorbance at 490 nm.

Figure 64 shows a comparison of chondrocyte number after treatment with or without Wild-type TIMP-3, or TIMP-3 mutants K26A/K45A and K42A/K110A for 48 h, either with or without IL-1 stimulation (10 ng/mL). SNP induces apoptotic cell death by production of hydrogen peroxide (Yamada et al., 1996) and was used as a control for cell death, while cells treated with neither TIMP-3 nor SNP served as untreated controls.

Chondrocytes treated with 50 or 100 nM Wild-type or mutant TIMP-3 for 48 h in the presence or absence of IL-1 showed no decrease in absorbance at 490 nm relative to untreated chondrocytes. This indicates that, at concentrations up to 100 nM, Wild-type and mutant TIMP-3 caused no reduction in cell metabolic activity. Therefore, it was unlikely that TIMP-3 or the mutants induced cell death at the concentrations used in the chondroprotection assays.

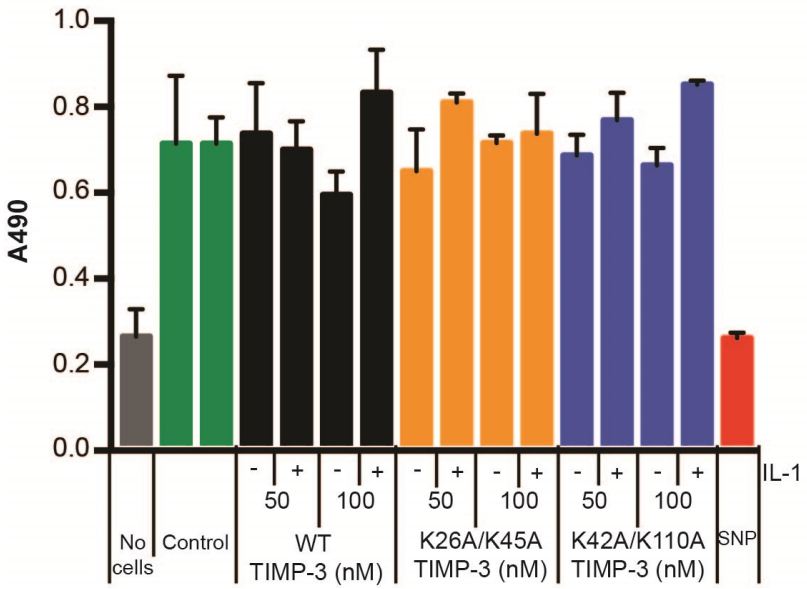


Figure 64: MTS assay of porcine cartilage explants treated with Wild-type and mutant TIMP-3.

Porcine cartilage explants were harvested from the metacarpophalangeal joints of 3-9 month old pigs were rested for 2 days in cartilage growth medium at one explant per well in a 48 well plate. Explants were then washed 3 times in serum-free cartilage growth medium and incubated in triplicate in 250 µL with or without Wild-type TIMP-3, TIMP-3 K26A/K45A or TIMP-3 K42A/K10A (50 or 100 nM) or sodium nitroprusside (SNP, 10 mM) in serum-free cartilage growth medium for 48 h, either with or without IL-1 stimulation (10 ng/mL) After 48 h, culture media were removed and fresh DMEM (200 µL, supplemented with 0.1 % v/v FCS) and MTS reagent (40 µL) were added. Cell number was evaluated by quantifying the coloured formazan product in triplicate after incubation for 35 mins (37 ^{o}C, 5 % CO_2) by measuring absorbance at 490 nm. Data represents mean ± SD.

6.2.2.4. Inhibition of porcine articular cartilage explant degradation by N-TIMP-3

The inhibitory effect of N-TIMP-3 on IL-1-stimulated GAG release from cartilage explants has been previously documented by our group, with a minimal concentration of 100 nM required to inhibit cartilage degradation (Gendron et al., 2003; Lim et al., 2010). We set about quantifying N-TIMP-3 inhibition of cartilage degradation in porcine articular cartilage explants in order to reproduce the published data, and thereby validate our experimental conditions and technique for analysis of the activity of Wild-type TIMP-3 and the K26A/K4A and K42A/K110A mutants.

Porcine cartilage explants were harvested from the metacarpophalangeal joints of 3-9 month old pigs using a 4 mm biopsy punch (Section 2.3.1) and rested for 2 days in 500 µL of cartilage growth medium, with one explant per well in a 48 well plate. They were then washed 3 times in serum-free cartilage growth medium, and stimulated in triplicate in 250 µL of serum-free cartilage growth medium for 2 days with IL-1 (10 ng/ml) and/or N-TIMP-3 (0, 10 or 100 nM). The volume of medium was reduced to 250 µL and the experiment conducted in 48-well plates to minimize the volume of TIMP-3 required for analysis. Conditioned media were harvested and GAG release quantified in triplicate using the DMMB assay (Section 2.3.1.1)(Farndale et al., 1982).

Addition of IL-1 stimulated a 5-fold increase in GAG release, as measured by the DMMB assay (Figure 65). This GAG release was inhibited fully by 100 nM N-TIMP-3, and partially by 10 nM N-TIMP-3. This is in line with previous reports by Gendron et al. (2003) and Lim et al. (2010). The optimised

experimental conditions were thus suitable for quantifying inhibition of GAG release by full-length Wild-type TIMP-3 and the TIMP-3 mutants.

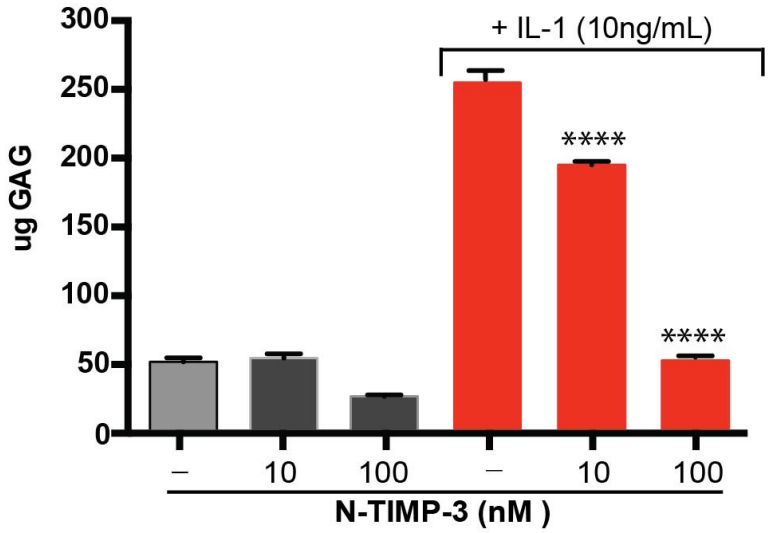


Figure 65: N-TIMP-3 inhibits IL-1-stimulated GAG release from porcine articular cartilage explants.

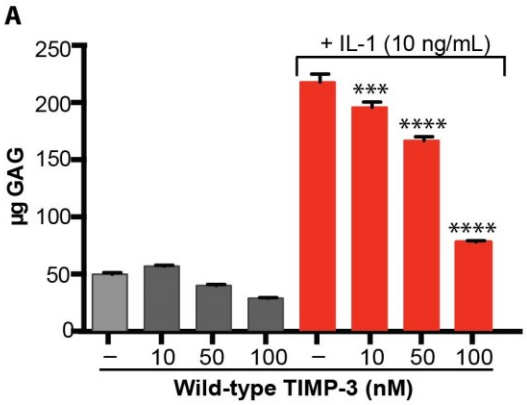
Porcine cartilage explants were harvested using a 4 mm biopsy punch and rested for 2 days in a 12-well plate in 500 µL of cartilage growth medium. Explants were then washed into serum-free cartilage growth medium and treated in triplicate with or without IL-1 (10 ng/mL IL-1) and/or N-TIMP-3 (0, 10 or 100 nM) for 48 h. Conditioned media were harvested and analysed for GAG content in triplicate using the DMMB assay *(n=1).* Statistical differences were determined by a One-Way Anova followed by Dunnett's *post-hoc* test where **** $P \leq 0.0001$.

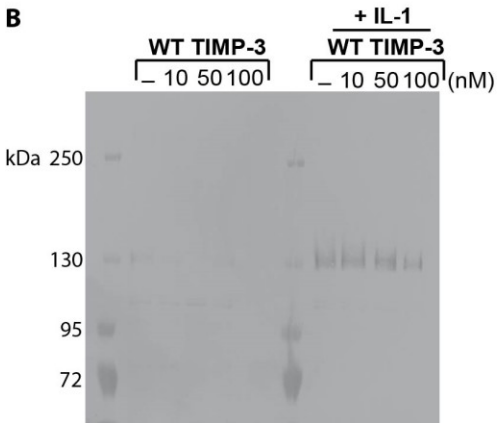
6.2.2.5. Inhibition of porcine articular cartilage explant degradation by full-length Wild-type TIMP-3

Inhibition of IL-1-stimulated GAG release from bovine and porcine cartilage by the N-terminal inhibitory domain of TIMP-3 has been previously reported (Gendron et al., 2003; Lim et al., 2010) and confirmed in Section 6.2.2.4. However, inhibition of IL-1-stimulated GAG release from cartilage explants by full length Wild-type TIMP-3 has not previously been reported. We

set about quantifying the chondroprotective efficacy of full-length Wild-type TIMP-3 using the newly optimised conditions.

Porcine cartilage explants were harvested from the metacarpophalangeal joints of 3-9 month old pigs using a 4 mm biopsy punch (Section 2.3.1) and rested for 2 days in 500 µL of cartilage growth medium, with one explant per well in a 48 well plate. They were then washed 3 times in serum-free cartilage growth medium, and stimulated for 2 days in 250 µL of serum-free cartilage growth medium containing IL-1 (10 ng/ml) and/or full-length Wild-type TIMP-3 (0, 10, 50 or 100 nM). Conditioned media were harvested and GAG release quantified in triplicate using the DMMB assay (Section 2.3.1.1)(Farndale et al., 1982). Samples were analysed also for release of the AGEG neo-epitope fragment of aggrecan by immunoblotting (Section 2.3.2).





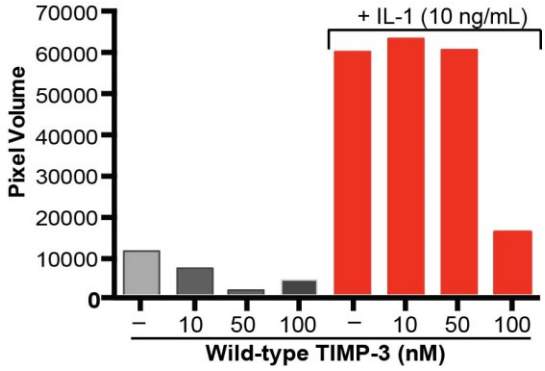


Figure 66 shows that 100 nM Wild-type TIMP-3 inhibits IL-1 stimulated GAG release from cartilage explants. This is in line with the concentration of N-TIMP-3 previously found to inhibit GAG release (Section 6.2.2.4, Gendron et al., 2003; Lim et al., 2010). By DMMB assay, partial inhibition was observed with 50 nM TIMP-3, and minimal inhibition with 10 nM TIMP-3. By neo-epitope immunoblotting, no inhibition was seen at either 50 or 10 nM. This is most likely due to the fact that the DMMB assay measures all GAG fragments released into the conditioned medium, while the anti-AGEG antibody only recognizes those fragments containing an N-terminal AGEG sequence. Additionally, the two analysis methods are likely to have different linear ranges.

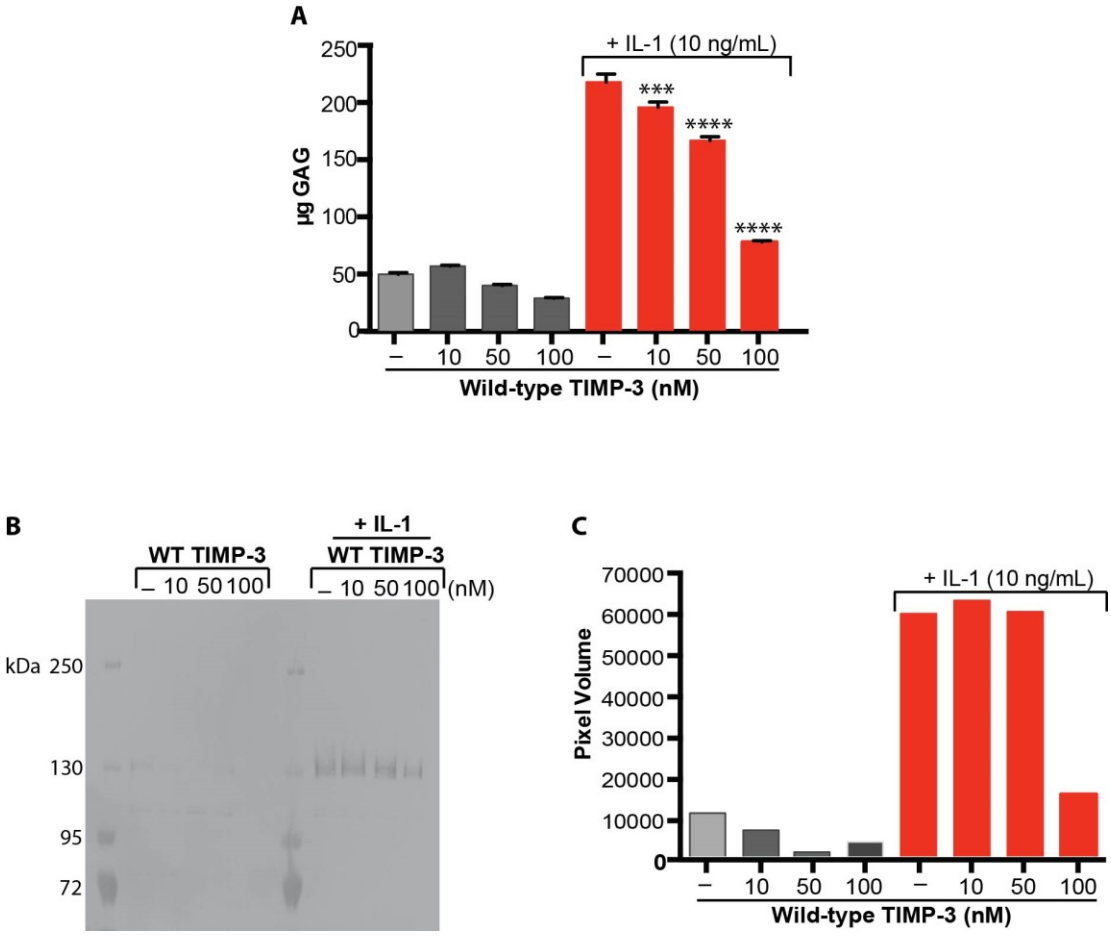


Figure 66: 100 nM Wild-type TIMP-3 inhibits GAG release from cartilage.

Porcine cartilage explants were harvested using a 4 mm biopsy punch and rested for 2 days in a 12-well plate in 500 µL of cartilage growth medium. Explants were washed into serum-free cartilage growth medium and treated in triplicate with or without IL-1 (10 ng/mL IL-1) and Wild-type TIMP-3 (1, 10, 50 and 100 nM) for 48 h. (**A**) Conditioned media were analysed in triplicate for GAG content using the DMMB assay. Media (2.5 µL) were mixed with DMMB dye (200 µL) in a 96-well plate and absorbance at 525 nm determined, (n=1). (**B**). Conditioned media were deglycosylated in 2x GAG buffer (200 mM, sodium acetate, 100 mM Tris-HCl pH 8.0, 100 mM EDTA) with 0.05 U each of chondroitinase ABC and keratanase (overnight, 37 ^{o}C). Samples (10 µL) were separated on a 6 % Tris-glycine gel and analysed by immunoblotting with an anti-AGEG primary antibody (1:1000 dilution of anti-serum) and an anti-rabbit IgG AP-conjugated antibody (1:5000). Bands were visualised using Western blue stabilised substrate for AP and the reaction stopped using AP stop (20 mM Tris-HCl pH 7.5, 10 mM EDTA). **(C)** Pixel volume of (**B**) was quantified using Phoretix ID Gel Analysis software. Statistical differences were determined by a One-Way Anova followed by Dunnett's *post-hoc* test where *** $P \leq 0.001$ and **** $P \leq 0.0001$

6.2.2.6. Inhibition of GAG release from cartilage explants by TIMP-3 mutant K26A/K45A

Having successfully shown that Wild-type TIMP-3 inhibits GAG release from porcine articular cartilage explants (Section 6.2.2.5), We set about quantifying inhibition of IL-1-stimulated GAG release from porcine articular cartilage by TIMP-3 K26A/K45 using the optimised conditions.

We have previously shown that this TIMP-3 mutant is resistant to endocytosis by the HTB94 cell line (Section 4.2.3.4) and (Section 6.2.1). It also has a comparable affinity for TIMP-3 target metalloproteinases (Sections 5.2.5) and retains ECM binding ability (Section 5.2.6). Therefore, it was expected that TIMP-3 K26A/K45 would inhibit ADAMTS-5 activity and so inhibit GAG release ex vivo.

Porcine cartilage explants were harvested from the metacarpophalangeal joints of 3-9 month old pigs using a 4 mm biopsy punch (Section 2.3.1) and rested for 2 days in 500 µL of cartilage growth medium, with one explant per well in a 48 well plate. They were then washed 3 times in serum-free cartilage growth medium and stimulated in triplicate in 250 µL of serum-free cartilage growth medium for 2 days with IL-1 (10 ng/ml) and/or full-length TIMP-3 K26A/K45 (0, 10, 50 or 100 nM). Conditioned media were harvested and GAG release quantified in triplicate using the DMMB assay (Section 2.3.1.1)(Farndale et al., 1982). Samples were also analysed for release of the AGEG neo-epitope fragment of aggrecan immunoblotting (Section 2.3.2).

The chondroprotective activity of TIMP-3 K26A/K45 was analysed in 7 independent experiments. Figure 67A shows results from a single representative experiment, with the error reflecting the variability of the DMMB assay. Each data point on Figure 67B indicates GAG release per condition in each of the 7 replicate experiments. This demonstrates the high reproducibility of the data. By both DMMB assay and AGEG neo-epitope immunoblotting, TIMP-3 K26A/K45A inhibited cartilage degradation (Figure 67). As with Wild-type TIMP-3, TIMP-3 K26A/K45A did not inhibit cartilage degradation at 10 nM. However, in contrast with Wild-type TIMP-3, TIMP-3 K26A/K45A showed increased protective activity at 50 nM. Looking at the average of the 7 replicate experiments, it is evident that cartilage degradation was inhibited by ~50% by 50 nM TIMP-3 K26A/K45A, which indicates that TIMP-3 K26A/K45A has an improved chondroprotectivity relative to Wild-type TIMP-3.

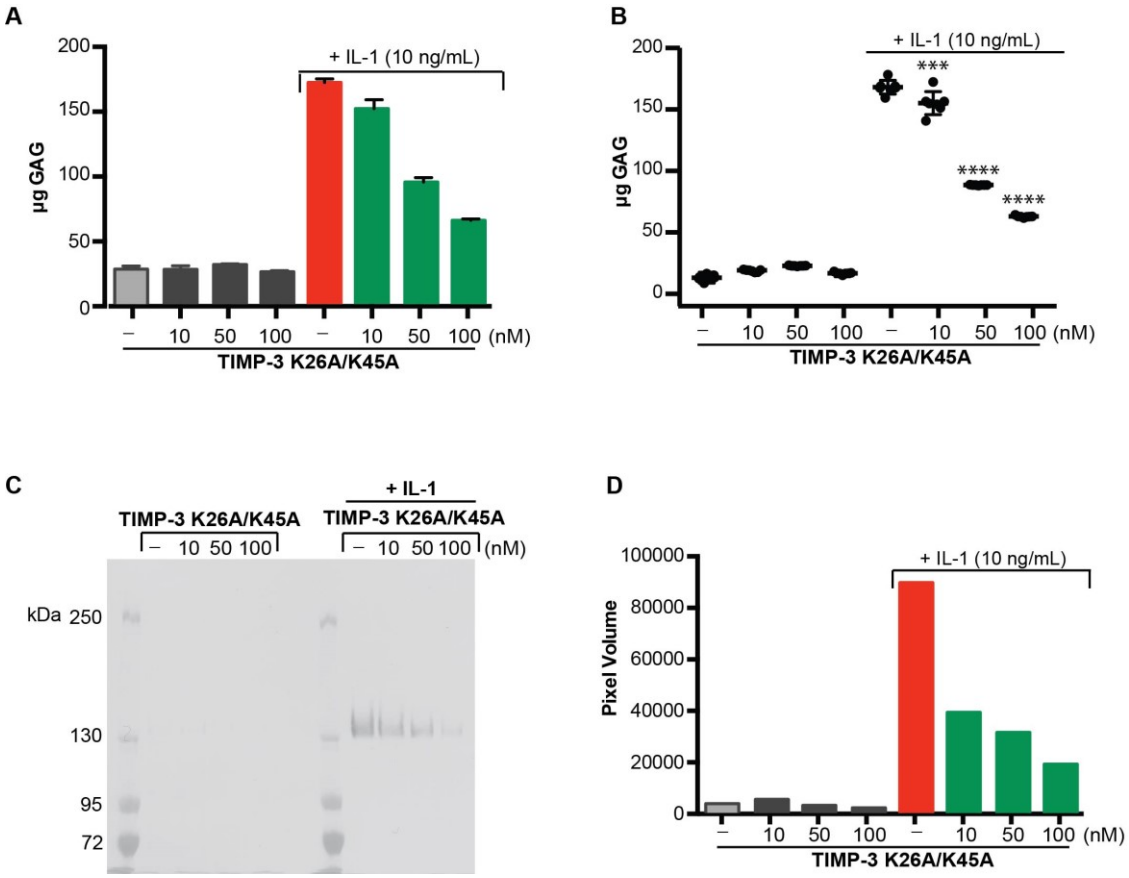


Figure 67: Inhibition of GAG release from porcine cartilage explants by TIMP-3 K26A/K45A.

Porcine cartilage explants were harvested using a 4 mm biopsy punch and rested for 2 days in a 48-well plate in 500 µL of cartilage growth medium with 10% FCS. Explants were then washed into 250 µL of serum-free cartilage growth medium and treated with or without IL-1 (10 ng/mL) and/or TIMP-3 K26A/K45A (10, 50 or 100 nM) for 48 h. (**A, B**) Conditioned media were analysed for GAG content using the DMMB assay. Media (2.5 µL) were mixed with DMMB dye (200 µL) in a 96-well plate and absorbance at 525 nm determined. (**A**) shows a single representative experiment, and (**B**) shows 7 replicate experiments, data shows mean ± SEM . (**C**) Conditioned media from (**A**) were deglycosylated in 2x GAG buffer (200 mM, sodium acetate, 100 mM Tris-HCl pH 8.0, 100 mM EDTA) with 0.05 U each of chondroitinase ABC and keratanase (overnight, 37 ^{o}C) Samples (10 µL) were separated on a 6 % Tris-glycine gel and analysed by immunoblotting with an anti-AGEG primary antibody (1:1000 dilution of anti-serum) and an anti-rabbit IgG AP-conjugated antibody (1:5000). Bands were visualised using Western blue stabilised substrate for AP and the reaction stopped using AP stop (20 mM Tris-HCl pH 7.5, 10 mM EDTA). **(D)** Pixel volume in (**C**) was quantified using Phoretix ID Gel Analysis software. Statistical differences were determined by a One-

Way Anova followed by Dunnet's *post-hoc* test where * $P \leq 0.05$ *** $P \leq 0.001$ and **** $P \leq 0.0001$.

6.2.2.7. Inhibition of GAG release from cartilage explants by TIMP-3 mutant K42A/K110A

TIMP-3 K26A/K45A was found to have increased inhibition of GAG release relative to that of Wild-type TIMP-3 (Section 6.2.2.6). Here, we quantify the inhibition of IL-1-stimulated GAG release from porcine explants by TIMP-3 K42A/K110A by DMMB assay and immunoblotting.

We have previously shown that TIMP-3 K42A/K110A is resistant to endocytosis by the HTB94 chondrosarcoma cell line (Section 4.2.4) and primary porcine chondrocytes (Section 6.2.1). It also has a comparable binding affinity for Wild-type TIMP-3 target metalloproteinases (Section 5.2.5), but has reduced ECM binding affinity (Section 5.2.6). Therefore, we expected that TIMP-3 K42A/K110A would inhibit ADAMTS-5 activity and so inhibit GAG release ex-vivo.

Porcine cartilage explants were harvested from the metacarpophalangeal joints of 3-9 month old pigs using a 4 mm biopsy punch (Section2.3.1) and rested for 2 days in 500 µL of cartilage growth medium containing 10 % FCS, with one explant per well in a 48 well plate. They were then washed 3 times in serum-free cartilage growth medium and stimulated in 250 µL of serum-free DMEM cartilage growth medium for 2 days with IL-1 (10 ng/ml) and/or full-length TIMP-3 K42A/K110A (0, 10, 50 or 100 nM). Conditioned media were harvested and GAG release quantified in triplicate using the DMMB assay (Section 2.3.1.1)(Farndale et al., 1982). Samples were analysed also for release of the AGEG neo-epitope fragment of aggrecan by immunoblotting (Section 2.3.2).

The chondroprotective activity of TIMP-3 K42A/K110A was analysed in 3 independent experiments. Figure 68A shows results from a single representative experiment, with the error reflecting the error of the DMMB assay. Each point on Figure 68B indicates GAG released per condition in each of the 3 replicate experiments, and thus demonstrates the high reproducibility of the experiments.

By DMMB assay, IL-1-stimulated GAG release was inhibited by 50 nM TIMP-3 K42A/K110A. Both 50 nM and 100 nM TIMP-3 K42A/K110A inhibiting DMMB release by 50 % (Figure 68B). Similar results were obtained by anti-AGEG neo-epitope immunoblotting, with inhibition observed with 50 nM TIMP-3 K42A/K110A (Figure 68C and D). This indicates that TIMP-3 K42A/K110 has increased chondroprotectivity relative to Wild-type TIMP-3.

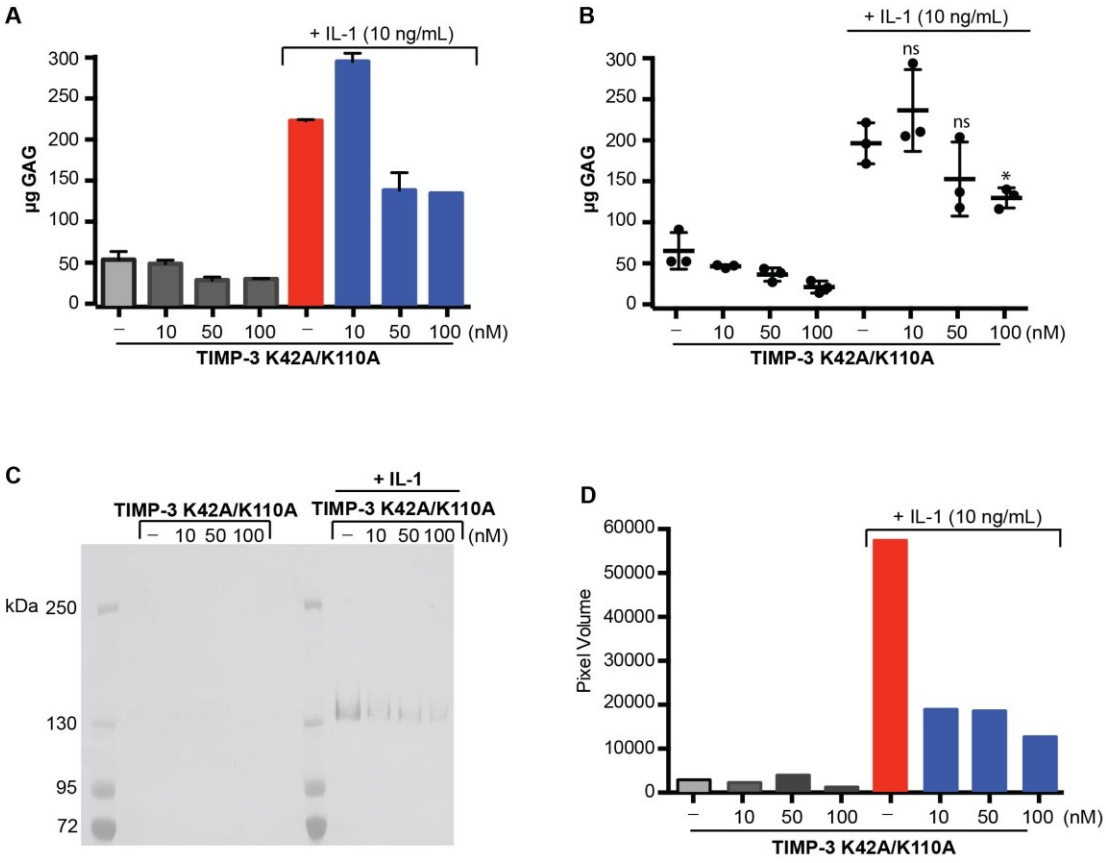


Figure 68: Inhibition of GAG release from porcine cartilage explants by TIMP-3 K42A/K110A quantified by DMMB assay.

Porcine cartilage explants were harvested using a 4 mm biopsy punch and rested for 2 days in a 48-well plate in 500 µL of cartilage growth medium with 10% FCS. Explants were then washed into 250 µL of serum-free cartilage growth medium and treated with or without IL-1 (10 ng/mL) and/or TIMP-3 K42A/K110A (10, 50 or 100 nM) for 48 h. (**A, B**) Conditioned media were analysed for GAG content using the DMMB assay. Media (2.5 µL) were mixed with DMMB dye (200 µL) in a 96-well plate and absorbance at 525 nm determined. (**A**) shows a single representative experiment, and (**B**) shows 3 replicate experiments, data shows mean ± SEM. (**C**) Conditioned media from (**A**) were deglycosylated in 2x GAG buffer (200 mM, sodium acetate, 100 mM Tris-HCl pH 8.0, 100 mM EDTA) with 0.05 U each of chondroitinase ABC and keratanase (overnight, 37 °C). Samples (10 µL) were separated on a 6 % Tris-glycine gel and analysed by immunoblotting with an anti-AGEG primary antibody (1:1000 dilution of anti-serum) and an anti-rabbit IgG AP-conjugated antibody (1:5000). Bands were visualised using Western blue stabilised substrate for AP and the reaction stopped using AP stop (20 mM Tris-HCl pH 7.5, 10 mM EDTA). **(D)** Pixel volume in (**C**) was quantified using Phoretix ID Gel Analysis software. Statistical differences were

determined by a One-Way Anova followed by Dunnet's multiple *post-hoc* test where ns: no statistical difference, * $P \leq 0.05$.

6.2.2.8. Effect of pre-incubation on chondroprotective activity of TIMP-3 K26A/K45A and TIMP-3 K42A/K110A

TIMP-3 K26A/K45A and TIMP-3 K42A/K110A have been shown to exhibit reduced endocytosis by LRP-1 in chondrocytes (Section 6.2.1) and improved inhibition of aggrecan degradation in porcine cartilage explants (Section 6.2.2.6 and Section 6.2.2.7). However, these experiments do not directly show that the observed inhibition of aggrecan degradation and the reduction in endocytosis by LRP-1 are causally linked. If the protective inhibitory activity were due to resistance to LRP-1-mediated endocytosis, then the TIMP-3 mutants should have an increased half-life in cartilage, and so remain in the cartilage for longer than Wild-type TIMP-3. An experiment was designed to test this hypothesis.

Porcine cartilage explants were harvested from the metacarpophalangeal joints of 3-9 month old pigs using a 4 mm biopsy punch (Section 2.3.1) and rested for 2 days in 500 µL of cartilage growth medium containing 10 % FCS, with one explant per well in a 48 well plate. Explants were washed 3 times in serum-free cartilage growth medium and pre-incubated with Wild-type TIMP-3, TIMP-3 K26A/K45A or TIMP-3 K42A/K110A (100 nM) for 0, 24, 48 or 72 h in 250 µL of serum-free DMEM cartilage growth medium, and then stimulated by addition of IL-1 (10 ng/ml) for 24 h. Conditioned media were harvested and GAG release quantified in triplicate using the DMMB assay (Section 2.3.1.1)(Farndale et al., 1982).

As expected, IL-1 stimulation produced an increase in GAG release from the explant to the medium. After pre-incubation on cartilage for 24 h, Wild-type TIMP-3 inhibited GAG release. This protection was progressively lost with

increasing pre-incubation such that after 3 days of pre-incubation, Wild-type TIMP-3 was unable to inhibit GAG release upon addition of IL-1. A similar pattern was observed for TIMP-3 K42A/K110A.

However, pre-incubation had a markedly reduced effect on TIMP-3 K26A/K45A. Even after 3 days of pre-incubation on cartilage, TIMP-3 K26A/K45A substantially inhibited GAG release upon addition of IL-1. This indicates that this mutant has greater chondroprotective activity than either Wild-type TIMP-3 or TIMP-3 K42A/K110A.

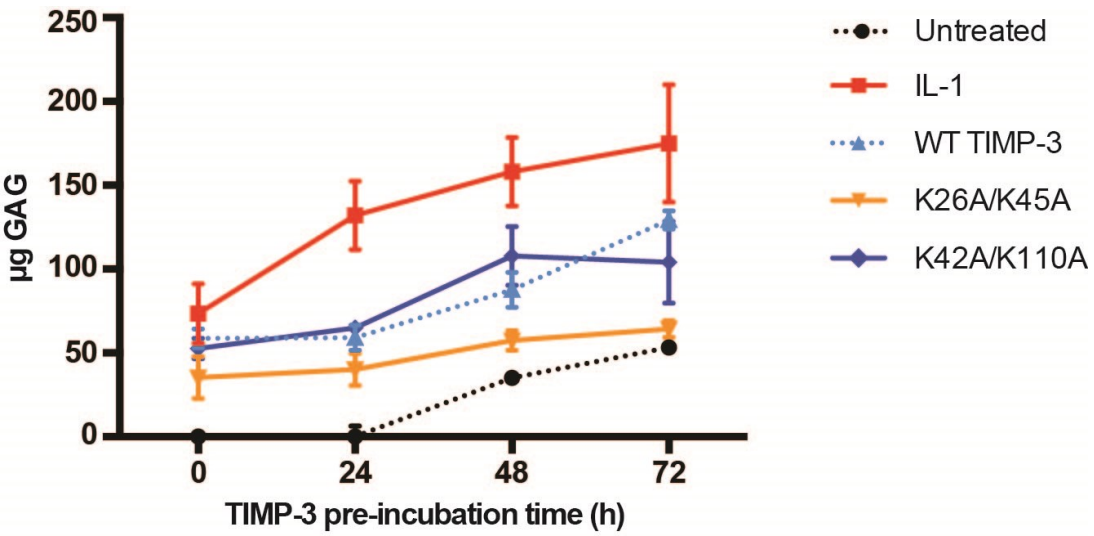


Figure 69: TIMP-3 K26A/K45A retains chondroprotective effect after pre-incubation on cartilage.

Porcine cartilage explants were harvested using a 4 mm biopsy punch and rested for 2 days in a 48-well plate in 500 µL of cartilage growth medium with 10% FCS. Explants were then washed into 250 µL serum-free cartilage growth medium and incubated with or without Wild-type TIMP-3, TIMP-3 K26A/K45A or TIMP-3 K42A/K110A (100 nM) for 0, 24, 48 or 72 h and then stimulated with IL-1 (10 ng/ml) for 24 h. Conditioned media were harvested 24 h after IL-1 stimulation and analysed for GAG content using the DMMB assay. Media (3 µL) were mixed with DMMB dye (200 µL) in a 96-well plate and absorbance at 525 nm determined. Preliminary data (n=1), showing mean ± SD.

6.2.2.9. Effect of TIMP-3 K26A/K45A on time course of GAG release

TIMP-3 K26A/K45A has been shown to have an improved ability to inhibit aggrecan degradation in porcine cartilage explants (Sections 6.2.2.6). These experiments show quantification of cumulative GAG release over the 48 hours following stimulation in an endpoint analysis. Here, I investigate the relative improvement in the inhibition of aggrecan degradation by TIMP-3 K26A/K45A compared with Wild-type TIMP-3 over time. We hypothesised that the improved inhibitory activity of TIMP-3 K26A/K45A was due to its resistance to endocytosis by LRP-1, and predicted that it should inhibit GAG release for a longer time than Wild-type TIMP-3. An experiment was designed to test this hypothesis.

Porcine cartilage explants were harvested from the metacarpophalangeal joints of 3-9 month old pigs using a 4 mm biopsy punch (Section 2.3.1) and rested for 2 days in in 500 µL of cartilage growth medium containing 10 % FCS, with one explant per well in a 48 well plate. They were then washed 3 times in serum-free cartilage growth medium and stimulated in 300 µL of serum-free cartilage growth medium for 4 days with IL-1 (10 ng/ml) and/or full-length Wild-type TIMP-3 or TIMP-3 K42A/K110A (50 nM). Conditioned media were harvested (6 µL) at the required time-points (0, 0.5, 1, 1.5, 2, 2.5, 3 and 4 days) and GAG release quantified using the DMMB assay (Section 2.3.1.1)(Farndale et al., 1982).

It has been shown that 100 nM Wild-type TIMP-3 is required to inhibit porcine explant GAG release during a 2-day stimulation with IL-1 (Section 6.2.2.5). However under the same conditions, 50 nM TIMP-3 K26A/K45A inhibited GAG release by ~50% (Section 6.2.2.6). Therefore, 50 nM Wild-type

TIMP-3 and TIMP-3 K26A/K45A were used to compare their relative inhibitory activity over time.

IL-1 stimulation increased GAG release across all time-points and Wild-type TIMP-3 treatment (50 nM) did not show inhibition of GAG release at any of the time-points investigated (Figure 70A). This was expected, seeing as 100 nM Wild-type TIMP-3 was required to inhibit IL-1 stimulated GAG release over 48 hours (Section 6.2.2.5).

TIMP-3 K26A/K45A completely inhibited stimulated GAG release 1 day after addition of IL-1, and a ~50 % reduction in GAG release was also observed 2 days after stimulation. Even after 4 days of stimulation, explants treated with TIMP-3 K26A/K45A showed a ~36% decrease in GAG release compared to Wild-type TIMP-3 treated explants at this time-point (Figure 70B). TIMP-3 K26A/K45A this showed increased protection over time compared to Wild-type TIMP-3.

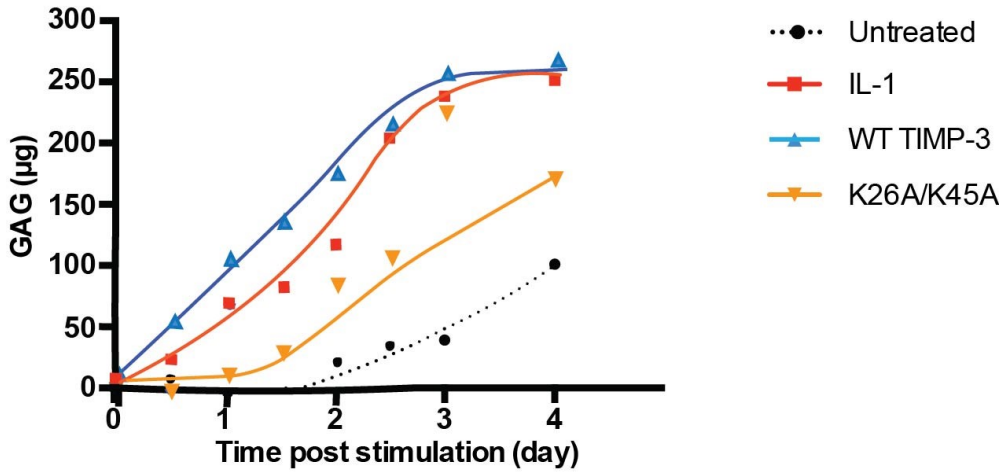


Figure 70: TIMP-3 K26A/K45A shows improved inhibition of GAG release over time.

Porcine cartilage explants were harvested using a 4 mm biopsy punch and rested for 2 days in a 48-well plate in 500 µL of cartilage growth medium with 10% FCS. Explants were then washed into 250 µL of serum-free cartilage growth medium and treated with or without IL-1 (10 ng/mL) and/or Wild-type TIMP-3 or TIMP-3 K26A/K45A (50 nM). Conditioned media were harvested at the indicated times. Conditioned media were analysed for GAG content using the DMMB assay. Media (2.5 µL) were mixed with DMMB dye (200 µL) in a 96-well plate and absorbance at 525 nm determined. GAG detected in conditioned media of explants treated with or without IL-1 (10 ng/mL) and/or Wild-type TIMP-3 (50 nM) or TIMP-3 K26A/K45A (50 nM) is shown. Preliminary data (n=1), showing mean ± SD.

6.3. Discussion

From a starting list of 22 potentially endocytosis-resistant TIMP-3 mutants, TIMP-3 K26A/K45A and TIMP-3 K42A/K110A were shortlisted as having shown delayed endocytosis in the HTB94 chondrosarcoma cell line. Both mutants also retained inhibitory activity against Wild-type TIMP-3 target metalloproteinases with comparable affinity (Section 5.2.5). In this Chapter, we determined that the delayed endocytosis observed in HTB94 cells (Section 5.2.3) also occurs in primary porcine chondrocytes (Section 6.2.1) and cartilage

explant cultures. We also determined that the TIMP-3 mutant endocytosis resistance correlates with increased chondroprotectivity relative to Wild-type TIMP-3.

ADAMTS degradation of cartilage causes the release of aggrecan breakdown products, GAG fragments, which are detectable by DMMB assay (Farndale et al., 1982) and neo-epitope immunoblotting. In the DMMB assay, sulfated GAG fragments form a complex with the DMMB dye causing a shift in the absorption spectrum that can be measured in 96-well plates at 525 nm (Section 2.3.1.1.) This method is quick and requires only a small sample volume (< 4 µL) to quantify the GAG fragments present in the sample tested. However, it has a narrow linear range and is not selective for ADAMTS cleavage, as the dye detects all GAG fragments including those generated by the activity of other metalloproteinases.

ADAMTS-4 and ADAMTS-5 cleave aggrecan at several sites, including at Glu^{373}–Ala^{374} and Glu^{1819}–Ala^{1820} generating the ARGSV neo-epitope and the AGEG neo-epitope, respectively. These neo-epitopes can be detected with the BC-3 anti-ARGSV antibody (Innes et al., 2005) and our in-house generated rabbit anti-AGEG antibody. Immunoblotting using these antibodies is time consuming, requires larger sample volumes (100 µL) and is expensive as it requires enzymatic deglycosylation prior to SDS-PAGE. Such immunoblotting does, however, directly show that ADAMTSs are involved the aggrecan degradation observed.

In designing the experiment to quantify GAG release in a physiologically representative manner, we reviewed the literature and found that articular cartilage explants are most commonly used (Gendron et al., 2003; Lim et al.,

2010; Sandy et al., 1991; Von den Hoff et al., 1993). However, I chose to assess both porcine chondrocyte monolayer cultures and porcine cartilage explants to optimise quantification of GAG release for comparing the relative chondroprotectivity of Wild-type TIMP-3 and the TIMP-3 mutants K26A/K45A and K42A/K110A, as both systems have inherent advantages and disadvantages. Porcine articular chondrocyte monolayer cultures have the potential for high reproducibility, as an accurate cell number can be used per condition. However, the chondrocytes are isolated by collagenase digestion of cartilage, and so have low levels of associated aggrecan and so are not necessarily physiologically representative.

Porcine cartilage explants on the other hand retain ECM and aggrecan, and are more physiologically representative of cartilage. However, harvesting explants of equal size using published methods (Gendron et al., 2003) proved challenging. This issue was overcome by the use of a biopsy punch, which removed size variability and increased overall experiment reproducibility. There was variability associated with explant depth, but this was minimal and decreased with improved technique.

In comparing the porcine chondrocyte monolayer and explant cultures, I found that porcine chondrocyte monolayers released too little GAG to be detected by either DMMB assay or anti-AGEG neo-epitope immunoblotting. This indicates that the isolated chondrocytes had not secreted sufficient ECM during the culture period for detection by DMMB assay or neo-epitope immunoblotting, and that this system was therefore not suitable for quantifying the inhibition of aggrecan degradation.

The explant cultures on the other hand, showed a strong increase in IL-1-stimulated GAG release, which was detectable by both DMMB assay and anti-AGEG neo-epitope immunoblotting. By DMMB assay, stimulated GAG release increased by 3-4 fold for retinoic acid and IL-1 stimulation (Figure 61). As good stimulation and good reproducibility were observed between sample repeats, this cartilage explant system was chosen for quantifying aggrecan degradation.

It has previously been shown that aggrecanase-associated GAG release can be stimulated ex vivo with IL-1 (Dingle et al., 1979) and other cytokines including TNFα (Arner et al., 1998; Fushimi et al., 2008) and IL-6 (Stanton et al., 2011a), and also by retinoic acid (Von den Hoff et al., 1993). Despite IL-1 being a most commonly used method for stimulation of GAG release, its precise mechanism of action has remains debatable. IL-1α increases ADAMTS-5 mRNA expression in human chondrocytes (Young et al., 2005) and immortalized human chondrocytes (Koshy et al., 2002), but this is not observed in all systems (Fosang et al., 2008). It has been technically difficult to show that IL-1α increases ADAMTS protein expression or activity. A recent study by Ismail et al. successfully showed that ADAMTS-5 is the major aggrecanase in human chondrocytes at the activity level, and that IL-1 induces its activity via the JNK-2 signaling pathway (Ismail et al., 2015).

It was imperative to demonstrate that any observed increase or decrease GAG release was related to experimental conditions and not to TIMP-3 induced cell death. Therefore a cell viability assay was conducted on porcine cartilage explants under experimental conditions. From MTS assay results (Figure 64), it is clear that treatment of cartilage explants with 100 nM Wild-type or mutant

TIMP-3, either with or without co-treatment with IL-1, does not induce chondrocyte cell death within the 48 h time frame assessed.

With the aim of testing our experimental conditions. I sought to reproduce published data, and determine the minimal concentration of N-TIMP-3 required to inhibit IL-1-stimulated GAG release. The DMMB assay indicated that 100 nM N-TIMP-3 was required to fully inhibit GAG release (Figure 65). This was in keeping with published data (Gendron et al., 2003), demonstrating that the reduced scale optimized conditions were suitable for quantifying the chondroprotectivity of the full length Wild-type TIMP-3 and TIMP-3 mutant K26A/K45A and TIMP-3 mutant K42A/K110A.

As N-TIMP-3 is the inhibitory domain of TIMP-3, it was expected that full-length Wild-type TIMP-3 would also inhibit IL-1-stimulated GAG release at the same concentration, although this has not been previously reported. Both the DMMB assay and anti-AGEG neo-epitope immunoblotting showed that 100 nM

Wild-type TIMP-3 fully inhibited GAG release (

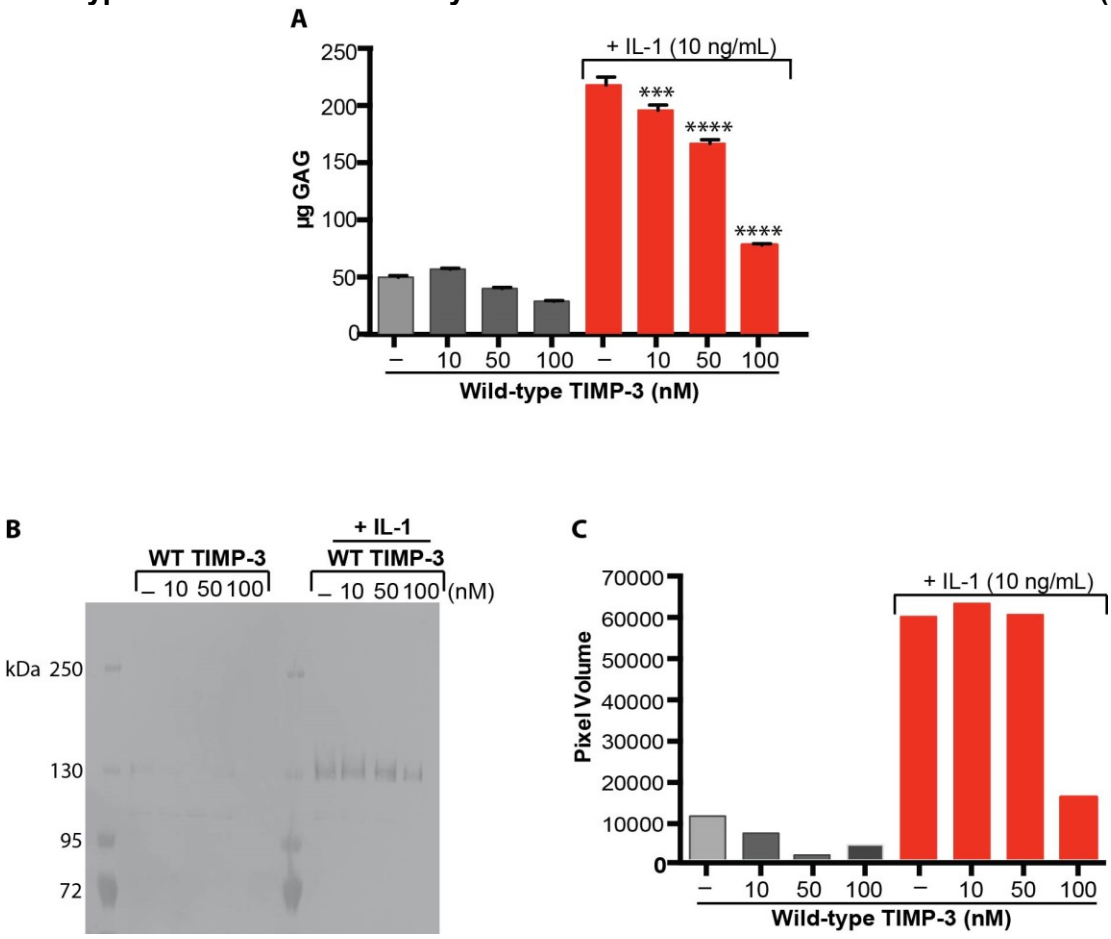


Figure 66). The DMMB assay showed a dose-dependent decrease in inhibition, with 50 nM TIMP-3 giving a ~25 % reduction in GAG release, and 10 nM TIMP-3

giving a ~10% reduction in GAG release (

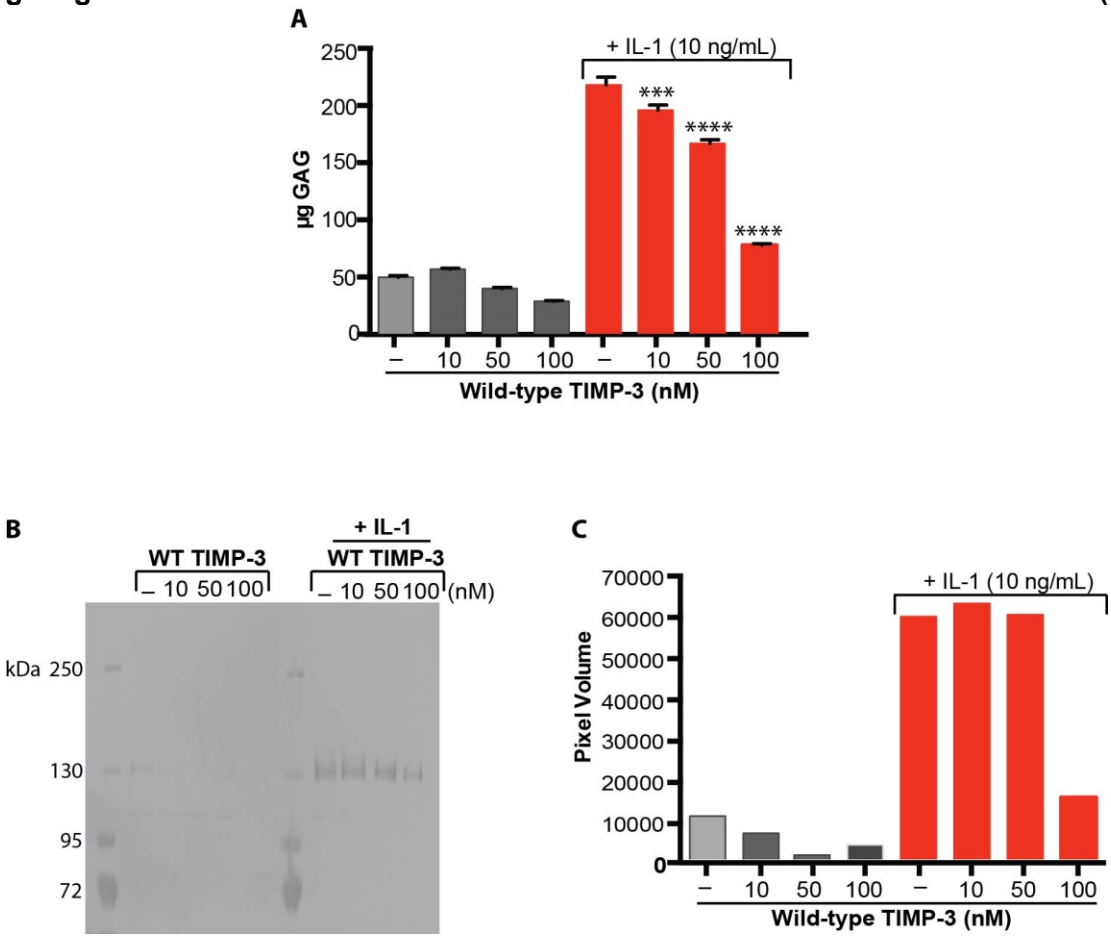


Figure 66A). By anti-AGEG neo-epitope immunoblotting, only 100nM TIMP-3 inhibited neo-epitope release fully, while lower concentrations had no effect.

The chondroprotective activity of TIMP-3 K26A/K45A was next assessed. By DMMB assay, TIMP-3 K26A/K45A inhibited GAG release completely at 100 nM, by ~45 % at 50 nM and by ~12 % at 10 nM (Figure 67 A and B). Interestingly, anti-AGEG neo-epitope immunoblotting showed stronger inhibition at each concentration (Figure 67C and D), with 100 nM TIMP-3 K26A/K45A inhibiting AGEG release by 58 %. This indicates that TIMP-3 K26A/K45A has increased chondroprotective activity relative to Wild-type TIMP-3.

TIMP-3 K42A/K110 also displayed increased chondroprotection relative to Wild-type TIMP-3. At 100 nM, TIMP-3 K42A/K110 completely inhibited GAG release (Figure 68A and B). At 50 nM, TIMP-3 K42A/K110 inhibited GAG release by ~50% by DMMB assay and ~43 % by anti-AGEG neo-epitope immunobloting. No protection was seen at 10 nM by either DMMB assay or anti-AGEG neo-epitope immunoblotting.

If either TIMP-3 mutant exhibited an increased half-life in cartilage relative to Wild-type TIMP-3, then that mutant would remain in the cartilage for longer, and it would display an increased chondroprotective activity. In Section 6.2.2.8, explants were incubated with Wild-type TIMP-3, TIMP-3 K26A/K45A or TIMP-3 K42A/K110A (100 nM) for 0, 24, 48 or 72 h before stimulation with IL-1 for 24 h. After 0 or 1 day of pre-incubation, TIMP-3 blocked GAG release completely. However, after more than 1 day of pre-incubation, the protective activity of TIMP-3 was lost, presumably due to its endocytosis by LRP-1. TIMP-3 K42A/K110A showed the same pattern of inhibition for each pre-incubation period. TIMP-3 K42A/K110A was thus no more effective in the cartilage explant system than Wild-type TIMP-3. However, TIMP-3 K26A/K45A strongly inhibited GAG release even after 3 days of pre-incubation on cartilage. Only minimal increase in GAG release was observed comparing 0 days of pre-incubation to 3 days pre-incubation (Figure 69). This indicates that TIMP-3 K26A/K45A has a much increased half-life in cartilage, enabling it to inhibit aggrecan degradation for longer than Wild-type TIMP-3.

I further analysed TIMP-3 K26A/K45A, by stimulating explants with IL-1 for 4 days in the presence of 50 nM Wild-type TIMP-3 or TIMP-3 K26A/K45A. At this concentration, Wild-type TIMP-3 had previously been found to be

ineffective **(**

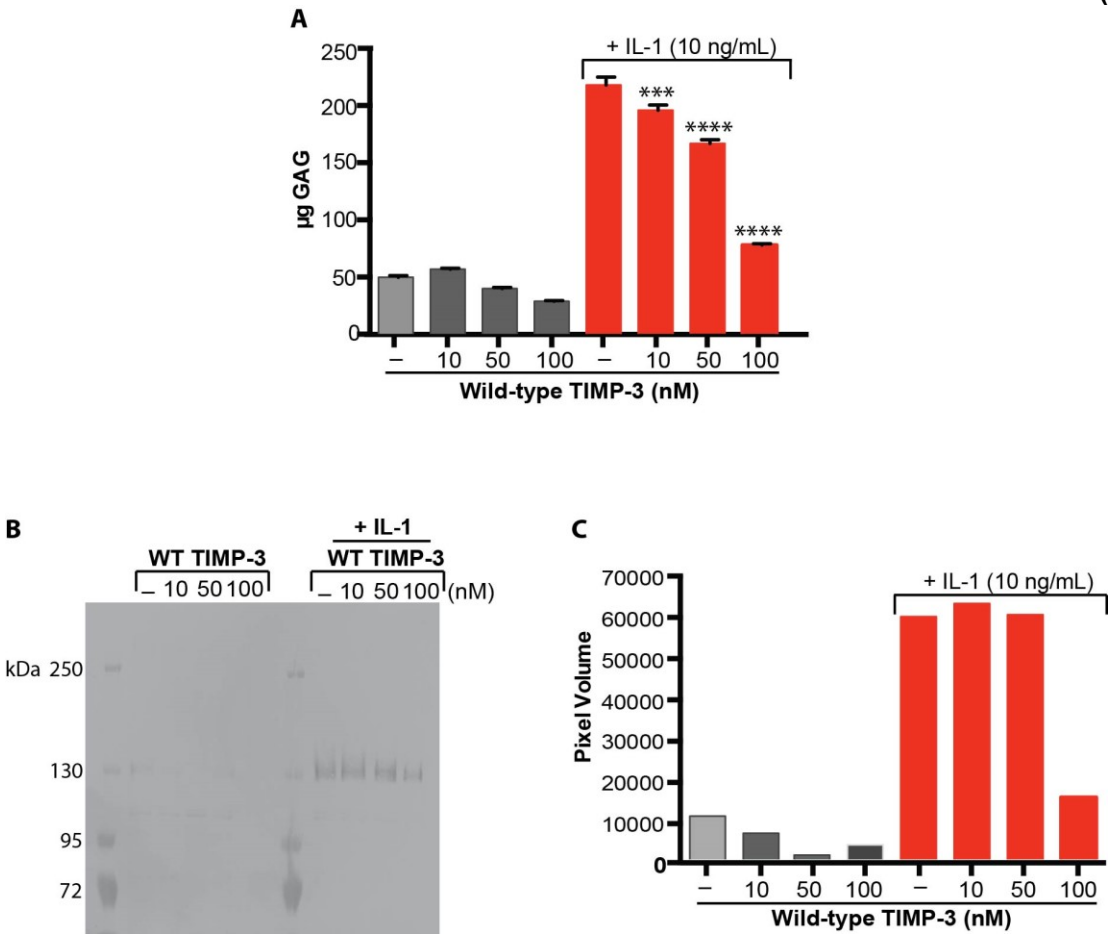


Figure 66), while TIMP-3 K26A/K45A showed a protective effect (Figure 67). Longer time periods were not analysed since it was observed that by day 5, that the growth medium had become acidic due to the accumulation of metabolic by-products. At 50 nM, Wild-type TIMP-3 failed to inhibit GAG release at any time-

point, in keeping with previous observations (

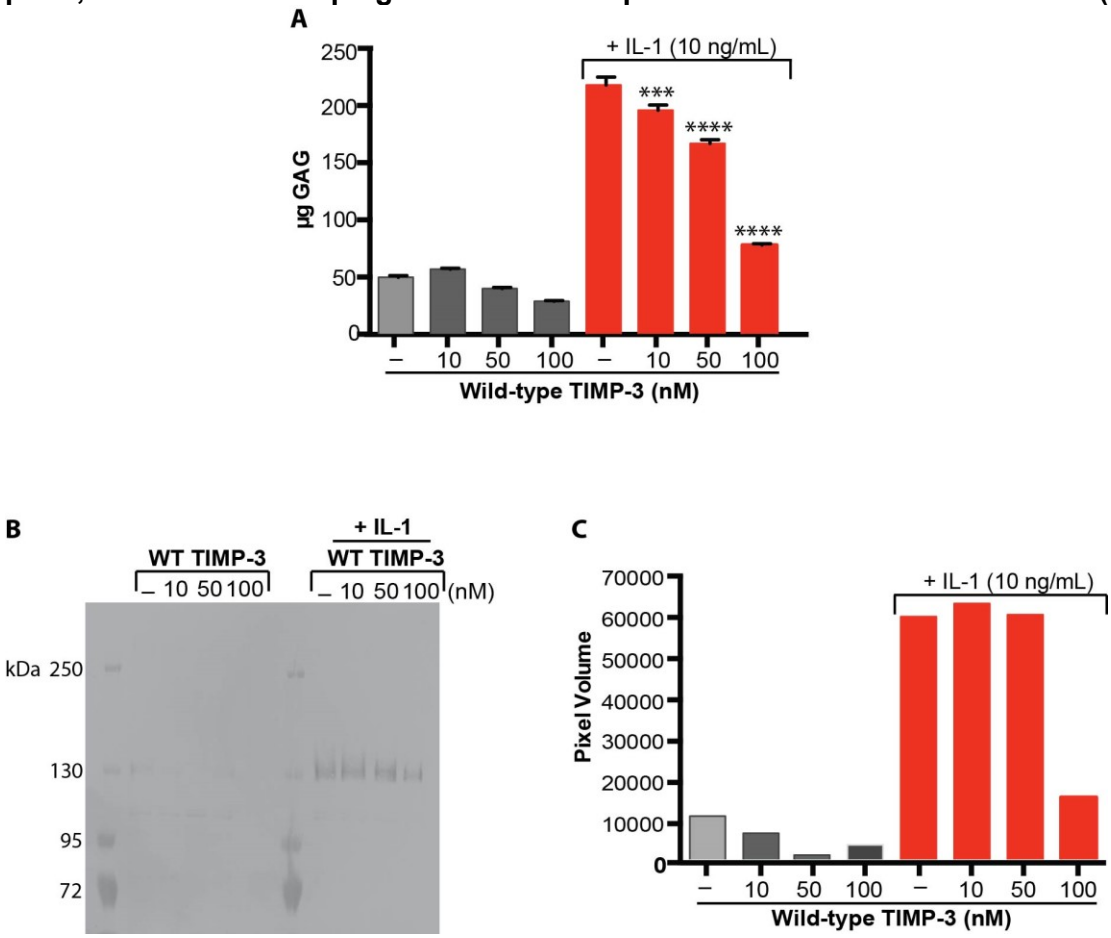


Figure 66), which demonstrated that 100 nM Wild-type TIMP-3 is required to inhibit GAG release. In contrast, 50 nM TIMP-3 K26A/K45A completely inhibited GAG release 1 day after IL-1 stimulation, and still inhibited GAG release by 36 % after 4 days of stimulation. This further supports the conclusion that TIMP-3 K26A/K45A has an increased half-life in cartilage, enabling it to display increased inhibition of GAG release compared to Wild-type TIMP-3.

Chapter 7: Discussion

7.1. Evaluation of proposed LRP-1-binding motif

Osteoarthritis is a degenerative disease of the joints for which there are currently no disease-modifying drugs. OA is characterised by degradation of cartilage, due to proteolytic breakdown of the primary ECM components, collagen and aggrecan, by matrix metalloproteinases (MMPs) and a disintegrin and metalloproteinase with thrombospondin motifs (ADAMTSs), respectively. Tissue inhibitor of metalloproteinase 3 (TIMP-3), the endogenous inhibitor of these enzymes, is present at lower levels in degraded human OA cartilage compared to normal cartilage (Morris et al., 2010). It has also been shown that *Timp3*-null mice have increased spontaneous cartilage degradation upon aging (Sahebjam et al., 2007) and that an intra-articular injection of TIMP-3 inhibits cartilage degradation in a rat meniscal tear model (Black et al., 2007). TIMP-3 is therefore considered a chondroprotective protein and a target for the development of novel OA therapies.

TIMP-3 has been shown to be endocytosed by chondrocytes via the endocytic receptor LDL receptor-related protein-1 (LRP-1) (Scilabra et al., 2013; Troeberg et al., 2008), reducing its in vivo half-life and therefore its chondroprotective activity. The aim of this study was to generate a TIMP-3 mutant that did not bind to LRP-1 but retained its affinity for target matrix metalloproteinases and sulfated proteoglycans of the ECM. We hypothesised that such a TIMP-3 mutant would have an increased half-life in cartilage and increased chondroprotective activity relative to Wild-type TIMP-3.

An LRP-1 ligand-binding motif had previously been identified to consist of a pair of lysine residues projecting outwards from the ligand surface and separated by 21 Å (Fisher et al., 2006; Jensen et al., 2006; Jensen et al.,

2009a; van den Bigglelaar et al., 2011). Using in silico molecular modeling of a proposed TIMP-3 structure, we identified 10 di-lysine pairs (composed of 12 constituent lysine residues) potentially satisfying this motif. We then performed site-directed mutagenesis of these lysine residues, individually (single mutants) and in pairs (double mutants) to identify an endocytosis-resistant TIMP-3. Two of these 10 TIMP-3 mutants, TIMP-3 K26A/K45A and TIMP-3 K42A/K110A, were successfully purified to the minimum concentration required for chondroprotective activity assays and found to have retained their affinity for prototypic matrix metalloproteinases.

7.2. LRP-1-binding residues of TIMP-3

Figure 71 shows localisation of di-lysine pairs K26/K45 and K42/K110 on the electrostatic charge surface-view of the full-length TIMP-3 model. Both di-lysine pairs are located within the extended basic patch on the face of the TIMP-3 opposite to the inhibitory ridge. This is in keeping with Scilabra et al. (Scilabra et al., 2013) who have previously shown that TIMP-3 in complex with LRP-1 retains its inhibitory activity, indicating that residues mediating metalloproteinase inhibition and LRP-1 binding are on opposite faces of the TIMP-3 molecule.

This is also supported by Troeberg et al. (Troeberg et al., 2014) who demonstrated that ECM-binding and LRP-1-binding sites overlap. Whilst all 8 remaining double mutants displayed endocytosis-resistance, their usefulness in future chondroprotective activity assays was limited by their low yield upon purification.

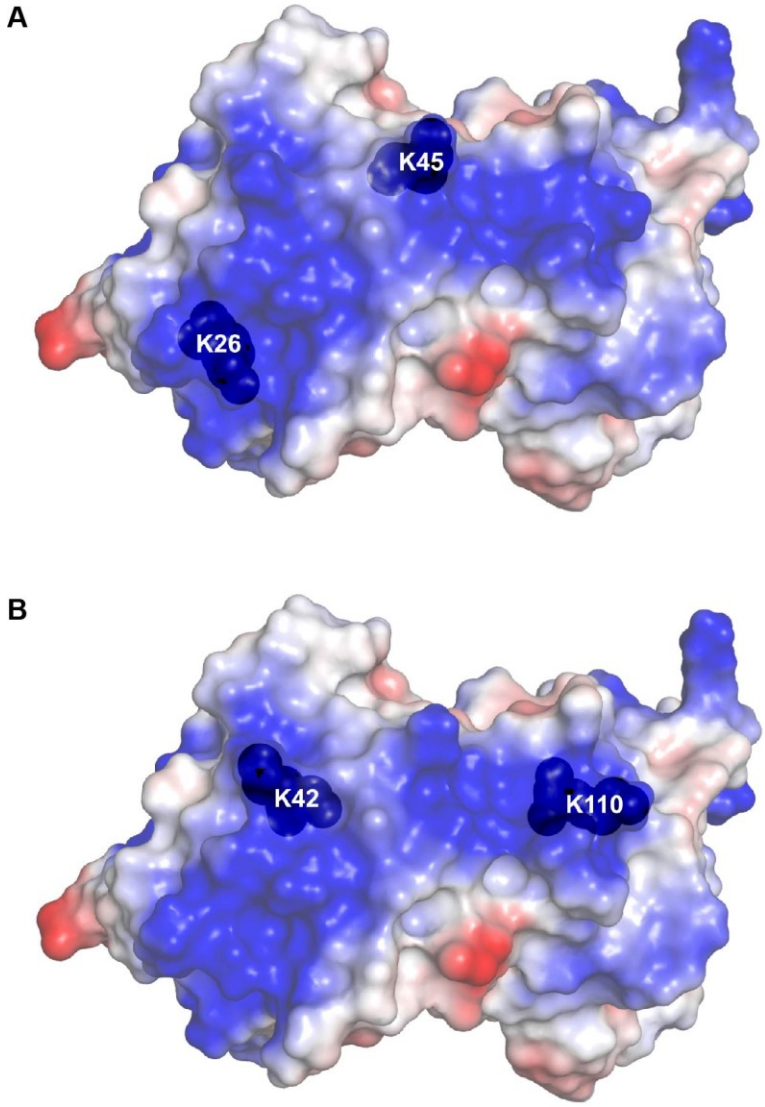


Figure 71: Localisation of di-lysine pairs on chondroprotective TIMP-3 mutants. Electrostatic charge surface views of 2 di-lysine pairs on TIMP-3 shown to mediate LRP-1 binding. Negatively charged areas are shown in red, positively charged areas in blue and uncharged areas are shown in white. Both di-lysine pairs are located along the TIMP-3 basic patch. (**A**) TIMP-3 K26/K45 and (**B**) TIMP-3 K42/K110.

The 10 di-lysine pairs were composed of 12 constituent single lysine residues, which were similarly individually assessed for endocytosis-resistance. The results of this study divided these 12 lysine residues into 2 overall groups, those that contributed to LRP-1-binding and those that did not. These groups were mapped onto the electrostatic charge surface-view of the full-length TIMP-3 model (Figure 72). Those lysine residues for which mutation

to alanine gave delayed TIMP-3 endocytosis are thought to contribute to LRP-1-binding and are shown in Figure 72A. With the exception of K157, these residues are closely packed and arranged centrally within a strongly basic region of the overall basic patch. Conversely, those lysine residues whose mutation to alanine had no effect on endocytosis are thought unlikely to contribute to LRP-1-binding. As shown in Figure 72B, these residues are arranged toward the outer boundary of the basic patch.

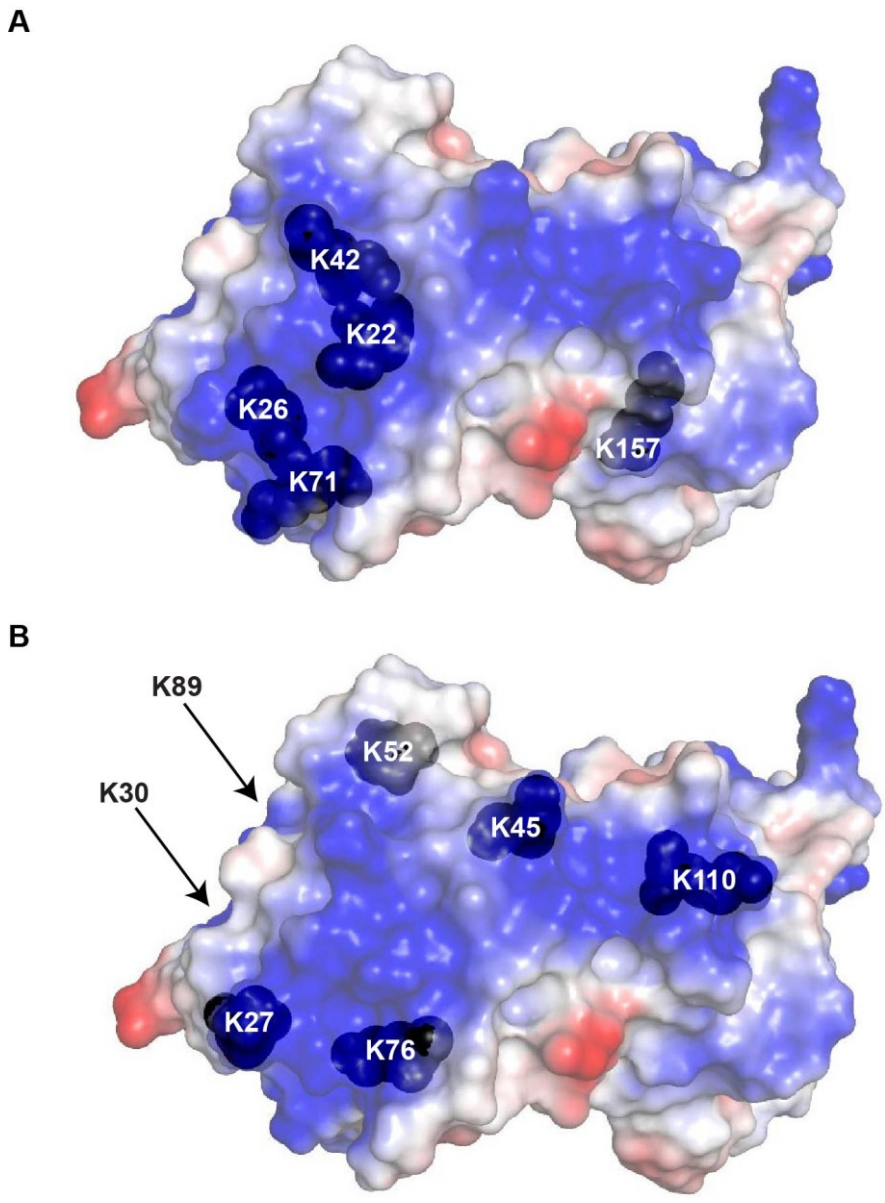


Figure 72: Localisation of lysine residues assessed for endocytosis-resistance on a TIMP-3 model.

The location of the 12 constituent TIMP-3 lysine residues of the 10 di-lysine pairs generated is shown and arranged on the electrostatic charge surface-view of the full-length TIMP-3 model. Negatively charged areas are shown in red, positively charged areas in blue and uncharged areas are shown in white. (**A**) mutation of K22, K26, K42, K71 and K157 reduced TIMP-3 endocytosis by LRP-1 (**B**) mutation K27, K30, K45, K52, K76, K89 and K110 had no effect on the TIMP-3 endocytosis by LRP-1.

While no single lysine residue was expected to solely mediate LRP-1 binding, the endocytosis screening also demonstrated that no di-lysine pair was solely responsible for LRP-1 binding either. These findings are in keeping with a recent study by van den Biggelaar et al., (van den Biggelaar et al., 2015) in which it is proposed that binding of factor VIII (fVIII) to LRP-1 may be mediated by an extended “hot spot” of lysine residues rather than the originally proposed di-lysine pair. Using hydrogen-deuterium exchange mass spectrometry and surface plasmon resonance analysis, van den Biggelaar et al. confirmed that lysine residues made the dominant contribution to fVIII-LRP-1 binding, and chemical modification of all fVIII lysine residues ablated binding to LRP-1 cluster II. However, no individual lysine residue accounted for cluster II binding, and an additive effect was observed with mutation of increasing numbers of lysine residues. This indicated that fVIII binds to LRP-1 via simultaneous interaction with multiple CRs. Each individual binding site was thought to be weak, but simultaneous binding of multiple sites enabled stronger binding and dissociation of one single lysine residue thus did not ablate binding. Using molecular modeling, it was found that the CRs in cluster II adapted to the fVIII surface topology with ease due to the flexibility of the CR chain within cluster II. Ionic interactions between the positively charged lysine residues on fVIII and

the negatively charged aspartic acid residues on the LRP-1 CRs resulted in close packing, which was proposed to be the main driving force of the interaction (van den Biggelaar et al., 2015).

This study proposed a new paradigm for LRP-1-ligand binding. Based on this, a TIMP-3-LRP-1 binding motif is proposed in Figure 73. The TIMP-3 basic patch containing those TIMP-3 lysine residues thought to contribute to LRP-1-binding aligns well with the aspartic acid residues of the CRs on LRP-1.

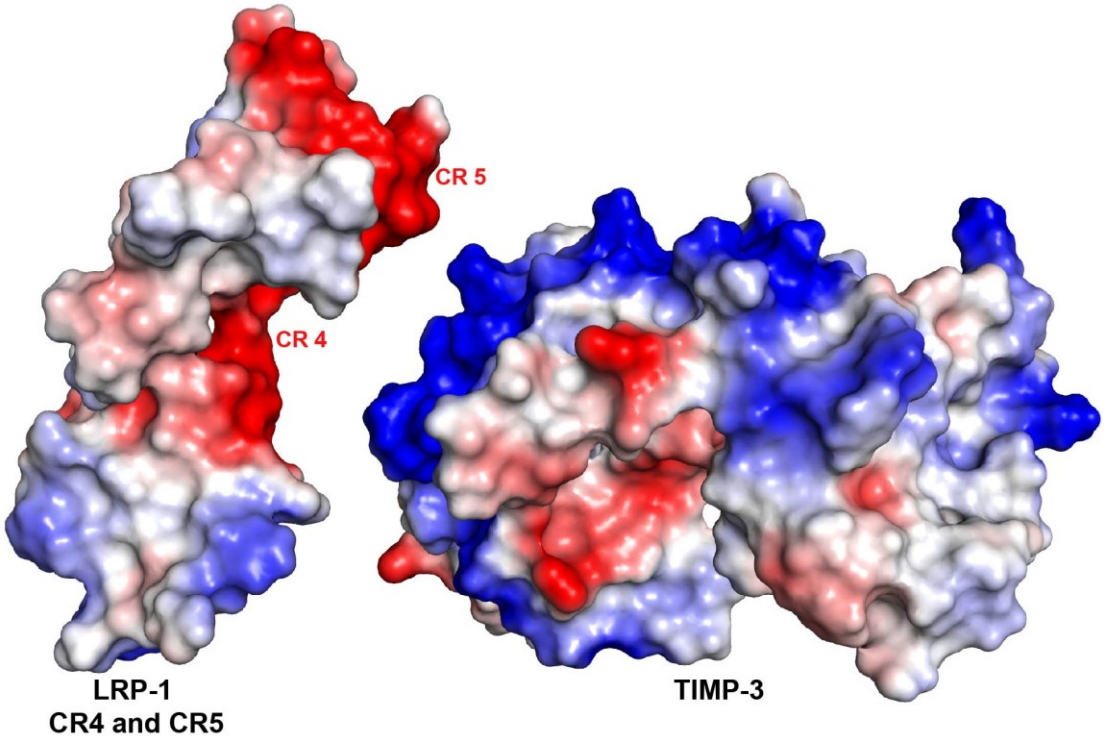


Figure 73: Proposed TIMP-3-LRP-1 binding

Alignment of electrostatic charge surface-view of LRP-1 CRs 4 and 5 with the electrostatic charge surface-view of the full-length TIMP-3 model. Negatively charged areas shown in red on CR 4 and 5 align with the TIMP-3 positively charged areas in blue. The TIMP-3 face interacting with the CRs includes those residues shown to give reduced TIMP-3 endocytosis on mutation, namely K22, K26, K42, K71 and K157.

In the future, it would be useful to test whether TIMP-3-LRP-1 binding is mediated by such a “hot spot” of lysine residues, as the current study has

demonstrated that all 10 di-lysine pairs tested here contributed to LRP-1-binding. A suitable approach would include the assessment of LRP-1-binding of mutated TIMP-3 di-lysine pairs which are separated by distances greater or less than 21 Å. Equally, mutation of increasing numbers of lysine residues followed by quantification of LRP-1-binding may also prove informative. We would predict that mutation of increasing numbers of lysine residues would further reduce LRP-1 binding. A suitable starting point would be combination of the mutations already shown to give delayed endocytosis. One potential drawback of this approach is that in our experience mutating more than 2 surface positive charges of TIMP-3 reduces expression yield considerably.

7.3. Biological effectiveness of mutants

The aim of this study was to generate an endocytosis-resistant TIMP-3 mutant with an improved chondroprotective activity. As TIMP-3 has previously been shown to induce cell apoptosis (Ahonen et al., 1998; Baker et al., 1999), there was a concern that TIMP-3 accumulation may lead to cell-death. However, following use of a cell viability assay, this was shown not to be the case in HTB94 and chondrocytes under the conditions of our endocytosis assays.

An interesting observation in the generation of HEK-293-EBNA mutant TIMP-3 stable cell lines was that higher mutant TIMP-3 protein expression was achieved with 8-fold lower levels of hygromycin B (100 µg/mL) than had been required for Wild-type TIMP-3 protein expression (800 µg/mL). Wild-type TIMP-3 protein expression at the higher hygromycin B level was thought to be linked to maintainance of low levels of TIMP-3 in the medium by rapid endocytosis, thereby preventing TIMP-3 apoptotic activity. However, as the TIMP-3 mutants

are endocytosis-resistant, their accumulation in cell media may have lead to apoptosis at higher hygromycin B levels. Therefore, increased TIMP-3 protein expression was observed at lower hygromycin B levels due to reduced cell toxicity. We thus cannot rule out that the endocytosis-resistant TIMP-3 mutants may cause increased apoptosis in chondrocytes if used at higher concentrations or for longer periods of time than tested in the current study.

To display improved chondroprotective activity, it was crucial that TIMP-3 K26A/K45A and TIMP-3 K42A/K110A retained prototypic TIMP-3 bioactivity, including unaltered affinity for target matrix metalloproteinases and ECM glycosaminoglycans. TIMP-3 achieves its chondroprotective function by inhibiting ECM-degrading enzymes including ADAMTS-4 and ADAMTS-5, but also by its ability to bind to the ECM increasing its affinity for target metalloproteinases including ADAMTS-5. TIMP-3 mutants displaying resistance to LRP-1-mediated endocytosis but having compromised affinity for either target metalloproteinases or ECM would not give improved chondroprotective activity.

It was successfully demonstrated that both TIMP-3 mutants had unaltered affinities for MMP-1, MMP-2, MMP-3, ADAMTS-4, ADAMTS-5. This was expected as Scilabra et al. (Scilabra et al., 2013) had previously indicated that residues mediating metalloproteinase inhibition and LRP-1 binding on TIMP-3 are on opposite faces of the TIMP-3 molecule.

The TIMP-3 positive patch, as shown in Figure 71 and Figure 72, is thought to mediate TIMP-3 binding to the strongly negatively charged GAGs in the ECM. As both TIMP-3 mutants include mutation of positive lysine residues within this region to neutral alanine residues, the binding of these mutants to

heparin and heparan sulfate was investigated to assess their ECM binding ability. Mutation of 6 basic residues (K26, K27, K30, K76, R163 and K167) within this positive patch had previously been demonstrated to ablate ECM binding of TIMP-3 (Lee et al., 2007). It was anticipated that mutation of 1 lysine residue would not ablate ECM binding, however the degree to which the double mutations would affect TIMP-3 ECM binding affinity was not known.

Wild-type TIMP-3 bound to both heparin and heparan sulfate with high affinity, TIMP-3 K26A/K45A showed an estimated 3-fold reduction in affinity and TIMP-3 K42A/K110A showing an estimated 10-fold reduction in affinity. It was not unexpected for TIMP-3 K26A/K45A to show a reduced ECM-binding affinity compared to Wild-type TIMP-3, as K26 had been identified by Lee at al. as one of the 6 residues mediating ECM-binding. However it was unexpected that TIMP-3 K42A/K110A showed an even greater reduction in ECM-binding affinity compared to TIMP-3 K26A/K45A, as these residues have not previously being associated with ECM-binding.

The affect of this reduced heparin-binding on the increase in TIMP-3 mutant affinity for ADAMTS-5 was investigated. Heparin similarly increased the affinity of TIMP-3 K26A/K45A to a value too low to be accurately determined, as was found for Wild-type TIMP-3. However no increase in affinity was observed for TIMP-3 K42A/K110A, which coincided with its greatly reduced heparin binding. Therefore TIMP-3 K26A/K45A retained sufficient GAG-binding affinity to display increased inhibitory activity when bound to the ECM, while TIMP-3 K42A/K110A did not. We thus predicted that TIMP-3 K42A/K110A would have reduced chondroprotective activity compared to TIMP-3 K26A/K45A, since its reduced GAG-binding would prevent it from displaying

increased inhibitory activity when bound to the ECM. This indeed was found to be the case and TIMP-3 K42A/K110A showed no increase in chondroprotective activity compared to Wild-type TIMP-3. TIMP-3 K26A/K45A however strongly inhibited GAG release even after 3 days preincubation with cartilage. This trend was also observed when GAG release was stimulated simultaneously with Wild-type TIMP-3 and TIMP-3 K26A/K45A treatment, indicating that TIMP-3 K26A/K45A had improved chondroprotective activity compared to Wild-type TIMP-3.

7.4. Conclusions and future directions

This study achieved its aim in the generation of an endocytosis-resistant TIMP-3 mutant, with TIMP-3 K26A/K45A giving improved chondroprotective activity, but is this mutant likely to be clinically useful?

In normal healthy tissue, the balance between ECM synthesis and degradation by MMPs and ADAMTSs is maintained in part, by TIMP-3. In osteoarthritic cartilage this balance is disturbed by the reduction in TIMP-3 levels, and an increase in metalloproteinase expression, shifting the balance in favour of catabolic activity and cartilage degradation. In either case, treatment of cartilage with endocytosis-resistant TIMP-3 K26A/K45A would redress this imbalance. However, due to their functions in normal balanced tissue turnover, pan-inhibition of matrix metalloproteinases by systemic administration of TIMP-3 K26A/K45A could have detrimental effects.

We have shown that TIMP-3 K26A/K45A gave improved chondroprotective activity in porcine cartilage explants. In the future, the chondroprotective activity of this TIMP-3 mutant should also be assessed in human cartilage explants. The use of mouse studies e.g. knock-in or a

transgenic mouse model would provide a very useful insight of the phenotype or any detrimental effects of this mutant than. A knock-in mouse model would be an appropriate approach as it is generated by targeted insertion of the desired gene into a specific locus in the target genome via homologous recombination. This ensures natural biological expression patterns and levels. In contrast, transgenic models use random integration of the desired gene, which could be placed under its own strong promoter, leading to high levels of expression and consequently an earlier or more robust phenotype.

MMPs have long been regarded as targets for cancer therapy and the attempts to bring such a drug to market highlight the challenges involved in the development of a synthetic MMP inhibitor. While preclinical studies investigating the efficacy of MMP suppression in tumour models were encouraging, clinical studies have been disappointing. The first generation of these synthetic MMP inhibitors such as Ilomastat and Batimastat were based on the structure of the collagen molecule, but showed poor oral bioavailability (Brown, 1997). These were replaced by a new generation of synthetic MMP inhibitors displaying excellent anticancer activity in tumour cells. However clinical performance was disappointing as they inhibited many differing MMPs and ADAMs and also induced dose-limiting muscular and skeletal pain in a number of patients (Durrant et al., 2011). Recent studies have shown that synthetic MMP inhibitors may even have paradoxical roles in tumour progression, with the inhibitors displaying both tumour-promoting and tumour suppressive effects in different contexts (Hua et al., 2011). The challenge in development of metalloproteinase inhibitors for disease treatment is that an

inhibitor is required to be highly selective for individual metalloproteinases to reduce toxicity.

However osteoarthritis is a disease of joints, which can be viewed as discrete treatment units. As such, direct administration of TIMP-3 K26A/K45A via intra-articular injection could be used to treat the diseased joint, while limiting undesirable systemic effects. The effectiveness of intra-articular injections of TIMP-3 K26A/K45A may be assessed in mouse models however the difficulty lies in purifying sufficient lipopolysaccharide-free amounts of the protein. Lipopolysaccharides are a key factor in septic shock in humans and induce a strong immune response in normal mammalian cells (Schletter et al., 1995).

The challenges in expressing and purifying TIMP-3 K26A/K45A to meaningful concentrations on an industrial scale make the development of small molecule inhibitors of TIMP-3 endocytosis an attractive alternative. The TIMP-3 K26A/K45A produced in this study could be used to generate a pharmacophore for the development of small molecule inhibitors of TIMP-3 endocytosis e.g. small GAG mimetics such as calcium pentosan polysulfate. The generation of a crystal structure for TIMP-3 K26A/K45A would provide a useful tool for designing such a pharmacophore. The challenge lies in the ability to reproducibly express and purify the protein to the minimum concentration required for crystallogenesis screening (10 mg/mL). While bacterial expression can produce high protein yields, the proteins do not contain posttranslational modifications generated by expression in mammalians cells. The use of insect cell protein expression may be a suitable approach to produce the required protein yields with posttranslational modifications similar to mammalian cells.

Insect cell protein expression also has the advantage of ease of scale-up as can readily be adapted to high-density suspension culture for large-scale expression. Should such a pharmacophore be successfully generated, it could be used for in-silico screening of drug libraries in order to select likely drug candidates.

OA is a chronic disease and as average life expectancy is increasing, any DMOAD developed would be expected to be suitable for long-term use. While low metabolic clearance is usually useful in drug development, in this case the induction of cell apoptosis by TIMP-3 makes it a major disadvantage. The endocytosis-resistance of TIMP-3 K26A/K45A would lead to increased TIMP-3 tissue levels and therefore may induce apoptosis. TIMP-3 has been shown to have a pro-apoptotic effect on normal and malignant human cells in culture and in vivo, with smooth muscle cells, HeLa human epithelial melanoma cell, HT1080 fibrosarcoma cells and MCF-7 breast cancer cells reportedly affected (Ahonen et al., 1998; Baker et al., 1999). It has been proposed that TIMP-3 promotes cell death by stabilising death receptors on the cell surface, leading to an increased susceptibility to apoptosis (Smith et al., 1997). It has been demonstrated that exposure to recombinant TIMP-3 or N-TIMP-3 and adenoviral expression of TIMP-3 stabilises several death receptors, including tumor necrosis factor receptor I (TNF-RI), Fas cell surface death receptor (FAS) and TNF-related apoptosis-inducing ligand receptor I (TRAIL-RI), thereby sensitizing cells to ligand-induced apoptosis (Ahonen et al., 2003). In this same study, it was also shown that TIMP-3 induced caspase-8-dependent apoptotic signaling of these death receptors. In a recent publication, Qi et al. found that TIMP-3-mediated apoptosis in endothelial cells was independent of

MMP inhibitory activity and was mediated by a caspase-independent cell death pathway, involving a focal adhesion kinase (FAK)-dependent survival pathway (Qi and Anand-Apte, 2015). Another possible disadvantage is that increasing levels of TIMP-3 could also inhibit those MMPs maintaining normal tissue turnover.

This endocytosis-resistant TIMP-3 mutant may have greater potential clinical application for acute treatments. For example, TIMP-3 plays an important role in regulating TNF release as it is the physiological inhibitor of TACE (TNFα converting enzyme or ADAM-17). *Timp3*-null mice have been shown to exhibit increased TACE activity leading to increased inflammation and reduced tissue repair in a liver regeneration model (Mohammed et al., 2004). Therefore an endocytosis-resistant TIMP-3 mutant could have applications in the treatment and prevention of acute inflammatory conditions such as sepsis and in the short-term treatment of chronic wounds.

Chapter 8: References

Abbaszade, I., Liu, R.Q., Yang, F., Rosenfeld, S.A., Ross, O.H., Link, J.R., Ellis, D.M., Tortorella, M.D., Pratta, M.A., Hollis, J.M., *et al.* (1999). Cloning and characterization of ADAMTS11, an aggrecanase from the ADAMTS family. J Biol Chem *274*, 23443-23450.
Afoke, N.Y., Byers, P.D., and Hutton, W.C. (1987). Contact pressures in the human hip joint. J Bone Joint Surg Br *69*, 536-541.
Ahonen, M., Baker, A.H., and Kahari, V.M. (1998). Adenovirus-mediated gene delivery of tissue inhibitor of metalloproteinases-3 inhibits invasion and induces apoptosis in melanoma cells. Cancer Res *58*, 2310-2315.
Ahonen, M., Poukkula, M., Baker, A.H., Kashiwagi, M., Nagase, H., Eriksson, J.E., and Kahari, V.M. (2003). Tissue inhibitor of metalloproteinases-3 induces apoptosis in melanoma cells by stabilization of death receptors. Oncogene *22*, 2121-2134.
Aigner, T., Sachse, A., Gebhard, P., and Roach, H. (2006). Osteoarthritis: Pathobiology—targets and ways for therapeutic intervention. Advanced Drug Delivery Reviews *58*, 128-149.
Amour, A., Knight, C.G., Webster, A., Slocombe, P.M., Stephens, P.E., Knauper, V., Docherty, A.J., and Murphy, G. (2000). The in vitro activity of ADAM-10 is inhibited by TIMP-1 and TIMP-3. FEBS Lett *473*, 275-279.
Amour, A., Slocombe, P.M., Webster, A., Butler, M., Knight, C.G., Smith, B.J., Stephens, P.E., Shelley, C., Hutton, M., Knauper, V., *et al.* (1998). TNF-alpha converting enzyme (TACE) is inhibited by TIMP-3. FEBS Lett *435*, 39-44.
Arandjelovic, S., Hall, B.D., and Gonias, S.L. (2005). Mutation of lysine 1370 in full-length human alpha2-macroglobulin blocks binding to the low density lipoprotein receptor-related protein-1. Arch Biochem Biophys *438*, 29-35.
Arner, E.C., Hughes, C.E., Decicco, C.P., Caterson, B., and Tortorella, M.D. (1998). Cytokine-induced cartilage proteoglycan degradation is mediated by aggrecanase. Osteoarthritis Cartilage *6*, 214-228.
Arner, E.C., Pratta, M.A., Trzaskos, J.M., Decicco, C.P., and Tortorella, M.D. (1999). Generation and characterization of aggrecanase - A soluble, cartilage-derived aggrecan-degrading activity. Journal of biological chemistry *274*, 6594-6601.
Ashcom, J.D., Tiller, S.E., Dickerson, K., Cravens, J.L., Argraves, W.S., and Strickland, D.K. (1990). The human alpha 2-macroglobulin receptor: identification of a 420-kD cell surface glycoprotein specific for the activated conformation of alpha 2-macroglobulin. J Cell Biol *110*, 1041-1048.
Aspberg, A. (2012). The different roles of aggrecan interaction domains. The journal of histochemistry and cytochemistry : official journal of the Histochemistry Society *60*, 987-996.
Baker, A.H., George, S.J., Zaltsman, A.B., Murphy, G., and Newby, A.C. (1999). Inhibition of invasion and induction of apoptotic cell death of cancer cell lines by overexpression of TIMP-3. British journal of cancer *79*, 1347-1355.
Balbin, M., Fueyo, A., Knauper, V., Lopez, J.M., Alvarez, J., Sanchez, L.M., Quesada, V., Bordallo, J., Murphy, G., and Lopez-Otin, C. (2001). Identification and enzymatic characterization of two diverging murine counterparts of human interstitial collagenase (MMP-1) expressed at sites of embryo implantation. J Biol Chem *276*, 10253-10262.
Barnes, H., Ackermann, E.J., and van der Geer, P. (2003). v-Src induces Shc binding to tyrosine 63 in the cytoplasmic domain of the LDL receptor-related protein 1. Oncogene *22*, 3589-3597.

Barnes, H., Larsen, B., Tyers, M., and van Der Geer, P. (2001). Tyrosine-phosphorylated low density lipoprotein receptor-related protein 1 (Lrp1) associates with the adaptor protein SHC in SRC-transformed cells. J Biol Chem *276*, 19119-19125.
Bau, B., Gebhard, P.M., Haag, J., Knorr, T., Bartnik, E., and Aigner, T. (2002). Relative messenger RNA expression profiling of collagenases and aggrecanases in human articular chondrocytes in vivo and in vitro. Arthritis Rheum *46*, 2648-2657.
Bauer, E.A., Stricklin, G.P., Jeffrey, J.J., and Eisen, A.Z. (1975). Collagenase production by human skin fibroblasts. Biochem Biophys Res Commun *64*, 232-240.
Behrens, J. (2000). Control of beta-catenin signaling in tumor development. Ann N Y Acad Sci *910*, 21-33; discussion 33-25.
Bertaux, B., Hornebeck, W., Eisen, A.Z., and Dubertret, L. (1991). Growth stimulation of human keratinocytes by tissue inhibitor of metalloproteinases. J Invest Dermatol *97*, 679-685.
Bieth, J.G. (1995a). Theoretical and Practical Aspects of Proteinase Inhibition Kinetics. Meth Enzymol *248*, 59-84.
Bieth, J.G. (1995b). Theoretical and practical aspects of proteinase inhibition kinetics. Methods Enzymol *248*, 59-84.
Billinghurst, R.C., Dahlberg, L., Ionescu, M., Reiner, A., Bourne, R., Rorabeck, C., Mitchell, P., Hambor, J., Diekmann, O., Tschesche, H.*, et al.* (1997). Enhanced cleavage of type II collagen by collagenases in osteoarthritic articular cartilage. J Clin Invest *99*, 1534-1545.
Bitton, R. (2009). The economic burden of osteoarthritis. Am J Manag Care *15*, S230-235.
Black, R.A. (2002). Tumor necrosis factor-alpha converting enzyme. Int J Biochem Cell Biol *34*, 1-5.
Black, R.A., Castner, B., Slack, J., Tocker, J., Eisenman, J., Jacobsen, E., Delaney, J., Winters, D., Hecht, R., and Bendele, A. (2007). Injected TIMP-3 protects cartilage in a rat meniscal tear model. Osteoarthritis and Cartilage *14*, S23-24.
Black, R.A., Rauch, C.T., Kozlosky, C.J., Peschon, J.J., Slack, J.L., Wolfson, M.F., Castner, B.J., Stocking, K.L., Reddy, P., Srinivasan, S.*, et al.* (1997). A metalloproteinase disintegrin that releases tumour-necrosis factor-alpha from cells. Nature *385*, 729-733.
Bond, M., Murphy, G., Bennett, M.R., Amour, A., Knauper, V., Newby, A.C., and Baker, A.H. (2000). Localization of the death domain of tissue inhibitor of metalloproteinase-3 to the N terminus. Metalloproteinase inhibition is associated with proapoptotic activity. J Biol Chem *275*, 41358-41363.
Boucher, P., Gotthardt, M., Li, W.P., Anderson, R.G., and Herz, J. (2003). LRP: role in vascular wall integrity and protection from atherosclerosis. Science *300*, 329-332.
Brennan, F.M., Maini, R.N., and Feldmann, M., 368–384 (1995). Cytokine expression in chronic inflammatory disease British Medical Bulletin *51*, 368-384.
Brew, K., and Nagase, H. (2010). The tissue inhibitors of metalloproteinases (TIMPs): an ancient family with structural and functional diversity. Biochim Biophys Acta *1803*, 55-71.
Brown, P.D. (1997). Matrix metalloproteinase inhibitors in the treatment of cancer. Med Oncol *14*, 1-10.

Brueckl, W.M., Grombach, J., Wein, A., Ruckert, S., Porzner, M., Dietmaier, W., Rummele, P., Croner, R.S., Boxberger, F., Kirchner, T.*, et al.* (2005). Alterations in the tissue inhibitor of metalloproteinase-3 (TIMP-3) are found frequently in human colorectal tumours displaying either microsatellite stability (MSS) or instability (MSI). Cancer letters *223*, 137-142.
Buckwalter, J.A., Mow, V.C., and Ratcliffe, A. (1994). Restoration of Injured or Degenerated Articular Cartilage. The Journal of the American Academy of Orthopaedic Surgeons *2*, 192-201.
Capurro, M.I., Shi, W., and Filmus, J. (2012). LRP1 mediates Hedgehog-induced endocytosis of the GPC3-Hedgehog complex. J Cell Sci *125*, 3380-3389.
Cardellini, M., Menghini, R., Martelli, E., Casagrande, V., Marino, A., Rizza, S., Porzio, O., Mauriello, A., Solini, A., Ippoliti, A.*, et al.* (2009). TIMP3 is reduced in atherosclerotic plaques from subjects with type 2 diabetes and increased by SirT1. Diabetes *58*, 2396-2401.
Caterson, B., Flannery, C.R., Hughes, C.E., and Little, C.B. (2000). Mechanisms involved in cartilage proteoglycan catabolism. Matrix Biol *19*, 333-344.
Cawston, T.E., Galloway, W.A., Mercer, E., Murphy, G., and Reynolds, J.J. (1981). Purification of rabbit bone inhibitor of collagenase. Biochem J *195*, 159-165.
Chaillan, F.A., Rivera, S., Marchetti, E., Jourquin, J., Werb, Z., Soloway, P.D., Khrestchatisky, M., and Roman, F.S. (2006). Involvement of tissue inhibition of metalloproteinases-1 in learning and memory in mice. Behavioural brain research *173*, 191-198.
Chen, A., Gupte, C., Akhtar, K., Smith, P., and Cobb, J. (2012). The Global Economic Cost of Osteoarthritis: How the UK Compares. Arthritis *2012*, 698709.
Chung, L., Shimokawa, K., Dinakarpandian, D., Grams, F., Fields, G.B., and Nagase, H. (2000). Identification of the (183)RWTNNFREY(191) region as a critical segment of matrix metalloproteinase 1 for the expression of collagenolytic activity. J Biol Chem *275*, 29610-29617.
Creemers, E.E., Davis, J.N., Parkhurst, A.M., Leenders, P., Dowdy, K.B., Hapke, E., Hauet, A.M., Escobar, P.G., Cleutjens, J.P., Smits, J.F.*, et al.* (2003). Deficiency of TIMP-1 exacerbates LV remodeling after myocardial infarction in mice. American journal of physiology Heart and circulatory physiology *284*, H364-371.
Davis, C.G., Goldstein, J.L., Sudhof, T.C., Anderson, R.G., Russell, D.W., and Brown, M.S. (1987). Acid-dependent ligand dissociation and recycling of LDL receptor mediated by growth factor homology region. Nature *326*, 760-765.
De Strooper, B., Annaert, W., Cupers, P., Saftig, P., Craessaerts, K., Mumm, J.S., Schroeter, E.H., Schrijvers, V., Wolfe, M.S., Ray, W.J.*, et al.* (1999). A presenilin-1-dependent gamma-secretase-like protease mediates release of Notch intracellular domain. Nature *398*, 518-522.
Diekmann, O., and Tschesche, H. (1994). Degradation of kinins, angiotensins and substance P by polymorphonuclear matrix metalloproteinases MMP 8 and MMP 9. Brazilian journal of medical and biological research = Revista brasileira de pesquisas medicas e biologicas / Sociedade Brasileira de Biofisica [et al] *27*, 1865-1876.
Dingle, J.T., Barrett, A.J., and Weston, P.D. (1971). Cathepsin D. Characteristics of immunoinhibition and the confirmation of a role in cartilage breakdown. Biochem J *123*, 1-13.
Dingle, J.T., Saklatvala, J., Hembry, R., Tyler, J., Fell, H.B., and Jubb, R. (1979). A cartilage catabolic factor from synovium. Biochem J *184*, 177-180.

Doege, K.J., Sasaki, M., Kimura, T., and Yamada, Y. (1991). Complete coding sequence and deduced primary structure of the human cartilage large aggregating proteoglycan, aggrecan. Human-specific repeats, and additional alternatively spliced forms. J Biol Chem *266*, 894-902.
Dolmer, K., Campos, A., and Gettins, P.G. (2013). Quantitative dissection of the binding contributions of ligand lysines of the receptor-associated protein (RAP) to the low density lipoprotein receptor-related protein (LRP1). J Biol Chem *288*, 24081-24090.
Durrant, J.D., de Oliveira, C.A., and McCammon, J.A. (2011). Pyrone-based inhibitors of metalloproteinase types 2 and 3 may work as conformation-selective inhibitors. Chemical biology & drug design *78*, 191-198.
Dvir-Ginzberg, M., Gagarina, V., Lee, E.J., and Hall, D.J. (2008). Regulation of cartilage-specific gene expression in human chondrocytes by SirT1 and nicotinamide phosphoribosyltransferase. J Biol Chem *283*, 36300-36310.
Ehrlich, M.G., Mankin, H.J., Jones, H., Wright, R., Crispen, C., and Vigliani, G. (1977). Collagenase and collagenase inhibitors in osteoarthritic and normal cartilage. J Clin Invest *59*, 226-233.
Enghild, J.J., Salvesen, G., Brew, K., and Nagase, H. (1989). Interaction of human rheumatoid synovial collagenase (matrix metalloproteinase 1) and stromelysin (matrix metalloproteinase 3) with human alpha 2-macroglobulin and chicken ovostatin. Binding kinetics and identification of matrix metalloproteinase cleavage sites. J Biol Chem *264*, 8779-8785.
Eyre, D.R., Weis, M.A., and Wu, J.J. (2006). Articular cartilage collagen: an irreplaceable framework? Eur Cell Mater *12*, 57-63.
Fariss, R.N., Apte, S.S., Luthert, P.J., Bird, A.C., and Milam, A.H. (1998). Accumulation of tissue inhibitor of metalloproteinases-3 in human eyes with Sorsby's fundus dystrophy or retinitis pigmentosa. The British journal of ophthalmology *82*, 1329-1334.
Farndale, R.W., Sayers, C.A., and Barrett, A.J. (1982). A direct spectrophotometric microassay for sulfated glycosaminoglycans in cartilage cultures. Connect Tissue Res *9*, 247-248.
Fedak, P.W.M., Smookler, D.S., Kassiri, Z., Ohno, N., Leco, K.J., S, V., Mickle, D.A.G., Watson, K.L., Hojilla, C.V., and Khokha, R. (2004). TIMP-3 deficiency leads to dilated cardiomyopathy. Circulation *110*, 2401-2409.
Felson, D.T. (2013). Osteoarthritis as a disease of mechanics. Osteoarthritis Cartilage *21*, 10-15.
Felson, D.T., Couropmitree, N.N., Chaisson, C.E., Hannan, M.T., Zhang, Y., McAlindon, T.E., LaValley, M., Levy, D., and Myers, R.H. (1998). Evidence for a Mendelian gene in a segregation analysis of generalized radiographic osteoarthritis: the Framingham Study. Arthritis Rheum *41*, 1064-1071.
Fernandez-Catalan, C., Bode, W., Huber, R., Turk, D., Calvete, J.J., Lichte, A., Tschesche, H., and Maskos, K. (1998). Crystal structure of the complex formed by the membrane type 1-matrix metalloproteinase with the tissue inhibitor of metalloproteinases-2, the soluble progelatinase A receptor. Embo J *17*, 5238-5248.
Fisher, C., Beglova, N., and Blacklow, S.C. (2006). Structure of an LDLR-RAP complex reveals a general mode for ligand recognition by lipoprotein receptors. Molecular Cell *22*, 277-283.

Flannery, C.R., Little, C.B., Hughes, C.E., and Caterson, B. (1999). Expression of ADAMTS homologues in articular cartilage. Biochem Biophys Res Commun *260*, 318-322.
Fosang, A.J., Last, K., Knauper, V., Murphy, G., and Neame, P.J. (1996). Degradation of cartilage aggrecan by collagenase-3 (MMP-13). FEBS Lett *380*, 17-20.
Fosang, A.J., Last, K., Knauper, V., Neame, P.J., Murphy, G., Hardingham, T.E., Tschesche, H., and Hamilton, J.A. (1993). Fibroblast and neutrophil collagenases cleave at two sites in the cartilage aggrecan interglobular domain. Biochem J *295 (Pt 1)*, 273-276.
Fosang, A.J., Neame, P.J., Hardingham, T.E., Murphy, G., and Hamilton, J.A. (1991). Cleavage of cartilage proteoglycan between G1 and G2 domains by stromelysins. J Biol Chem *266*, 15579-15582.
Fosang, A.J., Neame, P.J., Last, K., Hardingham, T.E., Murphy, G., and Hamilton, J.A. (1992). The interglobular domain of cartilage aggrecan is cleaved by PUMP, gelatinases, and cathepsin B. J Biol Chem *267*, 19470-19474.
Fosang, A.J., Rogerson, F.M., East, C.J., and Stanton, H. (2008). ADAMTS-5: the story so far. Eur Cell Mater *15*, 11-26.
Fujita, N., Matsushita, T., Ishida, K., Kubo, S., Matsumoto, T., Takayama, K., Kurosaka, M., and Kuroda, R. (2011). Potential involvement of SIRT1 in the pathogenesis of osteoarthritis through the modulation of chondrocyte gene expressions. Journal of orthopaedic research : official publication of the Orthopaedic Research Society *29*, 511-515.
Fushimi, K., Troeberg, L., Nakamura, H., Lim, N.H., and Nagase, H. (2008). Functional differences of the catalytic and non-catalytic domains in human ADAMTS-4 and ADAMTS-5 in aggrecanolytic activity. J Biol Chem *283*, 6706-6716.
Gabriely, G., Wurdinger, T., Kesari, S., Esau, C.C., Burchard, J., Linsley, P.S., and Krichevsky, A.M. (2008). MicroRNA 21 promotes glioma invasion by targeting matrix metalloproteinase regulators. Mol Cell Biol *28*, 5369-5380.
Galloway, W.A., Murphy, G., Sandy, J.D., Gavrilovic, J., Cawston, T.E., and Reynolds, J.J. (1983). Purification and characterization of a rabbit bone metalloproteinase that degrades proteoglycan and other connective-tissue components. Biochem J *209*, 741-752.
Garofalo, M., Di Leva, G., Romano, G., Nuovo, G., Suh, S.S., Ngankeu, A., Taccioli, C., Pichiorri, F., Alder, H., Secchiero, P.*, et al.* (2009). miR-221&222 regulate TRAIL resistance and enhance tumorigenicity through PTEN and TIMP3 downregulation. Cancer Cell *16*, 498-509.
Gendron, C., Kashiwagi, M., Hughes, C., Caterson, B., and Nagase, H. (2003). TIMP-3 inhibits aggrecanase-mediated glycosaminoglycan release from cartilage explants stimulated by catabolic factors. FEBS Lett *555*, 431-436.
Gendron, C., Kashiwagi, M., Lim, N.H., Enghild, J.J., Thogersen, I.B., Hughes, C., Caterson, B., and Nagase, H. (2007). Proteolytic activities of human ADAMTS-5: comparative studies with ADAMTS-4. J Biol Chem *282*, 18294-18306.
Glasson, S.S., Askew, R., Sheppard, B., Carito, B., Blanchet, T., Ma, H.L., Flannery, C.R., Peluso, D., Kanki, K., Yang, Z.*, et al.* (2005). Deletion of active ADAMTS5 prevents cartilage degradation in a murine model of osteoarthritis. Nature *644*, 644-648.
Gleghorn, J.P., Jones, A.R., Flannery, C.R., and Bonassar, L.J. (2009). Boundary mode lubrication of articular cartilage by recombinant human lubricin. Journal of

orthopaedic research : official publication of the Orthopaedic Research Society *27*, 771-777.
Gliem, M., Muller, P.L., Mangold, E., Holz, F.G., Bolz, H.J., Stohr, H., Weber, B.H., and Charbel Issa, P. (2015). Sorsby Fundus Dystrophy: Novel Mutations, Novel Phenotypic Characteristics, and Treatment Outcomes. Invest Ophthalmol Vis Sci *56*, 2664-2676.
Gliemann, J., Nykjaer, A., Petersen, C.M., Jorgensen, K.E., Nielsen, M., Andreasen, P.A., Christensen, E.I., Lookene, A., Olivecrona, G., and Moestrup, S.K. (1994). The multiligand alpha 2-macroglobulin receptor/low density lipoprotein receptor-related protein (alpha 2MR/LRP). Binding and endocytosis of fluid phase and membrane-associated ligands. Ann N Y Acad Sci *737*, 20-38.
Goldring, M.B., and Goldring, S.R. (2010). Articular cartilage and subchondral bone in the pathogenesis of osteoarthritis. Annals of the New York Academy of Sciences *1192*, 230-237.
Goldring, M.B., and Marcu, K.B. (2012). Epigenomic and microRNA-mediated regulation in cartilage development, homeostasis, and osteoarthritis. Trends in molecular medicine *18*, 109-118.
Goldstein, J.L., and Brown, M.S. (1973). Familial hypercholesterolemia: identification of a defect in the regulation of 3-hydroxy-3-methylglutaryl coenzyme A reductase activity associated with overproduction of cholesterol. Proc Natl Acad Sci U S A *70*, 2804-2808.
Gomis-Ruth, F.X., Maskos, K., Betz, M., Bergner, A., Huber, R., Suzuki, K., Yoshida, N., Nagase, H., Brew, K., Bourenkov, G.P.*, et al.* (1997). Mechanism of inhibition of the human matrix metalloproteinase stromelysin-1 by TIMP-1. Nature *389*, 77-81.
Greene, G.W., Banquy, X., Lee, D.W., Lowrey, D.D., Yu, J., and Israelachvili, J.N. (2011). Adaptive mechanically controlled lubrication mechanism found in articular joints. Proc Natl Acad Sci U S A *108*, 5255-5259.
Greene, J., Wang, M., Liu, Y.E., Raymond, L.A., Rosen, C., and Shi, Y.E. (1996). Molecular cloning and characterization of human tissue inhibitor of metalloproteinase 4. J Biol Chem *271*, 30375-30380.
Gross, J., and Lapiere, C.M. (1962). Collagenolytic activity in amphibian tissues: a tissue culture assay. Proc Natl Acad Sci U S A *48*, 1014-1022.
Gross, J., and Nagai, Y. (1965). Specific degradation of the collagen molecule by tadpole collagenolytic enzyme. Proc Natl Acad Sci U S A *54*, 1197-1204.
Guan, Z., Zhang, J., Song, S., and Dai, D. (2013). Promoter methylation and expression of TIMP3 gene in gastric cancer. Diagnostic pathology *8*, 110.
Guttman, M., Prieto, J.H., Handel, T.M., Domaille, P.J., and Komives, E.A. (2010). Structure of the minimal interface between ApoE and LRP. J Mol Biol *398*, 306-319.
Hamze, A.B., Wei, S., Bahudhanapati, H., Kota, S., Acharya, K.R., and Brew, K. (2007). Constraining specificity in the N-domain of tissue inhibitor of metalloproteinases-1; gelatinase-selective inhibitors. Protein Sci *16*, 1905-1913.
Hashimoto, G., Aoki, T., Nakamura, H., Tanzawa, K., and Okada, Y. (2001). Inhibition of ADAMTS4 (aggrecanase-1) by tissue inhibitors of metalloproteinases (TIMP-1, 2, 3 and 4). FEBS Lett *494*, 192-195.
Hass, M.R., Sato, C., Kopan, R., and Zhao, G. (2009). Presenilin: RIP and beyond. Seminars in cell & developmental biology *20*, 201-210.

Hayakawa, T., Yamashita, K., Ohuchi, E., and Shinagawa, A. (1994). Cell growth-promoting activity of tissue inhibitor of metalloproteinases-2 (TIMP-2). J Cell Sci *107 (Pt 9)*, 2373-2379.
Hayakawa, T., Yamashita, K., Tanzawa, K., Uchijima, E., and Iwata, K. (1992). Growth-promoting activity of tissue inhibitor of metalloproteinases-1 (TIMP-1) for a wide range of cells. A possible new growth factor in serum. FEBS Lett *298*, 29-32.
Heinegård, D., and Saxne, T. (2011). The role of the cartilage matrix in osteoarthritis. Nature Reviews Rheumatology, *7*, 50–56.
Herz, J., Clouthier, D.E., and Hammer, R.E. (1992). LDL receptor-related protein internalizes and degrades uPA-PAI-1 complexes and is essential for embryo implantation. Cell *71*, 411-421.
Herz, J., Goldstein, J.L., Strickland, D.K., Ho, Y.K., and Brown, M.S. (1991). 39-kDa protein modulates binding of ligands to low density lipoprotein receptor-related protein/alpha 2-macroglobulin receptor. J Biol Chem *266*, 21232-21238.
Herz, J., Hamann, U., Rogne, S., Myklebost, O., Gausepohl, H., and Stanley, K.K. (1988). Surface location and high affinity for calcium of a 500-kd liver membrane protein closely related to the LDL-receptor suggest a physiological role as lipoprotein receptor. Embo J *7*, 4119-4127.
Herz, J., Kowal, R.C., Goldstein, J.L., and Brown, M.S. (1990). Proteolytic processing of the 600 kd low density lipoprotein receptor-related protein (LRP) occurs in a trans-Golgi compartment. Embo J *9*, 1769-1776.
Herz, J., and Strickland, D.K. (2001). LRP: a multifunctional scavenger and signaling receptor. Journal of Clinical Investigation *108*, 779-784.
Hirsch, R., Lethbridge-Cejku, M., Hanson, R., Scott, W.W., Jr., Reichle, R., Plato, C.C., Tobin, J.D., and Hochberg, M.C. (1998). Familial aggregation of osteoarthritis: data from the Baltimore Longitudinal Study on Aging. Arthritis Rheum *41*, 1227-1232.
Hollander, A.P., Pidoux, I., Reiner, A., Rorabeck, C., Bourne, R., and Poole, A.R. (1995). Damage to type II collagen in aging and osteoarthritis starts at the articular surface, originates around chondrocytes, and extends into the cartilage with progressive degeneration. J Clin Invest *96*, 2859-2869.
Horton, W.E., Yamada, Y., and Hassell, J.R. (1987). Retinoic acid rapidly reduces cartilage matrix synthesis by altering gene transcription in chondrocytes. Developmental biology *123*, 508-516.
Howell, B.W., and Herz, J. (2001). The LDL receptor gene family: signaling functions during development. Current opinion in neurobiology *11*, 74-81.
Hu, K., Yang, J., Tanaka, S., Gonias, S.L., Mars, W.M., and Liu, Y. (2006). Tissue-type plasminogen activator acts as a cytokine that triggers intracellular signal transduction and induces matrix metalloproteinase-9 gene expression. J Biol Chem *281*, 2120-2127.
Hua, H., Li, M., Luo, T., Yin, Y., and Jiang, Y. (2011). Matrix metalloproteinases in tumorigenesis: an evolving paradigm. Cell Mol Life Sci *68*, 3853-3868.
Hughes, C.E., Little, C.B., Buttner, F.H., Bartnik, E., and Caterson, B. (1998). Differential expression of aggrecanase and matrix metalloproteinase activity in chondrocytes isolated from bovine and porcine articular cartilage. J Biol Chem *273*, 30576-30582.
Hunter, D.J., and Felson, D.T. (2006). Osteoarthritis. British medical journal *332*, 639-642B.

Iadonato, S.P., Bu, G., Maksymovitch, E.A., and Schwartz, A.L. (1993). Interaction of a 39 kDa protein with the low-density-lipoprotein-receptor-related protein (LRP) on rat hepatoma cells. Biochem J *296 (Pt 3)*, 867-875.
Innes, J.F., Little, C.B., Hughes, C.E., and Caterson, B. (2005). Products resulting from cleavage of the interglobular domain of aggrecan in samples of synovial fluid collected from dogs with early- and late-stage osteoarthritis. American journal of veterinary research *66*, 1679-1685.
Ismail, H.M., Yamamoto, K., Vincent, T.L., Nagase, H., Troeberg, L., and Saklatvala, J. (2015). Interleukin-1 Acts via the JNK-2 Signaling Pathway to Induce Aggrecan Degradation by Human Chondrocytes. Arthritis Rheumatol *67*, 1826-1836.
Ito, A., Mukaiyama, A., Itoh, Y., Nagase, H., Thogersen, I.B., Enghild, J.J., Sasaguri, Y., and Mori, Y. (1996). Degradation of interleukin 1beta by matrix metalloproteinases. J Biol Chem *271*, 14657-14660.
Jaworski, D.M., Soloway, P., Caterina, J., and Falls, W.A. (2006). Tissue inhibitor of metalloproteinase-2(TIMP-2)-deficient mice display motor deficits. Journal of neurobiology *66*, 82-94.
Jensen, G., Andersen, O.M., Bonvin, A.M.J.J., Bjerrum-Bohr, I., Etzerodt, M., Thorgersen, H.C., O'Shea, C., Poulsen, F.M., and Kragelund, B.B. (2006). Binding site structure of one LRP-RAP complex: Implications for a common ligand-receptor binding motif. J Mol Biol *362*, 700-716.
Jensen, J.K., Dolmer, K., and Gettins, P.G. (2009a). Specificity of binding of the low density lipoprotein receptor-related protein to different conformational states of the clade E serpins plasminogen activator inhibitor-1 and proteinase nexin-1. J Biol Chem *284*, 17989-17997.
Jensen, J.K., Dolmer, K., Schar, C., and Gettins, P.G. (2009b). Receptor-associated protein (RAP) has two high-affinity binding sites for the low-density lipoprotein receptor-related protein (LRP): consequences for the chaperone functions of RAP. Biochem J *421*, 273-282.
Jensen, K.J., Domer, K., and Gettins, P.G.W. (2009c). Specificity of binding of the low density lipoprotein receptor-related protein to different conformational states of the Clade E serpins plasminogen activator inhibitor-1 and proteinase nexin-1. J Biol Chem *284*, 17989-17997.
Jensen, P.H., Moestrup, S.K., and Gliemann, J. (1989). Purification of the human placental alpha 2-macroglobulin receptor. FEBS Lett *255*, 275-280.
Jin, G., Huang, X., Black, R., Wolfson, M., Rauch, C., McGregor, H., Ellestad, G., and Cowling, R. (2002). A continuous fluorimetric assay for tumor necrosis factor-alpha converting enzyme. Analytical biochemistry *302*, 269-275.
Jordan, K., Clarke, A.M., Symmons, D.P.M., Fleming, D., Porcheret, M., T Kadam, U., and Croft, P. (2007). Measuring disease prevalence: a comparison of musculoskeletal disease using four general practice consultation databases. Brit J Gen Pract *57*, 7-14.
Jourquin, J., Tremblay, E., Bernard, A., Charton, G., Chaillan, F.A., Marchetti, E., Roman, F.S., Soloway, P.D., Dive, V., Yiotakis, A*., et al.* (2005). Tissue inhibitor of metalloproteinases-1 (TIMP-1) modulates neuronal death, axonal plasticity, and learning and memory. Eur J Neurosci *22*, 2569-2578.
Kanekiyo, T., Zhang, J., Liu, Q., Liu, C.C., Zhang, L., and Bu, G. (2011). Heparan sulphate proteoglycan and the low-density lipoprotein receptor-related protein 1 constitute major pathways for neuronal amyloid-beta uptake. J Neurosci *31*, 1644-1651.

Kashiwagi, M., Enghild, J.J., Gendron, C., Hughes, C., Caterson, B., Itoh, Y., and Nagase, H. (2004). Altered proteolytic activities of ADAMTS-4 expressed by C-terminal processing. J Biol Chem *279*, 10109-10119.
Kashiwagi, M., Tortorella, M., Nagase, H., and Brew, K. (2001). TIMP-3 is a potent inhibitor of aggrecanase 1 (ADAM-TS4) and aggrecanase 2 (ADAM-TS5). J Biol Chem *276*, 12501-12504.
Kempson, G.E. (1982). Relationship between the Tensile Properties of Articular-Cartilage from the Human Knee and Age. Ann Rheum Dis *41*, 508-511.
Kinoshita, A., Shah, T., Tangredi, M.M., Strickland, D.K., and Hyman, B.T. (2003). The intracellular domain of the low density lipoprotein receptor-related protein modulates transactivation mediated by amyloid precursor protein and Fe65. J Biol Chem *278*, 41182-41188.
Knauer, M.F., Orlando, R.A., and Glabe, C.G. (1996). Cell surface APP751 forms complexes with protease nexin 2 ligands and is internalized via the low density lipoprotein receptor-related protein (LRP). Brain research *740*, 6-14.
Knight, G.C., Willenbrock, F., and Murphy, G. (1992). A novel coumarin-labelled peptide for sensitive continuous assays of the matrix metalloproteinases. FEBS Lett *296*, 263-266.
Koshy, P.J., Lundy, C.J., Rowan, A.D., Porter, S., Edwards, D.R., Hogan, A., Clark, I.M., and Cawston, T.E. (2002). The modulation of matrix metalloproteinase and ADAM gene expression in human chondrocytes by interleukin-1 and oncostatin M: a time-course study using real-time quantitative reverse transcription-polymerase chain reaction. Arthritis Rheum *46*, 961-967.
Koskivirta, I., Kassiri, Z., Rahkonen, O., Kiviranta, R., Oudit, G.Y., McKee, T.D., Kyto, V., Saraste, A., Jokinen, E., Liu, P.P.*, et al.* (2010). Mice with tissue inhibitor of metalloproteinases 4 (Timp4) deletion succumb to induced myocardial infarction but not to cardiac pressure overload. J Biol Chem *285*, 24487-24493.
Kristensen, T., Moestrup, S.K., Gliemann, J., Bendtsen, L., Sand, O., and Sottrup-Jensen, L. (1990). Evidence that the newly cloned low-density-lipoprotein receptor related protein (LRP) is the alpha 2-macroglobulin receptor. FEBS Lett *276*, 151-155.
Kuettner, K.E., Hiti, J., Eisenstein, R., and Harper, E. (1976). Collagenase inhibition by cationic proteins derived from cartilage and aorta. Biochem Biophys Res Commun *72*, 40-46.
Laatsch, A., Panteli, M., Sornsakrin, M., Hoffzimmer, B., Grewal, T., and Heeren, J. (2012). Low density lipoprotein receptor-related protein 1 dependent endosomal trapping and recycling of apolipoprotein E. PLoS One *7*, e29385.
Laemmli, U.K. (1970). Cleavage of structural proteins during the assembly of the head of bacteriophage T4. Nature *227*, 680-685.
Langton, K.P., Barker, M.D., and McKie, N. (1998). Localization of the functional domains of human tissue inhibitor of metalloproteinases-3 and the effects of a Sorsby's fundus dystrophy mutation. J Biol Chem *273*, 16778-16781.
Langton, K.P., McKie, N., Curtis, A., Goodship, J.A., Bond, P.M., Barker, M.D., and Clarke, M. (2000). A novel tissue inhibitor of metalloproteinases-3 mutation reveals a common molecular phenotype in Sorsby's fundus dystrophy. J Biol Chem *275*, 27027-27031.
Langton, K.P., McKie, N., Smith, B.M., Brown, N.J., and Barker, M.D. (2005). Sorsby's fundus dystrophy mutations impair turnover of TIMP-3 by retinal pigment epithelial cells. Hum Mol Genet *14*, 3579-3586.

Leco, K., Waterhouse, P., Sanchez, O.H., Gowing, K.L., Poole, A.R., Wakeham, A., Mak, T.W., and Khokha, R. (2001). Spontaneous air space enlargement in the lungs of mice lacking tissue inhibitor of metalloproteinases-3 (TIMP-3). Journal of Clinical Investigation *108*, 817-829.
Lee, D., Walsh, J.D., Mikhailenko, I., Yu, P., Migliorini, M., Wu, Y., Krueger, S., Curtis, J.E., Harris, B., Lockett, S.*, et al.* (2006). RAP uses a histidine switch to regulate its interaction with LRP in the ER and Golgi. Mol Cell *22*, 423-430.
Lee, M.H., Atkinson, S., and Murphy, G. (2007). Identification of the extracellular matix (ECM) binding motifs of Tissue Inhibitors of Metalloproteinases (TIMP-3 and effective transfer to TIMP-1. J Biol Chem *282*, 6887-6898.
Lee, M.H., Rapti, M., and Murphy, G. (2005). Total conversion of tissue inhibitor of metalloproteinase (TIMP) for specific metalloproteinase targeting: fine-tuning TIMP-4 for optimal inhibition of tumor necrosis factor-{alpha}-converting enzyme. J Biol Chem *280*, 15967-15975.
Lee, M.H., Verma, V., Maskos, K., Becherer, J.D., Knauper, V., Dodds, P., Amour, A., and Murphy, G. (2002). The C-terminal domains of TACE weaken the inhibitory action of N-TIMP-3. FEBS Lett *520*, 102-106.
Li, F., and Curry, T.E., Jr. (2009). Regulation and function of tissue inhibitor of metalloproteinase (TIMP) 1 and TIMP3 in periovulatory rat granulosa cells. Endocrinology *150*, 3903-3912.
Li, W.Q., and Zafarullah, M. (1998). Oncostatin M up-regulates tissue inhibitor of metalloproteinases-3 gene expression in articular chondrocytes via de novo transcription, protein synthesis, and tyrosine kinase- and mitogen-activated protein kinase-dependent mechanisms. Journal of Immunology *161*, 5000-5007.
Lijnen, H.R., Arza, B., Van Hoef, B., Collen, D., and Declerck, P.J. (2000). Inactivation of plasminogen activator inhibitor-1 by specific proteolysis with stromelysin-1 (MMP-3). J Biol Chem *275*, 37645-37650.
Lillis, A.P., Van Duyn, L.B., Murphy-Ullrich, J.E., and Strickland, D.K. (2008). LDL receptor-related protein 1: unique tissue-specific functions revealed by selective gene knockout studies. Physiol Rev *88*, 887-918.
Lim, N.H., Kashiwagi, M., Visse, R., Jones, J., Enghild, J.J., Brew, K., and Nagase, H. (2010). Reactive-site mutants of N-TIMP-3 that selectively inhibit ADAMTS-4 and ADAMTS-5: biological and structural implications. Journal of Biological Chemistry *431*, 113-122.
Limana, F., Esposito, G., D'Arcangelo, D., Di Carlo, A., Romani, S., Melillo, G., Mangoni, A., Bertolami, C., Pompilio, G., Germani, A.*, et al.* (2011). HMGB1 attenuates cardiac remodelling in the failing heart via enhanced cardiac regeneration and miR-206-mediated inhibition of TIMP-3. PLoS One *6*, e19845.
Little, C.B., Barai, A., Burkhardt, D., Smith, S.M., Fosang, A.J., Werb, Z., Shah, M., and Thompson, E.W. (2009). Matrix metalloproteinase 13-deficient mice are resistant to osteoarthritic cartilage erosion but not chondrocyte hypertrophy or osteophyte development. Arthritis Rheum *60*, 3723-3733.
Little, C.B., Mittaz, L., Belluoccio, D., Rogerson, F.M., Campbell, I.K., Meeker, C.T., Bateman, J.F., Pritchard, M.A., and Fosang, A.J. (2005). ADAMTS-1-knockout mice do not exhibit abnormalities in aggrecan turnover in vitro or in vivo. Arthritis Rheum *52*, 1461-1472.
Liu, Q., Zhang, J., Tran, H., Verbeek, M.M., Reiss, K., Estus, S., and Bu, G. (2009). LRP1 shedding in human brain: roles of ADAM10 and ADAM17. Molecular neurodegeneration *4*, 17.

Liu, X.W., Bernardo, M.M., Fridman, R., and Kim, H.R. (2003). Tissue inhibitor of metalloproteinase-1 protects human breast epithelial cells against intrinsic apoptotic cell death via the focal adhesion kinase/phosphatidylinositol 3-kinase and MAPK signaling pathway. J Biol Chem *278*, 40364-40372.
Lochter, A., Galosy, S., Muschler, J., Freedman, N., Werb, Z., and Bissell, M.J. (1997). Matrix metalloproteinase stromelysin-1 triggers a cascade of molecular alterations that leads to stable epithelial-to-mesenchymal conversion and a premalignant phenotype in mammary epithelial cells. J Cell Biol *139*, 1861-1872.
Loukinova, E., Ranganathan, S., Kuznetsov, S., Gorlatova, N., Migliorini, M.M., Loukinov, D., Ulery, P.G., Mikhailenko, I., Lawrence, D.A., and Strickland, D.K. (2002). Platelet-derived growth factor (PDGF)-induced tyrosine phosphorylation of the low density lipoprotein receptor-related protein (LRP). Evidence for integrated co-receptor function betwenn LRP and the PDGF. J Biol Chem *277*, 15499-15506.
Lozano, R., Naghavi, M., Foreman, K., Lim, S., Shibuya, K., Aboyans, V., Abraham, J., Adair, T., Aggarwal, R., Ahn, S.Y.*, et al.* (2012). Global and regional mortality from 235 causes of death for 20 age groups in 1990 and 2010: a systematic analysis for the Global Burden of Disease Study 2010. Lancet *380*, 2095-2128.
Majid, M.A., Smith, V.A., Newby, A.C., and Dick, A.D. (2007). Matrix bound SFD mutant TIMP-3 is more stable than wild type TIMP-3. The British journal of ophthalmology *91*, 1073-1076.
Malik, S., and Balkwill, F.R. (1988). Tumour necrosis factor. British Medical Journal *296*, 1214.
Mantuano, E., Lam, M.S., and Gonias, S.L. (2013). LRP1 assembles unique co-receptor systems to initiate cell signaling in response to tissue-type plasminogen activator and myelin-associated glycoprotein. J Biol Chem *288*, 34009-34018.
Matsumoto, K., Shionyu, M., Go, M., Shimizu, K., Shinomura, T., Kimata, K., and Watanabe, H. (2003). Distinct interaction of versican/PG-M with hyaluronan and link protein. J Biol Chem *278*, 41205-41212.
Matthews, R.T., Gary, S.C., Zerillo, C., Pratta, M., Solomon, K., Arner, E.C., and Hockfield, S. (2000). Brain-enriched hyaluronan binding (BEHAB)/brevican cleavage in a glioma cell line is mediated by a disintegrin and metalloproteinase with thrombospondin motifs (ADAMTS) family member. J Biol Chem *275*, 22695-22703.
May, P., Reddy, Y.K., and Herz, J. (2002). Proteolytic processing of low density lipoprotein receptor-related protein mediates regulated release of its intracellular domain. J Biol Chem *277*, 18736-18743.
Melching, L.I., and Roughley, P.J. (1990). Studies on the interaction of newly secreted proteoglycan subunits with hyaluronate in human articular cartilage. Biochim Biophys Acta *1035*, 20-28.
Mi, K., and Johnson, G.V. (2007). Regulated proteolytic processing of LRP6 results in release of its intracellular domain. J Neurochem *101*, 517-529.
Migliorini, M.M., Behre, E.H., Brew, S., Ingham, K.C., and Strickland, D.K. (2003). Allosteric modulation of ligand binding to low density lipoprotein receptor-related protein by the receptor-associated protein requires critical lysine residues within its carboxyl-terminal domain. J Biol Chem *278*, 17986-17992.
Mikhailenko, I., Battey, F.D., Migliorini, M., Ruiz, J.F., Argraves, K., Moayeri, M., and Strickland, D.K. (2001). Recognition of alpha 2-macroglobulin by the low density

lipoprotein receptor-related protein requires the cooperation of two ligand binding cluster regions. J Biol Chem *276*, 39484-39491.
Mikhailenko, I., Considine, W., Argraves, K.M., Loukinov, D., Hyman, B.T., and Strickland, D.K. (1999). Functional domains of the very low density lipoprotein receptor: molecular analysis of ligand binding and acid-dependent ligand dissociation mechanisms. J Cell Sci *112 (Pt 19)*, 3269-3281.
Milla, M.E., Leesnitzer, M.A., Moss, M.L., Clay, W.C., Carter, H.L., Miller, A.B., Su, J.L., Lambert, M.H., Willard, D.H., Sheeley, D.M.*, et al.* (1999). Specific sequence elements are required for the expression of functional tumor necrosis factor-alpha-converting enzyme (TACE). J Biol Chem *274*, 30563-30570.
Milner, J.M., Elliott, S.F., and Cawston, T.E. (2001). Activation of procollagenases is a key control point in cartilage collagen degradation. Arthritis Rheum *44*, 2084-2096.
Mochizuki, S., Shimoda, M., Shiomi, T., Fujii, Y., and Okada, Y. (2004). ADAM28 is activated by MMP-7 (matrilysin-1) and cleaves insulin-like growth factor binding protein-3. Biochem Biophys Res Commun *315*, 79-84.
Moestrup, S.K., and Gliemann, J. (1989). Purification of the rat hepatic alpha 2-macroglobulin receptor as an approximately 440-kDa single chain protein. J Biol Chem *264*, 15574-15577.
Moestrup, S.K., Gliemann, J., and Pallesen, G. (1992). Distribution of the alpha 2-macroglobulin receptor/low density lipoprotein receptor-related protein in human tissues. Cell Tissue Res *269*, 375-382.
Moestrup, S.K., Holtet, T.L., Etzerodt, M., Thogersen, H.C., Nykjaer, A., Andreasen, P.A., Rasmussen, H.H., Sottrup-Jensen, L., and Gliemann, J. (1993). Alpha 2-macroglobulin-proteinase complexes, plasminogen activator inhibitor type-1-plasminogen activator complexes, and receptor-associated protein bind to a region of the alpha 2-macroglobulin receptor containing a cluster of eight complement-type repeats. J Biol Chem *268*, 13691-13696.
Mohammed, F.F., Smookler, D.S., Taylor, S.E.M., Fingleton, B., Kassiri, Z., Sanchez, O.H., English, J.L., Matrisian, L.M., Yeh, W.C., and Khokha, R. (2004). Abnormal TNF activity in Timp3-/- mice leads to chronic hepatic inflammation and failure of liver regeneration. Nat Genet *36*, 969-977.
Moon, R.T., Brown, J.D., and Torres, M. (1997). WNTs modulate cell fate and behavior during vertebrate development. Trends in genetics : TIG *13*, 157-162.
Morris, K.J., Cs-Szabo, G., and Cole, A.A. (2010). Characterisation of TIMP-3 in human talar cartilage. Connective Tissue Research *51*, 478-490.
Mouw, J.K., Ou, G., and Weaver, V.M. (2014). Extracellular matrix assembly: a multiscale deconstruction. Nat Rev Mol Cell Biol *15*, 771-785.
Murphy, F.R., Issa, R., Zhou, X., Ratnarajah, S., Nagase, H., Arthur, M.J., Benyon, C., and Iredale, J.P. (2002). Inhibition of apoptosis of activated hepatic stellate cells by tissue inhibitor of metalloproteinase-1 is mediated via effects on matrix metalloproteinase inhibition: implications for reversibility of liver fibrosis. J Biol Chem *277*, 11069-11076.
Murphy, G., Cartwright, E.C., Sellers, A., and Reynolds, J.J. (1977). The detection and characterisation of collagenase inhibitors from rabbit tissues in culture. Biochim Biophys Acta *483*, 493-498.
Murphy, G., Houbrechts, A., Cockett, M.I., Williamson, R.A., O'Shea, M., and Docherty, A.J. (1991). The N-terminal domain of tissue inhibitor of

metalloproteinases retains metalloproteinase inhibitory activity. Biochemistry *30*, 8097-8102.
Murphy, G., and Nagase, H. (2008). Reappraising metalloproteinases in rheumatoid arthritis and osteoarthritis: destruction or repair? Nat Clin Pract Rheumatol *4*, 128-135.
Murray, C.J., Vos, T., Lozano, R., Naghavi, M., Flaxman, A.D., Michaud, C., Ezzati, M., Shibuya, K., Salomon, J.A., Abdalla, S.*, et al.* (2012). Disability-adjusted life years (DALYs) for 291 diseases and injuries in 21 regions, 1990-2010: a systematic analysis for the Global Burden of Disease Study 2010. Lancet *380*, 2197-2223.
Nagase, H., Fields, C.G., and Fields, G.B. (1994a). Design and characterization of a fluorogenic substrate selectively hydrolyzed by stromelysin 1 (matrix metalloproteinase-3). J Biol Chem *269*, 20952-20957.
Nagase, H., Itoh, Y., and Binner, S. (1994b). Interaction of alpha 2-macroglobulin with matrix metalloproteinases and its use for identification of their active forms. Ann N Y Acad Sci *732*, 294-302.
Nagase, H., and Kashiwagi, M. (2003). Aggrecanases and cartilage matrix degradation. Arthritis Res Ther *5*, 94-103.
Nagase, H., Visse, R., and Murphy, G. (2006). Structure and function of matrix metalloproteinases and TIMPs. Cardiovasc Res *69*, 562-573.
Naito, S., Shiomi, T., Okada, A., Kimura, T., Chijiiwa, M., Fujita, Y., Yatabe, T., Komiya, K., Enomoto, H., Fujikawa, K.*, et al.* (2007). Expression of ADAMTS4 (aggrecanase-1) in human osteoarthritic cartilage. Pathology international *57*, 703-711.
Nakamura, H., Fujii, Y., Inoki, I., Sugimoto, K., Tanzawa, K., Matsuki, H., Miura, R., Yamaguchi, Y., and Okada, Y. (2000). Brevican is degraded by matrix metalloproteinases and aggrecanase-1 (ADAMTS4) at different sites. J Biol Chem *275*, 38885-38890.
Nakamura, H., Fujii, Y., Ohuchi, E., Yamamoto, E., and Okada, Y. (1998). Activation of the precursor of human stromelysin 2 and its interactions with other matrix metalloproteinases. Eur J Biochem *253*, 67-75.
Nakopoulou, L., Giannopoulou, I., Stefanaki, K., Panayotopoulou, E., Tsirmpa, I., Alexandrou, P., Mavrommatis, J., Katsarou, S., and Davaris, P. (2002). Enhanced mRNA expression of tissue inhibitor of metalloproteinase-1 (TIMP-1) in breast carcinomas is correlated with adverse prognosis. The Journal of pathology *197*, 307-313.
Neels, J.G., van Den Berg, B.M., Lookene, A., Olivecrona, G., Pannekoek, H., and van Zonneveld, A.J. (1999). The second and fourth cluster of class A cysteine-rich repeats of the low density lipoprotein receptor-related protein share ligand-binding properties. J Biol Chem *274*, 31305-31311.
Nemeth, J.A., Rafe, A., Steiner, M., and Goolsby, C.L. (1996). TIMP-2 growth-stimulatory activity: a concentration- and cell type-specific response in the presence of insulin. Exp Cell Res *224*, 110-115.
Neuhold, L.A., Killar, L., Zhao, W., Sung, M.L., Warner, L., Kulik, J., Turner, J., Wu, W., Billinghurst, C., Meijers, T.*, et al.* (2001). Postnatal expression in hyaline cartilage of constitutively active human collagenase-3 (MMP-13) induces osteoarthritis in mice. J Clin Invest *107*, 35-44.
Newton, C.S., Loukinova, E., Mikhailenko, I., Ranganathan, S., Gao, Y., Haudenschild, C., and Strickland, D.K. (2005). Platelet-derived growth factor receptor-beta (PDGFR-beta) activation promotes its association with the low

density lipoprotein receptor-related protein (LRP). Evidence for co-receptor function. J Biol Chem *280*, 27872-27878.
Noe, V., Fingleton, B., Jacobs, K., Crawford, H.C., Vermeulen, S., Steelant, W., Bruyneel, E., Matrisian, L.M., and Mareel, M. (2001). Release of an invasion promoter E-cadherin fragment by matrilysin and stromelysin-1. J Cell Sci *114*, 111-118.
Nothnick, W.B. (2001). Reduction in reproductive lifespan of tissue inhibitor of metalloproteinase 1 (TIMP-1)-deficient female mice. Reproduction *122*, 923-927.
Nykjaer, A., and Willnow, T.E. (2002). The low-density lipoprotein receptor gene family: a cellular Swiss army knife? Trends in cell biology *12*, 273-280.
Pavloff, N., Staskus, P.W., Kishnani, N.S., and Hawkes, S.P. (1992). A new inhibitor of metalloproteinases from chicken: ChIMP-3. A third member of the TIMP family. J Biol Chem *267*, 17321-17326.
Polakis, P. (2000). Wnt signaling and cancer. Genes & development *14*, 1837-1851.
Polakis, P. (2001). More than one way to skin a catenin. Cell *105*, 563-566.
Pratta, M.A., Yao, W., Decicco, C., Tortorella, M.D., Liu, R.Q., Copeland, R.A., Magolda, R., Newton, R.C., Trzaskos, J.M., and Arner, E.C. (2003). Aggrecan protects cartilage collagen from proteolytic cleavage. J Biol Chem *278*, 45539-45545.
Qi, J.H., and Anand-Apte, B. (2015). Tissue inhibitor of metalloproteinase-3 (TIMP3) promotes endothelial apoptosis via a caspase-independent mechanism. Apoptosis : an international journal on programmed cell death *20*, 523-534.
Qin, S., Zhu, Y., Ai, F., Li, Y., Bai, B., Yao, W., and Dong, L. (2014). MicroRNA-191 correlates with poor prognosis of colorectal carcinoma and plays multiple roles by targeting tissue inhibitor of metalloprotease 3. Neoplasma *61*, 27-34.
Rocks, N., Paulissen, G., El Hour, M., Quesada, F., Crahay, C., Gueders, M., Foidart, J.M., Noel, A., and Cataldo, D. (2008). Emerging roles of ADAM and ADAMTS metalloproteinases in cancer. Biochimie *90*, 369-379.
Rodriguez, E., and Roughley, P. (2006). Link protein can retard the degradation of hyaluronan in proteoglycan aggregates. Osteoarthritis Cartilage *14*, 823-829.
Rogerson, F.M., Chung, Y.M., Deutscher, M.E., Last, K., and Fosang, A.J. (2010). Cytokine-induced increases in ADAMTS-4 messenger RNA expression do not lead to increased aggrecanase activity in ADAMTS-5-deficient mice. Arthritis Rheum *62*, 3365-3373.
Roughley, P.J., Geng, Y., and Mort, J.S. (2014). The non-aggregated aggrecan in the human intervertebral disc can arise by a non-proteolytic mechanism. Eur Cell Mater *28*, 129-136; discussion 136.
Rozanov, D.V., Hahn-Dantona, E., Strickland, D.K., and Strongin, A.Y. (2004). The low density lipoprotein receptor-related protein LRP is regulated by membrane type-1 matrix metalloproteinase (MT1-MMP) proteolysis in malignant cells. J Biol Chem *279*, 4260-4268.
Sahebjam, S., Khokha, R., and Mort, J.S. (2007). Increased collagen and aggrecan degradation with age in the joint of TIMP-3 -/- mice. Arthritis Rheum *56*, 905-909.
Salic, A., Lee, E., Mayer, L., and Kirschner, M.W. (2000). Control of beta-catenin stability: reconstitution of the cytoplasmic steps of the wnt pathway in Xenopus egg extracts. Mol Cell *5*, 523-532.
Sandy, J.D. (2006). Editorial - A contentious issue finds some clarity: on the independent and complementary roles of aggrecanase activity and MMP activity in human joint aggrecanolysis. Osteoarthritis and Cartilage *14*, 95-100.

Sandy, J.D., Flannery, C.R., Neame, P.J., and Lohmander, L.S. (1992). The structure of aggrecan fragments in human synovial fluid. Evidence for the involvement in osteoarthritis of a novel proteinase which cleaves the Glu 373-Ala 374 bond of the interglobular domain. J Clin Invest *89*, 1512-1516.
Sandy, J.D., Neame, P.J., Boynton, R.E., and Flannery, C.R. (1991). Catabolism of Aggrecan in Cartilage Explants - Identification of a Major Cleavage Site within the Interglobular Domain. Journal of biological chemistry *266*, 8683-8685.
Sapolsky, A.I., Altman, R.D., Woessner, J.F., and Howell, D.S. (1973). The action of cathepsin D in human articular cartilage on proteoglycans. J Clin Invest *52*, 624-633.
Sapolsky, A.I., Keiser, H., Howell, D.S., and Woessner, J.F., Jr. (1976). Metalloproteases of human articular cartilage that digest cartilage proteoglycan at neutral and acid pH. J Clin Invest *58*, 1030-1041.
Sarafanov, A.G., Ananyeva, N.M., Shima, M., and Saenko, E.L. (2001). Cell surface heparan sulfate proteoglycans participate in factor VIII catabolism mediated by low density lipoprotein receptor-related protein. J Biol Chem *276*, 11970-11979.
Sasaki, T., Gohring, W., Mann, K., Maurer, P., Hohenester, E., Knauper, V., Murphy, G., and Timpl, R. (1997). Limited cleavage of extracellular matrix protein BM-40 by matrix metalloproteinases increases its affinity for collagens. J Biol Chem *272*, 9237-9243.
Sato, H., Kida, Y., Mai, M., Endo, Y., Sasaki, T., Tanaka, J., and Seiki, M. (1992). Expression of genes encoding type IV collagen-degrading metalloproteinases and tissue inhibitors of metalloproteinases in various human tumor cells. Oncogene *7*, 77-83.
Schletter, J., Heine, H., Ulmer, A.J., and Rietschel, E.T. (1995). Molecular mechanisms of endotoxin activity. Archives of microbiology *164*, 383-389.
Scilabra, S.D., Troeberg, L., Yamamoto, K., Emonard, H., Thogersen, I., Enghild, J.J., Strickland, D.K., and Nagase, H. (2013). Differential regulation of extracellular TIMP-3 levels by cell membrane-bound and shed LRP-1. J Biol Chem *288*, 332-342.
Sellam, J., and Berenbaum, F. (2010). The role of synovitis in pathophysiology and clinical symptoms of osteoarthritis. Nature reviews Rheumatology *6*, 625-635.
Selvais, C., D'Auria, L., Tyteca, D., Perrot, G., Lemoine, P., Troeberg, L., Dedieu, S., Noel, A., Nagase, H., Henriet, P.*, et al.* (2011). Cell cholesterol modulates metalloproteinase-dependent shedding of low-density lipoprotein receptor-related protein-1 (LRP-1) and clearance function. Faseb J *25*, 2770-2781.
Seo, D.W., Kim, S.H., Eom, S.H., Yoon, H.J., Cho, Y.R., Kim, P.H., Kim, Y.K., Han, J.W., Diaz, T., Wei, B.Y.*, et al.* (2008). TIMP-2 disrupts FGF-2-induced downstream signaling pathways. Microvasc Res *76*, 145-151.
Sheu, B.C., Hsu, S.M., Ho, H.N., Lien, H.C., Huang, S.C., and Lin, R.H. (2001). A novel role of metalloproteinase in cancer-mediated immunosuppression. Cancer Res *61*, 237-242.
Skeldal, S., Larsen, J.V., Pedersen, K.E., Petersen, H.H., Egelund, R., Christensen, A., Jensen, J.K., Gliemann, J., and Andreasen, P.A. (2006). Binding areas of urokinase-type plasminogen activator-plasminogen activator inhibitor-1 complex for endocytosis receptors of the low-density lipoprotein receptor family, determined by site-directed mutagenesis. FEBS J *273*, 5143-5159.

Smith, M.R., Kung, H., Durum, S.K., Colburn, N.H., and Sun, Y. (1997). TIMP-3 induces cell death by stabilizing TNF-alpha receptors on the surface of human colon carcinoma cells. Cytokine *9*, 770-780.
Smith, R.J., Rohloff, N.A., Sam, L.M., Justen, J.M., Deibel, M.R., and Cornette, J.C. (1989). Recombinant human interleukin-1 alpha and recombinant human interleukin-1 beta stimulate cartilage matrix degradation and inhibit glycosaminoglycan synthesis. Inflammation *13*, 367-382.
Song, R.H., Tortorella, M.D., Malfait, A.M., Alston, J.T., Yang, Z., Arner, E.C., and Griggs, D.W. (2007). Aggrecan degradation in human articular cartilage explants is mediated by both ADAMTS-4 and ADAMTS-5. Arthritis Rheum *56*, 575-585.
Sophia Fox, A.J., Bedi, A., and Rodeo, S.A. (2009). The basic science of articular cartilage: structure, composition, and function. Sports health *1*, 461-468.
Sorsby, A., and Mason, M.E. (1949). A fundus dystrophy with unusual features. The British journal of ophthalmology *33*, 67-97.
Stanton, H., Golub, S.B., Rogerson, F.M., Last, K., Little, C.B., and Fosang, A.J. (2011a). Investigating ADAMTS-mediated aggrecanolysis in mouse cartilage. Nature protocols *6*, 388-404.
Stanton, H., Melrose, J., Little, C.B., and Fosang, A.J. (2011b). Proteoglycan degradation by the ADAMTS family of proteinases. Biochim Biophys Acta *1812*, 1616-1629.
Stanton, H., Rogerson, F.M., East, C.J., Golub, S.B., Lawlor, K.E., Meeker, C.T., Little, C.B., Last, K., Farmer, P.J., Campbell, I.K*., et al.* (2005). ADAMTS5 is the major aggrecanse in mouse cartilage in vivo and in vitro. Nature *434*, 648-652.
Stockwell, R.A. (1967). The cell density of human articular and costal cartilage. Journal of anatomy *101*, 753-763.
Strongin, A.Y., Collier, I., Bannikov, G., Marmer, B.L., Grant, G.A., and Goldberg, G.I. (1995). Mechanism of Cell-Surface Activation of 72-Kda Type-Iv Collagenase - Isolation of the Activated Form of the Membrane Metalloprotease. Journal of biological chemistry *270*, 5331-5338.
Su, S., Dehnade, F., and Zafarullah, M. (1996). Regulation of tissue inhibitor of metalloproteinases-3 gene expression by transforming growth factor-beta and dexamethasone in bovine and human articular chondrocytes. DNA and cell biology *15*, 1039-1048.
Su, S., DiBattista, J.A., Sun, Y., Li, W.Q., and Zafarullah, M. (1998). Up-regulation of tissue inhibitor of metalloproteinases-3 gene expression by TGF-beta in articular chondrocytes is mediated by serine/threonine and tyrosine kinases. Journal of cellular biochemistry *70*, 517-527.
Suzuki, K., Kan, C.C., Hung, W., Gehring, M.R., Brew, K., and Nagase, H. (1998). Expression of human pro-matrix metalloproteinase 3 that lacks the N-terminal 34 residues in Escherichia coli: autoactivation and interaction with tissue inhibitor of metalloproteinase 1 (TIMP-1). Biol Chem *379*, 185-191.
Tamai, K., Semenov, M., Kato, Y., Spokony, R., Liu, C., Katsuyama, Y., Hess, F., Saint-Jeannet, J.P., and He, X. (2000). LDL-receptor-related proteins in Wnt signal transduction. Nature *407*, 530-535.
Taube, M.E., Liu, X.W., Fridman, R., and Kim, H.R. (2006). TIMP-1 regulation of cell cycle in human breast epithelial cells via stabilization of p27(KIP1) protein. Oncogene *25*, 3041-3048.
Thevenard, J., Verzeaux, L., Devy, J., Etique, N., Jeanne, A., Schneider, C., Hachet, C., Ferracci, G., David, M., Martiny, L*., et al.* (2014). Low-density lipoprotein receptor-

related protein-1 mediates endocytic clearance of tissue inhibitor of metalloproteinases-1 and promotes its cytokine-like activities. PLoS One *9*, e103839.
Thomas, L. (1956). Reversible collapse of rabbit ears after intravenous papain, and prevention of recovery by cortisone. The Journal of experimental medicine *104*, 245-252.
Tortorella, M.D., Burn, T.C., Pratta, M.A., Abbaszade, I., Hollis, J.M., Liu, R., Rosenfeld, S.A., Copeland, R.A., Decicco, C.P., Wynn, R.*, et al.* (1999). Purification and cloning of aggrecanase-1: a member of the ADAMTS family of proteins. Science *284*, 1664-1666.
Tortorella, M.D., Liu, R.Q., Burn, T., Newton, R.C., and Arner, E. (2002). Characterization of human aggrecanase 2 (ADAM-TS5): substrate specificity studies and comparison with aggrecanase 1 (ADAM-TS4). Matrix Biol *21*, 499-511.
Tortorella, M.D., Pratta, M., Liu, R.Q., Austin, J., Ross, O.H., Abbaszade, I., Burn, T., and Arner, E. (2000). Sites of aggrecan cleavage by recombinant human aggrecanase-1 (ADAMTS-4). J Biol Chem *275*, 18566-18573.
Towbin, H., Staehelin, T., and Gordon, J. (1979). Electrophoretic transfer of proteins from polyacrylamide gels to nitrocellulose sheets: procedure and some applications. Proc Natl Acad Sci U S A *76*, 4350-4354.
Troeberg, L., Fushimi, K., Khokha, R., Emonard, H., Ghosh, P., and Nagase, H. (2008). Calcium pentosan polysulfate is a multifaceted exosite inhibitor of aggrecanases. FASEB *22*, 3515-3524.
Troeberg, L., Fushimi, K., Scilabra, S.D., Nakamura, H., Dive, V., Thogersen, I.B., Enghild, J.J., and Nagase, H. (2009). The C-terminal domains of ADAMTS-4 and ADAMTS-5 promote association with N-TIMP-3. Matrix Biol *28*, 463-469.
Troeberg, L., Lazenbatt, C., Anower, E.K.M.F., Freeman, C., Federov, O., Habuchi, H., Habuchi, O., Kimata, K., and Nagase, H. (2014). Sulfated glycosaminoglycans control the extracellular trafficking and the activity of the metalloprotease inhibitor TIMP-3. Chemistry & biology *21*, 1300-1309.
Troeberg, L., Mulloy, B., Ghosh, P., Lee, M.H., Murphy, G., and Nagase, H. (2012). Pentosan polysulfate increases affinity between ADAMTS-5 and TIMP-3 through formation of an electrostatically driven trimolecular complex. Biochem J *443*, 307-315.
Tuuttila, A., Morgunova, E., Bergmann, U., Lindqvist, Y., Maskos, K., Fernandez-Catalan, C., Bode, W., Tryggvason, K., and Schneider, G. (1998). Three-dimensional structure of human tissue inhibitor of metalloproteinases-2 at 2.1 A resolution. J Mol Biol *284*, 1133-1140.
Ugwu, F., Van Hoef, B., Bini, A., Collen, D., and Lijnen, H.R. (1998). Proteolytic cleavage of urokinase-type plasminogen activator by stromelysin-1 (MMP-3). Biochemistry *37*, 7231-7236.
van den Biggelaar, M., Madsen, J.J., Faber, J.H., Zuurveld, M.G., van der Zwaan, C., Olsen, O.H., Stennicke, H.R., Mertens, K., and Meijer, A.B. (2015). Factor VIII Interacts with the Endocytic Receptor Low-density Lipoprotein Receptor-related Protein 1 via an Extended Surface Comprising "Hot-Spot" Lysine Residues. J Biol Chem *290*, 16463-16476.
van den Bigglelaar, M., Sellink, E., Klein Gebbinck, J.W.T.M., Mertens, K., and Meijer, A.B. (2011). A single lysine of the two-lysine recognition motif of the D3 domain of receptor-associated protein is sufficient to mediate endocytosis by low-density

lipoprotein receptor-related protein. The International Journal of Biochemistry & Cell Biology *43*, 431-440.
Vankemmelbeke, M.N., Holen, I., Wilson, A.G., Ilic, M.Z., Handley, C.J., Kelner, G.S., Clark, M., Liu, C., Maki, R.A., Burnett, D.*, et al.* (2001). Expression and activity of ADAMTS-5 in synovium. Eur J Biochem *268*, 1259-1268.
Vater, C.A., Mainardi, C.L., and Harris, E.D., Jr. (1979). Inhibitor of human collagenase from cultures of human tendon. J Biol Chem *254*, 3045-3053.
Verrouil, E., and Mazieres, B. (1995). Etiologic factors in finger osteoarthritis. Rev Rhum Engl Ed *62*, 9S-13S.
Verzijl, N., DeGroot, J., Ben Zaken, C., Braun-Benjamin, O., Maroudas, A., Bank, R.A., Mizrahi, J., Schalkwijk, C.G., Thorpe, S.R., Baynes, J.W.*, et al.* (2002). Crosslinking by advanced glycation end products increases the stiffness of the collagen network in human articular cartilage - A possible mechanism through which age is a risk factor for osteoarthritis. Arthritis Rheum *46*, 114-123.
Visse, R., and Nagase, H. (2003). Matrix metalloproteinases and tissue inhibitors of metalloproteinases: structure, function, and biochemistry. Circ Res *92*, 827-839.
von Arnim, C.A., Kinoshita, A., Peltan, I.D., Tangredi, M.M., Herl, L., Lee, B.M., Spoelgen, R., Hshieh, T.T., Ranganathan, S., Battey, F.D.*, et al.* (2005). The low density lipoprotein receptor-related protein (LRP) is a novel beta-secretase (BACE1) substrate. J Biol Chem *280*, 17777-17785.
Von den Hoff, H.W., van Kampen, G.P., and van der Korst, J.K. (1993). Proteoglycan depletion of intact articular cartilage by retinoic acid is irreversible and involves loss of hyaluronate. Osteoarthritis Cartilage *1*, 157-166.
Wang, B., Hsu, S.H., Majumder, S., Kutay, H., Huang, W., Jacob, S.T., and Ghoshal, K. (2010). TGFbeta-mediated upregulation of hepatic miR-181b promotes hepatocarcinogenesis by targeting TIMP3. Oncogene *29*, 1787-1797.
Wang, W.M., Ge, G., Lim, N.H., Nagase, H., and Greenspan, D.S. (2006). TIMP-3 inhibits the procollagen N-proteinase ADAMTS-2. Biochem J *398*, 515-519.
Warshawsky, I., Broze, G.J., Jr., and Schwartz, A.L. (1994). The low density lipoprotein receptor-related protein mediates the cellular degradation of tissue factor pathway inhibitor. Proc Natl Acad Sci U S A *91*, 6664-6668.
Watanabe, H., Yamada, Y., and Kimata, K. (1998). Roles of aggrecan, a large chondroitin sulfate proteoglycan, in cartilage structure and function. Journal of biochemistry *124*, 687-693.
Wayne, G.J., Deng, S.J., Amour, A., Borman, S., Matico, R., Carter, H.L., and Murphy, G. (2007). TIMP-3 inhibition of ADAMTS-4 (Aggrecanase-1) is modulated by interactions between aggrecan and the C-terminal domain of ADAMTS-4. J Biol Chem *282*, 20991-20998.
Weber, B.H., Vogt, G., Pruett, R.C., Stohr, H., and Felbor, U. (1994). Mutations in the tissue inhibitor of metalloproteinases-3 (TIMP3) in patients with Sorsby's fundus dystrophy. Nat Genet *8*, 352-356.
Wei, S., Kashiwagi, M., Kota, S., Xie, Z., Nagase, H., and Brew, K. (2005). Reactive site mutations in tissue inhibitor of metalloproteinase-3 disrupt inhibition of matrix metalloproteinases but not tumor necrosis factor-alpha-converting enzyme. J Biol Chem *280*, 32877-32882.
Welgus, H.G., Stricklin, G.P., Eisen, A.Z., Bauer, E.A., Cooney, R.V., and Jeffrey, J.J. (1979). A specific inhibitor of vertebrate collagenase produced by human skin fibroblasts. J Biol Chem *254*, 1938-1943.

Will, H., Atkinson, S.J., Butler, G.S., Smith, B., and Murphy, G. (1996). The soluble catalytic domain of membrane type 1 matrix metalloproteinase cleaves the propeptide of progelatinase A and initiates autoproteolytic activation. Regulation by TIMP-2 and TIMP-3. J Biol Chem *271*, 17119-17123.
Williams, S.E., Ashcom, J.D., Argraves, W.S., and Strickland, D.K. (1992). A novel mechanism for controlling the activity of alpha 2-macroglobulin receptor/low density lipoprotein receptor-related protein. Multiple regulatory sites for 39-kDa receptor-associated protein. J Biol Chem *267*, 9035-9040.
Williamson, R.A., Marston, F.A., Angal, S., Koklitis, P., Panico, M., Morris, H.R., Carne, A.F., Smith, B.J., Harris, T.J., and Freedman, R.B. (1990). Disulphide bond assignment in human tissue inhibitor of metalloproteinases (TIMP). Biochem J *268*, 267-274.
Williamson, R.A., Martorell, G., Carr, M.D., Murphy, G., Docherty, A.J., Freedman, R.B., and Feeney, J. (1994). Solution structure of the active domain of tissue inhibitor of metalloproteinases-2. A new member of the OB fold protein family. Biochemistry *33*, 11745-11759.
Willnow, T.E. (1999). The low-density lipoprotein receptor gene family: multiple roles in lipid metabolism. J Mol Med (Berl) *77*, 306-315.
Willnow, T.E., Orth, K., and Herz, J. (1994a). Molecular dissection of ligand binding sites on the low density lipoprotein receptor-related protein. J Biol Chem *269*, 15827-15832.
Willnow, T.E., Sheng, Z., Ishibashi, S., and Herz, J. (1994b). Inhibition of hepatic chylomicron remnant uptake by gene transfer of a receptor antagonist. Science *264*, 1471-1474.
Wisniewska, M., Goettig, P., Maskos, K., Belouski, E., Winters, D., Hecht, R., Black, R., and Bode, W. (2008). Structural determinants of the ADAM inhibition by TIMP-3: crystal structure of the TACE-N-TIMP-3 complex. J Mol Biol *381*, 1307-1319.
Wodarz, A., and Nusse, R. (1998). Mechanisms of Wnt signaling in development. Annual review of cell and developmental biology *14*, 59-88.
Woessner, J.F., Jr. (1973). Purification of cathepsin D from cartilage and uterus and its action on the protein-polysaccharide complex of cartilage. J Biol Chem *248*, 1634-1642.
Woolley, D.E., Roberts, D.R., and Evanson, J.M. (1975). Inhibition of human collagenase activity by a small molecular weight serum protein. Biochem Biophys Res Commun *66*, 747-754.
Wyckoff, M., Rodbard, D., and Chrambach, A. (1977). Polyacrylamide gel electrophoresis in sodium dodecyl sulfate-containing buffers using multiphasic buffer systems: properties of the stack, valid Rf- measurement, and optimized procedure. Analytical biochemistry *78*, 459-482.
Yamada, M., Momose, K., Richelson, E., and Yamada, M. (1996). Sodium nitroprusside-induced apoptotic cellular death via production of hydrogen peroxide in murine neuroblastoma N1E-115 cells. Journal of pharmacological and toxicological methods *35*, 11-17.
Yamamoto, K., Troeberg, L., Scilabra, S.D., Pelosi, M., Murphy, C.L., Strickland, D.K., and Nagase, H. (2013). LRP-1-mediated endocytosis regulates extracellular activity of ADAMTS-5 in articular cartilage. Faseb J *27*, 511-521.
Yang, M., Huang, H., Li, J., Li, D., and Wang, H. (2004). Tyrosine phosphorylation of the LDL receptor-related protein (LRP) and activation of the ERK pathway are

required for connective tissue growth factor to potentiate myofibroblast differentiation. Faseb J *18*, 1920-1921.
Young, D.A., Lakey, R.L., Pennington, C.J., Jones, D., Kevorkian, L., Edwards, D.R., Cawston, T.E., and Clark, I.M. (2005). Histone deacetylase inhibitors modulate metalloproteinase gene expression in chondrocytes and block cartilage resorption. Arthritis Res Ther *7*, R503-512.
Yu, Q., and Stamenkovic, I. (2000). Cell surface-localized matrix metalloproteinase-9 proteolytically activates TGF-beta and promotes tumor invasion and angiogenesis. Genes & development *14*, 163-176.
Yu, W.H., Yu, S., Meng, Q., Brew, K., and Woessner, J.F. (2000). TIMP-3 binds to sulfated glycosaminoglycans of the extracellular matrix. J Biol Chem *275*, 1226-1232.
Zheng, J., Luo, W., and Tanzer, M.L. (1998). Aggrecan synthesis and secretion. A paradigm for molecular and cellular coordination of multiglobular protein folding and intracellular trafficking. J Biol Chem *273*, 12999-13006.
Zilberberg, A., Yaniv, A., and Gazit, A. (2004). The low density lipoprotein receptor-1, LRP1, interacts with the human frizzled-1 (HFz1) and down-regulates the canonical Wnt signaling pathway. J Biol Chem *279*, 17535-17542.
Zurhove, K., Nakajima, C., Herz, J., Bock, H.H., and May, P. (2008). Gamma-secretase limits the inflammatory response through the processing of LRP1. Science signaling *1*, ra15.